Increasing the Capacity of Distributed Generation in Electricity Networks by Intelligent Generator Control

Aristides E. Kiprakis

A thesis submitted for the degree of Doctor of Philosophy.
The University of Edinburgh.
October 2005

Abstract

The rise of environmental awareness as well as the unstable global fossil fuel market has brought about government initiatives to increase electricity generation from renewable energy sources. These resources tend to be geographically and electrically remote from load centres. Consequently many Distributed Generators (DGs) are expected to be connected to the existing Distribution Networks (DNs), which have high impedance and low X/R ratios.

Intermittence and unpredictability of the various types of renewable energy sources can be of time scales of days (hydro) down to seconds (wind, wave). As the time scale becomes smaller, the output of the DG becomes more difficult to accommodate in the DN. With the DGs operating in constant power factor mode, intermittence of the output of the generator combined with the high impedance and low X/R ratios of the DN will cause voltage variations above the statutory limits for quality of supply. This is traditionally mitigated by accepting increased operation of automated network control or network reinforcement. However, due to the distributed nature of RES, automating or reinforcing the DN can be expensive and difficult solutions to implement. The Thesis proposed was that new methods of controlling DG voltage could enable the connection of increased capacities of plant to existing DNs without the need for network management or reinforcement.

The work reported here discusses the implications of the increasing capacity of DG in rural distribution networks on steady-state voltage profiles. Two methods of voltage compensation are proposed. The first is a deterministic system that uses a set of rules to intelligently switch between voltage and power factor control modes. This new control algorithm is shown to be able to respond well to slow voltage variations due to load or generation changes. The second method is a fuzzy inference system that adjusts the setpoint of the power factor controller in response to the local voltage. This system can be set to respond to any steady-state voltage variations that will be experienced. Further, control of real power is developed as a supplementary means for voltage regulation in weak rural networks. The algorithms developed in the study are shown to operate with any synchronous or asynchronous generation wherein real and reactive power can be separately controlled. Extensive simulations of typical and real rural systems using synchronous generators (small hydro) and doubly-fed induction generators (wind turbines) have verified that the proposed approaches improve the voltage profile of the distribution network. This demonstrated that the original Thesis was true and that the techniques proposed allow wider operation of greater capacities of DG within the statutory voltage limits.

Declaration of Originality

I hereby declare that, unless explicitly stated, the research recorded in this thesis, and the thesis itself, was composed and originated entirely by myself in the School of Engineering and Electronics at The University of Edinburgh.

Aristides E. Kiprakis

Acknowledgments

I have to admit that this page was the most difficult to compose from the whole Thesis, for it is not an easy task to thank all the people who have offered me help throughout these years, and at the same time make it sound as true and honest as it feels by avoiding commonalities. Especially when I write in English. I will try my best.

First of all, I would like to thank my supervisor, Dr Robin Wallace, for being a caring mentor, for his endless support, encouragement, trust and epic patience.

I also owe many thanks to my second supervisor, Dr Ewen Macpherson for being there every time I needed him, and for providing his valuable advice, especially during my writing-up stage.

My sincere thanks also go to Dr Gareth Harrison, for being an ideal collaborator within the RNET project, a good friend and a valuable "unofficial" but always willing advisor.

Lots of thanks to the whole IES community for being a pleasant group of people and a pleasure to work with. However, I have to put Simon (lately known as "Doctor Forrest") one step above, for being such a good friend and for making sure that during my studies in Edinburgh, I received the full Scottish education. Including whisky. And beer. And sambuca on fire. Sifis, a flask of tsikoudia is always waiting for us in Crete.

I owe many thanks to my parents Manolis and Sofia, my brother Dimitrios and my sister Irene for their everlasting love, patience and support in multiple ways (some of which required the assistance of ΕΛΤΑ and Royal Mail). Folks, I promise: I am done with my studies.

Finally, It was my family that made it possible for me to engage in this PhD study. It was somebody else's support that assisted me to complete it. Vasso, I am eternally indebted to you.

Contents

List of figures

List of tables

Acronyms and abbreviations

APFC	Automatic Power Factor Controller
AVPFC	Automatic Voltage / Power Factor Controller
AVR	Automatic Voltage Regulator
BSP	Bulk Supply Point
BWEA	British Wind Energy Association
CCGT	Combined Cycle Gas Turbine
CHP	Combined Heat and Power
GHG	Greenhouse Gases
DG	Distributed / Dispersed Generation
DFIG	Doubly Fed Induction Generator
DN	Distribution Network
EG	Embedded Generation
EHV	Extra High Voltage (400 kV and 275 kV)
EPSRC	Engineering and Physical Sciences Research Council
FLPFC	Fuzzy Logic Power Factor Controller
HG	Hydro Generator
HV	High Voltage (132 kV)
IG	Induction Generator
IM	Induction Machine
LDRC	Line Drop / Rise Compensation
LUT	Look Up Table
LV	Low Voltage (400 V and 230 V)
mHG	Mini-Hydro Generator
μHG	Micro-Hydro Generator
MV	Medium Voltage (11 kV and 33 kV)
OLTC	Online Tap Changer
PEC	Power Electronic Converter

PV	Photo-Voltaic panel
RES	Renewable Energy Sources
RNET	Renewable and New Energy Technologies
ROC	Renewables Obligation Certificate
SCIG	Squirrel Cage Induction Generator
SG	Synchronous Generator
SHG	Small Hydro Generator
SM	Synchronous Machine
UK	United Kingdom
WECS	Wind Energy Conversion System
WT	Wind Turbine

Contend with the powers of nature, force them to the yoke of superior purpose. Free that spirit which struggles within them and longs to mingle with that spirit which struggles within you. When a man fighting with chaos subdues a series of phenomena to the laws of his mind and strictly confines these laws within the boundaries of reason, then the world breathes, the voices are ranged in order, the future becomes clarified, and all the dark and endless quantities of numbers are freed by submitting to mystical quality.

Nikos Kazantzakis, *"Ascetic Life (Salvatores Dei)"*

Chapter 1
Introduction

1.1 Research Background

Increased environmental awareness has generated a number of directives both in the UK and internationally in order to motivate development of Renewable Energy Sources (RES) and Combined Heat and Power (CHP) plants. The EU Renewables Directive, the UK Renewables Obligation and revisions to energy trading agreements aim to significantly increase the European and UK capacity of Distributed Generators that will not operate in response to central dispatch. Most of the Renewable Energy Sources are located at remote ends of the Distribution Network (wind, marine, mini-hydro). The Renewables Obligation sets a target that by 2010 10%, and by 2020 20%, of total electricity supplied should be from RES plant. The goverment has also set a target of connecting 10 GW of fossil fuelled but very efficient Combined Heat and Power plants. In absolute terms this implies connection of around 2000 MW of new Distributed Generation (DG) plant *every year* [2]. A great amount of this new generation (especially from RES) is typically found in remote rural areas where the loads are low, the Distribution Network (DN) is medium or even low voltage and designed for a unidirectional, downstream flow of energy [3]. The steady-state, slow and transient variations of voltage levels related to the connection of a DG can lead to undesired operation of voltage control equipment on transformers at the primary substations of the network. A net reversal or increase of power flow in lines due to the presence or the loss respectively of a DG, can cause unacceptable voltage variations, and the Distribution Network Operator (DNO) will likely then require that the DG be disconnected [4]. The resulting loss of revenue can be a barrier for the development of DG towards the 2010 targets. It is therefore clear that a technology and an operational framework has to be developed that will mitigate these adverse effects.

1.2 Basic Definitions

The following terms will be used in this document as described here:

Renewable Energy Source is any energy source that is replenished by natural processes at least as fast as it is used and its overall environmental impact during its life cycle (emergence/consumption) is negligible. Examples are wind, hydro (small only), solar, biomass, geothermal, wave and tidal current.

Transmission Network is the part of the electric power system that is used to interconnect large power stations and ship large quantities of energy from generators to bulk supply points. Its operation is actively managed and its voltage levels in the UK are 400 kV and 275 kV. Furthermore, in Scotland the 132 kV sub-system is also operated and considered as "sub-transmission" network.

Distribution Network is the part of the electric power system that is used to deliver energy to end customers (loads). Currently there are only a few active means of control over its function, such as transformers with online tap changing mechanisms. The voltage levels in the UK Distribution Network are 132 kV (England & Wales), 33 kV, 11 kV and low voltage (400 V and 230 V).

Distributed or Dispersed Generation is generation that is connected to the Distribution Network and not 'dispatched' *i.e.* not controlled by the power system operator. There is no formal definition of its capacity, but for this document this will be considered as less than 20 MW. The terms 'distributed' and 'dispersed' will be used interchangeably.

Embedded Generation is considered by many as equivalent to Distributed or Dispersed Generation. In this document an Embedded Generator is defined as a Distributed Generator that is physically attached to the same busbar as a load and its output is governed by the load requirements. An example of an Embedded Generator is a Combined Heat and Power plant that provides electricity as a by-product after serving a specific heat load.

1.3 Sustainable Electricity Systems

It is now understood that anthropogenic pollution of the atmosphere, mainly through burning of fossil fuels, makes a large contribution to climate change. The last century saw an increase of the global temperatures of 0.6^oC, while the Intergovernmental Panel on Climate Change (IPCC) has predicted that global temperatures will rise during the 21st Century by between 1.4^oC and 5.8^oC and that sea levels will rise by between 0.09 and 0.88 metres [5]. Energy production and consumption do more environmental damage in the world than any other human activity. Global energy demand is expected to increase 57% over the next two decades [6]. The result will be a further 60% increase in the emission of carbon dioxide (CO_2) and other Greenhouse Gases (GHG) [7], when the present concentration of CO_2 in the atmosphere is the highest for three million years. In the UK, electric power stations currently contribute 29% of the total CO_2 emissions. The breakdown of the contribution to GHG emissions by each source in the UK for 2002 is shown in Figure 1.1 [8].

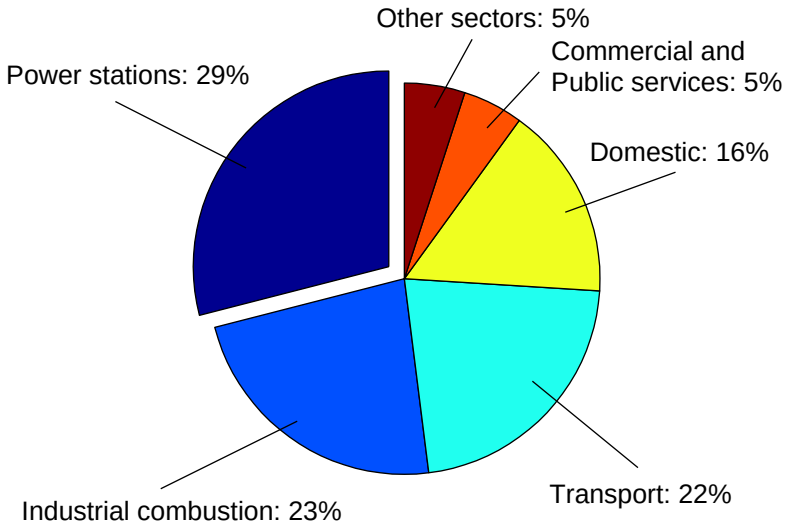

Figure 1.1: *Contribution to CO_2 emissions by various sources in the UK, 2002*

At Kyoto, the member states of the European Union (EU) agreed jointly to undertake an 8% reduction of six key greenhouse gases from 1990 to 2008-2012 [9]. The UK reduction target under EU burden sharing arrangements was 12.5%, but the UK government has committed itself to a 20% reduction of of carbon dioxide emissions by 2010 and has set

an ambitious target for a 60% reduction from the 1990 levels by 2050 [10].

Reduction of CO_2 emissions is not the only challenge for tomorrow's electricity generation system. Fuel poverty and depletion of conventional fuels in the next few decades are also threats that cannot be ignored. Energy consumption is correlated with the per capita income and is distributed inequitably around the world. It is estimated that one third of the world's population has no access to electricity [11]. At the same time, oil and all the other fossil fuels are finite resources. World oil production is expected to peak during the next few decades and then decline. Oil prices will therefore rise rapidly unless alternative fuels can be exploited [12].

To mitigate these problems there is a need for *Sustainable Energy Development* by utilising a policy, which will aim to reduce the need for energy by improving the effectiveness of its use (*Energy Efficiency*) and motivate use of energy from a source that does not result in the depletion of the earth's resources, whether this is from a central or local source (*Renewable Energy Supply*). The criteria that need to be satisfied in order for the operation of the electric power system to qualify as sustainable are:

- provision of electricity necessary to maintain and improve quality of life to all, both in physical and economic terms;
- constraint of pollutants within healthy levels;
- minimisation of the risk of future environmental or economic impact by limiting greenhouse gases, radioactive wastes and other long-lived toxins;
- development and promotion of cheap and environment-friendly technologies for electricity generation; and
- electricity pricing that reflects the actual costs of electricity provision, including environmental and other external costs.

An exact definition of energy technologies that meet the above criteria does not exist; but when observed from the electric power point of view, sustainability resides in two

large thematic areas: increased power system efficiency and development of Renewable Energy Sources (RESs).

1.4 Renewable Energy Sources in the UK Power System

Electricity generated from Renewable Energy Sources is considered as "green" because it has negligible emissions of greenhouse gases and other pollutants. Commercial interest in RES started in the mid-1970s shortly after the first oil shock and was driven mainly by the goal of minimising the dependence of the western countries on oil. Then, since the late 1990s a series of incidents occurred and this led to a radical change to the UK energy market:

- CO_2 emissions slowed down due to the decline of coal usage;
- oil (and consequently gas) prices rose from approximately \$10 to \$60 per barrel;
- wholesale prices fell and undermined future investment in the energy sector;
- the US energy colossus Enron collapsed along with its trading model;
- the UK became a net gas importer through the Interconnector and thus gas prices were linked to those of mainland Europe.

It is therefore clear that the UK (as most of the industrialised countries) has two growing concerns: the need for an improved environmental policy and the fact that it is already an importer of gas, and through gas, of electricity too, as gas is becoming the dominant fuel source for electricity [13]. As a consequence, the UK Renewables Obligation was introduced by the UK government (and the Renewables Directive in the rest of EU) in order to motivate and stimulate development of RES. The former sets a target that by 2010 a 10% (and 20% by 2020) of total electricity supplied in the UK should be from RE plant. Further, the Renewables Obligation aims to increase installed capacity of CHP

generation to 10 GW. With the current legislation, method of operation of the power system and initiatives (or lack thereof), these targets are now proving very difficult to meet. Figure 1.2 shows the generating capacity per plant type in the UK from 1996 to 2002 [14]. The total generating capacity at the end of 2002 was 76.6 GW.

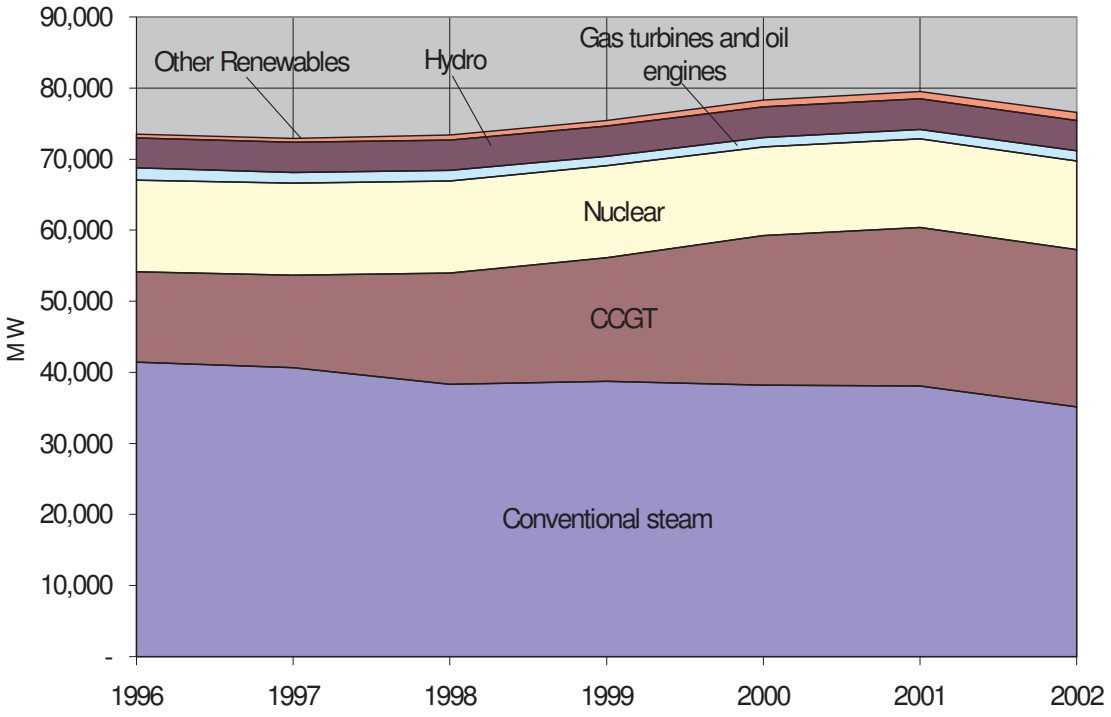

Figure 1.2: *Capacity per plant type in the UK from 1996 to 2002, DUKES 2002*

Although still small, Renewable Energy stations' capacity has been increased by 123% in these 6 years to reach the 2002 capacity of 1.13 GW. The non-renewable but highly efficient Combined Cycle Gas Turbine (CCGT) plant capacity has also been significantly increased by 74% during the same period (22.1 GW in total). On the contrary, all the non-sustainable plants have seen a decrease in their capacity, with most significant the conventional steam plants (15.2%). This is partially due to the UK non-fossil commitment, but was further assisted by the fact that some of the coal-fired plants were already at the end of their life cycles. Finally the capacity of the large hydro-electric plants (including pumped storage) has been increased by 1.24% up to 4.25 GW over these six years, although during 2002 there was a decline due to the reduction of

the output of some stations in order for them to conform to (and benefit from) the pro- Distributed Generation regulations that apply to RES plants with capacity under 20 MW. The contribution of each technology to the total generation capacity at the end of 2002 is shown in Figure 1.3.

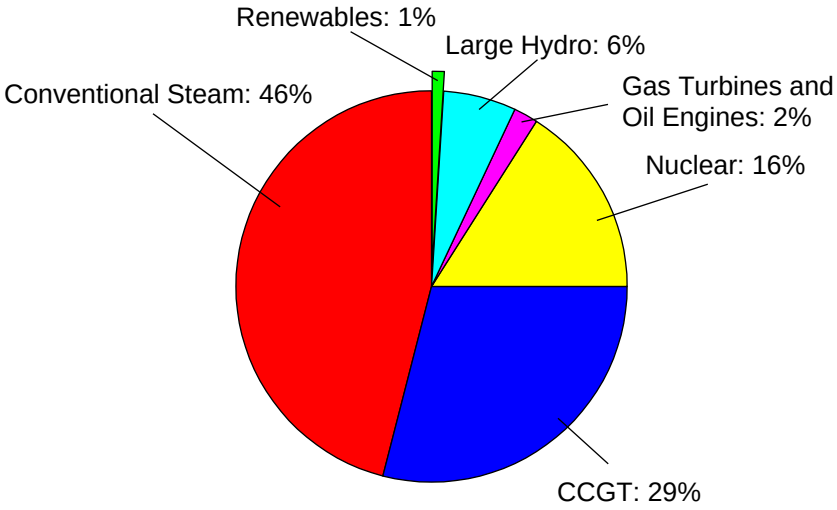

Figure 1.3: *Contribution of each generation type to the total UK capacity, DUKES 2002*

In the effort to achieve the 2010 and 2020 targets, management of a power system with such a high RES penetration is expected to impose major challenges to the network operators. The Royal Commission on Environmental Pollution in its report "Energy - The Changing Climate", published in 2000, proposes that these challenges may be overcome by installing large capacities of conventional fossil fuelled generating plants that will be used only for short intervals when the RES output does not suffice [10]. It is easy to understand that such a strategy would have an extremely high capital cost. Additionally, each renewable energy technology has its own characteristic impact on the environment and the power system and has to be assessed on an individual basis. The RE technologies that already are developed, or expected to develop, in the UK distribution systems are:

- wind (on-, near- and offshore);
- small hydro;

- biomass;
- solar photovoltaic; and
- marine (wave, tidal current).

Large hydro-electricity plants are not categorised among the RESs despite their zero-emission operation. The reasons are their high capital cost and their adverse environmental effects both upstream (large area flood and significant impacts to the habitat) and downstream (quality and quantity of water flow). Also, they are usually connected to the transmission rather than the distribution network through dedicated power lines. The above list should also contain the Combined Heat and Power (CHP) plants because, although they are not fed by a RES, they are highly efficient and therefore qualify as sustainable generation by reducing the need for conventional, inefficient steam power plant. Wind Energy Conversion Systems and Small Hydro Generators are discussed in the following sections as they are the main types of generation studied in this research.

1.5 The RNET Project

The work reported here was a part of a research project funded by the UK Engineering and Physical Sciences Research Council (EPSRC) that emerged in response to the EPSRC's Renewable and New Energy Technologies (RNET) programme (Ref. RNET1/084). The title of the project was "Maximising the Integration of Embedded Renewable and New Generation into Existing Distribution Networks" and it was carried out by the Institute for Energy Systems at the University of Edinburgh (led by Dr Robin Wallace) with the collaboration of the Manchester Centre For Electrical Energy at the University of Manchester, Institute of Science and Technology (led by Prof. Goran Strbac). The project was supported by a number of industrial collaborators including SP Power Systems, East of Scotland Water, IPSA Power Engineering and others. Work was initiated in October 2000 and ended in September 2003 and involved 4 academic staff, 2 research associates and this PhD studentship.

The objective of the whole RNET project, as stated in the project proposal, was to develop a body of knowledge and software simulation toolset that would:

1. Determine the amount of Embedded, Renewable and new Generation (ERG) that can be connected to distribution networks subject to existing and revised system restrictions;
2. Embody stochastic energy production and load demand as time-series data;
3. Apply probabilistic analysis techniques to optimise ERG production, distribution system optimal power flow and voltage profiles;
4. Identify and validate possible changes to network operation and configuration to integrate a greater capacity of ERG ;
5. Quantify the economic interaction between the ERG and the network;
6. Investigate local and regional voltage reprofiling - both static and dynamic - to optimise capacity and energy production of ERG;
7. Investigate active and reactive power control techniques of, or at, the ERG that will maximise production and reduce impact on the distribution system.

These tasks were shared among the collaborators, and this report is on work mainly concerned with task 7.

1.6 Project Objectives and Scope

In this work the main objective was to explore the possibility of alternative control and dispatch of Distributed Generators, in order to maximise production with minimum impact on the power system. This was implemented through a number of tasks. It modelled power and voltage influenced excitation and governor control of Synchronous Generators and studied the dispatch of active and reactive power from Doubly Fed Induction Generators by rotor voltage control. Further, DG control algorithms were

developed to maximise production, ensuring at the same time that the generator will operate within pre-defined voltage and reactive power generation limits.

1.7 Thesis

The thesis of the work was that: Intelligent voltage and reactive power control algorithms of small-scale generators, which are connected to weak distribution networks, can allow increase of their capacity before the statutory voltage limits for quality of supply are violated. Particularly, novel control schemes of:

i. Distributed Generators featuring Synchronous Machines and,

ii. Wind Energy Conversion Systems (WECS) based on Doubly Fed Induction Generators (DFIGs),

can mitigate the adverse effects of increased generation capacity on Distribution Network voltage quality.

1.8 Contribution to Knowledge and Deliverables

This study contributed to knowledge by creation of appropriate control algorithms to assist developers and network operators to increase penetration of distributed generation. Furthermore, this research generated a set of models for power systems simulation that focuses on control of distributed generation. This allowed evaluation of the impact that smart DG controllers introduce to the system, as well as the development of algorithms and methods for maximising power production and injection into a weak network. Finally, it established a set of rules that may be used to define when and which technology should be utilised, in order to achieve the most efficient generation and transport of power, taking into account the technical and economic issues in each case.

There are three main deliverables from this research:

- the establishment of combined generation, control and network models for detailed investigation of novel control algorithms for DGs connected to weak distribution networks;
- a set of novel control algorithms for Synchronous and Doubly Fed Induction Generators that will assist injection of power generated by DGs; and
- an assessment on the application of these algorithms on machines and devices connected to a (simulated) existing DN.

1.9 Thesis Outline

This chapter was the introduction of this thesis. Chapter 2 explains the issues related to increased penetration of Renewable and Embedded Generation in the Distribution Network. Then Chapter 3 describes modelling of distribution networks as well as generation plants based on synchronous machines such as Small-Hydroelectric Generators (SHGs). Chapter 4 presents the modelling of wind energy conversion systems and builds a full wind-to-wire dynamic model of a variable speed wind turbine including a doubly fed induction generator. Chapter 5 presents the developed control algorithms for Distributed Generators that improve steady-state voltages. Chapter 6 presents the performance of the developed algorithms through a case study that considers connection of various DGs in a part of the Scottish Distribution Network, and then it discusses the findings. Finally, Chapter 7 makes the conclusions of this work and summarises the thesis.

Chapter 2
Embedded and Renewable Generation in the Distribution Network

2.1 Introduction

This chapter provides a background on Electricity Distribution Networks and explains the problems related to increased penetration of Renewable and Embedded Generation in the MV grid and in particular in weak rural networks. The characteristics of a typical distribution system are shown and then the obstacles for the connection of Renewable and Embedded Generation to it are presented. The most important of these is the alteration of voltage profiles throughout the distribution network due to the addition of DG, and therefore this is further discussed. The power flow between two buses is derived and used as an example to depict the voltage rise problem. The effects of different conductor sizes and voltage levels on voltage rise are presented through a series of simulations and finally the structure of voltage control within a distribution system is presented.

2.2 UK Regulations on Voltage Variation in DNs

The Distribution Network Operators (DNOs) are obliged to provide electricity that complies with statutory levels for quality of supply. Voltage fluctuation is one of the monitored indices. Electricity Supply Regulations 1988 (Regulation 30) requires that the voltage variation at a consumers supply terminals at a voltage less than 132 kV should not exceed 6% above or below the declared nominal voltage. The 1994 amendment of Regulation 30 (passed in order to make it compliant with the

European Standard EN50160:1994), sets the permissible voltage variation at a low voltage consumers supply terminals between 10% above or 6% below nominal.

The Electricity Supply Regulations 1988 was replaced by the Electricity Safety, Quality and Continuity Regulations 2002. As defined in Regulation 27, the voltage limits for the distribution and transmission networks in the UK are:

- 10% above or 6% below the declared voltage at the declared frequency for voltage levels between 50V and 1kV,
- 6% above or below the declared voltage at the declared frequency for voltage levels below 132kV, and
- 10% above or below the declared voltage at the declared frequency for voltage levels above 132kV (transmission level).

Traditionally in the distribution networks these limits are preserved through use of transformers with fixed taps and by using on-line tap changers on transformers at some of the bulk supply points. However, with the introduction of distributed generation these measures may not be sufficient to maintain an acceptable voltage profile throughout the network. However it should be noted that DNOs may operate well within the ones defined above in order to enhance security and quality of supply.

2.3 Distribution Network Structure

Historically, Distribution Networks (DNs) were designed to convey electrical energy from the central power stations that were connected to the High-Voltage (HV) Transmission Network (TN), to consumers connected to medium (MV) and low (LV) voltage circuits [15]. The most common topology of DNs in rural areas is long radial feeders. Particularly in Scotland, the DN is characterised by long overhead line circuits at 132, 33 and 11kV. Depending on the area, there may be some interconnection at 132kV, but this can be sparse at 33kV and non-existent at 11kV. Overall impedance that has increased with circuit length is not reduced by parallel circuit combination

as it would be at transmission level. The reduced loads typically found in rural areas allowed the network to be extended radially from the bulk supply points. While the fixed geometry of the conductors of 33 and 11kV overhead lines bring about a nearly uniform reactance, increasingly tapered circuits see the resistance rise with reduced conductor cross-sectional area towards the edges of the network. The diagram of a typical radial network is shown in Figure 2.1.

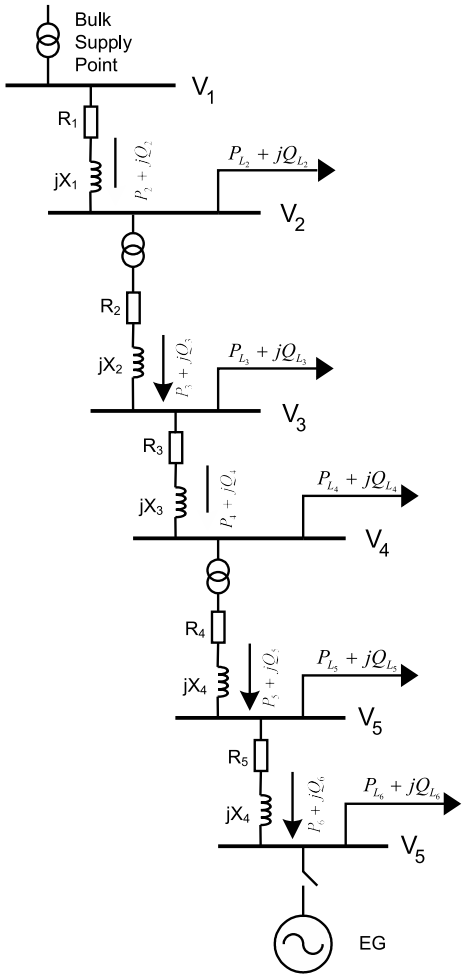

Figure 2.1: *A section of a common distribution network consisting of a tapered radial feeder with loads*

The distribution system was designed on the basis that power flows were unidirectional; real and reactive power were flowing from the Bulk Supply Point to the loads [16]. In addition, consumer load patterns (and therefore network power flows) were to a

great extent predictable, with periodic patterns lasting from days to seasons. Voltage profiles were established by a radially tapered conductor system, and off-load voltages (and on-load profiles) were set by initial adjustment of fixed off-load taps in the LV transformers at 11000:430V. It was operated in a passive fit-and-forget manner and was maintained on a planned routine basis. At the most remote ends of the 11kV network, voltage was passively controlled by means of transformers with fixed taps adjusted to set the on-load voltage within statutory limits. Transformers at the Bulk Supply Points (11:33kV or 33:132kV) were equipped with On-Line Tap Changers (OLTCs), which operated actively in response to voltage change with power flow [17]. Statutory voltage limits were set in order to maintain quality of supply (±6% for MV in the UK) and to ensure this, DNOs often planned and operated their networks in a ±3% voltage envelope [18].

2.3.1 Conductor Sizing and Spacing

Typically, population density and demand for electricity tends to reduce along the feeder and towards its rural edge. This fact allows the DNOs to reduce their development costs by reducing the capacity of the feeder as it approaches its remote end. This is usually done by reducing the cross-sectional area of the conductors. However, this means that the network resistance R_{km} per kilometer increases, as:

$$R_{km} = \rho \frac{l}{\pi r^2} \qquad \text{ohm/km} \tag{2.1}$$

where: ρ = resistivity,
l = conductor length (m),
and r = conductor radius (m).

In the simplest case of balanced currents and a three-phase line with its conductors symmetrically spaced in a triangular configuration as shown in Figure 2.2, the line inductance per phase per kilometer length is shown in by Equation 2.2 [19].

$$L_{km} = 0.2ln\frac{d}{re^{-\frac{1}{4}}} \qquad \text{mH/km} \tag{2.2}$$

where: d = conductor spacing (m).

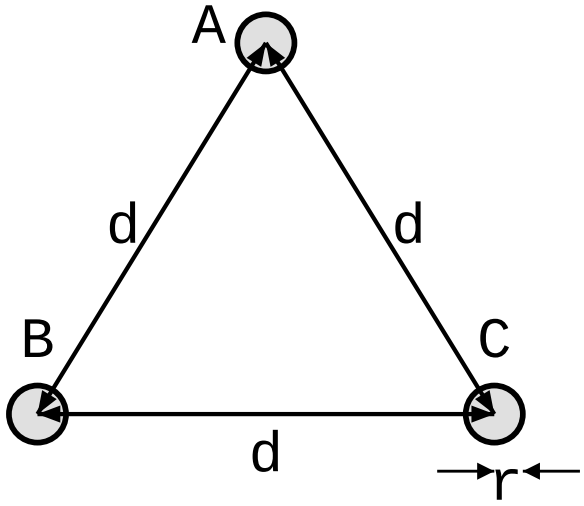

Figure 2.2: *Three-phase line with symmetrical spacing*

The most commonly used conductor setup in distribution systems is the in-line configuration depicted in Figure 2.3 (left). Being asymmetric, the line inductance in this setup differs from phase to phase. One way to regain symmetry in good measure is to use conductor transposition as shown in Figure 2.3 (right). However this technique is not very common in distribution levels.

It can be shown that in this case the inductance per phase per kilometre length for a solid round conductor is

$$L_{km} = 0.2ln\frac{GMD}{re^{-\frac{1}{4}}} \qquad \text{mH/km} \tag{2.3}$$

where GMD is the geometric mean distance and equals to

$$GMD = \sqrt[3]{D_{AB}D_{BC}D_{AC}} \tag{2.4}$$

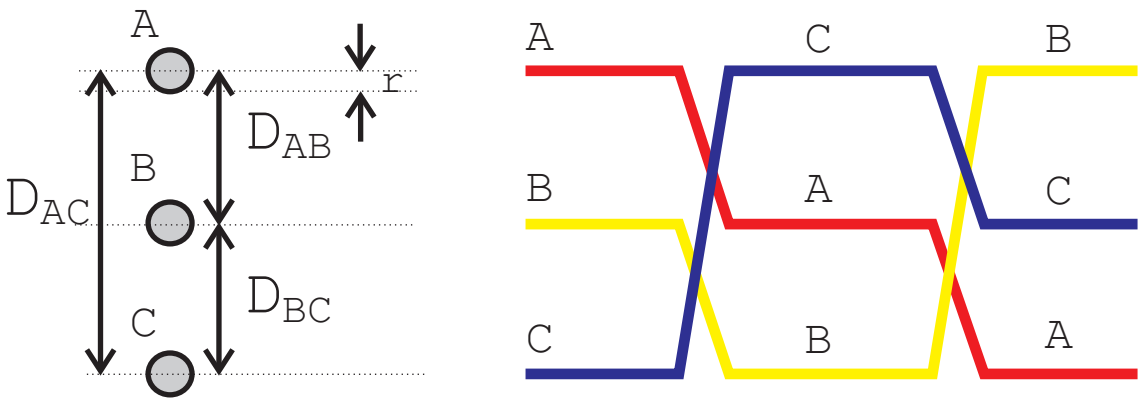

Figure 2.3: *In-line configuration of conductors of a three-phase line (left) and conductor transposition (right)*

In the case of a stranded conductor with n strands, Equation 2.3 is modified by replacing the term $re^{-\frac{1}{4}}$ with the Geometric Mean Radius (GMR):

$$GMR = \sqrt[n^2]{(D_{aa}D_{ab}\cdots D_{an})\cdots(D_{na}D_{nb}\cdots D_{nn})}, \tag{2.5}$$

where $D_{aa} = D_{bb} = \cdots = D_{nn}$ are the radii of each strand and D_{ij} for $i, j \in [1, n]$ and $i \neq j$ are the distances between the centres of the strands. Line reactance X_{km} per kilometre is:

$$X_{km} = L \times 2\pi f \qquad \text{ohm/km} \tag{2.6}$$

where f = network frequency (Hz)

In all cases equations 2.1 through 2.6 show that r is a significantly more important factor in R than in X. Line inductance is mainly geometry dependent. However, the geometry of the lines tends not to change much, hence X remains largely constant and therefore the $X : R$ ratio decreases rapidly with reduction of the conductor cross-sectional area. This has serious implications on the development of DG projects located close to the remote ends of the DN as the increased R will exaggerate the variation of voltage due to generated real power export. It should be noted here that for other conductor topologies, line reactance X differs from the value given by Equations 2.6 and 2.3 but the effect of r on it is of the same magnitude. A set of typical conductor sizes and their characteristics is shown in Table 2.1.

Conductor type	Resistance R Ω/km	Reactance X Ω/km (50Hz)	Thermal limit MVA	Investment costs £/km
ACSR 34/6	0.848	0.4	7.4	7,870
ACSR 54/9	0.536	0.4	9.9	9,200
AAC 132	0.219	0.4	17.5	11,470

Table 2.1: *Typical conductor sizes and their characteristics. Data taken from [1].*

The three conductors presented in Table 2.1 are named after their size and type. Hence, the first represents a conductor with $34mm^2$ of aluminum wire strands and a $6mm^2$ steel core reinforcement, the second with $54mm^2$ of aluminum wire strands and a $9mm^2$ steel core, and the third with $132mm^2$ of aluminum wire strands and no core. It is shown that although the reactance remains practically constant, the resistance varies widely with changing cross-sectional area, with high values for small areas and vice-versa. The thermal limit of the line is increasing with the cross-sectional area (which means that more power can be shipped through the line) and finally the investment cost also rises for heavier conductors as expected.

2.3.2 Selection of Distribution Network Operating Voltage

The capital cost of a distribution system can also be lowered by using lower voltage levels in low demand areas. This is done by installing step-down transformers. Table 2.2 shows the relative capital cost per kilometre, the maximum possible feeder length due to overvoltage constraints and the power losses per km for four nominal DN voltages (under the same loading conditions). It should be noted that the 6.6 and 20kV levels are not used in the UK, but are shown for comparison.

For all three parameters the $11kV$ voltage level is taken as reference. It is seen that the capital cost for a $33kV$ overhead line can be over 30% higher than for an $11kV$ for the same feeder length. However, the table shows that a $33kV$ operating voltage will allow the feeder length to be increased 9 times before voltage violations become a problem as the reduced resistance will cause less voltage rise/drop. Additionally, the power losses for the same distance will be reduced to one tenth [1]. Switchgear,

Voltage kV	Capital Cost/km %	Feeder Length %	Power Losses/km %
6.6	93	41	278
11	100	100	100
20	112	331	30
33	131	900	11

Table 2.2: *Relative characteristics of overhead lines in the distribution network. From [1].*

protection and transformer costs will also rise with operating voltage, but on the other hand the number of substations will be reduced due to the reduced voltage rise/drop. Hence, the decision of the operating voltage can only be made on an individual basis, also considering the long-term development projection of the covered area.

2.4 Power Flows and Voltages in a Two-Bus System

The simplest case of a power system consists of two buses connected by a single line. One of the buses is considered as the infinite bus, *i.e.* a bus that is assumed to have fixed voltage magnitude and angle, while the second bus hosts a load. Such a system is depicted in Figure 2.4.

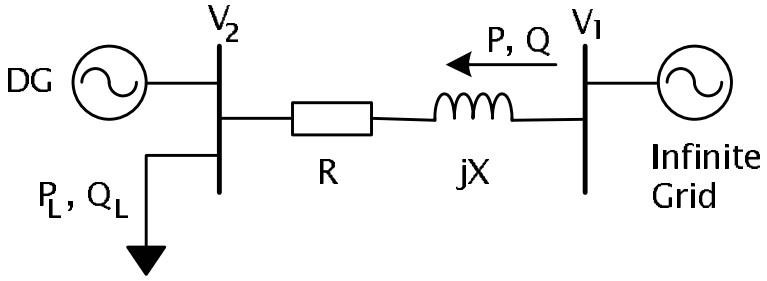

Figure 2.4: *A simple two-bus system*

In this system a distributed generator is connected to the load bus and therefore the real and reactive power P_B and Q_B that the load bus exchanges with the network is the difference between the P_G and Q_G of the generator and the P_L and Q_L of the load.

The complex power exchanged between the infinite bus and the rest of the system S depends on the bus voltage and the line current and is defined by:

$$\bar{S} = P + jQ = \bar{V_1} \times \bar{I}^* \tag{2.7}$$

By solving Equation 2.7 for $\bar{I}$ we get:

$$\bar{I} = \frac{P - jQ}{\bar{V_1}^*} \tag{2.8}$$

Application of Kirchoff's voltage law on the two-bus system gives:

$$\bar{V_2} = \bar{V_1} - (R + jX) \times \bar{I}, \tag{2.9}$$

where R and X are the line's resistance and reactance respectively. Using the above expression for the current and by combining it with Kirchoff's voltage law it is possible to derive the voltage on the load bus:

$$\bar{V_2} = \bar{V_1} - (R + jX)\frac{P - jQ}{\bar{V_1}^*} \tag{2.10}$$

Equation 2.10 calculates the voltage on the load bus for a given state of infinite bus power and voltage. This equation can be further simplified by choosing the infinite bus voltage as phase reference, (therefore $\bar{V_1} = \bar{V_1}^* = V_1 \angle 0^o = V_1$), allowing Equation 2.10 to be rewritten as:

$$\bar{V_2} = V_1 - \frac{RP + XQ}{V_1} - j\frac{XP - RQ}{V_1} \tag{2.11}$$

It can be shown that if the values of P_L, Q_L, P_G, Q_G and V_2 were given instead, the same process would give:

$$\bar{V_1} = V_2 - \frac{RP_B + XQ_B}{V_2} - j\frac{XP_B - RQ_B}{V_2}, \tag{2.12}$$

where $P_B = P_L - P_G$ and $Q_B = Q_L - Q_G$.

In real life however, it is the voltage on the infinite bus and the power demands on the load bus that are given. Therefore it is not possible to solve Equation 2.12 algebraically,

as there is a nonlinear relationship between V_2 and powers P_B and Q_B. It should be noted here that the power that the load bus exchanges with the line does not equal the power the latter exchanges with the infinite bus, as there are the real and reactive power losses on the line due to the resistance and reactance respectively. Equation 2.12 is the simplest case of a *load flow* problem that is typically solved using classic iterative algorithms such as Newton-Raphson, Gauss-Seidel and their variations.

The voltage rise $D\bar{V}$ on the line can be calculated from Equation 2.12:

$$D\bar{V} = V_2 - \bar{V_1} = \frac{RP_B + XQ_B}{V_2} + j\frac{XP_B - RQ_B}{V_2} \tag{2.13}$$

Equation 2.13 describes the voltage vector diagram of the system that is shown in Figure 2.5.

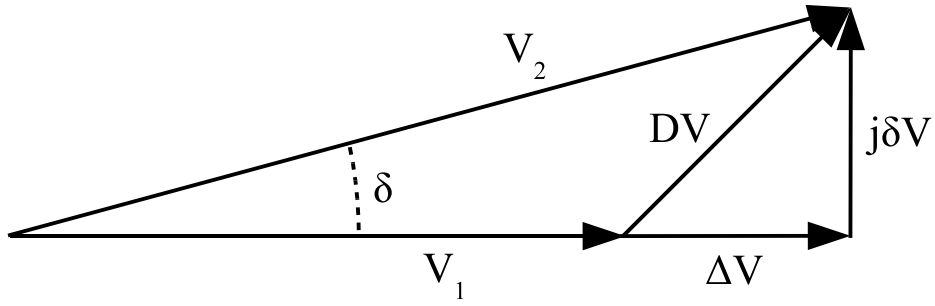

Figure 2.5: *Vector diagram of the two-bus system*

According to (2.13), the real and imaginary parts of the voltage rise in this figure ΔV and $j\delta V$ respectively are given by:

$$\Delta V = \frac{RP_B + XQ_B}{V_2}, \tag{2.14}$$

and

$$\delta V = \frac{XP_B - RQ_B}{V_2}. \tag{2.15}$$

The imaginary component of the voltage rise $j\delta V$ in this diagram has been exaggerated

as it is normally very small relative to the real part ΔV. This is because in distribution networks R is high (and comparable to X). For the same reason Equation 2.13 is often simplified to:

$$DV = \Delta V = \frac{RP_B + XQ_B}{V_2} \tag{2.16}$$

In weak distribution systems, the high X/R ratios typical in the transmission network are replaced with X/R ratios dominated by resistance. Therefore the DNs are more vulnerable to RP/V than to XQ/V terms in the voltage rise, and this has commercial implications as the voltage limits are easily reached with small increases of the generator's output.

2.4.1 Illustration of the Effects of Conductor Sizing

The voltage response on the load bus of the two-bus system of Figure 2.4 to increasing load is shown in Figure 2.6. In this example the line has been modelled as a $1km$ long feeder consisting of the three alternative conductor types presented in Table 2.1. The load is increased from zero to $10MVA$ at 0.9 power factor and there is no generation.

The effect of different conductor sizing is apparent in this graph. This example shows that selection of the smaller conductor type (ACSR 34/6) would clearly lead to undervoltages well below the -6% statutory limit, while the next size (ACSR 54/9) would just reside within the limit. It should be noted that in reality none of these two types would be selected as both of them have lower power transfer capacity, with a thermal limit of $7.4MVA$ and $9.9MVA$ respectively. Use of conductor type AAC 132 would give acceptable voltage results and would also be able to cope with the higher power transfer.

Figure 2.7 shows the effects on local voltage of adding a distributed generator on the load bus of the same two-bus system. In this example the local load was held constant at $10MVA$, 0.9 power factor and the generation increased from zero to $25MVA$ ($PF = 0.9$).

While generation was below the local demand, voltage remained below $1.0pu$. With

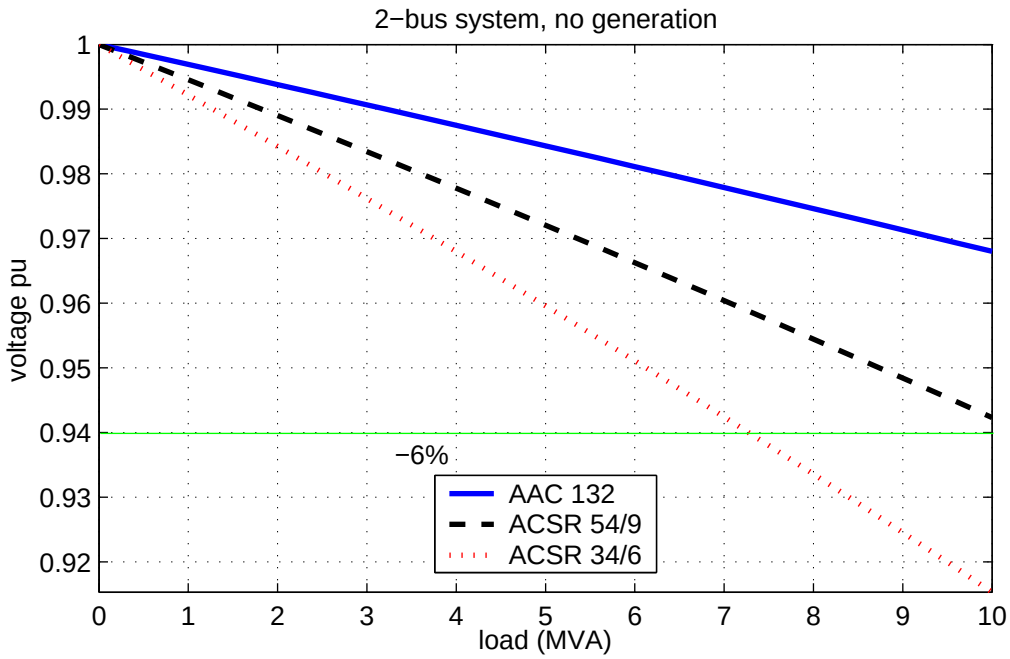

Figure 2.6: *Voltage drop due to load increase on the two-bus system*

the reversal of power transfer ($S_G > S_L$) voltage crossed unity for all three conductor types. However, an important observation is that the weaker the line is (i.e higher resistance - lower X/R ratio), the wider the fluctuation becomes. This results in a lower power output from the generator before the statutory limit is violated. With the ACSR 34/6 type the +6% limit was reached at $18MVA$ (28% below rated DG output), while ACSR 54/9 allowed generation of ($22MVA$ 13% below rated DG output). Type AAC 132 resulted in a voltage well below $1.06pu$ even for $25MVA$ generation. The financial implications of this difference are significant. With the current UK wholesale price of approximately 2 pence/kWh for DG, the 28% reduction of output in the case of ACSR 34/6 would incur a reduction in revenue of £3,360 per day for the 25MW generator. Respectively, the loss in the case of ACSR 54/9 would be £1,440/day.

The effects of distributed generation on power losses on the network are depicted in Figure 2.8. As expected, it can be seen that for generation up to the level of local demand the power losses on the line are reduced, to become zero when generation matches the load on the bus.

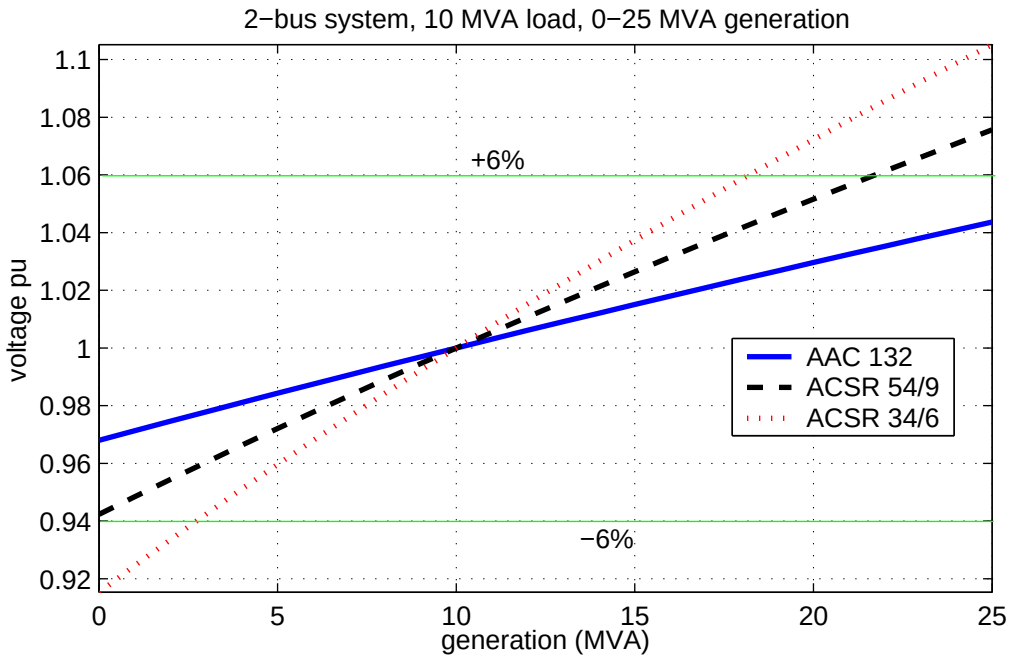

Figure 2.7: *Voltage effect of increasing generation on the two-bus system*

It should be noted here that this graph shows the power loss (P_{loss}) for the simple case that generation power factor is equal to load's PF (*i.e.* $P_G = P_L$ and $Q_G = Q_L$). In most cases $PF_G \neq PF_L$ and therefore the losses on the line cannot be zeroed.

Once again it is apparent that the effects of weak lines are more significant. Nevertheless, in all cases connection of a generator in the distribution network will improve system operation as the losses will generally be reduced, unless the generator output is higher than the local demand. Power losses are closely related to thermal loading, as the lost power on the line is dissipated as heat, and each conductor type has a limit on the power that can be dissipated without overheating. Consequently, line losses (together with transformer ratings) determine the maximum power transmission capacity of the feeder.

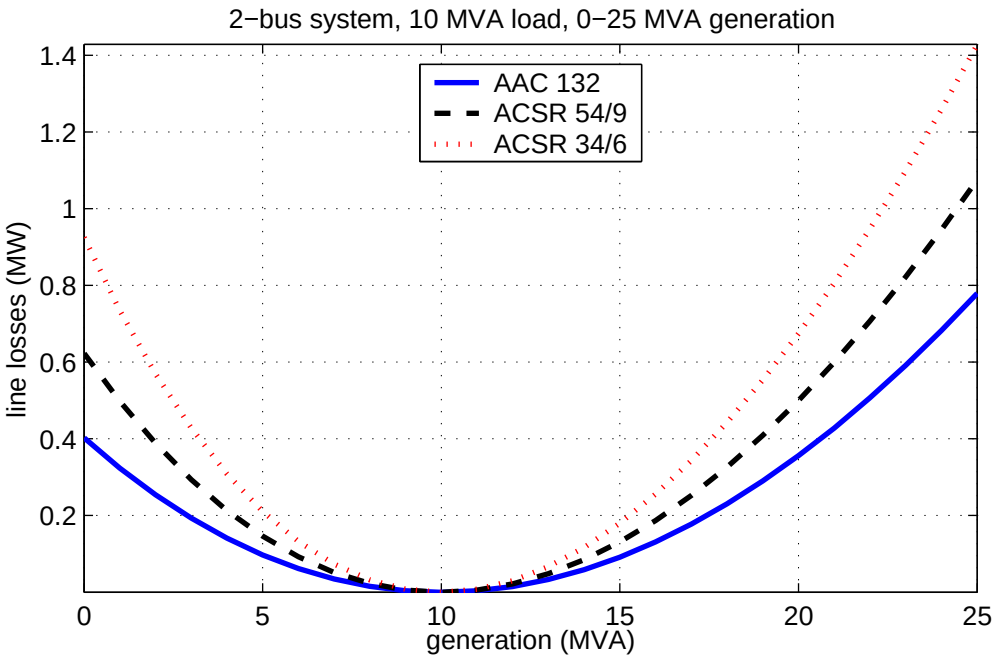

Figure 2.8: *Power losses on the line for the two-bus system*

2.4.2 Illustration of the Effects of Voltage Level

The operating voltage level of a distribution network has a significant effect on the power flows and the voltage variation. Equation 2.7 indicates that for the same power exchange from/to a bus, a higher bus voltage would result in proportionally lower line current. Since the voltage drop on the line is proportional to current (Equation 2.9), a high operating voltage is desired in order to reduce current and voltage fluctuations with varying power flows. This is depicted in Figure 2.9.

The excursion is significantly wider (and unacceptable as it crosses the ±6% margins) for the $11kV$ system. It is shown that in the modelled system the highest power output that could be safely accommodated using an 11kV line would be 20MVA. In monetary terms this would mean a £2,400 reduction of revenue per day for the 25MW generator, assuming it can otherwise generate at capacity for 24 hours a day. Deviation decreases with operating voltage and the smallest is experienced for the $33kV$ system. The reduction of line current with increasing system voltage will also lead to lower losses as $P_{loss} = \Re(\bar{I} \times Z_{line})$. This is illustrated in Figure 2.10.

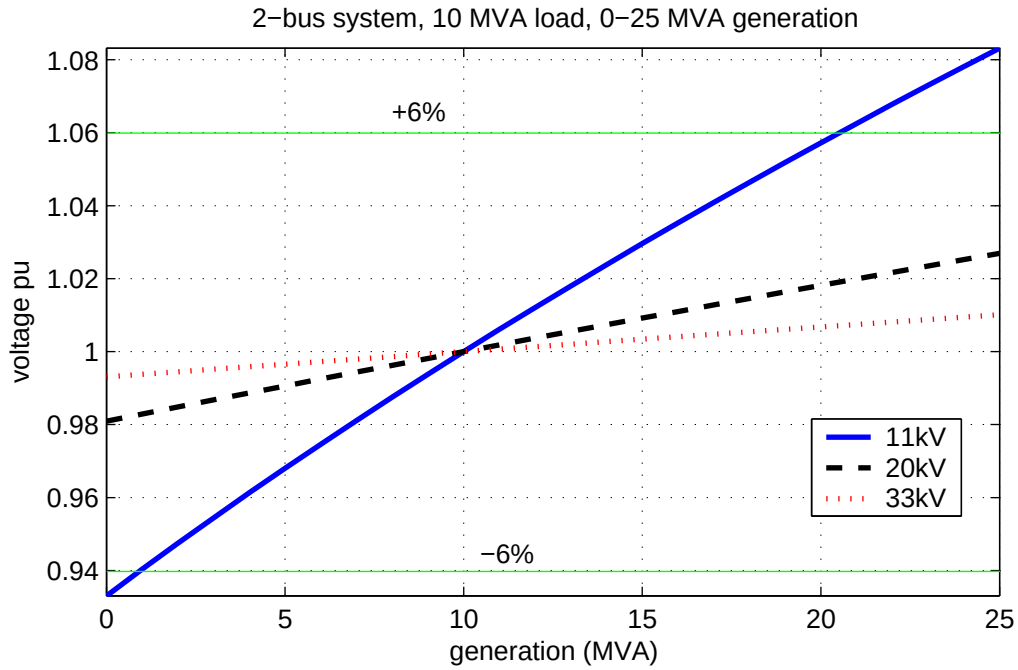

Figure 2.9: *Voltage variation at the load bus of the two-bus system for type ACSR54/9 conductor and for three operating voltage levels*

2.5 Voltage Variation in the Distribution Network

Typically, distribution systems consist of long, radially tapered feeders such as the one shown in Figure 2.1. Assuming that the transformers operate at a fixed tap, in such a system the bus voltages in per unit are derived from the equation:

$$\overline{V_{n+1}} = \overline{V_1} - \sum_{k=1}^{n} \frac{(R_k + jX_k)(P_{k+1} - jQ_{k+1})}{\overline{V_{k+1}^*}} \quad \text{pu} \tag{2.17}$$

As Equation 2.17 shows, the distributed loads (as well as the loading of each branch) affect the voltage profile across the feeder. A common way for network operators to tackle the voltage drop problem is to raise the voltage at the Bulk Supply Point (BSP) and therefore throughout the whole feeder. Table 2.3 shows the electrical data of an example network with the same topology as the one in Figure 2.1. The voltage profile across that network is presented in in Figure 2.11.

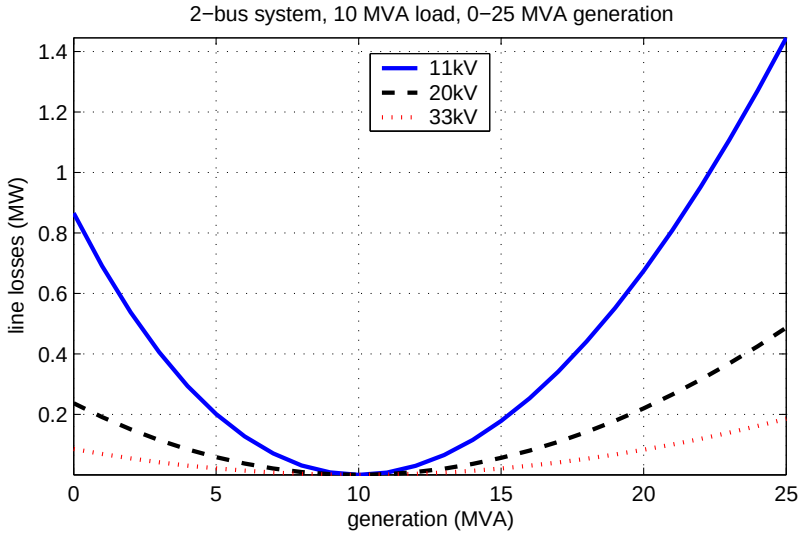

Figure 2.10: *Power losses on the line for three operating voltage levels*

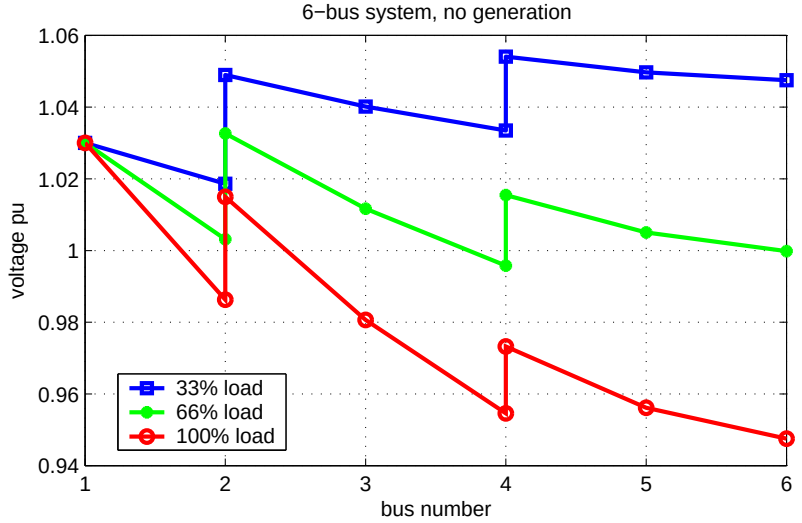

Figure 2.11: *Voltage profile of the six-bus system of Figure 2.1 with no embedded generation*

The voltage at the BSP was selected to be 3% above the nominal voltage of $11kV$ to compensate for the voltage drop along the long line. Two transformers were installed to serve the same purpose at positions further down the feeder. As shown in Figure 2.11 the voltage variation for three different load levels (100%, 66% and 33% of the maximum)

System voltage	$11kV$
Conductor type	ACSR 54/9
R_{km}	$0.536\Omega/km$
X_{km}	$0.4\Omega/km$
Branch length	$1km$
T_1 ratio	$+3\%$
X_{T1}	0.0363Ω
T_2 ratio	$+2\%$
X_{T2}	0.0363Ω
Loads	$1.5MVA$ each
Embedded Generator	$2MVA$

Table 2.3: *Electrical data of the network of Figure 2.1*

is just within the statutory limits. Addition of an embedded generator at the farthest bus of the feeder would raise the voltage of all the buses above the +6% limit for the low load case as shown in Figure 2.12.

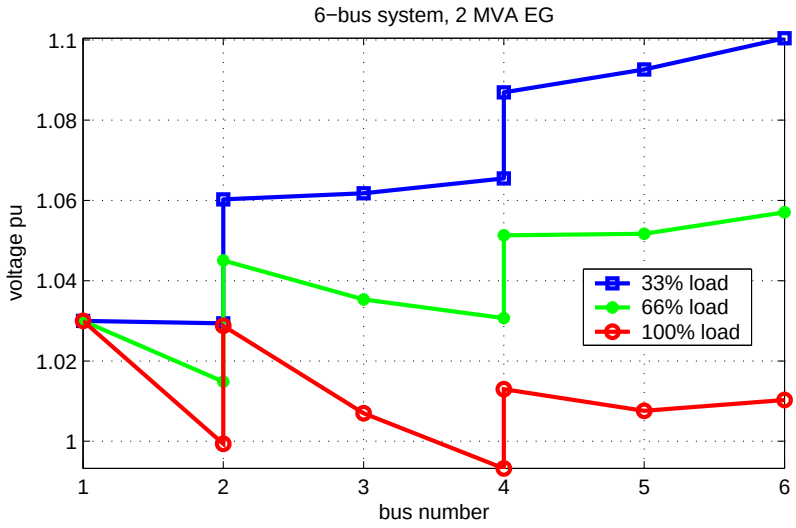

Figure 2.12: *Voltage profile of the six-bus system of Figure 2.1 with 2 MVA of embedded generation on bus 6*

The problem could be resolved by readjusting the tap positions on the transformers to 1.0 or less as shown in Figure 2.13. However, since an embedded or renewable generator is inherently intermittent, the risk of undervoltages in case of an output reduction (or

even complete disconnection) would be greatly increased.

It should be noted here that for the purpose of these simulations, the BSP was represented by the slack bus. In a real network, BSP is the point of connection of the local distribution system to the transmission grid. However, in the Scottish network, the BSP is often considered to be at 33kV, or (in some remote, low demand areas) even at 11kV.

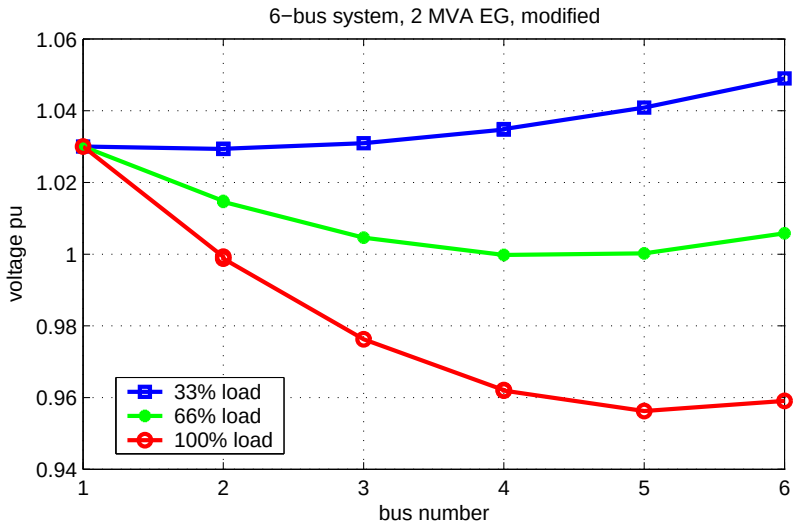

Figure 2.13: *Voltage profile of the six-bus system of Figure 2.1 modified to accommodate 2 MVA of embedded generation on bus 6 (transformer 1:1)*

2.6 Voltage Control in the Distribution Network

Control of voltage in a power system is generally performed according to a three-level hierarchical structure. The reasons of using such a mode of control are the size, structure and complexity of the system, as well as the difficulty of collecting and managing the amount of information needed to control such a system from a central location. A system of the size of a distribution network may contain areas with conflicting objectives and in need of different methods of control. A hierarchical scheme can be divided into sections, each with its own control strategy, performed by a dedicated controller. This way the computational burden is also reduced.

The three levels of control of a power system are primary, secondary and tertiary. *Primary control* involves the second by second (instantaneous) control of a generating plant using its governor, Automatic Voltage Regulator (AVR), Power System Stabiliser (PSS) etc. to regulate voltage and power output in a safe and acceptable manner during steady-state and transient operation of the system. *Secondary control* ensures that the steady-state voltage profiles in the controlled area are within the statutory limits of quality of supply. Secondary control is performed by inductors, capacitors and more rarely synchronous and Static VAr Compensators (SVCs) installed throughout the network. All these devices regulate voltage by adjusting the amount of reactive power exchanged with the power system. OLTC transformers are also utilised for (direct) secondary voltage control. Finally *tertiary control* ensures an optimal voltage profile of the system and coordination of the tertiary control mechanisms according to safety and economic criteria. Tertiary control is generally performed centrally on large transmission networks in a time frame of tens of minutes, by sending commands to the generators to adjust their operating point according to system's estimated requirements.

In this work it is proved that the distributed generators themselves can be used for tertiary voltage control.

2.7 Further Effects of Increased Generating Capacity within the Distribution Network

It is well understood that voltage rise is the number one issue concerning the increasing generating capacity within distribution networks. However, there is a series of other significant obstacles that are associated with distributed generation.

As already discussed, distribution networks were designed for unidirectional power flow from the heavily reinforced transmission system to the consumer, via radial-feed overhead lines. Connection of generators at the former receiving-ends will under certain circumstances cause severe situations such as undesirable function of automatic control voltage equipment, increment of fault levels, effects on system protection and reduction

of system stability [16, 20, 21].

Connection of a DG to a distribution network will increase the fault levels everywhere, but most in the neighbourhood of the connection point. If the fault levels before the connection of the DG are already close to the design limits, the fault contribution of the DG may increase them to unacceptable levels. Towards the remote ends of the distribution network, the fault levels are lower and the problem becomes more apparent [2, 22].

Distributed generation schemes based on synchronous generators can both export and absorb reactive power and can therefore cause a steady state voltage rise or fall. Consequently they will generally improve voltage and frequency stability. Induction generators will contribute real power to system thus increasing capacity and hence frequency stability. In case of induction generators, a three-phase fault would inhibit supply of reactive power to the generator, hence its excitation will be discontinued and therefore its contribution to fault currents will be constrained only in the subtransient period [23–25].

A great concern should be dedicated to the islanding issue. In case that the grid supply is interrupted for any reason, any EG connected to the "islanded" part of the network is required to be disconnected for safety reasons. The network voltage must be absolutely equal with that of the EG in terms of amplitude, frequency and phase upon reconnection, otherwise this would lead to asynchronous connection and possibly the destruction of the EG. It should be noted that an induction generator cannot maintain voltage amplitude and frequency. DGs should be reconnected only after synchronisation with the network voltage. Islanding may also cause security issues for the consumers and the repair personnel, or leave the DG without earth. Engineering Recommendation G.59/1 describes the way that an DG should behave in the event of loss-of-mains [2, 23, 26].

Flicker is an engineering expression for short-lived voltage variations in the electrical grid, which may cause connected light bulbs to flicker. A wind turbine connected to a weak grid may cause voltage flicker, as momentary wind variations will cause

fluctuations in power output. When the blades of the turbine pass in front of the tower, the reduction of the torque due to the wind shadowing causes a reduction of real power export and voltage variation with a frequency around 10Hz. Flicker effect is reduced when many wind turbines work in parallel. Moreover, the time-varying output of photovoltaic systems can cause flicker [23].

DGs that incorporate line commutated power electronic converters will introduce harmonics to the system that (depending on converter size and technology) may be outside the statutory limits set out by Engineering recommendation G.77. However, modern inverter-based DGs, such as photovoltaic systems and variable-speed wind turbines use power electronic converters based on Insulated Gate Bipolar Transistors (IGBTs) operating at frequencies that are well outside the bandwidth of the network (typically 10kHZ) and thus are filtered out. Harmonics are considered as "voltage pollution" and are the reason for problems like machine and transformer overheating as well as the malfunction of line-commutated rectifiers. Excessive levels of harmonic distortion may require operation of the network at reduced ratings. Engineering recommendation G.77 has been issued by the Electricity Association in order to set the limitations regarding harmonics in the transmission/distribution network. Although large inverter-based plants do not exist at the moment, advances of converter design and power electronic devices may increase their utilisation [23, 27].

2.8 Summary

Distributed renewable generation cannot be dispatched. It can be constrained 'off' (or be asked to reduce its output) by agreement with the DNO by using protection mechanisms that restrict network impacts such as overvoltage at times of low local demand. However, it cannot be constrained 'on', or be asked to increase its output, as it is always depended on the primary energy source. Where the energy source is time varying, power flows and voltage profiles in the network take on a time variation, which if unchecked can lead to violations in supply quality of the voltage. This can be of a high incidence and a highly varying nature where the energy source is extremely

variable such as in the case of wind. Longer term, more steady reversals in power flow can occur with biomass or Combined Heat & Power (CHP) plants that are crop- or heat-led.

The loss of possible generation in a distribution network due to its weakness can be quite significant. To accommodate the power flow characteristics of distributed generation in a weak rural system, where the renewable energy resources are mainly located, within acceptable limits on supply quality either will require the extensive and deep reinforcement of the network to mitigate voltage variation, or a very high level of active management. The investment in new plant could be drastically increased, and operating costs would rise by an order of magnitude. A better understanding of the nature, operation and control of distributed generation is therefore necessary if the set targets of DG penetrations are to be met. The next step would be to devise modes of operation and control strategies for the DGs such that they can contribute to tertiary control. The following chapters discuss the modelling and control of such generators and provide the basis for the proposed control algorithms.

Chapter 3
Modelling of Hydro Generation within the Distribution Network

3.1 Introduction

During the conversion of energy from its original state (e.g. wind, hydro, chemical) to electricity a number of distinct processes are taking place. In order to build a system model that is both functional and intuitive, the process has to be broken down to several subsystems according to their function, and each of them has to be modelled individually. This chapter discusses the dynamic model of a Small-Hydro Generation Plant that can be used for voltage variation studies. Further, it presents a Distribution Network model based on power flow analysis and its interfacing with the SHG model. A model for an On-line Tap Changing transformer is then presented and the chapter closes with a set of simulation results that illustrate the combined operation of the developed models.

3.2 Modelling of Distributed Generation

It is possible to build a system model where its top level block diagram is common for many different types of energy sources and conversion schemes. Use of a standardised top level model allows direct comparisons of the operation and performance of such systems, as well as easy transfer and evaluation of applicable control techniques between them [28]. Such a top level diagram for dispersed generation schemes is depicted in Figure 3.1.

In large scale, conventional power stations the energy source is completely controllable and can be considered constant (e.g. coal, large hydro, nuclear). Therefore, their

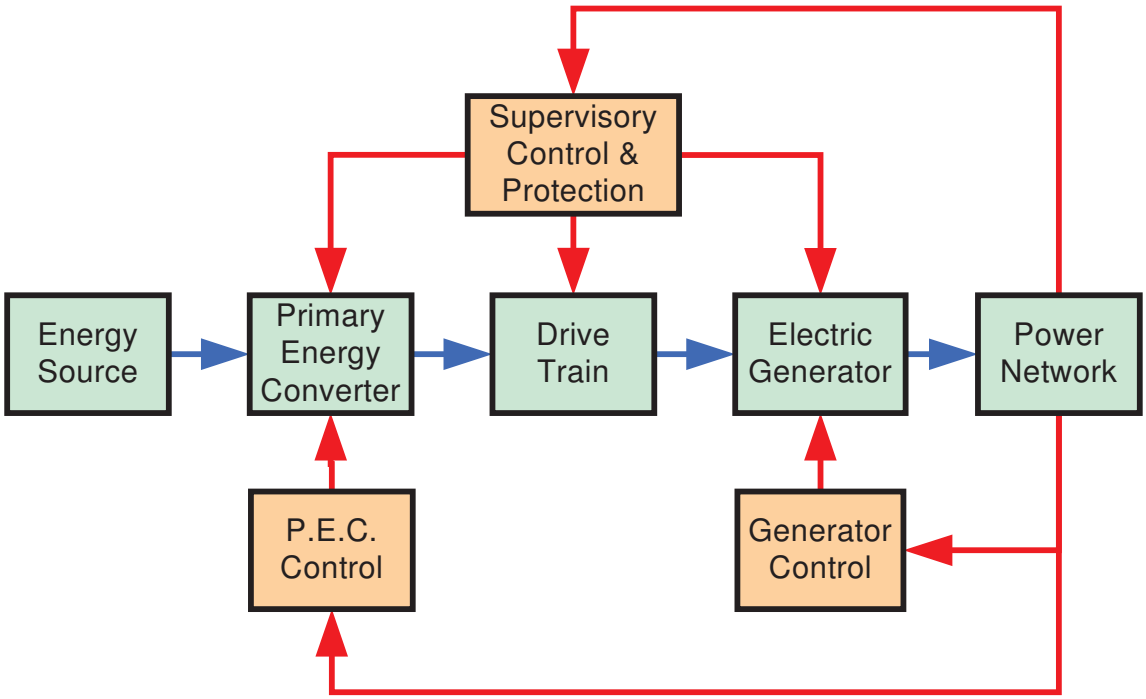

Figure 3.1: *Source-to-electricity block diagram of a power conversion scheme. Blue arrows represent energy flow and red arrows represent control signals.*

modelling can be omitted if the simulation focuses on the electrical aspects of the system. This is not the case with dispersed generation, where in most cases the primary energy resource is variable due to natural (wind, water flow, sunlight, sea state), or technical (varying demand on combined heat & power) reasons. Natural resources cannot be controlled and, additionally, in most cases are hard to predict, and the output of CHP plants is often governed by the heat load.

The prime mover translates the energy from its original form to rotational speed (torque) in order to drive the generator. This rotational speed can be variable, and well out of the operational range of the generator. Large wind turbines rotate at a speed of about 25 rev/min maximum and a gas or steam turbine can operate at up to several thousand rev/min. This speed has to be matched to the optimum value for the generator, which depending on its pole pairs number can be 3000 rev/min or less for a 50 Hz power network. This job is done by the drive train, which can be a constant ratio gearbox.

The electric generator in dispersed generation schemes is typically a Synchronous, Squirrel Cage Induction,or Doubly-Fed Induction Generator. The generator controller regulates one or more of the real and reactive power, the speed and the voltage. The primary energy converter is also used to regulate the mechanical power and/or the rotational speed of the generator. The supervisory control performs high-level control on the system in order to optimise the performance of the system as a whole and the protection systems are there to disconnect and lock the generator in case of emergency. Finally, the power network model includes all the components of the distribution system and can have varying levels of detail, depending on the type of simulation.

A model of a generator (and in general any component of the power system) can be categorised according to the time frame it is operating in. In that respect, there are three categories of models, namely steady-state, transient (dynamic) and sub-transient. Table 3.1 shows the possible applications for each type of DG model [29].

Model Type	Type of study
Steady-state (static)	Load and power flows
	Voltage variation
	Energy capture assessments
	Short-circuit studies
	Supervisory control design
Transient (dynamic)	Transient stability
	Small-signal stability
	Transient Response
	Low-level control
	Optimisation
Sub-transient	Start-up transients studies
	Load transients studies
	Fault operation
	Harmonics and sub-harmonics studies
	Control of power electronics
	Detailed optimisation

Table 3.1: *Possible applications of dispersed generator models in the three time frames*

Selection of the correct model for each type of study has a very high importance. Selecting a model of higher order than needed will increase simulation times without

offering more information, and a lower order model will generate suboptimal and/or erratic results [30, 31]. The static model of a dispersed generator is used in all steady and quasi-steady state analyses such as load and power flows (power delivery and voltage variation studies) as well as assessments of energy capture and calculation of fault levels. The static model is very basic and consists of a pure voltage source, a voltage and real power source, or a real and imaginary power source, depending on the type and mode of operation of the generator [32]. In each case the respective parameter(s) is (are) constant or adjusted according to the control strategy of the generator.

The transient model of a dispersed generator is one step more detailed and is used for studies that involve system dynamics such as small-signal stability and dynamic response to faults, as well as optimisation of controllers.

Finally the sub-transient model is of higher order and is needed for non-fundamental frequency analysis, short-lived transient effects such as the ones that occur during faults, generator start-up, power electronics simulation and control, and low-level controller design and optimisation. Study of such phenomena is not an object of this work and therefore sub-transient models will not be discussed.

3.3 Small Scale Hydro Power Generation

Small-scale Hydro Generators (SHGs) convert the kinetic energy of flowing water to electricity. Obviously, SHGs can only be built at places where adequate water flow is available, but if the resource exists they can generate clean and reliable energy as the technology is more mature compared to other RES such as solar and wind. On the other side, land costs and infrastructure usually raise the initial expenditure [11]. Additionally, an SHG plant can have minimal environmental impact if carefully designed. It can provide an alternative source of energy to remote loads, and due to its simple construction can be a viable option for rural electrification in many developing countries [33]. There is not a clear threshold between 'small' and 'large' Hydro Generation, but for this work anything less than 10 MW will be classified as 'small'. Mini- (mHG) and micro- (μHG) Hydro Generation installations are defined

by unit capacities of above and below 100 kW respectively and are usually connected to the LV network. The total UK capacity of technically and financially feasible sites was estimated to be approximately 240 MW [34]. At the end of 2002, a total capacity of 194 MW was installed [14]. Figure 3.2 illustrates the basic diagram of an SHG installation.

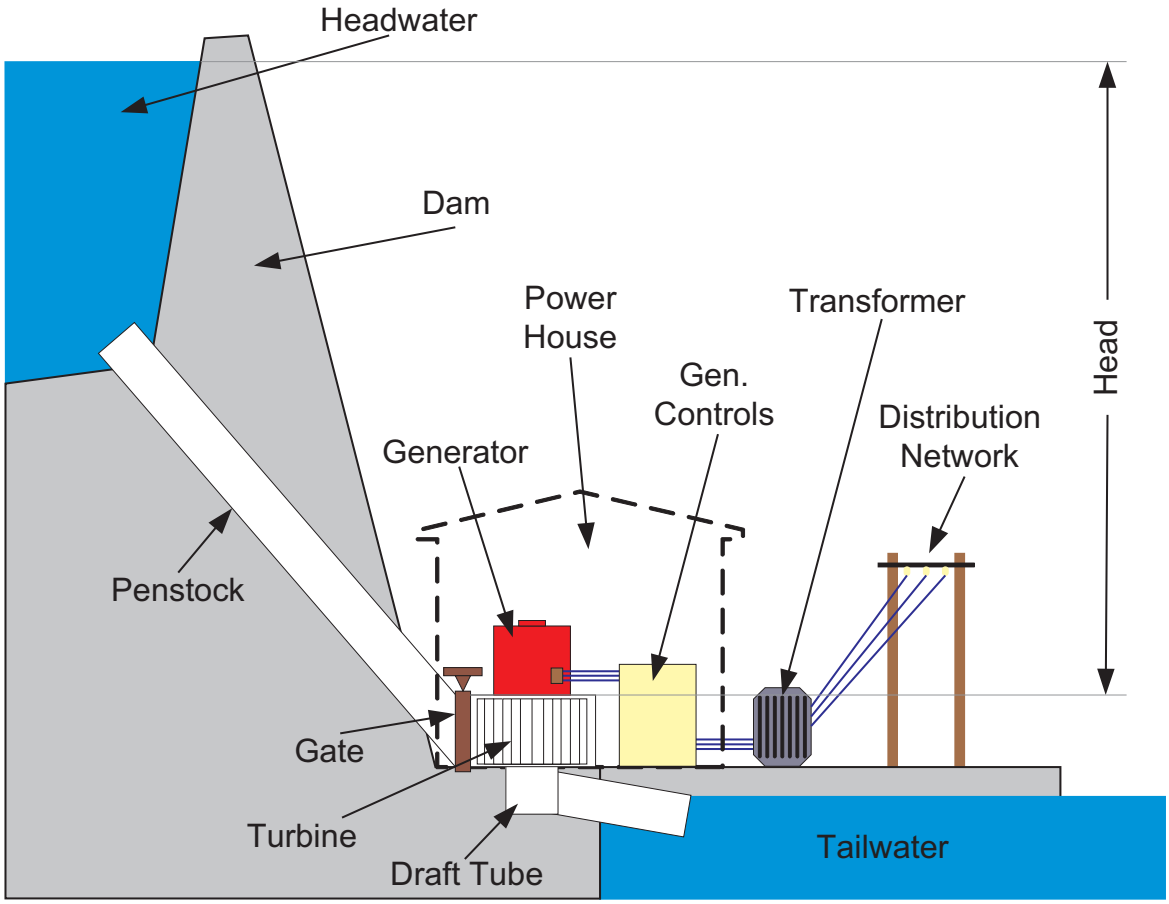

Figure 3.2: *Diagram of a Small Hydro Generator Installation.*

3.3.1 Hydro Turbine Selection and Modelling

As water flows downstream in a river (or within a penstock), its potential energy is transformed to kinetic energy. The transitional kinetic energy of the water is then transferred as rotational kinetic energy to the hydraulic turbine, and the water exits with a lower energy content. In a Francis (reaction) turbine water enters the turbine

tangentially through guide vanes (or gates) and exits axially. The guide vanes regulate water flow (and therefore output power) by increasing or decreasing the cross-sectional area of the gate.

The shaft output power is given by Equation 3.1 [35].

$$P = \rho \times g \times H \times Q \times \eta \qquad Watts \tag{3.1}$$

where: ρ is the density of water ($1000kg/m^3$);
g is the acceleration due to gravity ($9.81m/s^2$);
H is the hydraulic head in metres;
Q is the volume flow rate (m^3/s); and
η is the turbine efficiency.

From the equation above, the two variables that affect output power are the hydraulic head H and the volume flow rate Q. There are a number of different turbine types and their efficiency (and therefore their appropriateness for a particular site) is defined by the available operating head. Because energy density in the water varies with head, for lower heads a larger volume of flow is needed. Therefore it is clear that the hydraulic head defines the turbine type, physical size and mechanical power output. The water flow, and hence the torque of the generator is controlled by the governor. The most common turbine types are the Pelton wheel (impulse category), the turgo-impulse and the crossflow type (part impulse, part reaction), the Francis and the Kaplan types (reaction category) and finally the tubular and the bulb types [34]. Table 3.2 shows the head range of each turbine type.

3.3.2 Electric Generators for SHGs

The most common generator type in SHGs is the synchronous machine. Only in very small installations (mHGs and μHGs) are induction generators (IGs) utilised, and only when the generator is connected to the grid, which provides steady voltage and frequency, as when stand-alone, the induction generator's voltage and frequency vary

Turbine Type	**Head Range** (m)
Pelton	100 - 1400
Turgo	10 - 300
Crossflow	60 - 300
Francis	50 - 400
Kaplan	10 - 50
Tubular	4 - 20
Bulb	2 - 30

Table 3.2: *Types of hydro turbines and their head ranges*

with load and mechanical power input. Otherwise induction machines are an attractive option due to their robustness and cost-effectiveness. Another disadvantage of IGs is their inability to control power factor as the relationship between their real and reactive power output cannot be regulated. Although not widely used at the moment, recent developments on doubly fed induction generators (DFIGs) are expected to assist the utilisation of them in small hydro schemes.

When a synchronous generator is used standalone, the generated voltage is held constant by an Automatic Voltage Regulator (AVR), which directly or indirectly controls the magnetising (excitation) current for the rotor field. The operational frequency is determined by the rotational speed and the number of pole pairs. When connected to a network, a synchronous generator can independently regulate its real and reactive power by adjustment of its mechanical power input and excitation respectively.

3.3.3 Turbine - Generator Control

There are three types of excitation systems and two types of governors. The Synchronous Generator in SHG installations can be shunt or separately excited, and there are also some (small) SGs that have a permament magnet mounted on the shaft which provides the required EMF to the stator. Shunt excited generators do not need external supply for their excitation and therefore are ideal for off-grid plants. However, the excitation voltage is dependent on the stator voltage and therefore a sudden change of the load will induce a transient to the excitation, which may destabilise

the machine. Separately excited SGs can overcome this problem, but at the cost of requiring an external power supply.

A top-level block diagram of the developed model is shown in Figure 3.3. In the following sections its constituent blocks will be discussed.

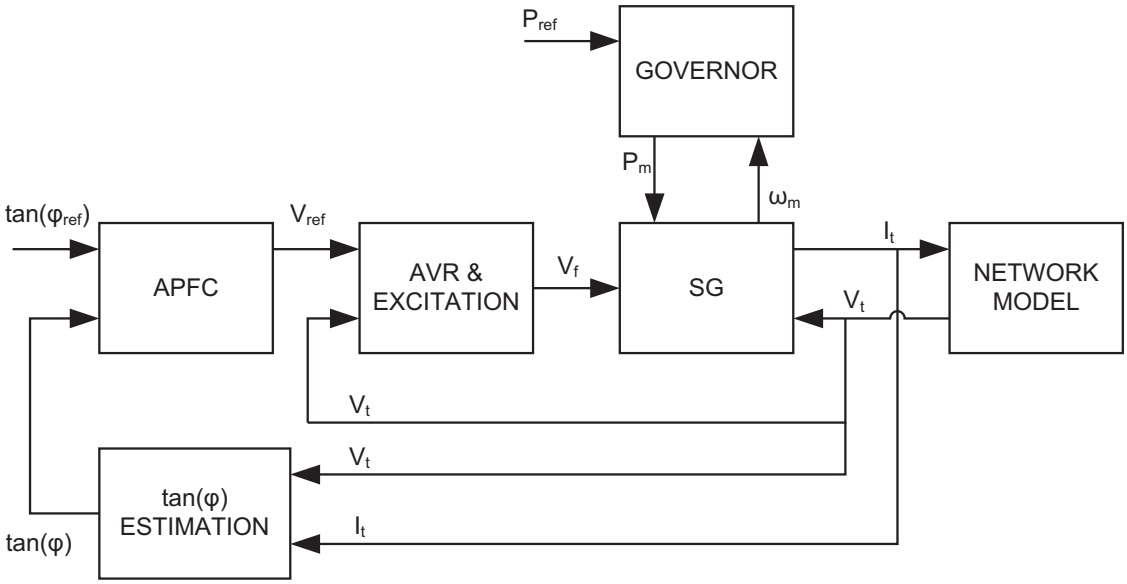

Figure 3.3: *Top-level block diagram of the developed model for the small-hydro plant*

3.4 Hydraulic Governor Model

The gate opening input of the hydraulic turbine has to be continuously controlled to react to load or turbine mechanical power (input) changes, otherwise the generator's output power would vary accordingly. This is performed by the speed governor, which measures the machine speed and adjusts the gate opening (and therefore the power input) to compensate the variability of the source or the load. Modern governors are electronically controlled, but due to the high associated forces there is a need for a combination of pneumatic, hydraulic and/or mechanical subsystems to assist gate control [36]. The block diagram of a Woodward-type governor [37] is shown in Figure 3.4 below.

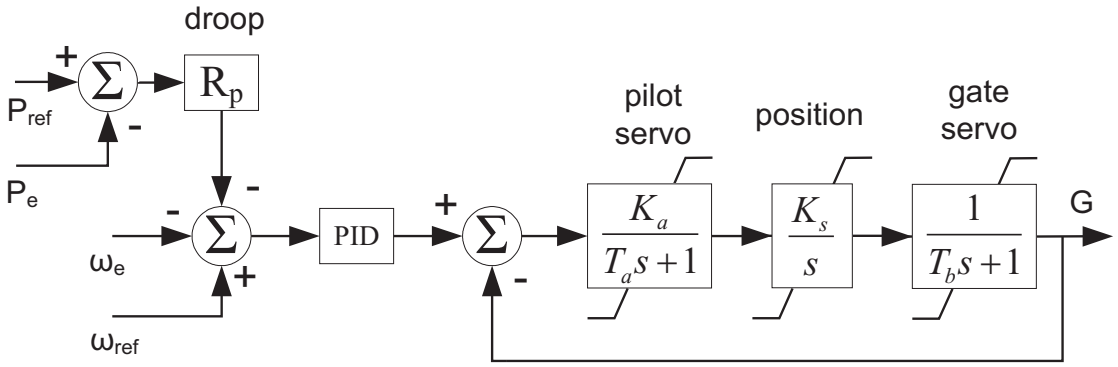

Figure 3.4: *Block diagram of the hydraulic governor*

In "island operation" (generator and local load not connected to a larger network), or during startup of the generator (pre-synchronisation), the governor is regulated by means of a feedback loop that provides a rotational speed error signal and a power error signal with a droop characteristic (if there are multiple generators running in parallel). When the generator is connected to the network, the speed error signal is disabled (since the generator is synchronised) [38, 39]. These error signals are fed to a Proportional-Integral-Derivative (PID) controller. The proportional part of the PID controller amplifies that error signal, thus accelerating the correction. However the higher the proportional term, the worse the stability of the system is. It is impossible to eliminate steady state error by pure P-control, as an error signal is always needed for the controller to produce a non-zero output. The integral action of the PID can assist in eliminating the offset error by providing an output proportional to the accumulated error signal over time. The hydraulic turbine is a non-minimum phase system, which means that the initial response is opposite to that of the gate position. This can be physically reasoned by the fact that a sudden opening of the gate would cause a reduction of the pressure across the penstock. However, due to water inertia the flow will not change immediately. As power is the product of flow times pressure, the initial power would be reduced. Then the water flow would accelerate with a time constant T_w until the turbine power has reached the steady state level for that gate opening. The derivative action of the PID controller mitigates that effect by boosting the short-term response to sudden load changes. The overall transfer function of the PID controller is

given by Equation 3.2:

$$C(s) = K_P + \frac{K_I}{s} + \frac{K_D \times s}{T_D \times s + 1}, \tag{3.2}$$

where: $K_P =$ proportional gain,
$K_I =$ integral gain,
$K_D =$ derivative gain,
and $T_D =$ derivative filter time constant (s).

An additional error signal derived by the difference between reference and electrical power (P_{ref} and P_e respectively) is added to the input of the PID controller to provide correction of the power mismatch. In order to ensure stable operation and load sharing among several generating units, a droop characteristic is given to the governor. The (steady-state) power droop R_P is of the range of 0.05 pu. This means that a power deviation of 5% would bring about a 100% change in gate opening and therefore power output. Finally each servo can be efficiently modelled by a first order, limited output transfer function as shown in the block diagram of Figure 3.4. The rate of change of gate position is also limited.

3.5 Synchronous Generator Model

The Synchronous Machine (SM) has been used for over a century in industrial and power applications. Many large loads are driven by synchronous motors, and synchronous generators are the cornerstone for power generation. The synchronous machine is also used as a synchronous condenser, to control network voltage by reactive power compensation [38]. Low-speed, salient pole synchronous generators are the most usual option for small hydro schemes [40]. Research on SM modelling was carried out extensively during the 20's and 30's, but more work has been done recently [38]. This section presents the dynamic SG model that will be used in the simulations throughout this thesis. It assumes knowledge of the physical and electrical properties of the synchronous machine that can be found in [38, 39, 41–43].

3.5.1 Electrical Subsystem

The mechanical speed ω_m of the SG in rad/s is given by:

$$\omega_m = \frac{\omega_e}{pp}, \tag{3.3}$$

where pp is the number of pole pairs, $\omega_e = 2\pi f_e$ and f_e is the network's electrical frequency. Due to their low mechanical speed, small hydro schemes utilise SGs with a large number of pole pairs in order to achieve an ω_m equal to $2 \times \pi \times 50$ (or $2 \times \pi \times 60$ for the US) rad/s.

The SG has three sets of windings, namely the armature (stator), the excitation or field (rotor) and (for salient pole machines) the damper windings. Power is transfered through the armature winding, while the excitation uses direct current to produce the required magnetic field to induce alternating voltage in the armature. Finally the damper windings provide electrical damping to the frequency oscillations. For the purpose of generator control, it is more convenient to use the $0dq$ model derived by the 3-phase model using the Park transformation [38, 39]. The main advantage of the $0dq$ model is that the fundamental frequency is eliminated and therefore all its components are constant and independent of time. In the $0dq$ model, the three components are perpendicular to each other. The d axis is aligned with the magnetic flux, rotates with the rotor and axis q follows it with a 90^o lag. In the dq plane all vector quantities are resultants of their respective d and q components according to:

$$\bar{U} = U_d + jU_q, \tag{3.4}$$

where U can be any vector quantity such as voltage, current, flux etc. The flux linkages of the synchronous generator in the per unit system are given by the following set of equations:

$$\Psi_0 = L_0 i_0 \tag{3.5}$$

$$\begin{bmatrix} \Psi_d \\ \Psi_f \\ \Psi_D \end{bmatrix} = \begin{bmatrix} L_d & kM_f & kM_D \\ kM_f & L_f & L_{fD} \\ kM_D & L_{fD} & L_D \end{bmatrix} \times \begin{bmatrix} i_d \\ i_f \\ i_D \end{bmatrix} \tag{3.6}$$

$$\begin{bmatrix} \Psi_q \\ \Psi_Q \end{bmatrix} = \begin{bmatrix} L_q & kM_Q \\ kM_Q & L_Q \end{bmatrix} \times \begin{bmatrix} i_q \\ i_Q \end{bmatrix} \tag{3.7}$$

In the above equations L and kM denote self and mutual inductance respectively, subscripts $_0$, $_d$, $_q$ denote the respective components of the armature, $_D$, $_Q$ the respective components of the damper windings and finally $_f$ denotes the field winding. For balanced and symmetrical systems the zero sequence component of current $i_0 = 0$, and since the system is assumed such, Equation 3.5 can be omitted.

The voltage equations of the synchronous generator (also in the $0dq$ reference frame) are the following:

For the stator:

$$\begin{aligned} v_0 &= -R_a i_0 - \dot{\Psi}_0 \\ v_d &= -R_a i_d - \dot{\Psi}_d - \omega_m \Psi_q \\ v_q &= -R_a i_q - \dot{\Psi}_q + \omega_m \Psi_d \end{aligned} \tag{3.8}$$

For the rotor:

$$\begin{aligned} v_f &= -R_f i_f - \dot{\Psi}_f \\ 0 &= -R_D i_D - \dot{\Psi}_D \\ 0 &= -R_Q i_Q - \dot{\Psi}_Q \end{aligned} \tag{3.9}$$

All quantities in the above equations are in the per unit system. As with the flux equations, the top equation of 3.8 can be omitted. The remaining can be rearranged and written in matrix format:

$$\begin{bmatrix} \dot{\mathbf{\Psi}}_{dq} \\ \dot{\mathbf{\Psi}}_{fDQ} \end{bmatrix} = - \begin{bmatrix} \mathbf{v}_{0dq} \\ \mathbf{v}_{fDQ} \end{bmatrix} - \begin{bmatrix} \mathbf{R}_a & \\ & \mathbf{R}_{fDQ} \end{bmatrix} \times \begin{bmatrix} \mathbf{i}_{0dq} \\ \mathbf{i}_{fDQ} \end{bmatrix} + \begin{bmatrix} \mathbf{\Omega} & \\ & \mathbf{0} \end{bmatrix} \times \begin{bmatrix} \mathbf{\Psi}_{dq} \\ \mathbf{\Psi}_{fDQ} \end{bmatrix}, \tag{3.10}$$

where $\mathbf{\Omega}$ is the rotation matrix and is given by:

$$\mathbf{\Omega} = \omega_m \times \begin{bmatrix} 0 & 0 & 0 \\ 0 & 0 & -1 \\ 0 & 1 & 0 \end{bmatrix} \tag{3.11}$$

The instantaneous electrical power P (under balanced operation) in the per unit system is equal to the air-gap torque T_e and is given by:

$$P = v_d \times i_d + v_q \times i_q = T_e \tag{3.12}$$

Similarly the reactive power in pu is given by:

$$Q = v_d \times i_q - v_q \times i_d \tag{3.13}$$

The steady state model of the synchronous generator emerges when the dynamic terms of the above equations are removed and the assumption $\omega_m = 1.0$ pu is made. The resulting equivalent circuit is depicted in Figure 3.5 below.

In the terminal voltage/current vector diagram of Figure 3.5 X_d is the synchronous reactance of the generator. In the per unit system and neglecting saliency, $X_d = X_q = L_d = L_q$. From that vector diagram, the basic equivalent circuit for the SG can be derived, and is shown in Figure 3.6. Voltage E_d in Figure 3.6 is the effective internal voltage of the machine which is equal to the excitation voltage due to the field current.

3.5.2 Mechanical Subsystem

The acceleration or deceleration of the machine is proportional to the difference between the mechanical torque T_m from the prime mover (or to the load, if motoring), which in this case is the hydraulic turbine, and the electrical torque T_e supplied to (or imported from) the grid. This is mathematically expressed by the following equation:

$$J\frac{d\omega_m}{dt} = T_m - T_e, \tag{3.14}$$

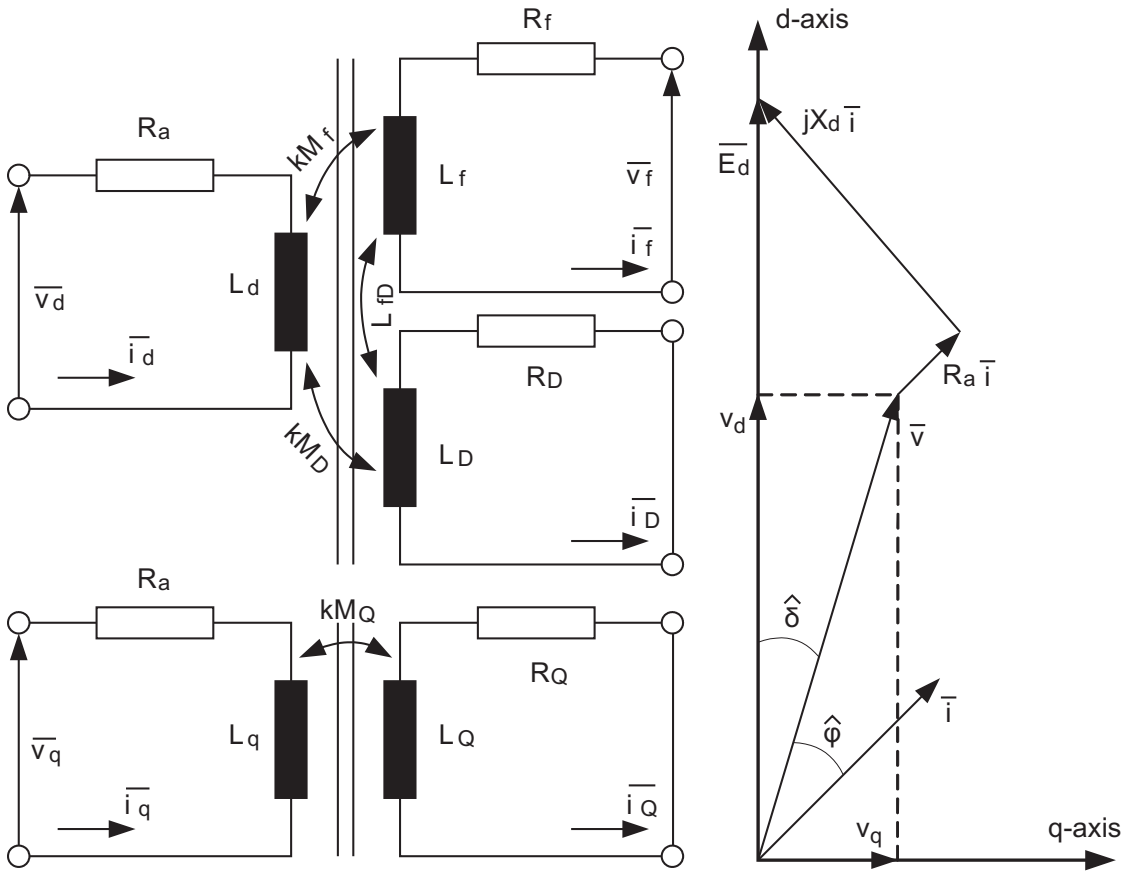

Figure 3.5: *Steady state equivalent circuit of the synchronous generator (left) and terminal voltage/current vector diagram*

where J is the sum of moments of inertia of the machine and the prime mover in kgm^2 and ω_m is the rotational speed of the rotor in rad/s. When a body rotates, its kinetic energy is equal to $0.5Jw_m^2$. Kinetic energy divided by the base apparent power S_{base} in VA (equal to rated VA of the machine for simplicity) equals the per unit inertia constant H, measured in seconds. Thus, Equation 3.14 becomes:

$$\frac{2HS_{base}}{\omega_{m0}^2}\frac{d\omega_m}{dt} = T_m - T_e, \tag{3.15}$$

where ω_{m0}^2 is the rated rotational speed in rad/s. By setting base torque $T_{base} = S_{base}/\omega_{m0}^2$ and then dividing Equation 3.15 by T_{base}, the swing equation for the machine

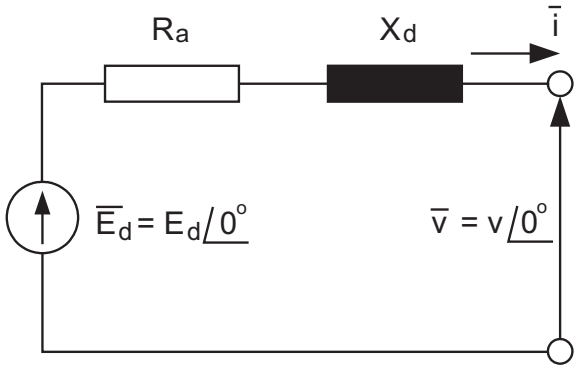

Figure 3.6: *Basic steady state equivalent circuit of the synchronous generator with saliency neglected*

is obtained:

$$2H\frac{d\omega_m}{dt} = T_m - T_e \tag{3.16}$$

Typical values for the per unit inertia constant H range from 2 to 4 seconds [38]. Equations 3.6, 3.7, 3.10, 3.12, 3.13 and 3.16 constitute the complete dynamic model of the synchronous generator that will be used throughout this thesis.

3.6 Operation and Control of the Synchronous Generator

The main advantage of the synchronous generator is that it has a well-understood, wide-range control over its basic quantities, i.e. terminal voltage, real and reactive power output. Additionally, real and reactive power controls can be individually controlled, allowing easy regulation of its output and power factor. While real power is governed by the prime mover, reactive power (and terminal voltage, when not connected on an infinite bus) is governed by the DC excitation. The Automatic Voltage Regulator (AVR) operates on the exciter according to a pre-defined control objective. This objective can be maintenance of constant terminal voltage, constant reactive power or constant power factor, depending on the level of connection (transmission or distribition) and the applicable regulations or agreements with the network operator.

3.6.1 Exciter & Excitation Control

A number of different technologies have been used for excitation of SGs, ranging from DC exciters utilising DC generators to provide the excitation current, to modern digitally controlled solid state active rectifiers [38, 39, 41, 44]. A basic functional diagram of such a system is shown in Figure 3.7. The excitation control acts on the exciter, which provides the field current (and hence voltage) for the synchronous generator. The feedback loop is closed by the voltage transducer, which measures the terminal voltage that is then compared to the setpoint and therefore an error signal is generated. The excitation system operation has a great impact on the performance of the overall plant, therefore care must be taken to ensure that it is optimally set up and tuned. Bad tuning of the AVR may lead to reduced performance, unstable operation and possibly damaging of the plant [45]. Excitation systems are often complemented by other components such as load compensators, power system stabilisers etc. However, their functionality is beyond the scope of this work and therefore will not be discussed here. Additional information on them can be found in [38, 39, 41, 44, 46].

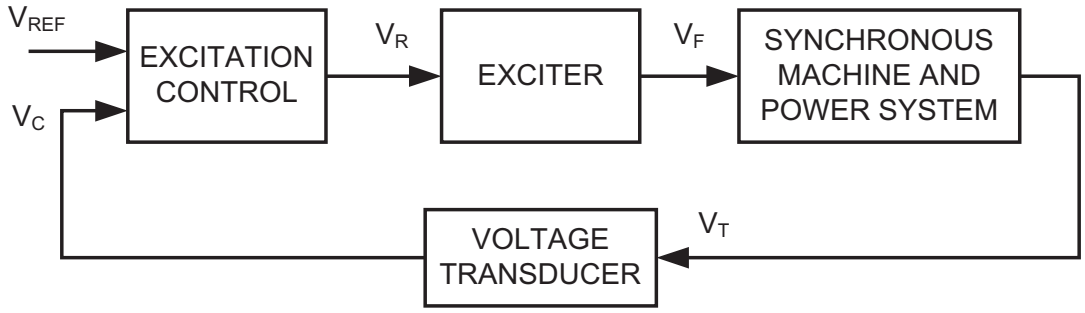

Figure 3.7: *Basic functional diagram of excitation system of a synchronous machine*

Additionally, the excitation system contains components such as current and voltage limiters in order to protect the generator and the exciter. IEEE in [44] has issued a recommendation for the modelling of excitation systems. A commonly used AVR / static exciter is type-ST1A. The complete ST1A model can be found in the above document. A simplified version of it (with load compensation and power system stabilisation omitted) will be used here. The block diagram of the simplified ST1A model is shown in Figure 3.8.

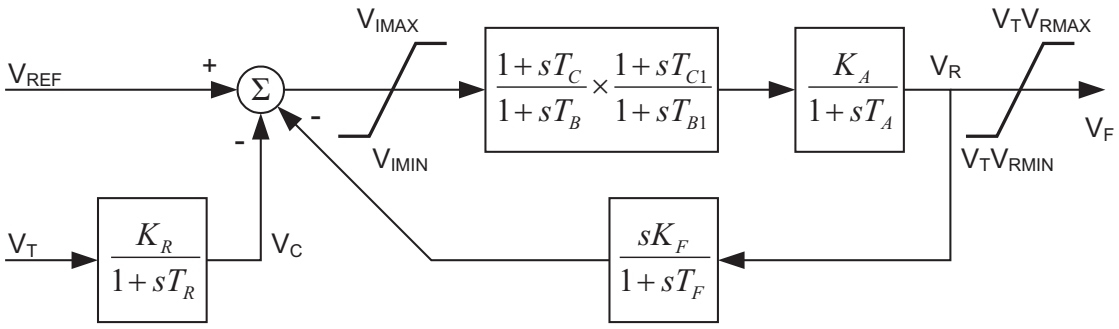

Figure 3.8: *Block diagram of the simplified ST1A excitation system model*

Since the dynamics of the (power electronics based) static exciter are significantly faster that the rest of the system, it can be assumed that exciter's action is instantaneous and hence an exciter block is not included in this model [41]. The main voltage regulator is modelled as a first order transfer function with gain K_A and time constant T_A. Its input is supplied by a Lead-Lag compensator with time constants T_B and T_C, which provides forward path transient gain reduction. Alternatively, rate feedback stabilisation may be included in the feedback path via the compensator (K_F, T_F). The feedback loop can be disabled (if transient gain reduction is performed in the forward path) by setting $K_F = 0$. Sometimes an extra component for transient gain increase is included in the forward path (T_{B1} and T_{C1}, with $T_{C1} > T_{B1}$). This section can also be disabled if not needed, by setting T_{B1} and T_{C1} equal to zero.

The error signal that is used to regulate the generator's voltage emerges by subtracting terminal voltage V_T from the reference V_{REF}. Before this happens, the former is passed through the transducer/filter (modelled here with the 1st order transfer function (K_R, T_R) that removes noise and scales the signal to the controller's input range.

The model also makes provision for limitation of the input and output of the excitation system. The input limits are represented by [V_{IMIN}, V_{IMAX}] and in many cases can be neglected [41]. However, the same document proposes that the output limits [$V_T V_{RMIN}$, $V_T V_{RMAX}$] should always be included in the model. The output limits are proportional to the terminal voltage because ST1A is a voltage source, controlled rectifier bridge system with its excitation power supplied by a transformer connected

directly on the generator terminals. If the exciter employs a fully controlled bridge (as in most cases), $V_{RMIN} < 0$. Otherwise the minimum excitation voltage will be equal to zero ($V_{RMIN} = 0$).

3.6.2 Automatic Power Factor Controller

When the generator operates in Automatic Voltage Control (AVC) mode, the voltage reference V_{REF} is set by a potentiometer or is provided (in modern AVRs) as an output from a computerised supervisory system. This is the standard mode of operation of generators connected to the transmission network. Distributed generators are required by the network operators to operate in Automatic Power Factor Control (APFC) mode except for very few cases that the DNOs allow AVC operation in order to enable generators connected to weak grids to perform voltage support. However, this is expected to happen more often in the future when the capacity of DG will increase. This has to be evaluated carefully because larger capacity SGs can cause AVC equipment on DNO transformers to operate in response.

Automatic power factor control is most easily applied when network impedance is low and when machines can export full capacity without a measurable increase in terminal voltage. SGs are usually loaded immediately after synchronising by increasing the speed setting in the governor, while simultaneously transferring the AVR from voltage control (AVC) for synchronising to power factor control (APFC). Thereafter active and reactive power ramp in constant ratio, up to any load limits. One method of implementing APFC is to include in the excitation system a separate control module that operates on the voltage setpoint of the AVR to hold the phase angle between generator terminal voltage and current constant. A possible configuration for such a system is shown in Figure 3.9. Terminal voltage $\bar{V_T}$ and current $\bar{I_T}$ are measured and the instantaneous real and imaginary powers are calculated using Equations 3.12 and 3.13 respectively. From these values the tangent of the voltage-current angle is calculated ($tan(\phi) = Q/P$) and used as an indicator for the actual power factor. Use of tangent instead of cosine ensures that the input term is always single-valued over the range of control. This value is compared to a reference and the resulting error signal is fed to a PID compensator

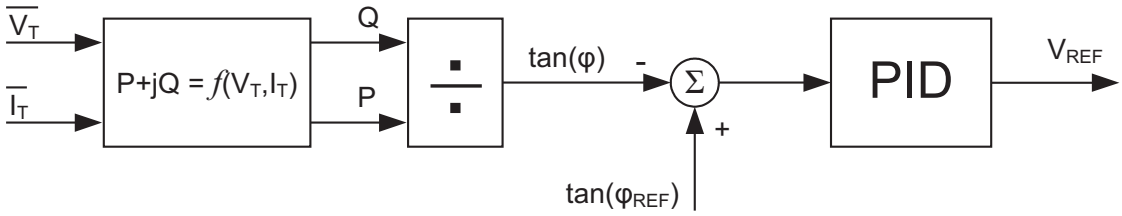

Figure 3.9: *Automatic power factor controller block diagram*

identical to the one discussed in Section 3.4, described by Equation 3.2. The PID compensator then provides the reference voltage for the AVR of Figure 3.8.

3.7 Voltage Regulation Using Transformers with On-Line Tap Changers

As already mentioned, distributed generation did not contribute to voltage regulation until recently. This was mainly performed by transformers with automated tap changing mechanisms installed at the bulk supply points. However, with the increase of distributed generation, transformers with On-Line Tap Changers (OLTCs) are increasingly being used at the points of DG connection in order to mitigate the increased voltage fluctuation due to the existence of the generator [47–52]. The OLTC mechanism acts on the taps on the primary winding of the transformer. The most common mode of operation is Automatic Voltage Control (AVC), where the OLTC regulates the voltage on the secondary winding through a voltage feedback signal. Therefore voltage at the DG busbar remains within the limits set in the OLTC control system. Figure 3.10 illustrates the working of such an OLTC mechanism.

A typical OLTC mechanism operates as follows [53]: First, the terminal voltage V_t on the secondary winding is measured. The measured voltage is then compared to the preset thresholds for tap action V_{min} and V_{max}. A command to raise (lower) the tap position is issued if V_t is higher (lower) than V_{max} (V_{min}), and if a time longer than the delay setting t_d has passed since the last tap change, and the tap changer has not

already reached its highest position. The time delay is used as a means to avoid hunting and rapid tap changes that may destabilise the system and cause quick wear-out of the tap contacts.

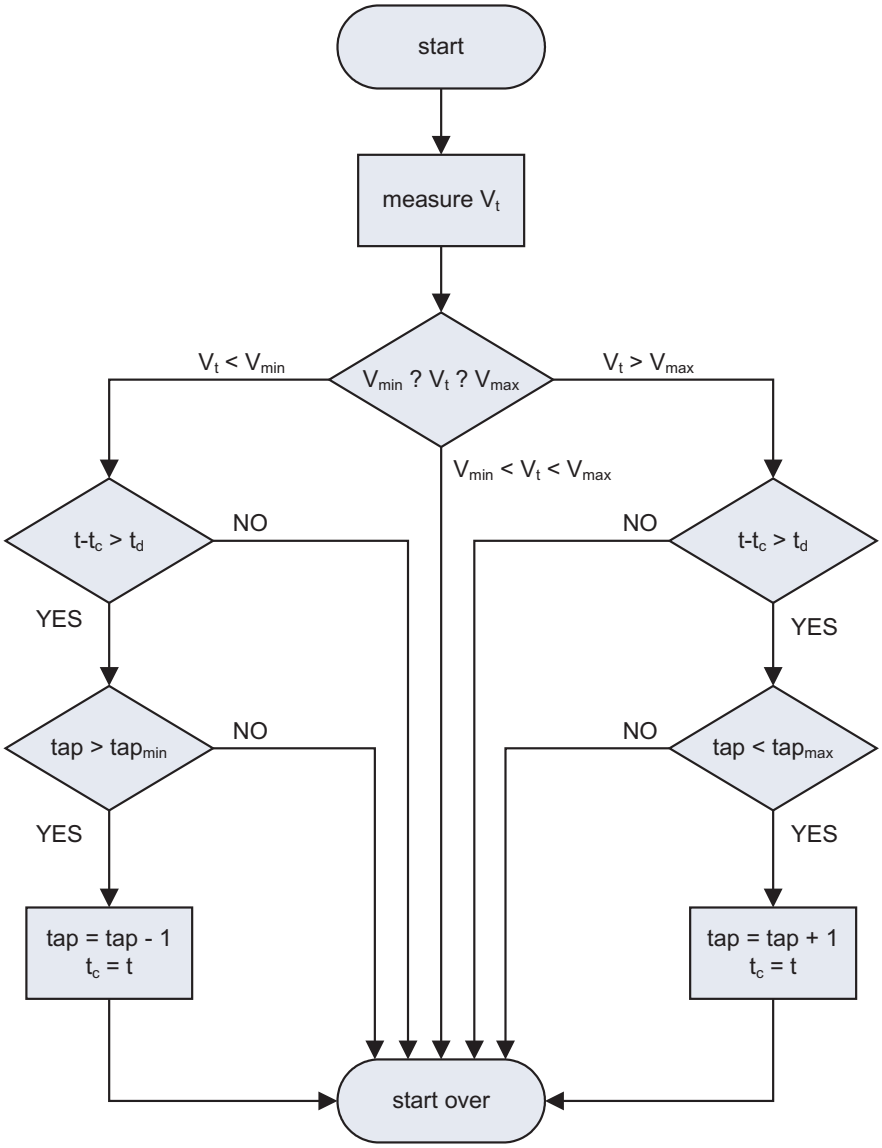

Figure 3.10: *Flow chart of the operation of an On-Line Tap Changing mechanism*

There are also cases where the transformer is located at another point in the network (usually upstream in the radial feeder) and controls the DG bus voltage by Line Drop/Rise Compensation (LDRC). This is achieved by including a circuit that emulates the impedance of the feeder, and by injecting samples of the measured voltage and

current, the voltage drop (or rise) across the feeder can be "virtually" measured. Then this voltage drop is used as a control signal to the OLTC [54]. The flow chart for the LDRC mode is the same with the one shown in Figure 3.10, with the only difference that measured V_t is the product of the emulating circuit. The operation of the OLTC mechanism is stepwise. At each tap change, a positive or negative voltage step V_{step} occurs. In addition, in order to avoid hunting and wear-out of the tap contacts, time delay circuits and voltage deadbands are included in the control system. However, these discontinuities degrade the quality of the controlled voltage by slowing down its response (time delay T_d) and reducing its sensitivity (deadband $V_{max} - V_{min}$). In addition, when operating in LDRC mode, the tolerance of the emulating circuit can also worsen the performance of the OLTC [54]. Table 3.3 shows a set of typical OLTC parameters [55].

The OLTC process described in Figure 3.10 was modelled in Matlab using the parameters of Table 3.3. The Simulink block diagram of the OLTC mechanism can be seen in Figure 3.11. In the developed model, the emulating circuit of the LDRC subsystem is assumed ideal. This simplifies the model as the voltage reading can be taken directly from the controlled bus, thus eliminating the need for inclusion of the emulating circuit in the model. However, in reality the emulating circuit is not 100% precise and therefore errors are introduced to the estimations of voltages at remote buses. Consequently, this decreases the accuracy of the control mechanism.

Parameter	**Value**	**Description**
tap_{max}	7	max. no. of taps above nominal position
tap_{min}	-7	max. no. of taps below nominal position
V_{step}	0.0125pu	voltage step per tap change
V_{dmax}	0.0125pu	high side of voltage deadband
V_{dmin}	0.0125pu	low side of voltage deadband
t_d	60 s	time delay between tap changes

Table 3.3: *A typical set of parameters for an OLTC mechanism*

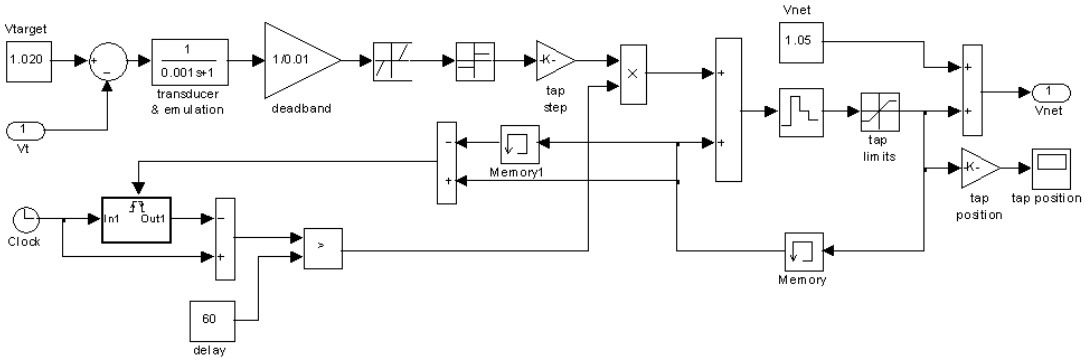

Figure 3.11: *Simulink block diagram of the OLTC mechanism*

3.8 The Synchronous Generator in a Distribution Network and its Operational Limitations

The limiting factors of the operation of a synchronous generator when connected to the distribution network can be divided in two categories: power plant protection and seamless operation of the distribution network. The former are related to the characteristics of the power plant itself, while the latter are imposed by the DNO in order to ensure security and quality of supply. The common way to display the power plant limitations, specifically the P, Q and V limits, is by using the capability diagram of the synchronous generator. A typical capability diagram is shown in Figure 3.12.

Detailed information on the construction of the capability diagram can be found in most power system analysis textbooks, such as [38, 39, 42]. The operational limits of the synchronous generator are drawn in the capability diagram as follows:

- **Stator heating limit:** Defines the maximum apparent power output (MVA) of the generator and is represented by the concentral circles with centre at O and radius S.
- **Prime mover limit:** Defines the maximum real power output of the generator and is represented by the horizontal lines.

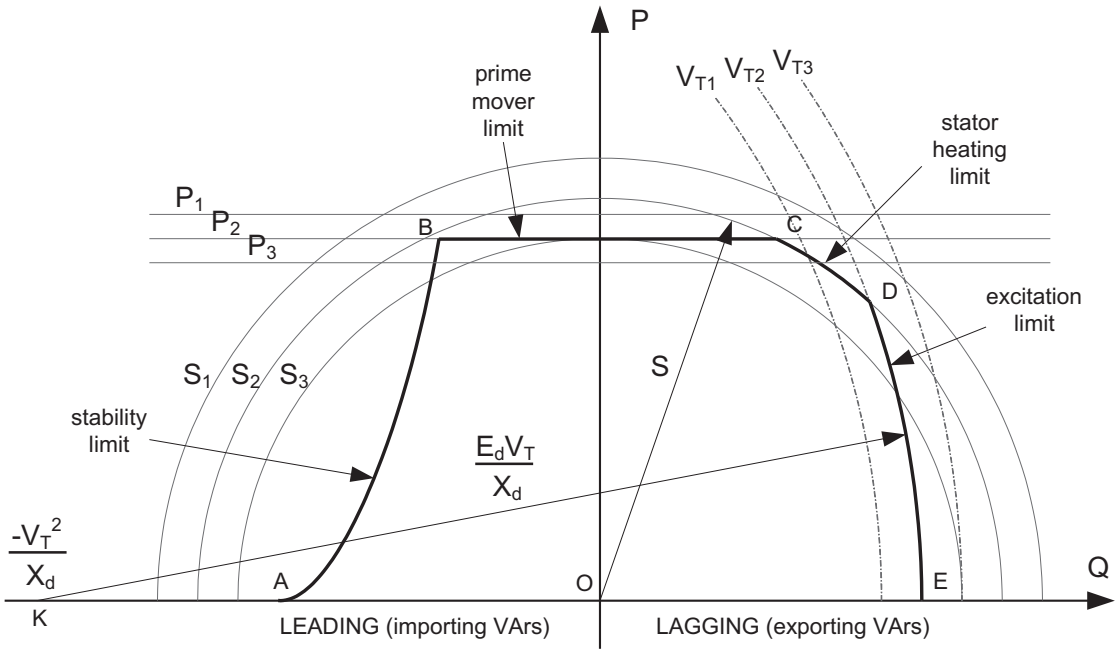

Figure 3.12: *Capability diagram of the synchronous generator*

- **Excitation limit:** Is defined by the maximum excitation voltage. Its locus is a circle with centre at $-\frac{V_T^2}{X_d}$ and radius $\frac{E_d V_T}{X_d}$.
- **Stability limit:** Defines the minimum excitation, beyond which the generator is at risk of losing stability. It is a function of excitation current and its construction is discussed in [42].

For a given set of S, V_T and P_{MAX}, the capability diagram of a generator with synchronous reactance X_d can be constructed, by connecting the pre-mentioned sections of the curve. The resulting curve ABCDE in Figure 3.12 is the capability diagram. It should be noted that for the construction of the capability diagram as discussed above, it is assumed that the generator is connected directly to the infinite grid and any change in real or imaginary power output is not reflected on the terminal voltage. Of course, as already discussed, this is not the case in the distribution network, where terminal voltage V_T may vary widely with power changes, depending on the network impedance at the point of connection [56]. The capability diagram as constructed above can not be used other than when $V_{gen} = 1.0pu$. The result of this fact is that the capability diagram

of a DG cannot be represented in the two-dimensional P-Q plane as in Figure 3.12, and a third dimension to accommodate voltage changes is needed. Figure 3.13 shows the resulting 3D capability diagram for a synchronous generator in the distribution system combined with the voltage surface for varying P and Q (note the change of direction of the Q axis compared to Figure 3.12). The generator convention is used, i.e. power is positive when exported.

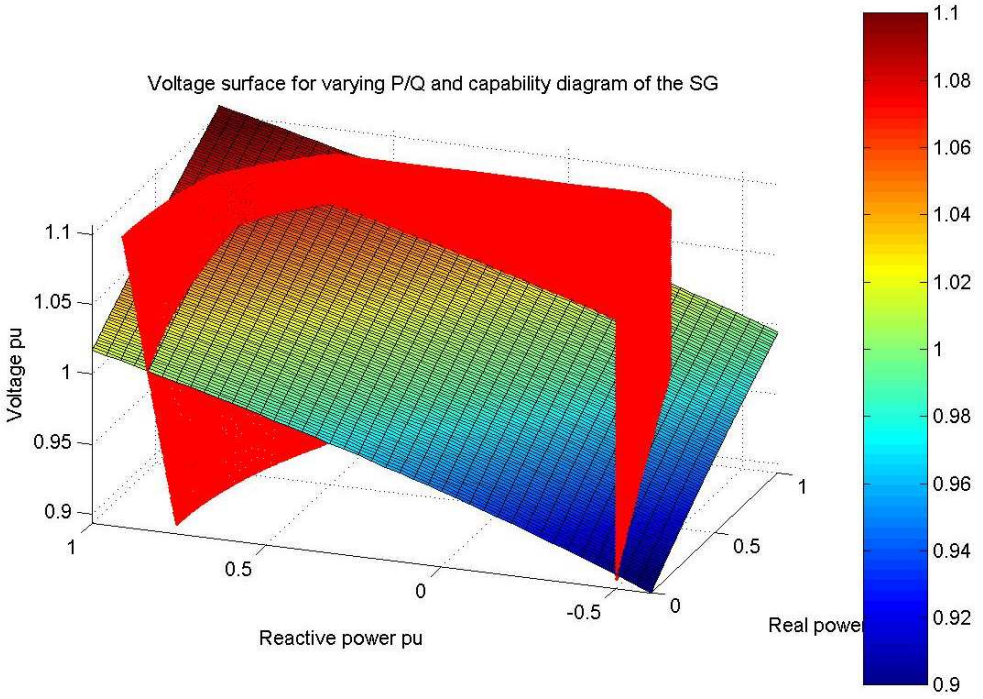

Figure 3.13: *Combined voltage surface and 3-dimensional capability diagram for a synchronous generator*

In this figure, the radius of the excitation limit (left side of the diagram) is scaled in proportion to V_T and therefore the "static" capability curve at each voltage level is different. The actual operational area of the DG in this case is the (non-planar) section of the voltage surface that is encompassed by the 3D capability diagram. An important aspect of the capability diagram is that in a real system it is "dynamic", i.e. it changes in time according to demand fluctuations and network reconfiguration. For

example, a decrease of demand would result in a voltage surface higher on the V-axis (and vice-versa), and disconnection of a feeder would bring about an increase of the voltage surface slope in both P and Q directions. Since the 3D capability diagram is machine-specific and therefore constant, a change of the voltage surface would alter the operational area of the generator. This change may move the operating point of the generator closer to (or farther from) its operational limits. This is further discussed in Chapter 5.

3.9 Power System Modelling

The task of the power network model is to calculate the power flows across the network as well as the associated voltage changes. Mathematically, the power network is described by a set of algebraic equations. For a network with p nodes, Equation 3.17 is the *nodal equation*:

$$\bar{\mathbf{I}} = \bar{\mathbf{Y}} \times \bar{\mathbf{V}} \tag{3.17}$$

where: $\bar{\mathbf{I}} = [I_1\ I_2\ \cdots\ I_p]^T$ current injections at nodes 1 to p,
$\bar{\mathbf{V}} = [V_1\ V_2\ \cdots\ V_p]^T$ voltages at nodes 1 to p,
and $\bar{\mathbf{Y}}$ nodal admittance matrix.

The nodal admittance matrix is equal to:

$$\bar{\mathbf{Y}} = \begin{bmatrix} \bar{Y_{11}} & \bar{Y_{12}} & \bar{Y_{13}} & \cdots & \bar{Y_{1p}} \\ \bar{Y_{21}} & \bar{Y_{22}} & \bar{Y_{23}} & \cdots & \bar{Y_{2p}} \\ \vdots & \vdots & \vdots & \ddots & \vdots \\ \bar{Y_{p1}} & \bar{Y_{p2}} & \bar{Y_{p3}} & \cdots & \bar{Y_{pp}} \end{bmatrix}, \tag{3.18}$$

where $\bar{Y_{ii}}$ is the self admittance of node i, equal to the sum of all admittances ending at node i, and $\bar{Y_{ij}}$ is the mutual admittance between nodes i and j and is equal to the negative of the branch series admittance between i and j.

When power injections are given, they can be converted to currents by:

$$I_i = \frac{S_i^*}{\bar{V}_i^*} = \frac{P_i - jQ_i}{\bar{V}_i^*}; \tag{3.19}$$

where P_i, Q_i are the real and imaginary power injections at node i respectively. Using powers instead of currents implies that the nodal equation cannot be solved algebraically, as, by substituting $\bar{\mathbf{I}}$ from Equation 3.19 into 3.17, $\bar{\mathbf{V}}$ appears on both sides of the equation in a non-linear fashion. Therefore an iterative algorithm has to be utilised for the solution, such as Newton-Raphson or Gauss-Seidel [19, 39].

Equations 3.17 and 3.19 are in the network reference frame (a,b) where the voltage of the infinite bus is assumed at an angle of zero degrees; however, the synchronous generator model described earlier is in the generator (d,q) reference frame. In order to be able to connect the generator model to any node of the network (where the voltage angle is arbitrary), the two systems must be aligned. This is performed by the transformation matrix as shown in Equation 3.20. The d-axis of the generator is shifted with respect to the network real axis a by the rotor angle δ. The terminal voltage can be transformed by:

$$\begin{bmatrix} v_a \\ v_b \end{bmatrix} = \begin{bmatrix} -\sin\delta & \cos\delta \\ \cos\delta & \sin\delta \end{bmatrix} \times \begin{bmatrix} v_p \\ v_q \end{bmatrix} \tag{3.20}$$

The rotor angle δ in radians is given by Equation 3.21:

$$\delta = \int (\omega_s - \omega_m) dt, \tag{3.21}$$

where ω_s and ω_m are the synchronous (network) angular speed and mechanical speed of rotation, both in radians, and $\omega_s - \omega_m = 0$ for $t = 0s$. Since the transformation matrix is unitary, the inverse transformation (from ab to dq) can be performed using the same matrix.

In the dynamic simulations throughout this work, energy sources are considered as current injections (as a function of generated power). Additionally, loads are assumed to be either constant or varying, but in both cases with no dynamic terms, and are modelled as power injections converted to currents by means of 3.19. A procedure for

solving the power flow in a distribution network is presented in [29]. This procedure has been implemented in Matlab and is used in all the simulations. The program receives as inputs the voltage of the infinite bus and the current injections at all nodes, and produces the node voltages. The source code of the program can be found in Appendix B. For the steady state simulations, a standard Matlab power flow program from [19] has been used, modified to include variable loads and On-Line Tap Changers (OLTCs) on the transformers. The modified code can also be found in Appendix B.

3.10 Simulation of the Developed SHG Model

A model of a small hydro scheme with a synchronous generator as described in this chapter has been built in Simulink. The block diagrams of the components of the model can be found in Appendix A. The model uses the Matlab code for the network solution that was presented in the previous section to solve the power flow. The top level diagram of the small hydro scheme block is shown in Figure 3.21. The modelled generator is a 12.5MVA, 10MW salient pole synchronous machine. The turbine is rated at 10.3MW output to account for the electrical losses. The generator and excitation system parameters of the plant were taken from [57]. The generator is connected to the infinite grid at 11kV through a feeder with $R_L = 0.5pu$ and $X_L = 0.4pu$ on a 100MVA base. Two tests of the developed model were performed; loading up the generator (post synchronisation) in APFC mode, and the response of the excitation system to a step change of the local load in AVC mode. Figure 3.14(a) below shows the process of loading up the generator.

On the generator bus, a 5MW, 0.9 lagging power factor load is connected. After synchronising, the power setpoint on the governor was increased linearly from zero to 1.0 per unit turbine output in 60 seconds, with the generator operating in automatic power factor control mode. The electrical power output of the generator shown in the top diagram of Figure 3.14(a) followed that increase. The increase stopped when the limit of the gate opening was reached. At that point the real power output of the generator was 0.8pu, or 10MW, which is the rating of the machine. At the same time

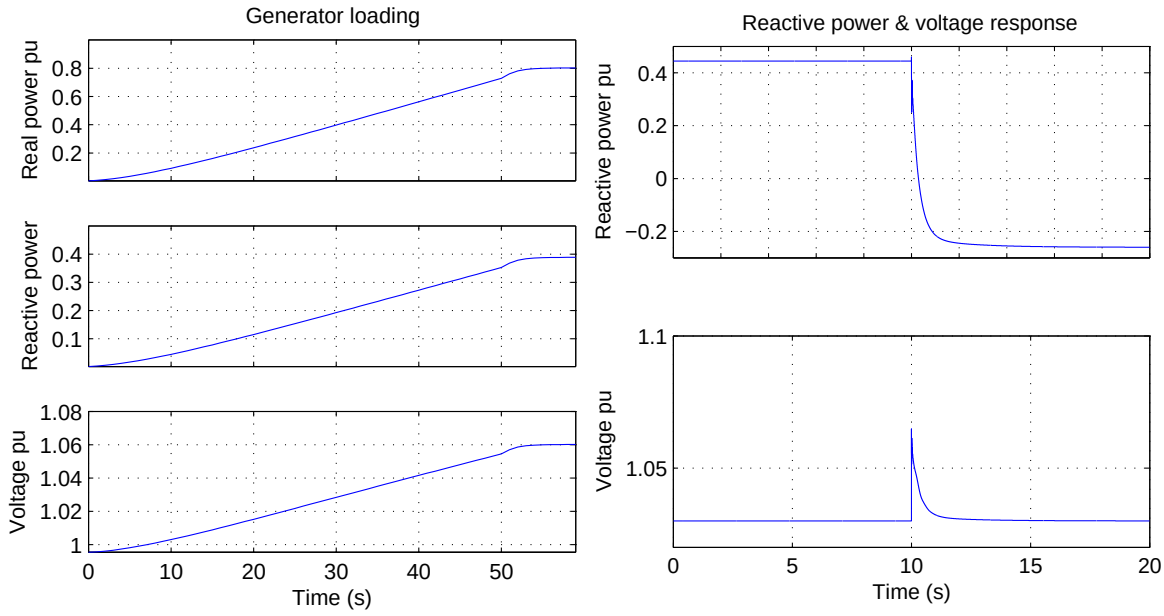

(a) **(b)**

Figure 3.14: *Synchronous generator loading up in APFC (a) and response to a load step change in AVC mode (b)*

the reactive power generated by the machine also increased in proportion so that the power factor remained constant at 0.9 lagging. The result of the simultaneous increase of P_{GEN} and Q_{GEN} was an increase of the terminal voltage to just above 1.06 pu. In a real situation the generator would not be allowed to reach that voltage level and would either have to constrain its output, or disconnect.

Figure 3.14(b) shows the response of the generator to a step change of the local load, with the AVR operating in automatic voltage control mode. The voltage reference was set at 1.03pu. At $t = 10$ seconds the local load was reduced stepwise from 10MW (0.9 PF) to 5MW. The top diagram of Figure 3.14(b) shows the reduction of reactive power from 0.45 pu (lagging) to -0.26pu (leading). By importing reactive power from the network, the bus voltage was maintained at 1.03pu. However the voltage spike once again violated the 1.06 pu statutory limit. Engineering Recommendation G59/1 [26] allows transient overvoltages with duration of less than 0.5s before the generator is disconnected.

3.11 Simulation of the OLTC in a Network with Varying Loads

The following simulations illustrates the operation of a transformer equipped with an On-Line Tap Changer in a radial system with a distributed generator and a varying load. The line diagram of the system is shown in Figure 3.15.

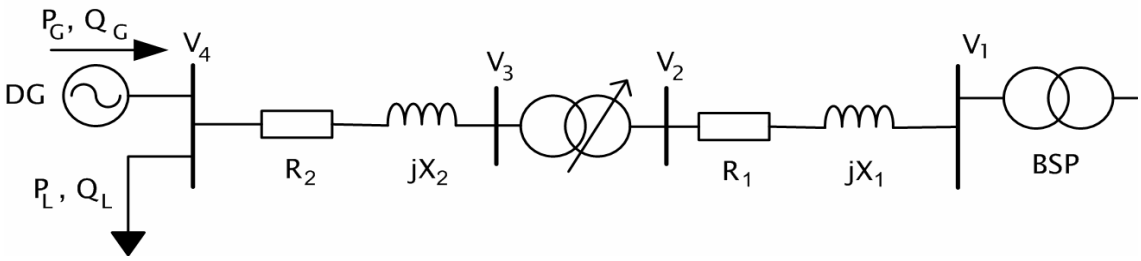

Figure 3.15: *The simulated 4-bus system with the OLTC*

In the first simulation the transformer was assumed to be directly connected on the DG bus and the OLTC operated in AVC mode. This was achieved by setting R_2 and X_2 equal to zero (so that $\bar{V_4} = \bar{V_3}$). In the second simulation R_2 and X_2 were given non-zero values and the OLTC operated in LDRC mode. In both simulations the OLTC settings were the ones presented in Table 3.3 with a target voltage of $1.0pu$. The profile of the load on the DG bus is shown in Figure 3.16 in per unit. It has been constructed using a 80% domestic and 20% industrial profile with data taken from [58]. Such a profile is typically found in rural areas. The system data for the simulation of the OLTC in AVC and in LDRC mode are shown collectively in Table 3.4.

3.11.1 Simulating the OLTC in AVC Mode

The system data for the simulation of the OLTC in AVC mode are shown in Table 3.4. Figure 3.17 shows the tap changer action throughout the simulated period. It is shown that at low demand periods, the tap changer raises the tap position, thereby reducing the transformer ratio and hence lowering the secondary winding voltage. Inverse action

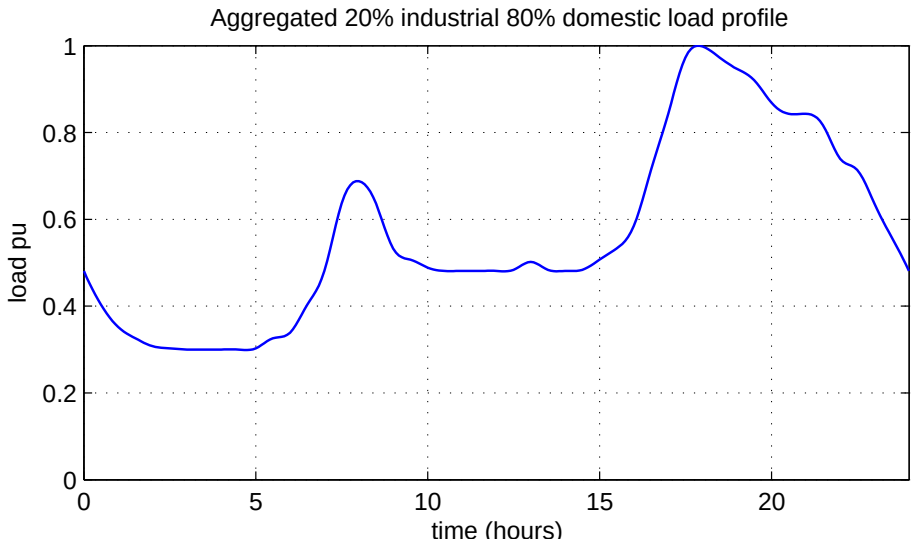

Figure 3.16: *24-hour varying load used in OLTC simulations*

takes place during high demand. The resulting voltage profile is represented by the red trace in Figure 3.18.

3.11.2 Simulating the OLTC in LDRC Mode

For the second simulation the impedance of the lines has been altered as shown in the third column of Table 3.4. There is now an impedance between the transformer's secondary and the DG bus. However The OLTC is still set to regulate V_4, thus operating in LDRC mode. The tap changer position is shown in Figure 3.19 and the voltages at buses 2, 3 and 4 in Figure 3.20. It can be observed that V_4 is still well regulated, however voltage V_3 (at the transformer's secondary terminals) is fluctuating widely to account for the voltage drop or rise across $R_2 + jX_2$. Nevertheless this is not a problem, as node 3 is a "virtual bus", i.e. it does not have any loads or generators connected.

Parameter	**Value (AVC test)**	**Value (LDRC test)**
Network		
S_{base}	$10MVA$	
V_{base}	$11kV$	
V_1 (slack)	$1.015pu$	
R_1	$0.125pu$	$0.030pu$
X_1	$0.100pu$	$0.020pu$
R_T	$0.003pu$	
X_T	$0.050pu$	
R_2	$0.000pu$	$0.060pu$
X_2	$0.000pu$	$0.040pu$
Load		
P_{Lmax}	$8MW$	
PF	0.9 lagging	
Generator		
P_G	$6MW$	
PF	0.95 lagging	

Table 3.4: *Parameters for the simulation of the OLTC operating in AVC and LDRC mode*

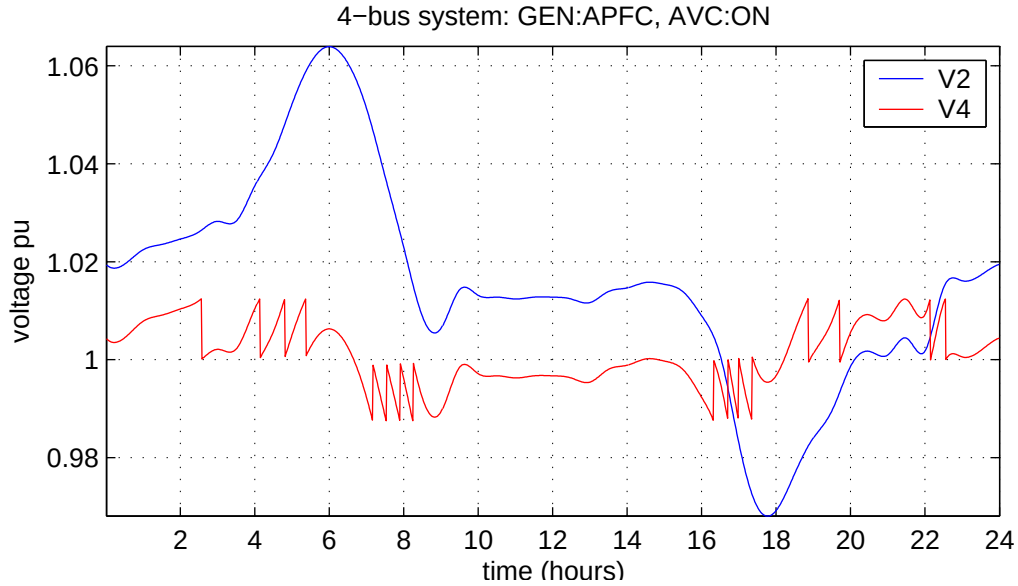

Figure 3.18: *Transformer primary and load bus voltage for the 24-hour simulation (AVC)*

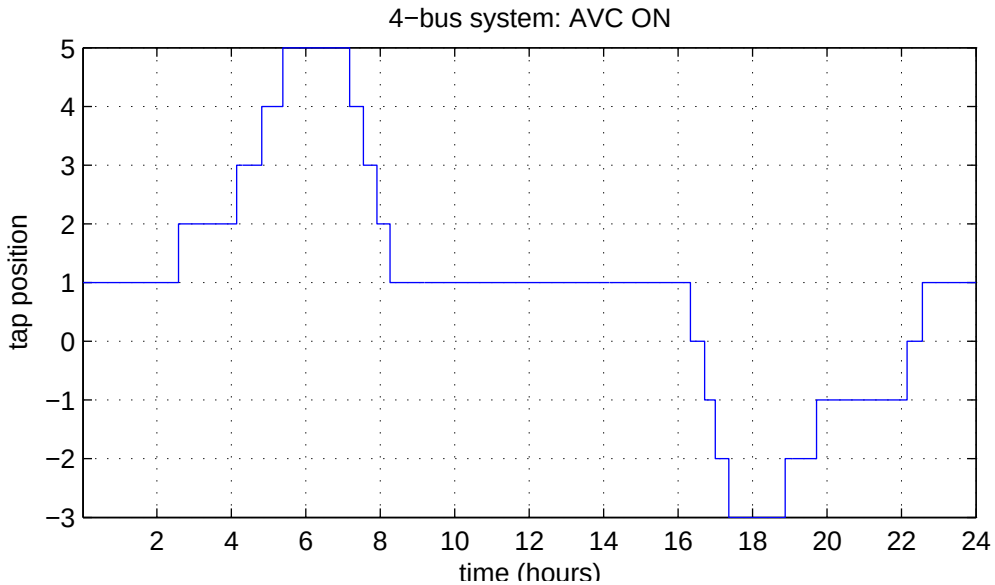

Figure 3.17: *OLTC tap position for the 24-hour simulation (AVC)*

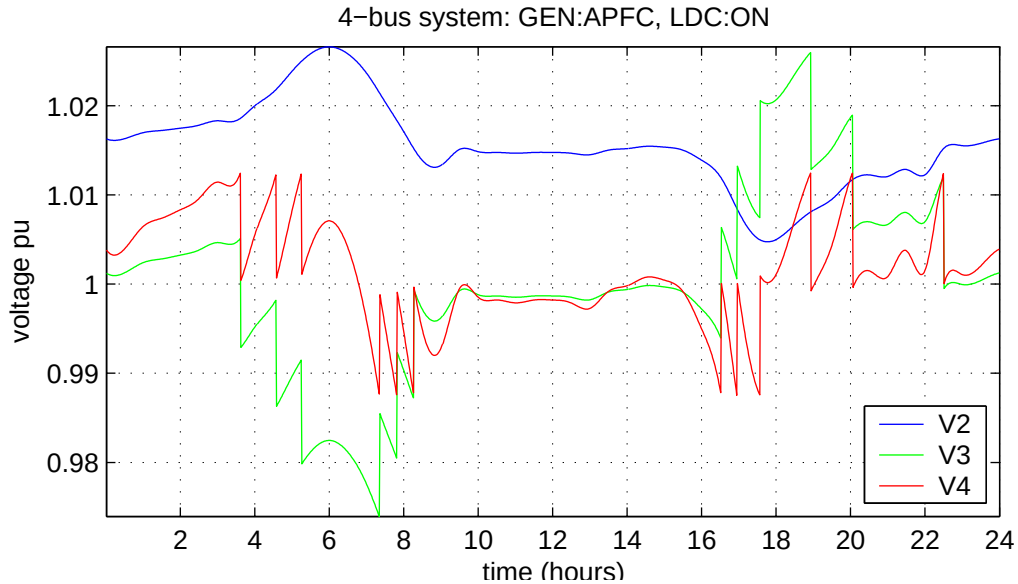

Figure 3.20: *Transformer primary and load bus voltage for the 24-hour simulation (LDRC)*

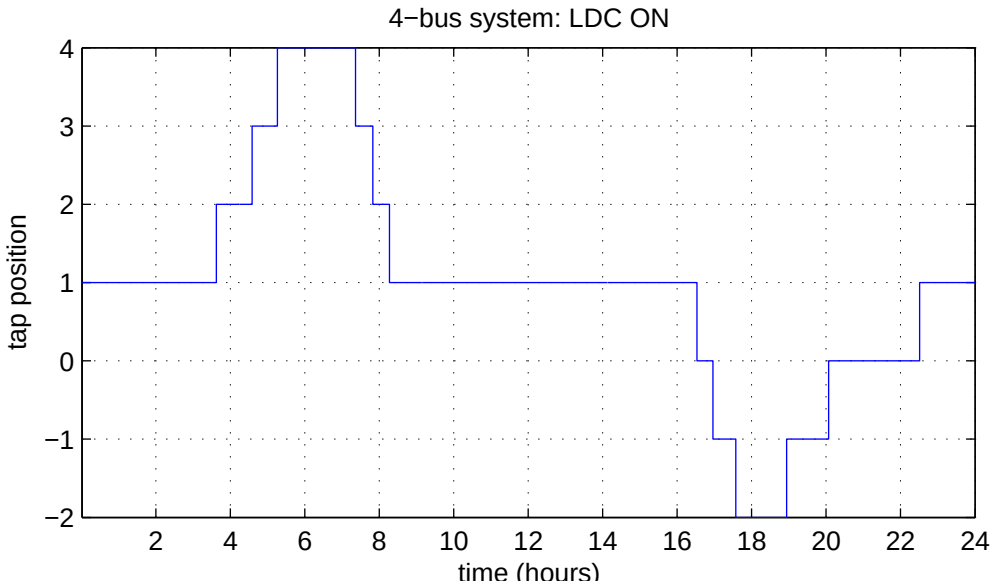

Figure 3.19: *OLTC tap position for the 24-hour simulation (LDRC)*

3.12 Summary

In this chapter the methodology for modelling a distributed generator within a distribution network was presented. A complete source-to-network model of a small hydro scheme has been constructed. The model is modular and therefore allows easy replacement of any of its components for further studies, e.g. control system development, or investigation of alternative means of power generation. The various components were represented using standard models found in the literature in order to allow comparison of the simulation results with related work. Automatic power factor mode and automatic voltage control mode, the two usual methods of operation of a synchronous generator were then presented. In addition, Automatic Voltage Control and Line Drop/Rise Compensation, two types of voltage control using transformers with On-Line Tap Changers were illustrated. The operation of the OLTC was assumed to be ideal. Further work could include consideration of the inaccuracies of the emulating circuit for the Line Drop Compensator. The operational aspects of utilisation of synchronous generators in distribution networks were also discussed, with particular interest on the determination of their range of allowed operation as defined by the machine characteristics and the DNO requirements. This was achieved

by representing the capability diagram of the synchronous generator as a 3D locus and combining it with the voltage surface on the $P - Q$ plane. This is a very useful tool for visualising and understanding how a synchronous machine based power plant will behave in a weak network. Finally the working of the developed small hydro scheme model was shown by simulating two characteristic events, namely generator loading and sudden loss of load, as well as operation of the OLTC in a network with a varying load. In the following chapter a similar procedure is followed to model and investigate the operation of a variable speed wind turbine including a Doubly Fed Induction Generator.

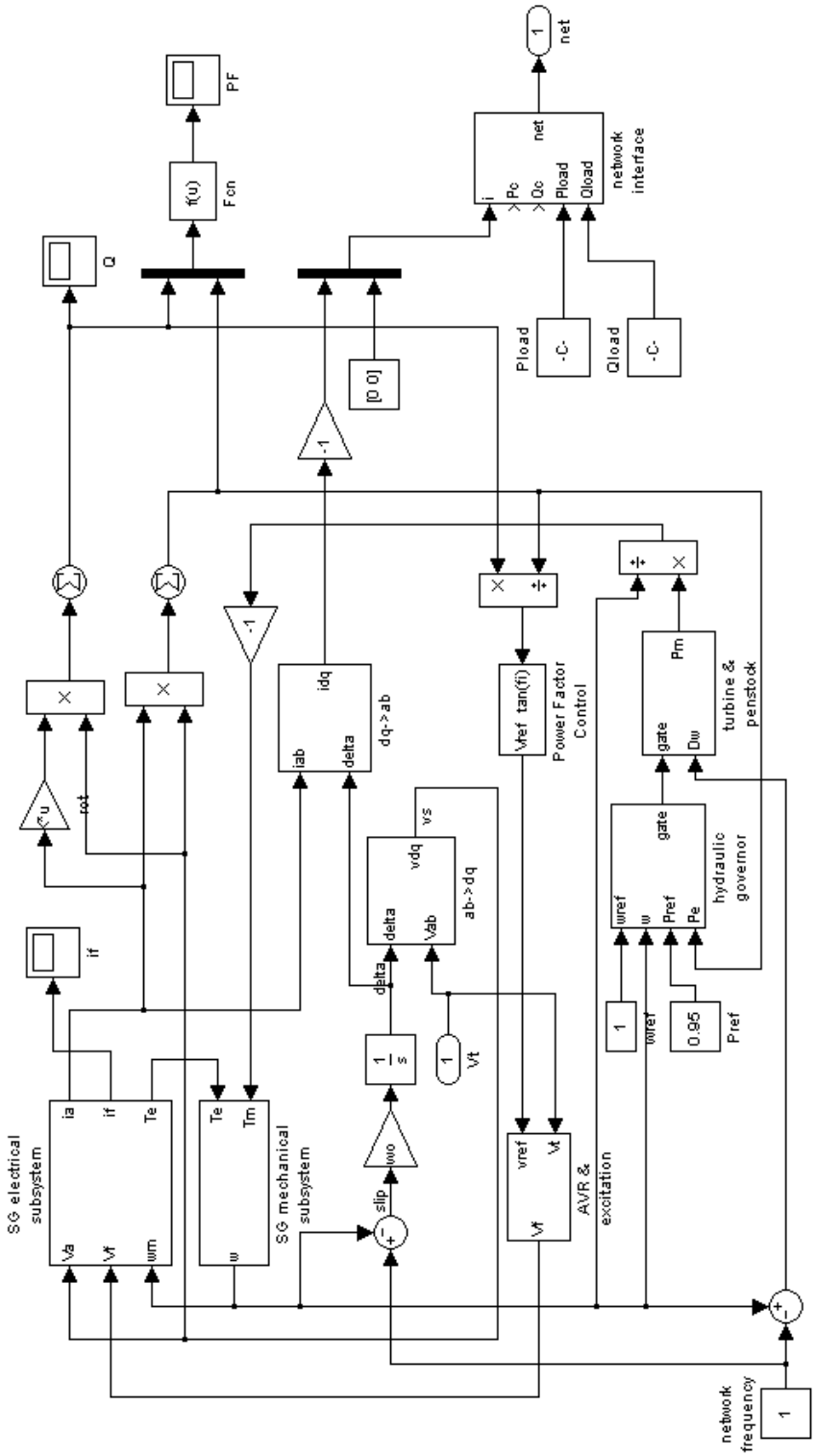

Figure 3.21: *Top-level block diagram of the Simulink small hydro scheme model*

Chapter 4
Modelling of Wind Energy Conversion Systems

4.1 Introduction

In this chapter the current technology and modelling of wind energy conversion systems is presented. In particular, a detailed model of wind speed is presented and then the model of a variable speed wind turbine with its drive train is shown. The various configurations available for a wind energy conversion system are then discussed, and the chapter ends with an analysis of the dynamic model of the doubly-fed induction generator.

4.2 Wind Energy Conversion System Modelling

There are a number of different designs of wind turbines (WTs) and selection is based upon their size and use. Hence wind turbines can be categorised as follows:

- large (MW range) or small (kW range);
- grid connected or isolated;
- onshore, nearshore or offshore.

The design of the mechanical part of the (grid connected) large onshore WECSs, which was studied in this work, follows invariably the 3-bladed, horizontal axis turbine model although some different old and experimental setups exist. A 3-D representation of the nacelle and rotor of a 3-bladed, horizontal axis wind turbine is depicted in

Figure 4.1. The most common design for the electrical part features a standard squirrel cage induction generator (SCIG) but due to its versatility, the doubly fed induction generator (DFIG) is nowadays being increasingly utilised. A third alternative is the Synchronous Generator (SG), either direct-drive or with a gearbox, and there are several implementations of WECS using SGs by various manufacturers.

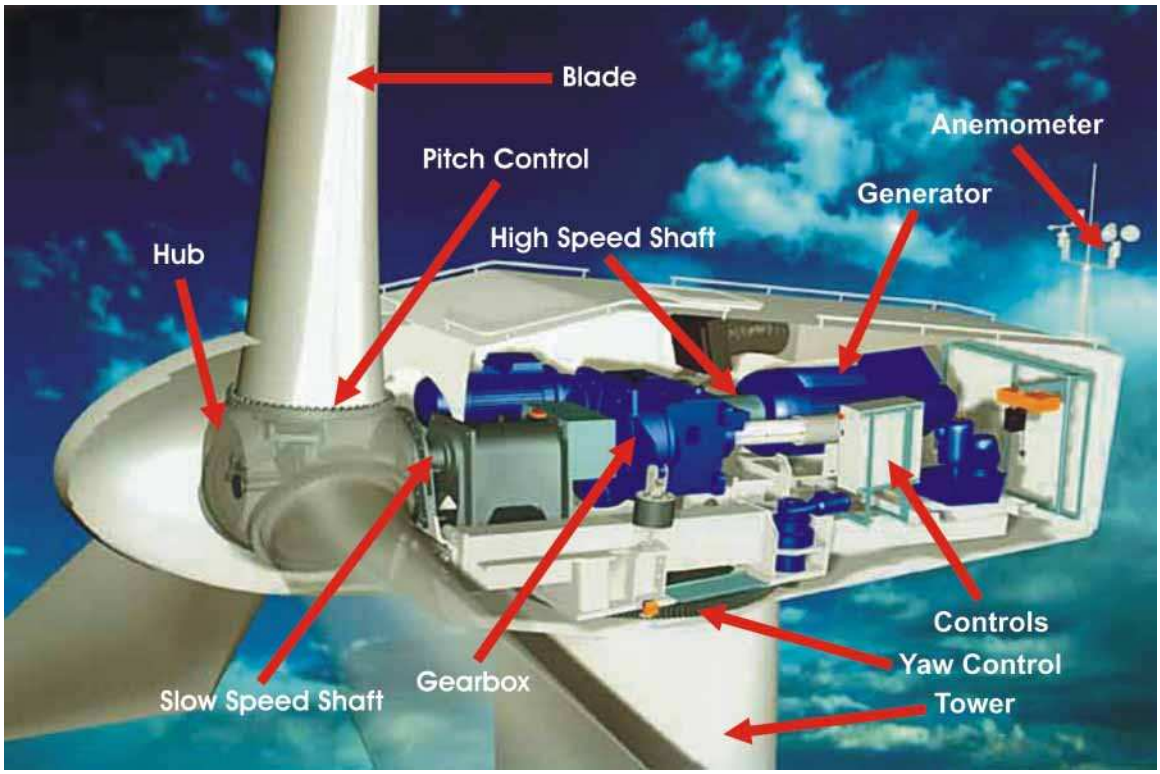

Figure 4.1: *Diagram of a 3-blade, horizontal axis wind turbine, image courtesy of Vestas*

Depending on the generator type the WT can be constant or variable speed. In a typical SCIG based WECS the slip, and hence the speed can vary typically only from 102% to 106% from nominal 104%; therefore the turbine operates nearly at constant speed. DFIG and SG based wind turbines can operate in a much wider range of speeds (typically up to ±30% of nominal) by decoupling the rotor mechanical speed and the network frequency through use of power electronic converters. Full variable speed operation of an SCIG can also be achieved by installing a power electronic converter between the generator and the network. A WT benefits from operating over a wide

range of speeds by the reduction of mechanical stresses on the blades and the WT body during wind gusts, as the extra wind energy is converted to increased (rotational) kinetic energy. Furthermore, this momentary storage of energy increases the efficiency of the WT and improves the quality of the electricity supplied by smoothing out the fluctuations of generated power [59, 60]. A disadvantage of variable speed operation is the need for a Power Electronic Converter (PEC) that decouples the network electrical frequency from the varying rotational speed of the WT. Use of PECs increases the overall cost of the WECS and can introduce harmonics [61].

The most common method of control of power flow within a constant speed WT is stall control, which is passive, as it constrains the rotor's rotational speed to its rated value by proper aerodynamic design of the blades. The design of the blades in a stall-controlled WT intrinsically regulates the power production. The blades have fixed pitch and operate near or at the optimal tip speed ratio at low wind speeds. The aerodynamics of the blades are such that with the increase of wind speed, the stall effect occurs on an increasingly larger part of the blade, thus reducing blade efficiency and therefore limiting output power. A stall regulated WT coupled to an SCIG is the so-called 'Danish' model and is the most common WT type installed today.

Variable speed WTs mainly use pitch control to actively regulate the rotational speed by altering the pitch angle of the blades (or parts of them). Below rated power such WTs operate at a fixed (optimal) pitch with a variable rotational speed in order to maintain an optimal tip speed ratio and therefore maximise efficiency and output power. When rated power is reached, pitch control is used to keep rotor speed within safe operation limits. While wind speed fluctuates, power output can be maintained almost constant by allowing the rotor to accelerate (thus storing energy) or to decelerate (thus supplying energy) [62]. Despite the associated cost rise, pitch control is attractive as it increases significantly the turbine efficiency [63]. Petersen in his 2000 work for the Danish Energy Agency showed that a pitch-regulated WT will yield 2.5% more energy than a dual-speed stall-regulated WT operating under the same conditions [64], and the increase in production will be even higher when compared to single-speed WTs. Figure 4.1 shows the diagram of an active pitch regulated WT made by Vestas, where

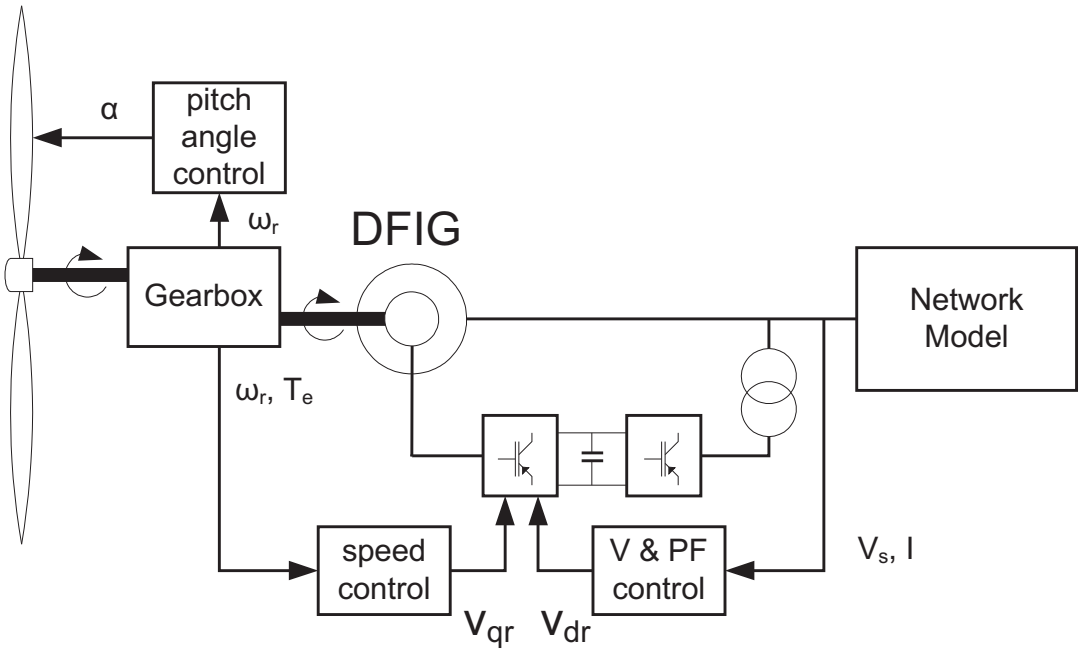

Figure 4.2: *Functional diagram and power transfer in a Wind Energy Conversion System*

the pitch control mechanism is located in the hub.

On the electrical side both real and reactive power may be controlled by appropriate action on a power electronic converter. Figure 4.2 shows the functional diagram of a WECS. Functionally, a WECS can be divided into four parts; rotor, drive train, generator and control system.

The wind turbine rotor consists of the blades and the hub, and is regarded as the most crucial element of the whole WECS because the overall efficiency of the WT is largely dependent on the aerodynamic design of the blades. Further, due to their size, their weight is an important factor from the design and cost standpoints [65]. The rotor diameter has increased from 12 m in late 1970's for a 50 kW turbine, to 120 m for the latest 4.5 MW turbines. Consequently, tower height has also increased from 25 m to 100 m [66].

4.2.1 Wind Modelling

The power in watts of a wind stream passing through an area A can be calculated from the following equation:

$$P_{wind} = \frac{1}{2} \times \rho \times A \times v_{wind}^3, \tag{4.1}$$

where ρ is the air density in kg/m^3 and v_{wind} is the instantaneous wind speed in m/s. Air density varies with the location and with time and it is approximately $1.26kg/m^3$ at 20^oC in a standard atmosphere. For wind turbines, A is the swept area of the blades and equals $\pi \times (\frac{D}{2})^2\ m^2$, where D is the diameter of the rotor in metres. It is therefore obvious that the wind power varies in proportion to the square of the WT diameter and the cube of the wind speed. However, Betz's law [67] proves that the theoretical maximum power that can be extracted from wind equals $16/27 \times P_{wind}$. Turbulent and non-homogeneous air flow, as well as friction losses typically reduce extracted power to about 0.5 of the power contained in the wind.

The variability of wind speed can be efficiently represented with a probability density function with a Weibull distribution according to the following equation [65]:

$$p(v_{wind}) = \left(\frac{k}{c}\right) \times \left(\frac{v_{wind}}{c}\right)^{k-1} \times e^{-\left(\frac{v_{wind}}{c}\right)^k}, \tag{4.2}$$

where k is the shape factor and c is the scale factor, both location-dependent parameters. These parameters can be calculated from the mean wind speed $\bar{v}$ (m/s) and the standard deviation σ_v using the following empirical equations [65]:

$$k = \left(\frac{\sigma_v}{\bar{v}}\right)^{-1.086}, \tag{4.3}$$

and

$$c = \bar{v} \times \left(0.568 + \frac{0.433}{k}\right)^{-\frac{1}{k}}. \tag{4.4}$$

For onshore sites, a typical pair of σ_v and $\bar{v}$ is 3.715 and 8 m/s, which gives $k = 2.3$ and $c = 9.033$. Figure 4.3 shows the probability density function for a wind speed time series with these characteristics.

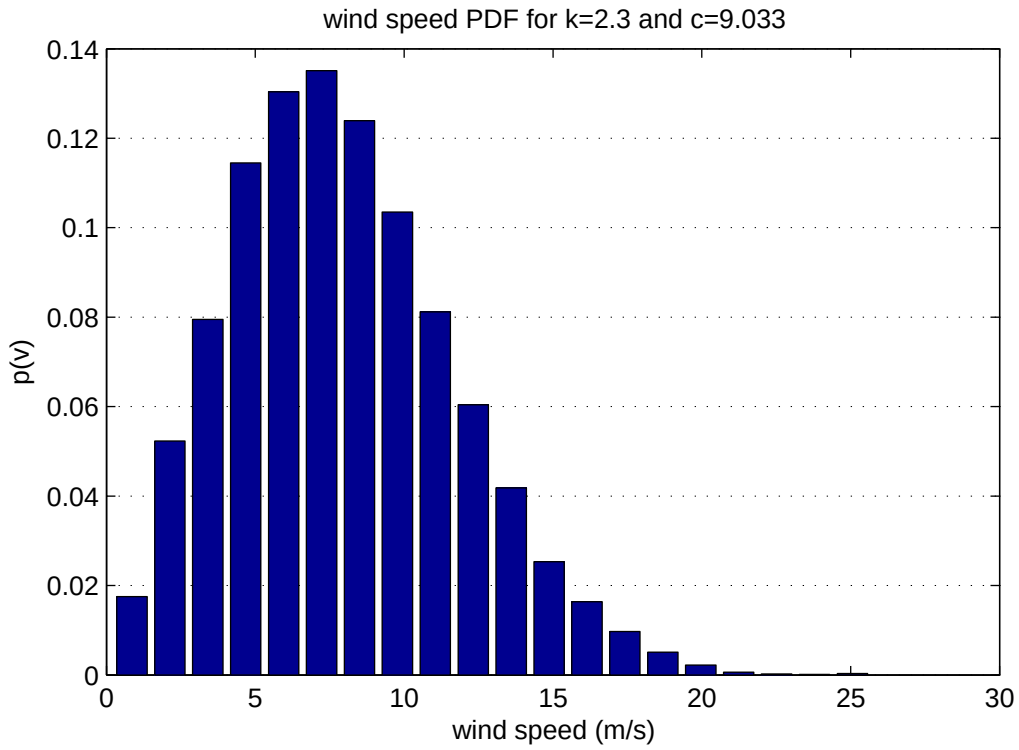

Figure 4.3: *Probability density function for a wind speed time series with k=2.3 and c=9.033.*

Wind speed can also be modelled as the Fourier series of a periodic signal. In this case, wind speed is given by:

$$v_{wind}(t) = \alpha_0 + \sum_{m=1}^{\infty} \alpha_m cos(2\pi m \Delta f t + \phi_m), \tag{4.5}$$

where: α_0 is the mean wind velocity in m/s,
Δf is the frequency interval in Hz,
m is the index of the frequency component, and
ϕ_m is the initial uniform random phase of the m_{th} frequency component, which varies from 0 to 2π.

Transitions between largely different wind speeds (i.e. wind gusts) are less likely to occur than smoother changes. For a given measured wind speed time series this tendency is described by the autocorrelation function:

$$R(r\Delta t) = \frac{1}{\sigma_v^2 \left(N_s - r\right)} \times \sum_{i=1}^{N_s - r} \left(u_i \times u_{i+r}\right), \tag{4.6}$$

where: r is the lag number,
Δt is the sample period and
N_s is the number of samples in the data series.

The autocorrelation function will start from 1.0 for $r = 0$ and will eventually decay to zero for an $r > 0$. The integral of $R(r\Delta t)$ over that period is called the integral time scale of turbulence and is a measure of the average time that the data are considered correlated over time. Typical values are below 10 seconds, but longer periods are possible too.

The frequency spectrum $S(f)$ is taken from [65] and is given by:

$$S(f) = \frac{4\sigma_v^2 \left(L/\bar{u}\right)}{\left[1 + 70.8 \left(fL/\bar{u}\right)^2\right]^{5/6}}, \tag{4.7}$$

where L is the integral length scale, which can be found by multiplying the mean wind speed with the integral time scale that throughout this thesis is set to be equal to $10s$ [65].

From this, the Fourier parameter α_m can be derived as:

$$\alpha_m = \sqrt{S(m\Delta f) \times \Delta f} \tag{4.8}$$

The wind speed time series used in this thesis was generated as follows. A 30 minute average of the wind speed over 24 hours is first generated. Then, for each half-hour

interval a time series is generated using equations 4.5 to 4.8. This results to a wind speed time series with a Weibull probability density function with the parameters shown in 4.3. This simulation represents a windy "day" at a location of a fairly flat grass field, a typical case of the Scottish landscape. In order to avoid periodicity of the generated signal the period interval $\Delta T = 1/\Delta f$ has to be longer than the duration of the signal, which in this case is $1800s$. Therefore it is set that $\Delta T = 2000s$ and $\Delta f = 5 \times 10^{-4} Hz$. In order to include frequencies up to $1Hz$, the frequency index m in Equation 4.5 is constrained to a maximum of 2000. The same procedure is repeated for all the 30 minute intervals of the 24 hours. Due to the large number of frequency components this can be a time consuming procedure if sufficient computing power is not available. For the purposes of this work, a wind speed time series for 24 hours, sampled at 1 Hz, was generated using the described method. Figure 4.4 shows a wind speed time series obtained by the this procedure (blue trace) together with the 30 minute average wind speed (red trace) for a period of 24 hours.

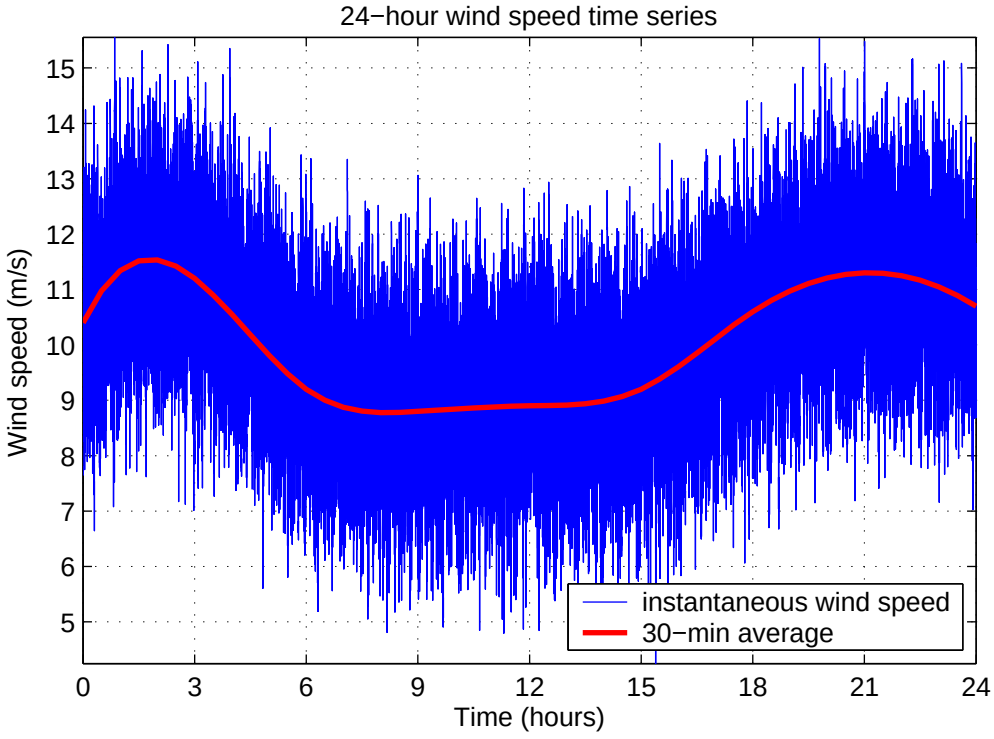

Figure 4.4: *Wind speed time series sampled at 1 Hz (blue) and 30 min. average (red)*

A 3-minute zoom (from 02:45 to 02:48) of the same time series is depicted in Figure 4.5. The mean wind speed of this period was $10m/s$. On this particular "day", the average wind speed is mostly flat at about $9m/s$, with two more "windy" periods at around 02.00 and 21.00 hours with maximum average speeds of about $11.6m/s$.

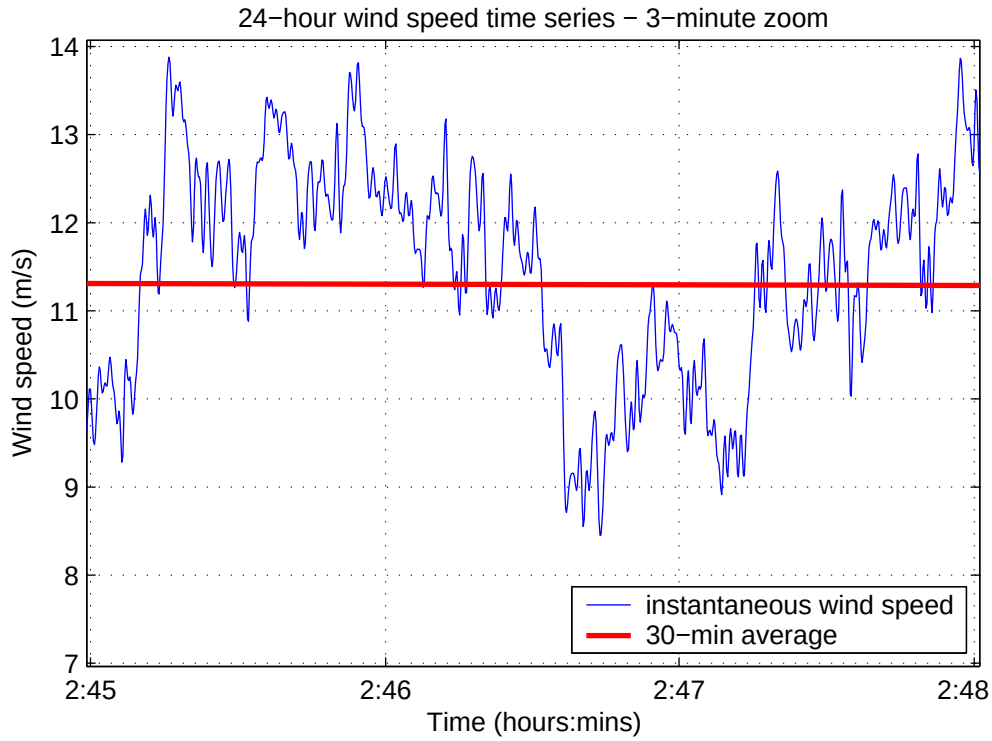

Figure 4.5: *A 3-minute zoom of the wind speed time series*

An alternative method to eliminate periodicity without the need for a high Δf is described in [68]. In this approach, a small, uniformly distributed random phase is added in Equation 4.5, in order to convert the stationary process to a quasi-stationary process.

Another wind speed model that takes into account the autocorrelation property of the wind speed can be obtained by using discrete Markov process theory [69]. The wind spectrum is divided into smaller regimes and the transition from one regime to another is governed by a Stochastic Transition Probability Matrix (STPM) which is constructed by processing measured wind speed time series or obtained by a Weibull PDF. Once again the STPM is site-specific and prone to periodic changes.

4.2.2 Dynamic Model of a Variable Pitch Wind Turbine

Complete aerodynamic modelling of a wind turbine leads to a set of high-order nonlinear equations. However, the scope of this thesis does not include the dynamics of the blades and therefore it allows significant simplifications of the wind turbine dynamics, as they do not impose a notable effect on the steady state operation of the WECS. Akhmatov *et al.* in [70, 71] propose that the wind turbine operation can be modelled as the Laplace transform of a 1st order differential equation. This is caused by a phenomenon known as spatial filtering. The total torque of the rotor is the sum of the torques of each blade element. However, wind speeds at all points of the rotor disk are not equal, therefore the applied torque to each blade element is not uniform. Hence the total torque variance is less than the variance of torque for each blade because turbulence factors of the blades partially cancel each other. The incident wind speeds of two points are correlated but this correlation is reduced with increasing distance from one another. Therefore on large wind turbines, the large swept area brings about an averaging of the wind speed, thus acting as a low pass filter of the form:

$$G(s) = K_w \times \frac{1 + sT_{w1}}{1 + sT_{w2}}. \tag{4.9}$$

The gain K_w and the time constants T_{w1} and T_{w2} are depended on the wind turbine design. Their approximation is based on emperical data and is based on the fact that a larger turbine will filter more effectively the wind turbulence. A medium size WT with an induction generator will have $K_w = 1$, $T_{w1} = 3.3$ s and $T_{w2} = 0.9$ s. A similar approximation is also discussed in [72].

As mentioned in the previous section, a wind turbine rarely achieves conversion of more than 50% of the available power in the wind. The power coefficient c_p of a variable speed WT varies with the blade pitch angle α (degrees) and the tip speed ratio λ, i.e. the ratio of the tangential velocity of the blade tip and the wind speed component that is prependicular to the rotor disk. Therefore the converted mechanical power of the WT becomes:

$$P_m = c_p(\lambda, \alpha) P_w = \frac{1}{2} c_p(\lambda, \alpha) \rho A v_{wind}^3 \tag{4.10}$$

From Equation 4.10 the definition of the power coefficient c_p can be derived as the ratio of extracted over available power:

$$c_p = \frac{P_m}{P_w} \tag{4.11}$$

The power coefficient has a non-linear relationship with blade pitch angle α and tip speed ratio λ. There are a number of methods followed to model this relationship, such as Look-Up Tables, splines, and linearisation using Taylor series. Another approach is to develop a numerical approximation of $c_p(\lambda, \alpha)$ curves generated from measurements on real turbines [73, 74]. This is the method that was followed here, using the numerical example presented in [74]. According to this, $c_p(\lambda, \alpha)$ can be calculated using the following two equations:

$$c_p(\lambda, \alpha) = c_1 \left(c_2 - c_3\alpha - c_4\alpha^x - c_5\right) e^{-c_6(\lambda,0)} \tag{4.12}$$

and

$$\frac{1}{\lambda_i} = \frac{1}{\lambda - 0.02\alpha} + \frac{0.003}{\alpha^3 + 1}. \tag{4.13}$$

The values of c_x parameters are selected as below [73]:

$c_1 = 0.73 \quad c_2 = 116/\lambda_i \; c_3 = 0.4$
$c_4 = 0.0 \quad c_5 = 5/\lambda_i \quad c_6 = 12.5/\lambda_i$

A series of $c_p(\lambda, \alpha)$ curves versus λ for some values of α is depicted in Figure 4.6 below. It is shown that power coefficient rises with decreasing pitch angle α. It is also notable that the optimum tip speed ratio is different for every blade pitch angle α.

The power output versus rotor speed of a 2 MW wind turbine with the above characteristics and a rotor diameter of 75 metres is shown in Figure 4.7 for various wind speeds. This graph was generated by combining Equations 4.10, 4.12 and 4.13.

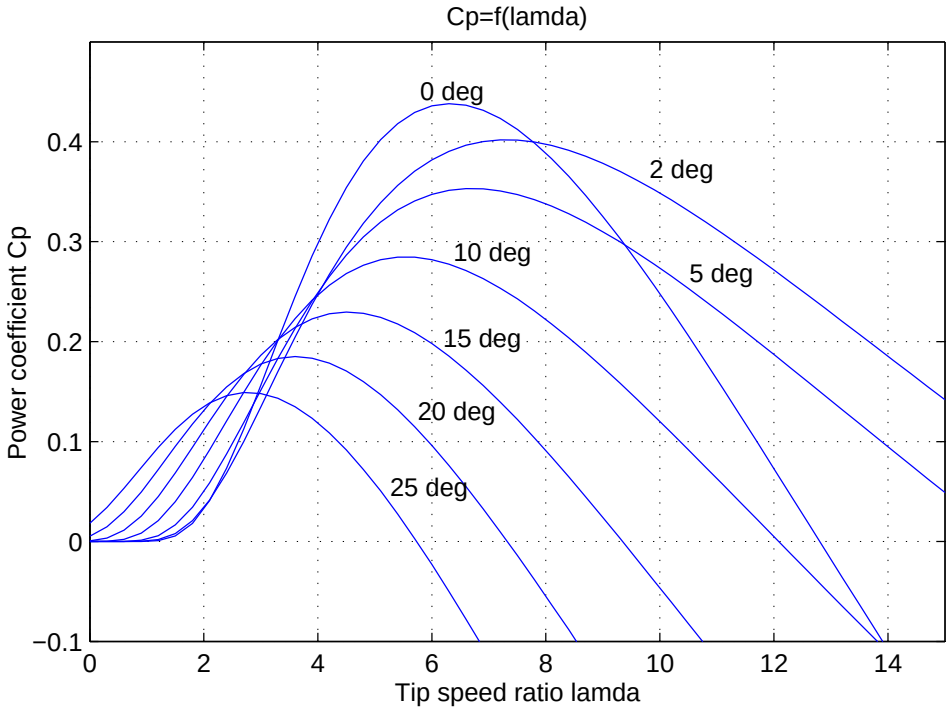

Figure 4.6: *Power coefficient versus tip speed ratio for various values of blade pitch angle. Regenerated after Slootweg* et al.*, 2001*

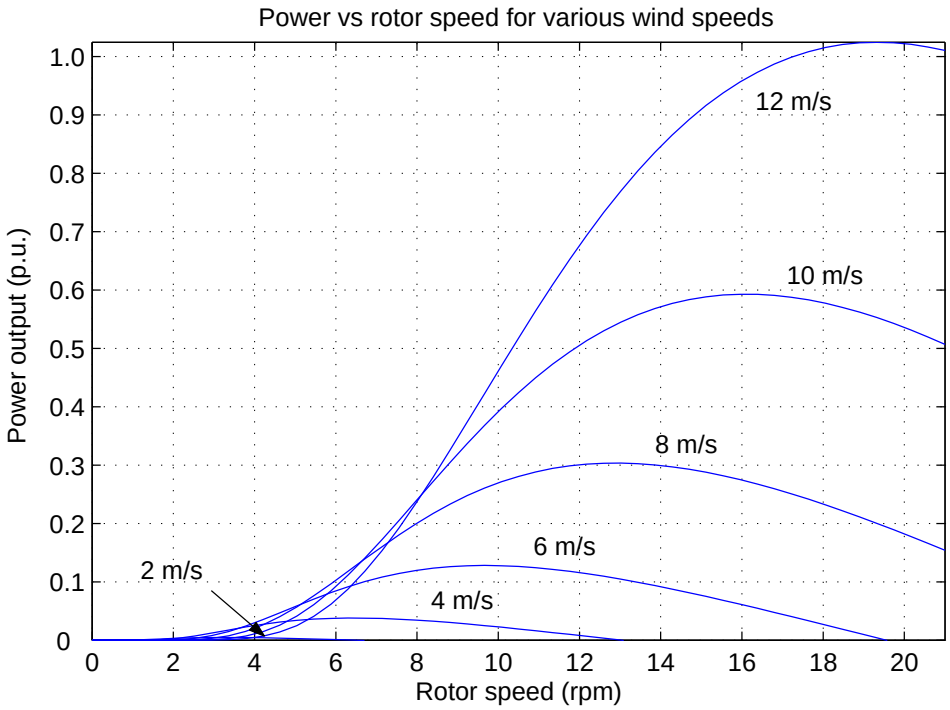

Figure 4.7: *Power capture versus rotor speed for various wind speeds*

The equation of motion of the wind turbine can be derived in the same manner as in the case of the small hydro generator that was presented in the previous chapter. In per unit terms it is given by:

$$2H\frac{d\omega_m}{dt} = T_m - T_e, \tag{4.14}$$

where H is the inertia constant in seconds, ω_m is the per unit mechanical angular velocity, T_m and T_e are the mechanical and electrical torques, respectively, in per unit. This model assumes no interaction between the drive train and tower dynamics and no periodic phenomena such as gravitational forces on the blades or shadowing of the tower.

4.2.3 Electric Generators for WECSs

The most common turbine-generator configurations are shown in Figure 4.8. The first one (a) is the typical "Danish" concept, which consists of a constant speed, stall regulated induction generator directly connected to the network. This is the cheapest and most robust solution and the vast majority of the installed WECSs follow this scheme. Its major disadvantage is the complete lack of active control of the generator. Diagram (b) shows the variable speed version of the "Danish" concept.

In the variable speed configuration the induction generator is connected to the network through a power electronic converter, which decouples the rotor's speed from the network frequency, allowing the WT to vary its rotational speed. This way the energy yield is higher as the turbine can be controlled to operate always at its highest efficiency (tip speed ratio). Additionally, the power surge during wind gusts is less severe, as the rotor is allowed to accelerate (or decelerate) thus acting as a short-term buffer. The disadvantages of this configuration are (i) the added cost of the converter and (ii) the harmonics that the power electronics introduce to the system, as the converter that is connected in series to the generator has to cater for the whole power transfer between the generator and the network. A similar scheme is shown in (c), where the induction generator has been replaced by a high-speed synchronous generator.

Diagram (d) shows a direct driven (no gearbox) synchronous generator based WECS.

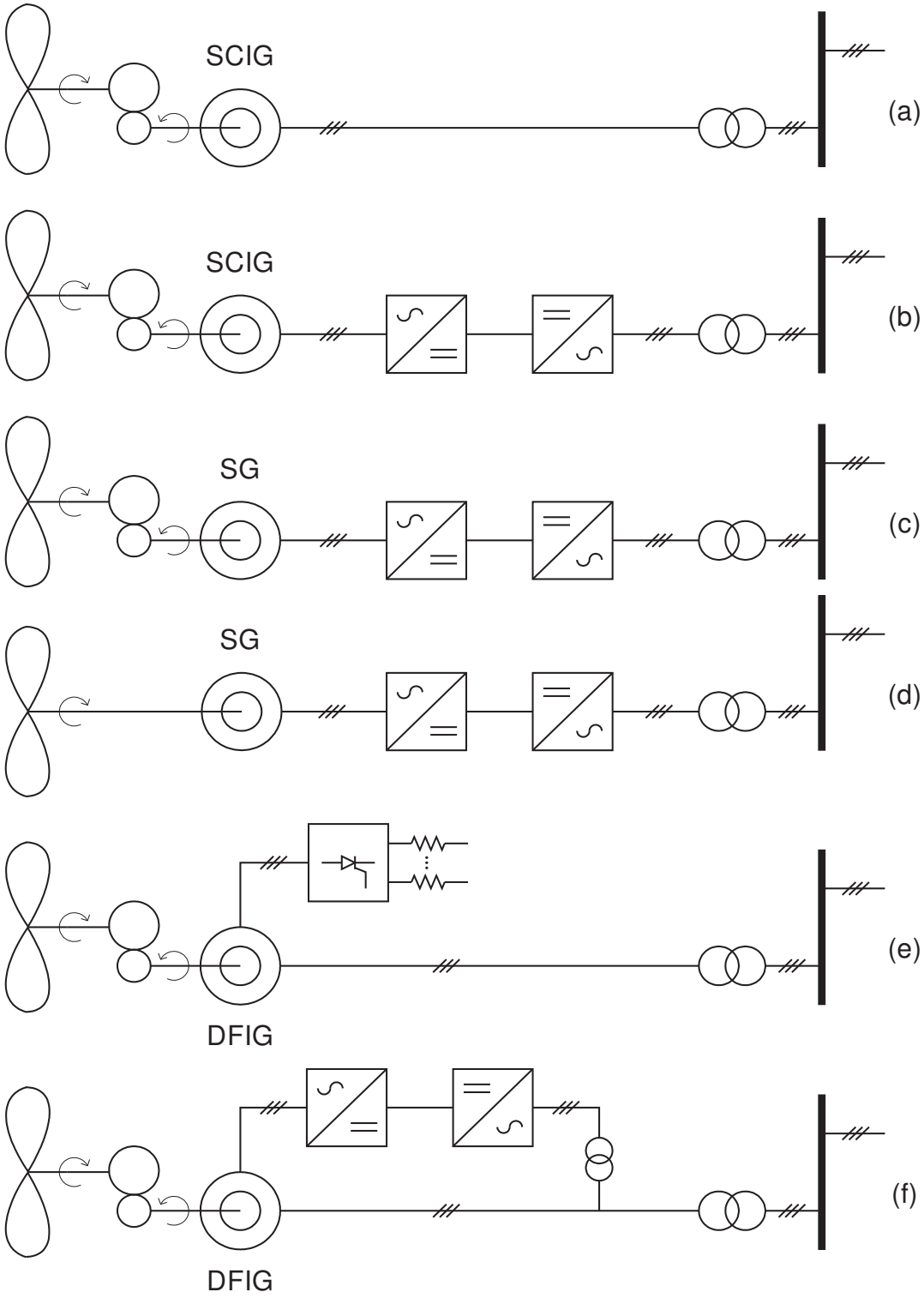

Figure 4.8: *Most common generator topologies of wind energy conversion systems*

The generator used in this case is a multi-pole, low-speed synchronous machine. This generator may be more expensive than the high-speed SG, but the extra cost is balanced by the savings due to the lack of a gearbox, which is the most expensive and sensitive part of a WECS.

The last two diagrams show WECSs that utilise the Doubly-Fed Induction Generator (DFIG). In (e) the speed of the generator can be increased by up to 20% over synchronous speed by altering the rotor circuit resistance by means of power electronic switches. Finally, diagram (f) shows a DFIG-based WT that is controlled by injecting a voltage to the rotor through a back-to-back power electronic converter. This configuration allows a ±30% variation around synchronous speed. By feeding only the rotor circuit, the converter can be significantly smaller than in cases (b), (c) and (d) (typically 30% of rated generator power) which means that it is much cheaper and generates less harmonics [75]. This is the system that will be mainly considered in this thesis.

4.2.4 Dynamic Model of the Doubly Fed Induction Generator

The dynamic model for the doubly fed induction generator will be constructed in the dq reference frame, as in the case of the synchronous generator in Chapter 3. The DFIG can be described in per unit by the following equations:

The generator convention is applied, which means that rotor and stator currents are positive when they are outputs.

$$v_{ds} = -R_s i_{ds} - \omega_s \psi_{qs} + \frac{d\psi_{ds}}{dt} \tag{4.15}$$

$$v_{qs} = -R_s i_{qs} + \omega_s \psi_{ds} + \frac{d\psi_{qs}}{dt} \tag{4.16}$$

$$v_{dr} = -R_r i_{dr} - s\omega_s \psi_{qr} + \frac{d\psi_{dr}}{dt} \tag{4.17}$$

$$v_{qr} = -R_r i_{qr} + s\omega_s \psi_{dr} + \frac{d\psi_{qr}}{dt} \tag{4.18}$$

where ω_s is the stator electrical frequency, ψ the flux linkage, s the rotor slip, indices

s and r are stator and rotor quantities, and finally d and q represent the direct and quadrature components. The rotor slip is given by:

$$s = \frac{w_s - pp \times w_m}{w_s}, \tag{4.19}$$

where pp is the number of pole pairs and ω_m is the mechanical angular speed of the generator in rad/s.

The dq reference frame is oriented so that the d-axis coincides with the maximum of the stator flux and q-axis is preceding the d-axis by 90^o. Therefore $\psi_{ds} = \psi_s$ and $\psi_{qs} = 0$. Hence, from Equations 4.15 and 4.16 results that $v_{ds} = 0$ and $v_{qs} = v_s$, which is equal to the terminal voltage.

The flux linkages in Equations 4.15 to 4.18 are given in per unit by:

$$\psi_{ds} = -(L_s + L_m)i_{ds} - L_m i_{dr} \tag{4.20}$$

$$\psi_{qs} = -(L_s + L_m)i_{qs} - L_m i_{qr} \tag{4.21}$$

$$\psi_{dr} = -(L_r + L_m)i_{dr} - L_m i_{ds} \tag{4.22}$$

$$\psi_{qr} = -(L_r + L_m)i_{qr} - L_m i_{qs} \tag{4.23}$$

where Lm represents mutual, L_s stator and L_r rotor leakage inductance respectively.

The real and reactive power generated (or consumed) by the doubly fed induction generator are given by:

$$P_g = v_{ds}i_{ds} + v_{qs}i_{qs} + v_{dr}i_{dr} + v_{qr}i_{qr} = P_s + P_r \tag{4.24}$$

$$Q_g = v_{qs}i_{ds} - v_{ds}i_{qs} + v_{qr}i_{dr} - v_{dr}i_{qr} = Q_s + Q_r \tag{4.25}$$

Assuming no losses within the turbine, the power given by Equation 4.10 equals the generated (and supplied to the network) electrical power of Equation 4.24. However, Equation 4.25 represents the reactive power *of the machine*, which is not necessarily equal to that exchanged with the network. Whereas the stator circuit is directly connected to the network (and therefore P_s and Q_s are directly exchanged with it), the

rotor circuit is connected through the power electronic converter. The network-side of the latter is able to generate or absorb reactive power independently and the rotor-side of it can provide the MVAr requirements of the DFIG rotor. Therefore Q_r disappears from Equation 4.25, and at its place Q_c is added. However, in order to reduce the rating (and hence the cost) and losses of the network-side converter, in most cases the converter control strategy is to keep $Q_c = 0$, although other strategies can be applied as well (e.g. $Q_{net} = Q_s + Q_c = 0$). It should be noted that the converter cannot store real power, therefore $P_r = P_c$ and $P_g = P_{net}$. The following equation gives the electro-mechanical torque developed by a doubly fed induction generator:

$$T_e = \psi_{ds} i_{qs} - \psi_{qs} i_{ds} \tag{4.26}$$

Substituting the fluxes in Equation 4.26, it becomes:

$$T_e = L_m \left(i_{qr} i_{ds} - i_{dr} i_{qs} \right) \tag{4.27}$$

The changes in generator speed that result from a difference in electrical and mechanical torque can be calculated using the generator equation of motion (4.14). Equations 4.9 to 4.27 have been modelled to constitute a complete, wind-to-wire, dynamic model of a variable speed wind energy conversion system equipped with a doubly fed induction generator. In the next sections the required controllers for such a generation system will be discussed.

4.2.5 Blade Pitch Angle Controller

The blade pitch angle controller is one of the two components of a variable speed WT that controls the rotor speed. However in this implementation it has only a secondary role, as the main speed control function is performed by the speed controller described in the next section. The block diagram of the blade pitch angle controller is shown in Figure 4.9.

The pitch angle controller operates during high wind speeds when the maximum torque

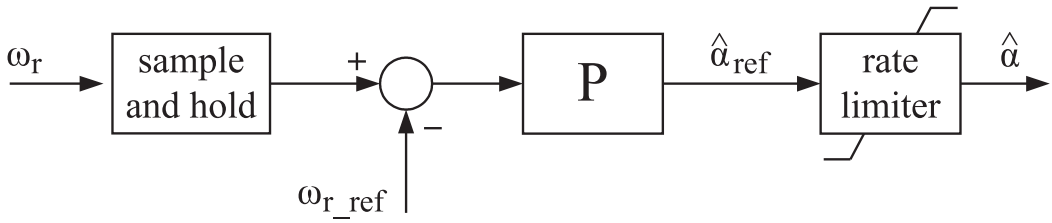

Figure 4.9: *Blade pitch controller for the wind turbine*

has been reached. Further increase of torque would overload the machine and the converter and therefore the pitch angle controller takes action by increasing the blade pitch, thus modifying the power coefficient curve $c_p(\lambda, \alpha)$ of the turbine as shown in Figure 4.6 [76]. The rotor's rotational speed ω_r (pu) is continuously sampled with a sample rate F_s typically about $2Hz$. The speed error between ω_r and reference (maximum) speed $\omega_{r_{ref}}$ is then fed to a Proportional (P) compensator, which outputs the reference pitch angle $\hat{\alpha_{ref}}$ (deg). By using a simple P compensator the rotor speed may overshoot by a 15%-20% from its nominal value, depending on the gain of the compensator. However this is acceptable as the WT structure can sustain such overspeeds and since the system is never in steady-state (due to the variability of wind), use of a Proportional-Integral (PI) compensator to minimise the offset error is not justified. The rate limiter models the function of the pitch mechanism, which has a finite rate of change (typically $3^o - 10^o$). It also constrains the pitch angle between the minimum and maximum values ($0^o - 30^o$).

4.2.6 Speed Controller

The speed controller is the main component used for rotor speed regulation. The controller objective described here is to optimise power extraction from wind. The blue trace Figure 4.10 shows graphically the relationship between rotor speed and power.

This curve, though, is sub-optimal for the reasons that will be discussed below. The optimal $P_m - \omega_r$ curve is represented by the red dashed trace. It consists of three rotor speed regions, divided by speeds at points A' and D'. At A' is the cut-in speed, below

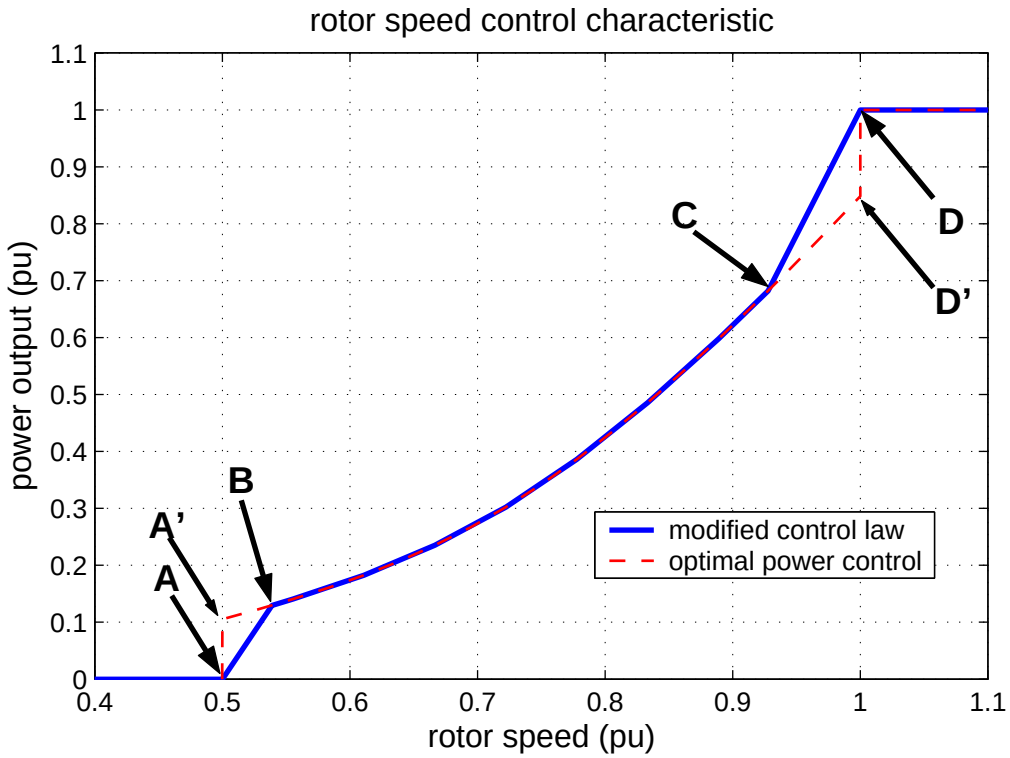

Figure 4.10: *Speed control characteristic for the DFIG*

which the wind turbine is turned off as the extracted power for these speeds will be very small and comparable to the losses. Between points A' and D', power rises in proportion to ω_r^3 and the objective of the speed controller is to track the maxima of the power coefficient curves for the particular wind speed (shown in Figure 4.6). When the rotor reaches its nominal speed, the speed controller objective changes to maintain power capture at rated value (1.0pu). That is the point that the blade pitch controller comes into play to constrain speed (and therefore power). However, the step changes at points A' and D' would bring about large power fluctuations when speed varies only a little around these values. Hence the step changes are replaced by the slopes A-B and C-D to allow a smoother change of power [77]. Obviously there is a trade-off between smooth operation and optimal power extraction as the farther the distance from A to B and C to D (smoother change of power), the greater the difference between optimal and actual power extraction will be [78]. Figure 4.11 shows the block diagram of the rotor speed controller.

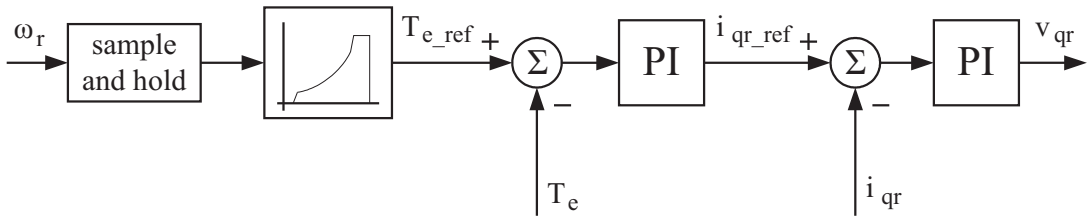

Figure 4.11: *Speed controller for the wind turbine*

Rotor speed is measured and sampled with a sample rate of a few tens of Hertz (typically $20Hz$). Using the sampled speed measurement and the control law depicted in Figure 4.10, a torque setpoint is generated by dividing the power derived from the graph with speed. It should be noticed that torque is used instead of power because it is proportional to i_{qr} and therefore makes control easier. Combining Equations 4.20 - 4.23, 4.31 - 4.34 and 4.26 and assuming that $r_s = 0$ it emerges that:

$$T_e = -\frac{L_m v_{qs}}{L_m + L_s} \times i_{qr} \tag{4.28}$$

The error between the derived torque setpoint and measured electrical torque is fed to a PI compensator to define the i_{qr} reference value. Then the error between $i_{qr_{ref}}$ and actual i_{qr} is fed in turn to a second PI in order to generate the v_{dr} reference, which is then sent to the rotor side inverter.

4.2.7 Voltage / Reactive Power Controller

One of the most important advantages of doubly fed induction generators over standard squirrel cage machines is that their reactive power can be controlled and this makes them a very attractive option especially when the network that the turbine or farm is going to be connected is weak [79, 80]. The reactive power exchanged between the DFIG and the network is regulated by the controller shown in Figure 4.12.

Assuming that $r_s = 0$, by combining Equations 4.31 - 4.34 and 4.24 - 4.25, it can be

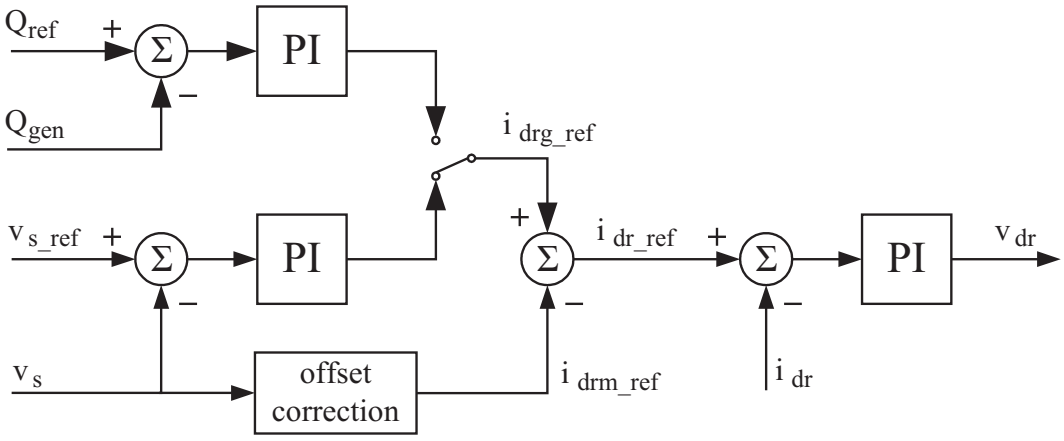

Figure 4.12: *Voltage / reactive power controller for the DFIG*

derived that the relationship between Q and i_{dr} is governed by the following equation:

$$Q_{gen} = -\frac{L_m i_{dr} v_{qs}}{L_m + L_s} - \frac{v_{qs}^2}{\omega_s (L_m + L_s)} \tag{4.29}$$

In the block diagram of Figure 4.12 the offset correction block calculates the current i_{drm} required for magnetising the rotor. This current can be found by the following equation:

$$i_{drm} = -\frac{v_{qs}^2}{\omega_s (L_m + L_s)} \tag{4.30}$$

If this value is used as a reference for i_{dr}, then the inverter will provide only the reactive power required for the magnetisation of the rotor and therefore no reactive power will be exchanged with the network and the DFIG will operate at unity power factor. In the block diagram of Figure 4.12, this would require the PI compensator responsible for voltage regulation (lower left) to be disabled. A reactive power setpoint could then be compared to generator's actual MVAr output, and with the assistance of the upper left PI compensator, the controller could perform Q or PF control. Alternatively the DFIG can operate in voltage control mode by selecting the lower left compensator.

4.3 Simulation of Wind Turbine Operation in a Distribution Network

The WECS model presented in this chapter has been constructed in Simulink. The top level diagram as well as the most important components of the WECS model are shown in Figure 4.14. In order for the model to be validated, it had to be comparable to that modelled and reported in the literature. Therefore the turbine and machine parameters presented in [74] have been used. These parameters are shown in Tables 4.1 and 4.2. Its main components are the wind turbine (as described by Equations 4.9 - 4.13), the DFIG (Equations 4.14 - 4.27), the real and reactive power controllers as shown in Figures 4.9 - 4.12 and finally the network model, which is implemented as a Matlab function. The 120 second wind speed time series shown in Figure 4.13 was used as an input to the model.

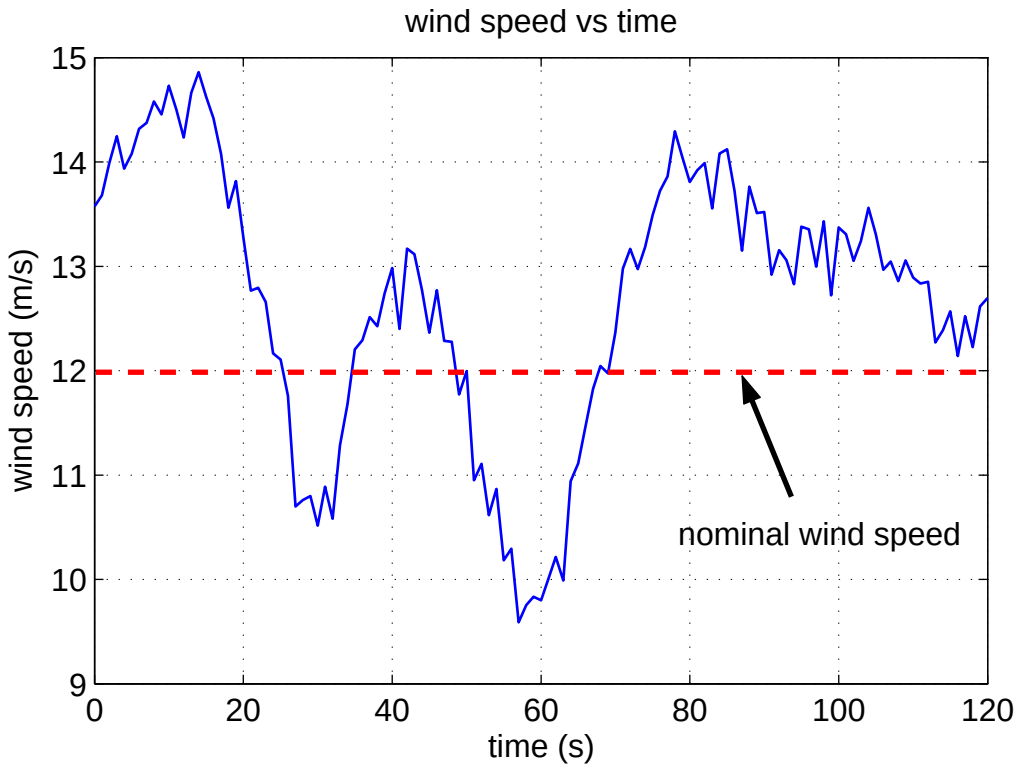

Figure 4.13: *120 second wind speed time series used for the simulations*

In the following simulations the network consists of a simple two-bus system, one of

which hosts the WT and the other is the slack bus. The two buses operate at 11kV and are connected by a line with $R_l + jX_l = 0.0443 + j0.0331$ pu on a 2MVA base. This is the equivalent of a 5km line made of a ACSR 54/9 type conductor.

rotor radius	37.5m
rotor speed range	9 - 21 rpm
rated power	2 MW
nominal wind speed	12 m/s
cut-in wind speed	3.5 m/s
gear box ratio	1:100
total moment of inertia	$5.9 \times 10^6 kgm^2$

Table 4.1: *Wind turbine characteristics*

pole pairs	2
generator speed range	900 - 2100 rpm
mutual inductance L_m	3.0pu
stator inductance L_s	0.1pu
rotor inductance L_r	0.08pu
stator resistance R_s	0.01pu
rotor resistance R_r	0.01pu
line resistance R_l	0.0443pu
line inductance L_l	0.331pu
network voltage	1.0pu
base voltage	11kV
base power MVA_{base}	2MVA

Table 4.2: *DFIG characteristics*

4.3.1 WT Operating at Constant Power Factor

The first simulation presents the conventional mode of operation of a wind turbine equipped with a doubly fed induction generator. At first, the voltage control component of the reactive power controller shown in Figure 4.12 is disabled and the power factor setpoint is set at 1.0 (no reactive power). Figure 4.15 shows the resulting real power export, rotor speed and blade pitch angle when the DFIG is operating at constant power factor mode.

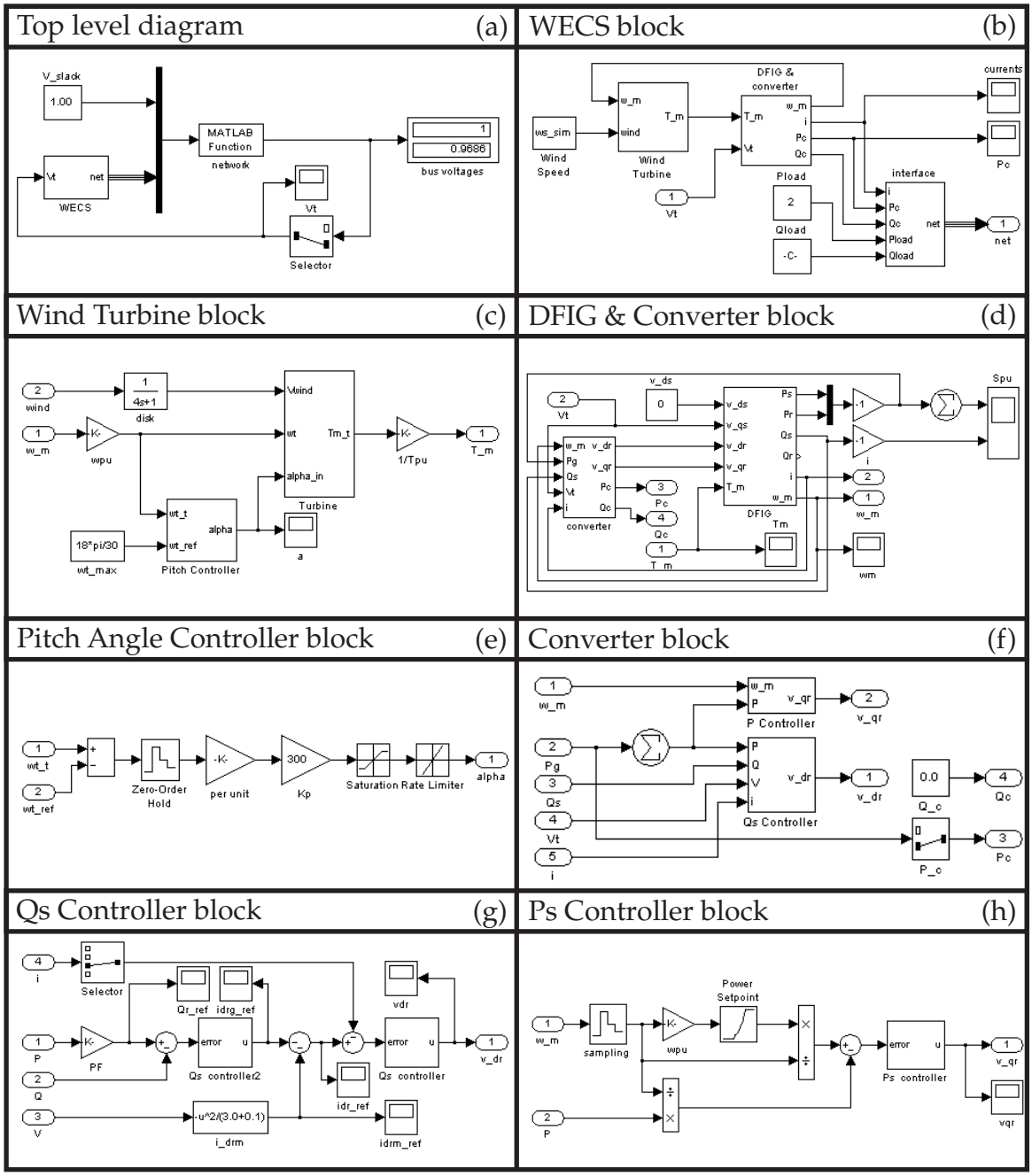

Figure 4.14: *Diagrams of the most significant blocks of the dynamic WECS model in Simulink. From (a) to (h): Top level diagram, WECS, wind turbine, DFIG and converter, pitch angle controller, power electronic converter, reactive power controller and real power controller. In (g) the Q_s controller has been set up to perform power factor control.*

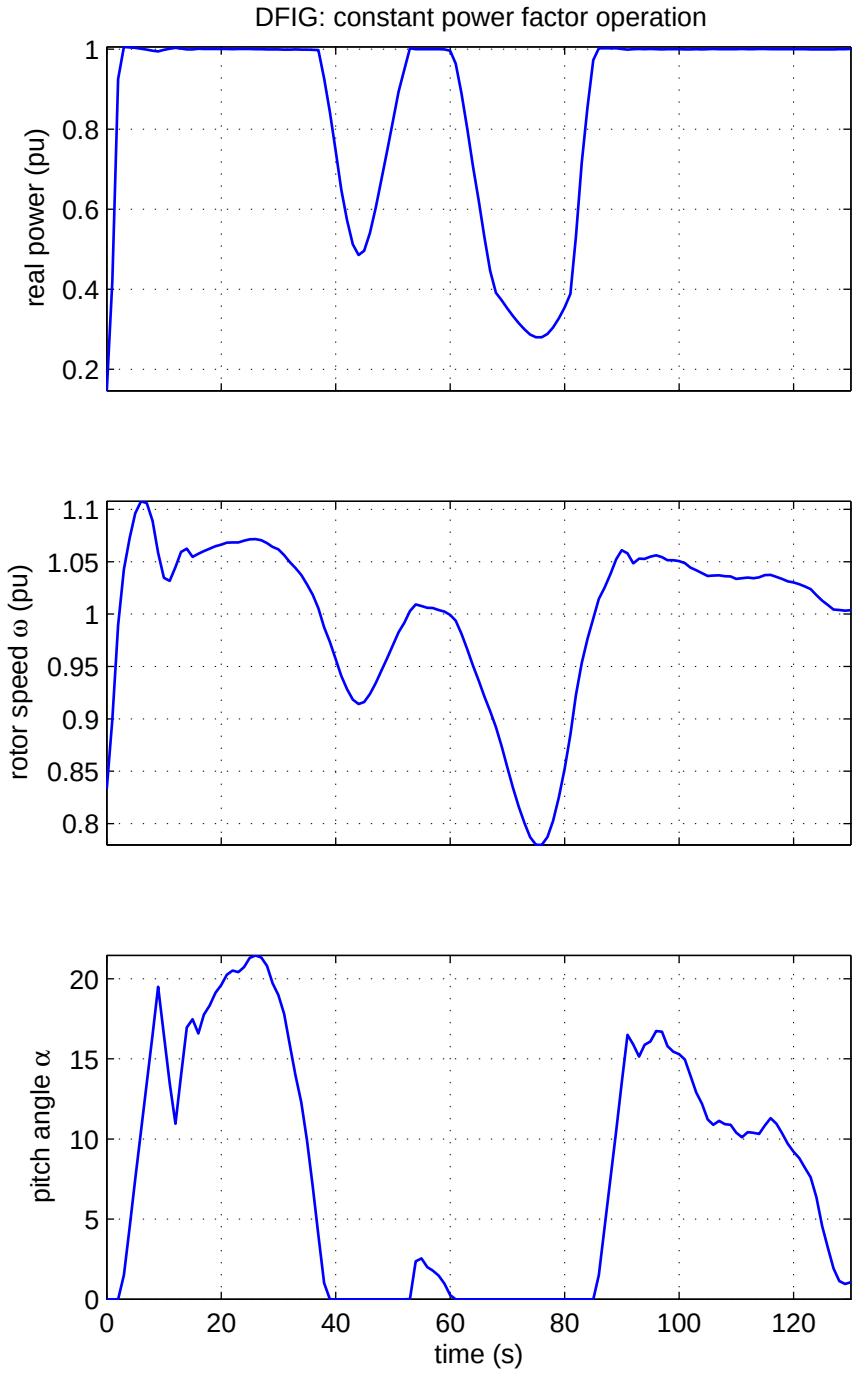

Figure 4.15: *Real power export, rotor speed and blade pitch angle for the DFIG in constant power factor operation*

The first observation is that the short-term transients of the wind speed have been smoothed away due to the averaging over the rotational area, the inertia of the system and the variable speed operation of the turbine, which acts as a short-term energy buffer. It is also shown that the speed varies between +10% and −20% even at rapid gusts, thus the turbine is operating safely, since the turbine can rotate with up to +30% deviation from nominal speed, depending on the converter ratings. Finally the operation of the pitch angle controller is depicted in the last graph of Figure 4.15. At times of high wind speed the controller increased the pitch angle up to 20 degrees for this particular time series in order to constrain the power output. Figure 4.16 shows the response of the power factor and the terminal voltage of the generator when it operates in constant power factor mode.

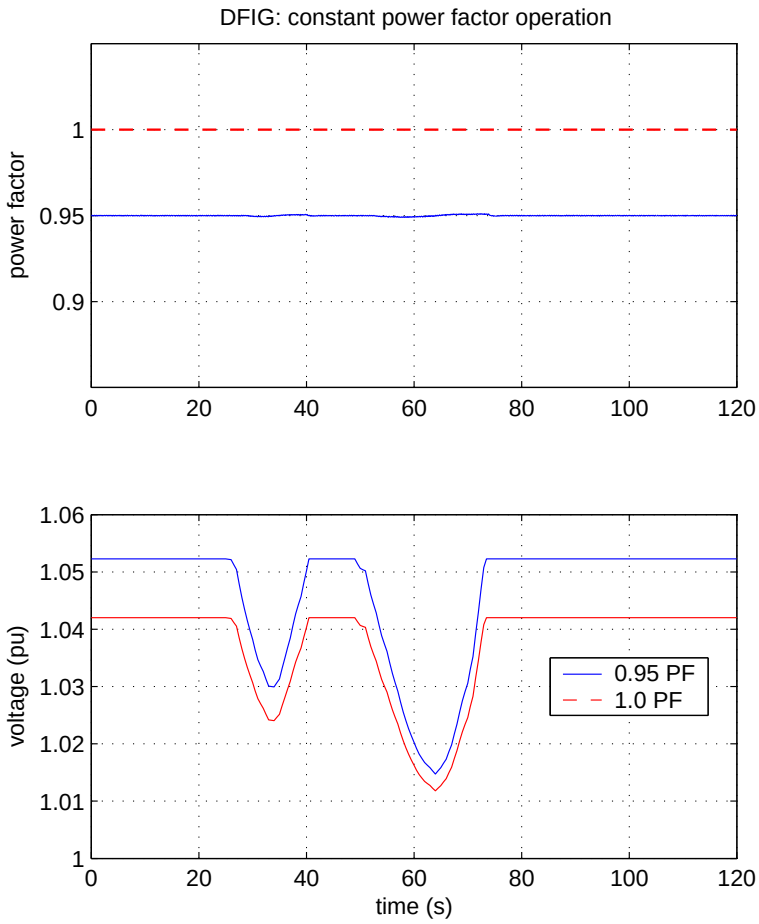

Figure 4.16: *Power factor and terminal voltage for the DFIG in constant power factor mode*

In this figure the blue trace represents a power factor setpoint of 1.0 and the red dashed trace shows the response for 0.95 PF lagging (exporting reactive power). It should be noted here that in both cases the responses of real power export, rotor speed and blade pitch angle were identical to the ones shown in Figure 4.15. The reactive power controller manages to fix power factor at the desired setpoints, but as a consequence the voltage varies with the changing power generation. It can be seen that the variation is wider in the case of lagging power factor than the one at unity, and this is explained by the fact that at unity the reactive power is zero, whereas at 0.95 lagging, the reactive power varies in proportion to the real power, thus increasing the effect of voltage fluctuation.

4.3.2 WT Operating at Constant Voltage

Although not widely practiced yet, wind turbines equipped with doubly fed induction generators can perform voltage control in a distribution system, thus assisting the DNOs to regulate the voltage profile of the network. However, for this to happen a solid regulatory framework has first to be developed. The response of the power factor and the terminal voltage of the generator when it operates in constant voltage mode is shown in Figure 4.17.

The V/Q controller is now set to perform voltage control, and fix the terminal voltage at 1.03 per unit. In this case also the responses of real power export, rotor speed and blade pitch angle were identical to the ones shown in Figure 4.15. However the power factor and voltage responses are quite different. Power factor has now settled at 0.95 leading (absorbing VArs), as due to the high real power output the voltage tends to rise over the 1.03 pu set point. It can be observed that terminal voltage remains practically constant at the setpoint value, but the power factor is increased during the two sudden reductions of wind speed at $t = 35s$ and $t = 65s$, as the voltage rise due to the real power export became smaller.

It should be noted that the results obtained in the last two sections agree with the results presented in [74], where the WECS data were taken from. Although the wind speed

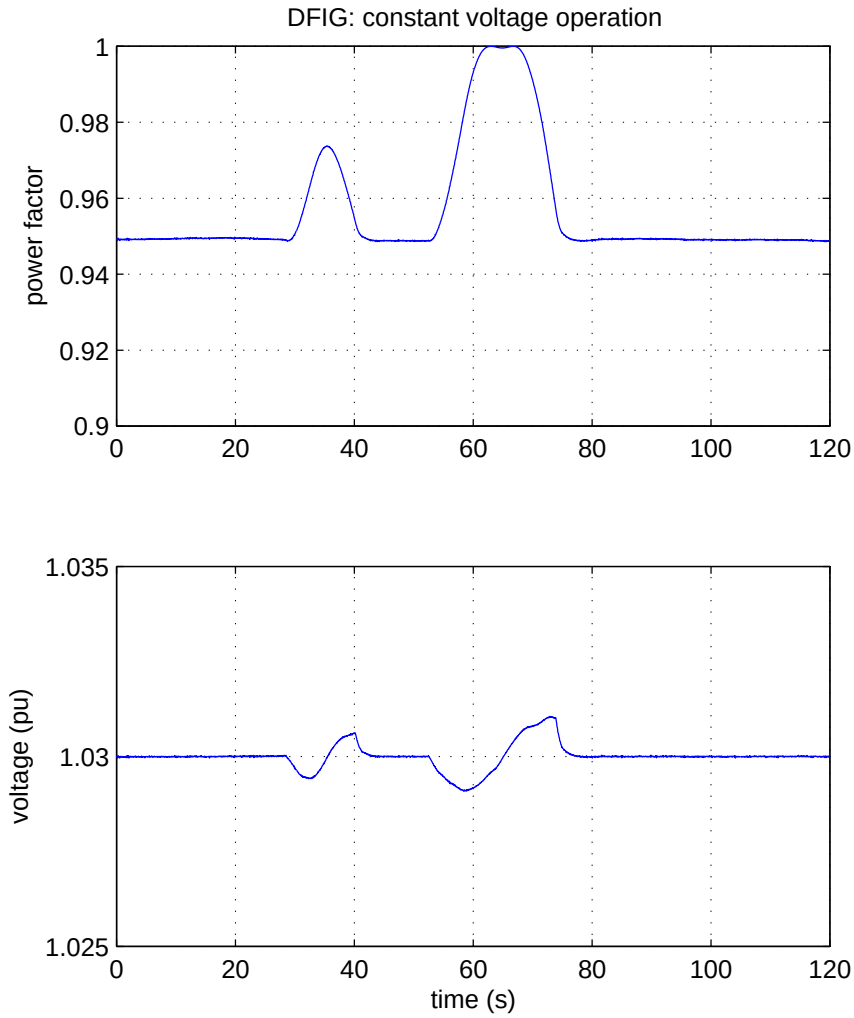

Figure 4.17: *Power factor and terminal voltage for the DFIG in constant voltage mode of operation*

input and the network characteristics are different in this case, the numerical values for power output, rotor speed and pitch angle are almost equal for the same wind speed. Some deviation is expected, as the systems are not at (but close to) steady-state. The voltage results agree with the results of a standard power flow for the same generated power and power factor (and in the same network). Therefore it is concluded that the model is accurate.

4.4 Steady State Model of the DFIG

Inclusion of the flux derivatives in Equations 4.15 to 4.18 would require a simulation step time well below $50ms$ that is a typical value for fundamental frequency dynamic simulations, hence drastically increasing the computational load. The full model is useful when studying the dynamic performance of the system (including the controllers), but does not provide more information for long term simulations than the steady state model. The above set of equations can be simplified to give the steady state model as follows. By allowing the generator to operate with variable speed, the torque does not experience rapid fluctuations. This has a smoothing effect on the generator currents as well (and hence the fluxes), and therefore the dynamic terms of Equations 4.15-4.18 have negligible effect and can be eliminated [65].

Taking into account the assumption discussed above and by substituting Equations 4.20-4.23 into Equations 4.15-4.18 the voltage equations for the DFIG become:

$$v_{ds} = 0 = -R_s i_{ds} + \omega_s \left[(Ls + L_m)\, i_{qs} + L_m i_{qr} \right] \tag{4.31}$$

$$v_{qs} = -R_s i_{qs} - \omega_s \left[(Ls + L_m)\, i_{ds} + L_m i_{dr} \right] \tag{4.32}$$

$$v_{dr} = -R_r i_{dr} + s\omega_s \left[(Lr + L_m)\, i_{qr} + L_m i_{qs} \right] \tag{4.33}$$

$$v_{qr} = -R_r i_{qr} - s\omega_s \left[(Lr + L_m)\, i_{dr} + L_m i_{ds} \right] \tag{4.34}$$

The above equations do not include a dynamic term and therefore can be used to draw the steady-state equivalent circuit of the DFIG. By considering Equations 4.31 - 4.34 the steady-state equivalent circuit of the DFIG as well as the corresponding phasor diagram can be derived as shown in Figure 4.18, where $X = \omega_s L$ and index m denotes magnetising quantities.

The power electronic converter that injects voltage in the rotor circuit can now be modelled as an ideal current source. The current setpoints are assumed to be instantaneously reached. This is a safe assumption as today's power electronic switches have response times well below the time frame in consideration. The set of equations

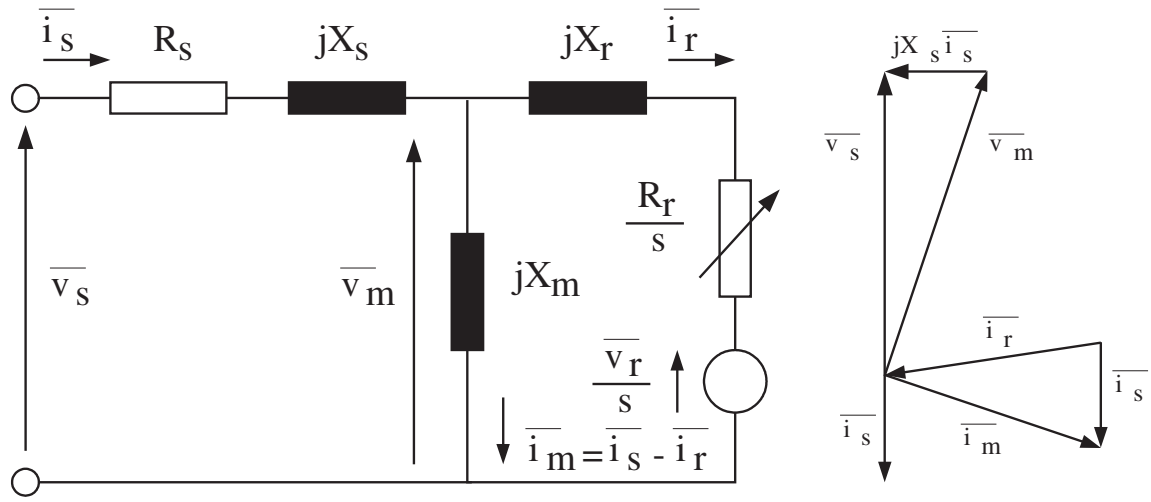

Figure 4.18: *Steady-state equivalent circuit for a DFIG and corresponding phasor diagram*

described in this section was utilised to construct the steady state model used in the following chapters for long term simulations.

4.5 Summary

In this chapter the modelling philosophy and the fundamental components for a wind-to-wire model of a wind energy conversion system were presented, namely the models of the wind speed, the wind turbine, the drive train and the doubly-fed induction generator. The advantages and disadvantages of the available configurations for WECS were discussed. Variable speed wind turbines are favoured by the industry due to their superior efficiency and controllability. From the available generators for variable speed WT schemes, the doubly-fed induction generator is most favoured and therefore this is the configuration that this work is based on. The dynamic model of a DFIG was presented in this chapter and two characteristic examples of its operation under constant power factor and constant voltage control were simulated. The results were in close match with other models in the published literature and therefore the constructed model can be relied upon. The next chapter uses the models developed here (and

in Chapter 3) to devise and validate intelligent control of distributed generators to overcome the voltage fluctuations brought about by the weakness (in electrical terms) of the distribution network.

Chapter 5
Intelligent Control of Distributed Generation

5.1 Introduction

This chapter proposes two methods of steady-state voltage control in remote parts of rural distribution networks that accommodate an increasing capacity of synchronous and doubly fed induction generators. The first of them is a deterministic system that uses a set of rules to switch intelligently between voltage and power factor control modes, while the second is based on a Fuzzy Inference System that adjusts the reference setting of the Automatic Power Factor Controller in response to the terminal voltage. Extensive simulations have verified that the proposed approaches increase the export of real power while maintaining voltage within the statutory limits.

5.2 The Need for Intelligent Control

The steady-state, slow and transient variations of voltage levels related to the connection of a DG can lead to undesired operation of voltage control equipment on transformers at the primary substations of the network. A net reversal of power flow in the distribution network line due to the presence of a DG can cause unacceptable voltage variations, and to protect quality of supply the Distribution Network Operator (DNO) may require that the DG be automatically disconnected by protection devices [4]. Operation of DGs in constant voltage or constant power factor (PF) mode, as required by most DNOs, may create a need for network reinforcement in order to reduce voltage variation and the cost of this work may be attributed to the connection costs of the DG. This may make potential schemes less attractive or even impossible to implement [3, 4].

The ability to export active and reactive power without voltage violation depends on network characteristics above the point of connection, and on the active and reactive power exported from the local busbar. Line power flow is reduced by local demand according to daily and seasonal patterns. The network impedance and X/R ratio can also vary due to automatic reconfiguration, but less frequently. Changes in local loading and network configuration causes local voltage excursions that can shut down the DG with loss of production and revenue. These effects are widely experienced by operators of DGs in rural areas. Depending on its capacity and the inherent voltage variation in the network, there may be merit in operating the DG with the excitation system in constant voltage mode as necessary. The ability to operate inside an acceptable voltage envelope and the opportunity to reduce network reinforcement costs could increase DG development.

Additionally, at times of high local load, or when changes in network impedance led to reduced voltage at the local busbar, the DG could be used to attempt to maintain voltage. While this could provide a measure of network support in the weak areas Distribution Network Operators need not accept this method of operation. An unconstrained machine in voltage control could attempt to define voltages that may conflict with their automatic voltage control equipment, and cause spurious operation of protection, particularly at times of light local load. If the DG tried to meet an excessive demand for reactive power, as voltage continued to fall, the AVR could attempt force excitation with potentially damaging results for the generator. While excitation overcurrent or busbar undervoltage protection should limit this they would shut the plant down, with loss of production and the need for a restart. There is a need to make best use of potential DG plants both from the developers' and the DNOs' point of view.

5.2.1 Universal Power Circle Diagram

Considering the simple two-bus system of Figure 5.1, if the DG produces $P_G + jQ_G$ and the local demand is $P_L + jQ_L$, the complex power delivered to the line in VA is:

$$S_{line} = P_{line} + jQ_{line} = (P_G - P_L) + j(Q_G - Q_L) \tag{5.1}$$

In Chapter 2 it was shown that the voltage rise due to the exported power from the DG bus would be:

$$D\bar{V} = \bar{V_2} - \bar{V_1} = \frac{RP_{line} + XQ_{line}}{V_2} + j\frac{XP_{line} - RQ_{line}}{V_2} \tag{5.2}$$

Equations 5.1 and 5.2 show that, where line power flow is dominated by DG production,

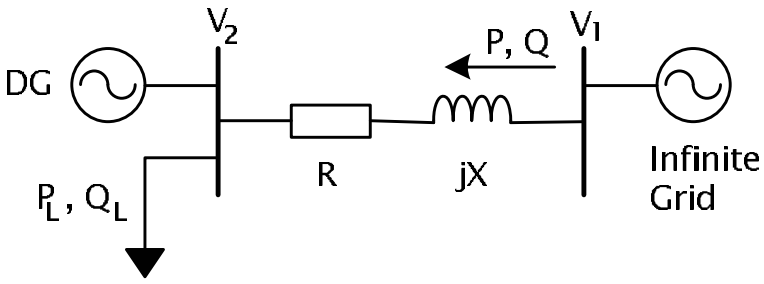

Figure 5.1: *Basic 2 bus system*

operating the generator at a constant power factor will result in voltage excursion as the plant tries to export reactive power in constant proportion to active power. Line impedance directly increases voltage rise. Line X/R ratio skews the effects of real and reactive power. A clearer appreciation of these may be obtained by considering the Universal Power Circle Diagram (UPCD) for a short distribution line shown in Figure 5.2. For $X_{line} >> R_{line}$ angle θ approaches -90^o degrees and the diagram resembles that of a synchronous generator connected to the infinite grid. At the edges of the distribution network, where the X/R ratio tends to be lower, θ is less than 90^o and the voltage origin and centre of constant V_2 circles rotates around a semicircle towards the -Q axis by less than 90^o. The complex power line drawn out of the PQ origin may be used to prescribe constant MVA circles and power factor lines at the remote end of the line, as shown in Figure 5.3. If the voltage at that end of the line

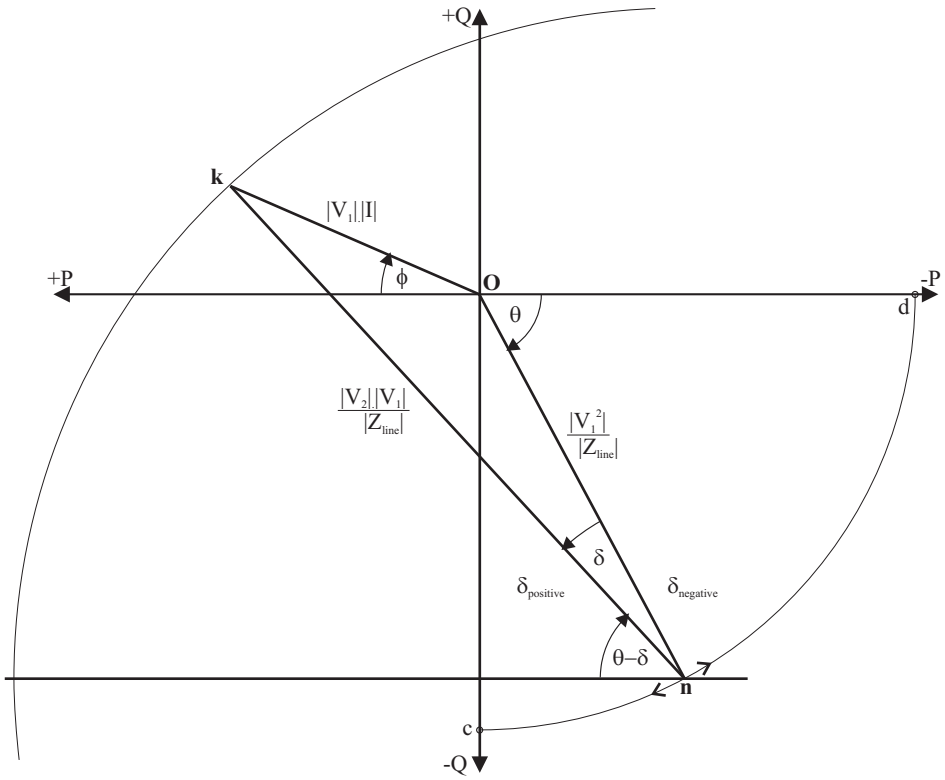

Figure 5.2: *Universal power circle diagram for a short distribution line*

is constant (nominally 1.0 pu) semi-circles of constant busbar voltage may be drawn, including voltage limits. The effects of changing network impedance may be separated from changing line power flow. Only increased complex power flow moves point k further away from the PQ origin, towards voltage limits. Where X/R ratios are high, dispatch of reactive power will rapidly take the busbar voltage to the overvoltage limit. Where the X/R ratio is lower reactive power flow has less effect and eventually active power flow becomes limited by the anti-clockwise rotation of the voltage phasors and voltage circles. Increased network impedance rescales the constant voltage circles to bring the limits closer to or inside point k and therefore dispatch of complex power is limited. While these diagrams are based on complex power flow in the line, they are useful to enable computation and examination of loci of busbar voltage as the DG is loaded or as local demand varies, while the plant is in constant power factor or constant voltage control. They also visualise the effects of network changes on the limits of operation and dispatch of DGs connected to the local busbar, particularly where the capacity of

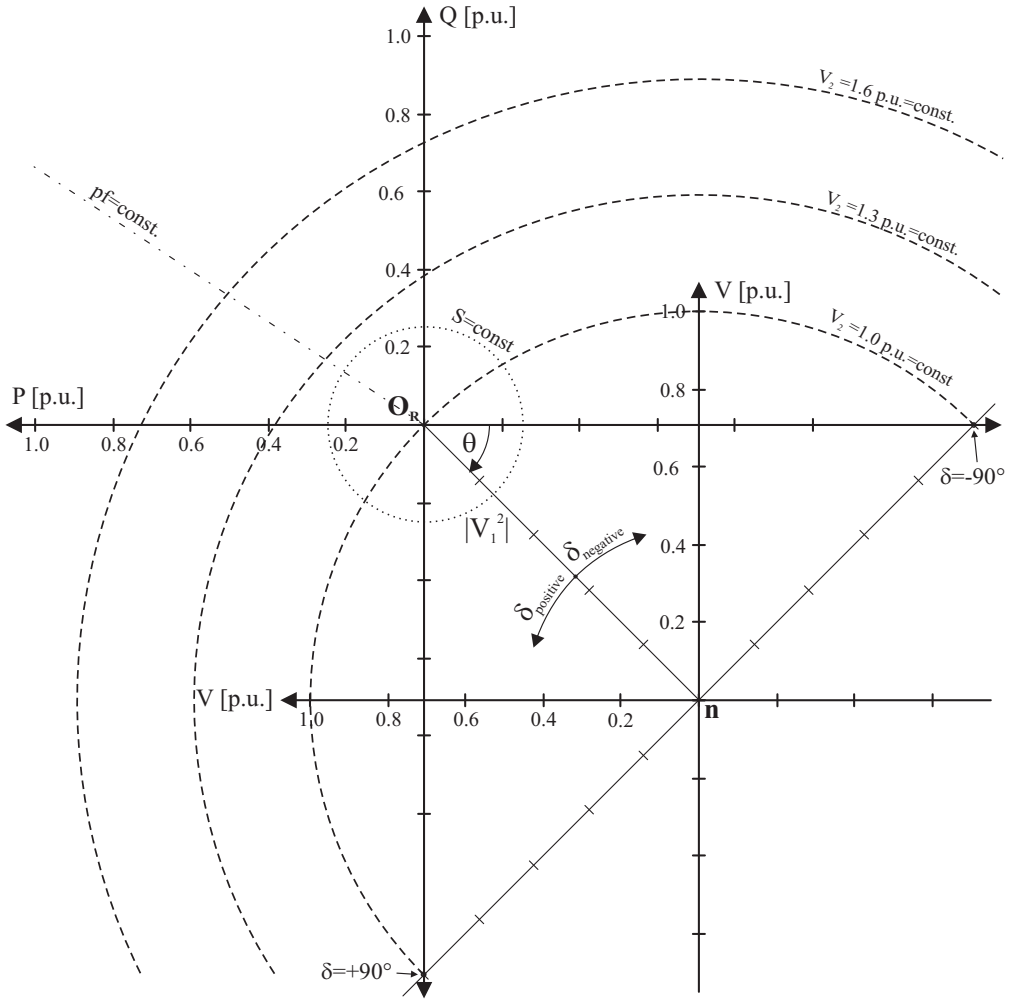

Figure 5.3: *Composite universal power circle diagram*

the generator is dominant. Finally they show that for an increasing MW export from the generator, the only way to maintain local voltage within limits is by reducing export and (should the generator be capable) even going further to import MVArs.

The universal power circle diagram focuses on the network impacts of varying power flows and line impedances. It would be useful to be able to combine the UPCD with the capability diagram of the generator in order to define the working limits of the whole system. However, the UPCD involves varying voltages for the generator bus, thus becoming incompatible with the capability diagram. In order to devise a control strategy for the generator, the network limitations should be reflected on the

machine's operational regime. This can be achieved by using 3D diagrams as shown in Figure 3.13. In this figure, the capability diagram of a synchronous machine connected to a distribution network scaled in the z-axis by terminal voltage, was superimposed to the voltage surface resulting from the real and reactive power loading of the generator. Figure 5.4 shows the same graph from the top. The black line is the intersection of the

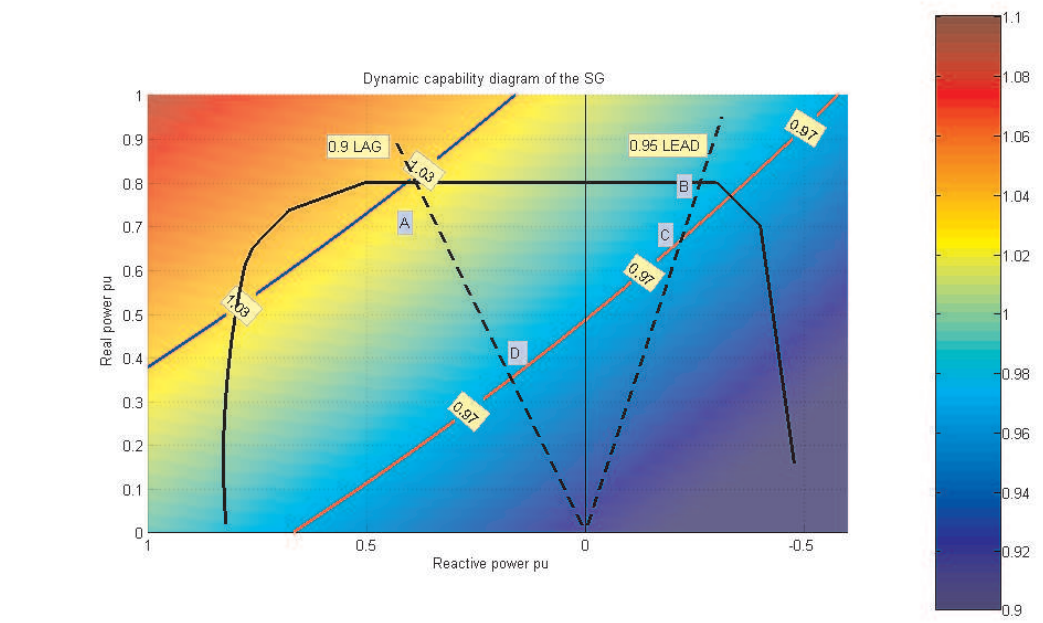

Figure 5.4: *Dynamic capability diagram for* $P_{load} = 0.6$ *pu,* $PF = 0.8$.

3D capability diagram with the voltage surface; in effect it depicts the actual operating limits for this generator in that particular network and load conditions. In this case the local load was $6MW/4.5MVAr$. The rating of the generator was $12MVA$, its reactance was $0.8pu$, the feeder's impedance was $0.8 + j0.6pu$ and the network's voltage was $1.0pu$. Base quantities were 11kV / 10MVA. On the same graph, the voltage and power factor limitations imposed by the DNO are shown. The dashed lines represent the power factor limits (in this case assumed to be 0.9 lagging - 0.95 leading), the blue line is the overvoltage limit set at $1.03pu$ and the red line is the undervoltage limit, at $0.97pu$. While the generator is able to operate safely anywhere within the capability diagram, should the DNO's demands be satisfied the operating area is constrained

to section ABCD, confined by the capability diagram and voltage and PF limits. It is shown that at rated output (0.8pu) the generator can use all the available power factor range, staying just below the overvoltage limit at 0.9 PF. In Figure 5.5 the local load was decreased to $4MW/3MVAr$. At its rated real power, the reactive power of the

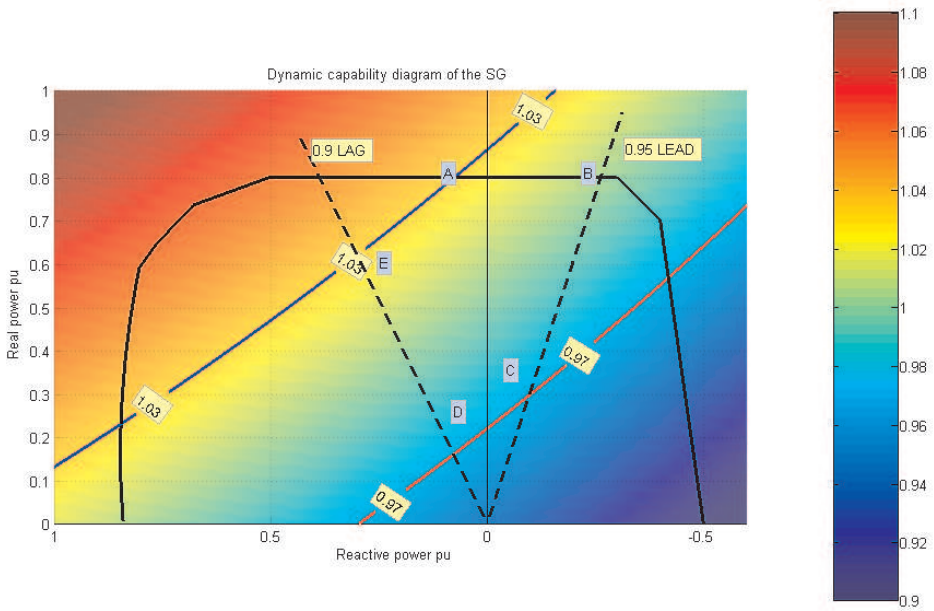

Figure 5.5: *Dynamic capability diagram for* $P_{load} = 0.45$ *pu,* $PF = 0.8$.

generator is now constrained by the overvoltage limit and the minimum (leading) power factor. The effective power factor limits are therefore 0.995 lagging - 0.95 leading. If the generator wanted to increase its reactive power output and yet remain within the voltage limits, it would have to reduce its real power output.

It is therefore apparent that due to the variability of the network conditions in a weak distribution system, operating at a fixed power factor assumes accepting the risk of hitting the over/undervoltage limits. Work done by the author for the purposes of this project, involving mixed voltage/PF control of DGs, have shown that by intelligently controlling the distributed generators, voltage variations can be mitigated and reinforcement may be avoided [4, 81, 82]. Utilisation of a Fuzzy Logic

(FL) Controller to control the DG may also prove to be a means of reducing voltage fluctuations [83]. In this chapter these control algorithms will be presented and it will be shown that the same method can be applied to both synchronous and doubly fed induction generators.

5.3 Artificially Intelligent Controllers

The term *Artificial Intelligence* (AI) is described as a

> "computer process that attempts to emulate the human thought processes that are associated with activities that require the use of intelligence"

There are a number of algorithms that can be categorised as AI controllers, such as expert systems, knowledge based systems, fuzzy logic controllers, neural networks, genetic algorithms etc. In this work two of these types of algorithms have been utilised: expert systems and fuzzy logic controllers. Artificial intelligence concepts have been investigated by several research groups as a means of improving voltage quality in electricity systems [49, 55, 84–91]

5.3.1 AI Controllers Based on Expert Systems

Expert systems are one of the most basic types of AI. The core of an expert system is the knowledge base, which contains the encoded problem solving knowledge for the particular application. A well known mechanism for knowledge representation is rule-based knowledge that takes the form of ***if*** *condition(s)* ***then*** *action(s)* statements. The expert system gathers information which it then uses to make decisions based on a pre-loaded set of rules. Their advantages are their ability to permanently encapsulate knowledge provided by human experts, their flexibility and their ability to generate answers quickly and with consistency. On the other hand, their disadvantages are that they are not adaptive to changing environments and they have difficulty in handling large amounts of data or use of large rule bases.

5.3.2 Fuzzy Logic Controllers

Fuzzy set theory was first discussed in the mid-sixties. Fuzzy controllers are being used with noisy, nonlinear and time-variant systems, tuning problems and with complex multiple input multiple output systems. In conventional logic the number 1 indicates that an object belongs to a set, while 0 indicates that the object is not a member of the set. The distinctive feature of fuzzy systems is that there are degrees of membership that vary from 0 to 1. A fuzzy logic system consists of four stages: the fuzzyfication stage, where crisp input information is converted to fuzzy values, the decision-making stage where it is decided how the fuzzy logic operations are performed, the knowledge base, which contains the decision-making rules and the defuzzyfication stage which converts the fuzzy information back to crisp information.

5.4 Hybrid Voltage / Power Factor Controller

The disadvantage of Figure 5.4 and 5.5 is that they are generator-specific. A generic diagram that includes both the network and generator limitations is shown in Figure 5.6. This vector diagram shows the operational limitations and the constraints (i.e. power factor values and ranges of permissible voltage) that the network operator imposes on the DG in the basic case of a 2-bus system such as the one shown in Figure 5.1. In this diagram V_{min} and V_{max} are the minimum and maximum acceptable voltages and PF_{min} and PF_{max} are the lines of constant minimum and maximum power factor, respectively. The allowable area of operation for the generator is the shadowed region between these boundaries. Ideally, therefore, a control system should constrain the operation of the distributed generator within these boundaries. The block diagram of a system that restricts operation of a synchronous generator within the shadowed area is shown in Figure 5.7. The details of excitation systems and synchronous machine modelling have been presented in Chapter 3.

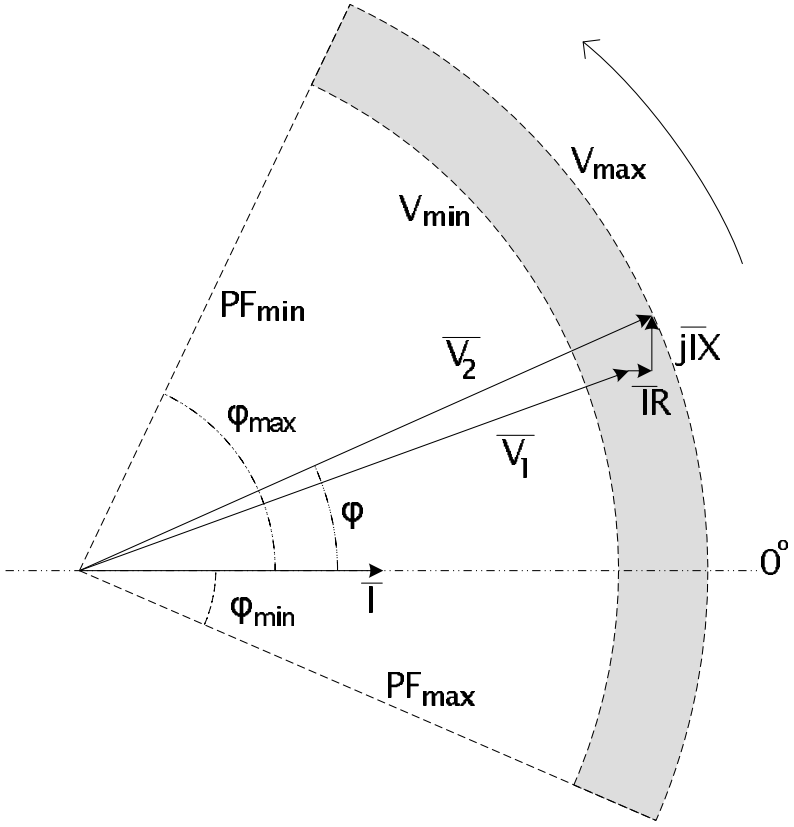

Figure 5.6: *Voltage vector diagram for the two-bus system of Figure 5.1*

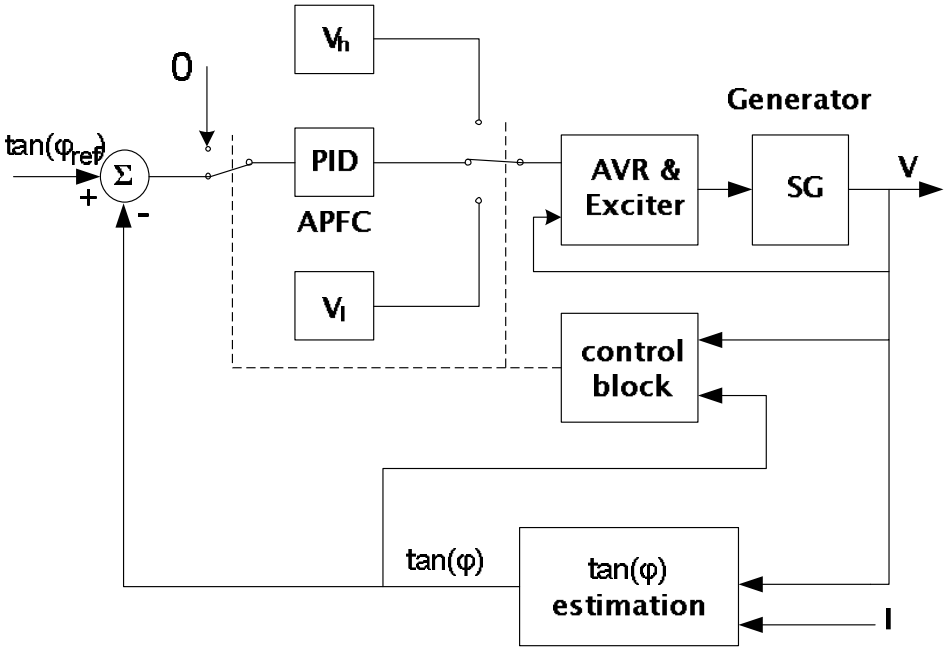

Figure 5.7: *AVPFC controlled synchronous generator block diagram*

There are two nested control loops in the block diagram of Figure 5.7. The inner loop performs voltage control and adjusts the terminal voltage of the generator according to the setpoint that is defined either from the output of the APFC, or the V_h and V_l setpoints. The external loop regulates the power factor of the generator according to the reference value given by $tan(\phi_{ref})$. The control block contains the heuristics of the expert system that ensure continuous operation of the generation within the shadowed area of Figure 5.6. The operation of this block is depicted in the flow chart of Figure 5.8. This constitutes the core of the expert system. The actions of the controller depend on

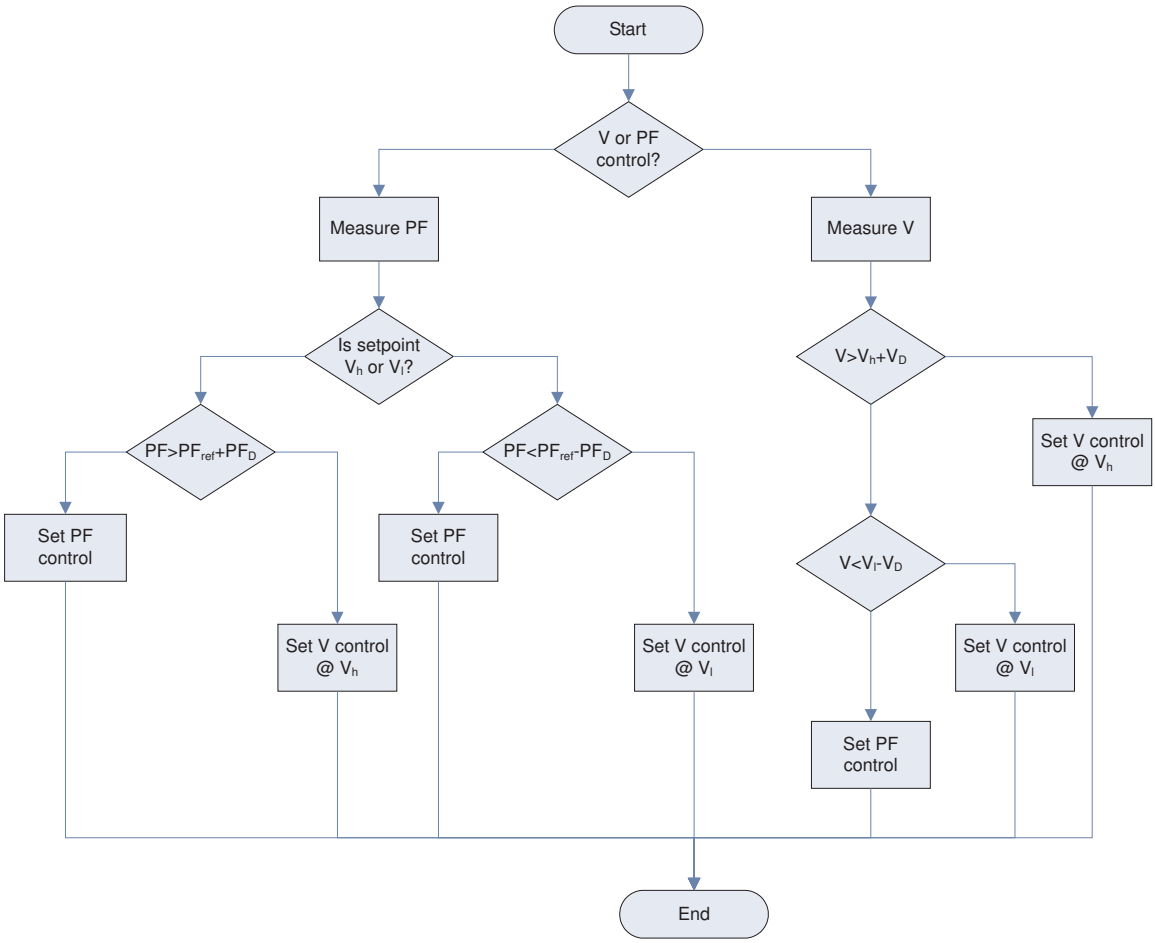

Figure 5.8: *The flow chart of the automatic voltage/power factor control algorithm*

its state, i.e. whether it is in voltage or power factor control mode:

- If the controller is in Automatic Power Factor Control (APFC) mode (right branch), terminal voltage is continuously measured and checked against two

values: the high voltage target V_h plus the deadband V_D, and the low voltage target V_l minus the deadband V_D. If the terminal voltage is higher than the first, or lower than the second, the controller switches to Automatic Voltage Control (AVC) with the reference voltage set at V_h or V_l respectively.

- If the controller is in AVC mode (left branch), the power factor (through $tan(\phi)$) is measured. Then, the measured PF value is compared to the PF target plus or minus the power factor deadband PF_D, depending on the current voltage setpoint (V_h or V_l respectively). As a result of this comparison, if the power factor is outside these limits, the controller switches to APFC.

After synchronisation, the DG could be brought towards capacity in constant power factor mode (travelling out on its constant power factor line) until the busbar voltage exceeds a pre-defined threshold voltage within the statutory limits. At that point APFC could be replaced with AVC to vary excitation and move the operating point around the constant voltage circle within the busbar overvoltage limit. Increased local load and reduction in terminal voltage could take the system back into APFC by sensing the increased demand for reactive power and therefore the reduction of power factor. Variations in network impedance would have a similar effect. This system, termed 'Automatic Voltage - Power Factor Controller' (AVPFC), would also enable voltage support at times of heavy local demand. On reaching a voltage just above the undervoltage limit the excitation system would be transferred to AVC to maintain local voltage. Excitation under- and over-voltage and over-current protection should protect the DG excitation and control system against prolonged forcing. When AVC is active the APFC module is disengaged, otherwise the non-zero power factor error signal would saturate the integrator of the internal PID compensator.

5.4.1 Determination of AVPFC mode selection rule set

The control block in Figure 5.7 is responsible for the control mode decision making. The system will attempt to regulate the DG operation around one of three possible setpoints: the power factor setting PF_{ref}, and the high or low voltage setting V_h and V_l,

respectively. Table 5.1 shows the heuristics of the control algorithm, *i.e.* the reference value which is applied to the controller for every combination of voltage and power factor conditions. In order to prevent hunting, a deadband exists around the decision thresholds. Voltage deadband is annotated as V_D and power factor deadband is PF_D.

	$V_2 \leq V_B$	$V_B < V_2 < V_T$	$V_T \leq V_2$
$PF \leq PF_B$	V_l	PF_{ref}	PF_{ref}
$PF_B < PF < PF_T$	V_l	PF_{ref}	V_h
$PF_T \leq PF$	PF_{ref}	PF_{ref}	V_h

Table 5.1: *AVPFC mode selection rules set*

where: $V_B = V_l - V_D$,
$V_T = V_h + V_D$,
$PF_B = PF_{ref} - PF_D$,
and $PF_T = PF_{ref} + PF_D$.

5.4.2 Performance of a Synchronous Machine Based DG under AVPFC control

In order to test model validity, the process of generator load-up was simulated under AVPFC control and the results compared with those under AVC and APFC modes. The radial test network in Figure 5.1 was used with its characteristics shown in Table 5.2.

The results of the DG loading-up, post-synchronisation, are shown in Figure 5.9. In this (hypothetical) case, local power demand is sufficiently high to result in the voltage at bus 2 (V_2) lying below the 0.94 pu limit. Normally, however, DNOs would ensure that voltage remained within statutory limits prior to connection. In the initial stages of load-up ($t \leq 45$s), local power demand exceeds DG output and in the case of the APFC-controlled DG, is sufficiently high to result in voltage V_2 being below 0.94 pu (a hypothetical situation as in general DNOs would ensure voltage remained within statutory limits prior to connection).

During the same period a fixed-voltage, AVC-controlled generator would try to hold

Network Data	
Machine size:	10 MW
Load size P_L, Q_L:	4 MW, 3 MVAr
Line resistance R:	0.124 pu
Line reactance X:	0.099 pu
Network Voltage V_1:	1.0 pu
Base Voltage V_{base}:	11 kV
Base Power S_{base}:	10 MVA
AVPFC Data	
V_h:	1.03 pu
V_l:	0.97 pu
V_B:	0.0025 pu
PF_{ref} :	0.9 lagging
PF_B:	0.0025
APFC Data	
PF_{ref} :	0.9 lagging
AVC Data	
V_{ref}:	1.03 pu

Table 5.2: *Test system data*

voltage at the 1.03 pu reference voltage leading to significant reactive power generation and a fall in the power factor wherein the DG excitation protection devices would shut the plant down. The AVPFC controller responded by fixing the terminal voltage at 0.97 pu. The low power factor would cause the protection devices to shut the generator down, albeit for a significantly shorter time than in the AVC case. Between $t = 45$s and $t = 125$s the AVPFC operated the generator in constant power factor mode as this would not result in voltage excursions outside the preset thresholds. For that period the response of the controller was identical to the response of APFC.

At $t = 125$s, the voltage of the APFC and AVPFC controlled generators reached 1.03 pu. Under AVPFC there was a switch to voltage control to maintain voltage, and from this point on its response is identical to that with AVC. The voltage under APFC continued to rise towards and through 1.06 pu - over-voltage protection would trip the DG at that point. This simulation showed that compared to APFC, hybrid voltage/PF control of a DG can improve the voltage profile in a weak network when the power transfer from or to the local bus is high, and at the same time will reduce import

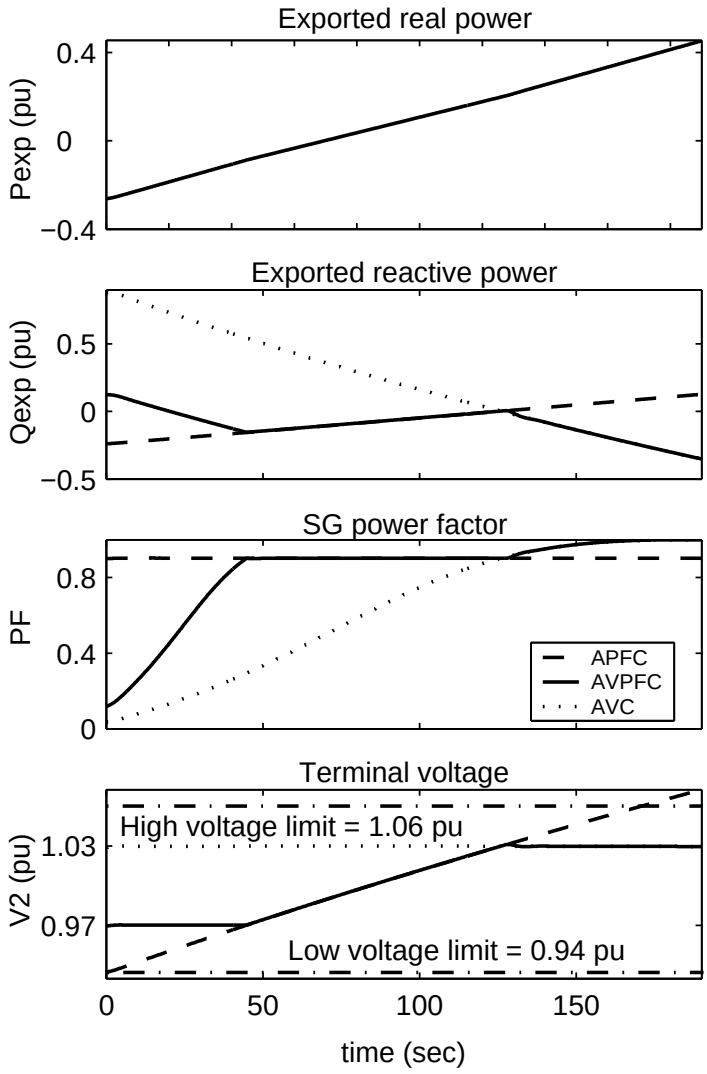

Figure 5.9: *DG loading-up under AVC, APFC and AVPFC control. Legend applies to all subfigures.*

or export of reactive power, compared to automatic voltage control. However, should another automatic voltage control device exist in the vicinity such as an On-Line Tap Changing (OLTC) transformer, the attempt of the AVPFC to hold voltage constant can potentially cause spurious operation of the OLTC mechanism, if the settings of the two control devices are not carefully selected.

5.5 Fuzzy Logic Power Factor Controller (FLPFC)

Artificial Intelligence has been applied successfully to solve many power system problems [92]. Being highly nonlinear, power systems are very difficult to control with conventional methods and linearisation techniques very often fail to produce models that resemble the actual characteristics of the system. The resulting ambiguities impose constraints on power system controller design. In addition to this, the stochastic variation of load, generation and topology of a power system exaggerate uncertainty and imprecision [89]. The use of a fuzzy inference-based approach can be shown to overcome these difficulties.

5.5.1 Formulation of the problem

As discussed in the previous section, hybrid voltage and power factor control of a DG can improve voltage quality in a weak network, but can only be applied when no other voltage control device exists in the vicinity, and at the same time will reduce the need to install such a device. On the other hand, with the rapid increase of distributed generation and the subsequent extension and improvement of the DN, it is expected that the DNOs will move toward more active control of the DN, and therefore the number of DN voltage control devices will increase. Hence, network operators in such areas may not allow generators to operate in any form of voltage control mode, including AVPFC. In that case, a method of reducing voltage fluctuations while in APFC mode is required. A conventional automatic power factor controller has a flat power factor characteristic over the permissible range of voltage. A human operator (or a specifically designed controller) of the DG plant would respond to voltage variation by altering the power factor setpoint in a way that the change in generated (or absorbed) reactive power regulated the terminal voltage. The DG should operate with constant power factor in a band spread about the middle of the permissible voltage range. When voltage falls the power factor should shift to a more lagging value so that the extra reactive power generated restores voltage. Conversely, increased voltage would require a move to a more leading power factor to compensate for the voltage increase. It is possible

to achieve such operation by adjusting the power factor reference rather than voltage refenernce in single AVC mode by means of a specifically designed fuzzy controller. The block diagram of a DG controlled in this manner is shown in Figure 5.10.

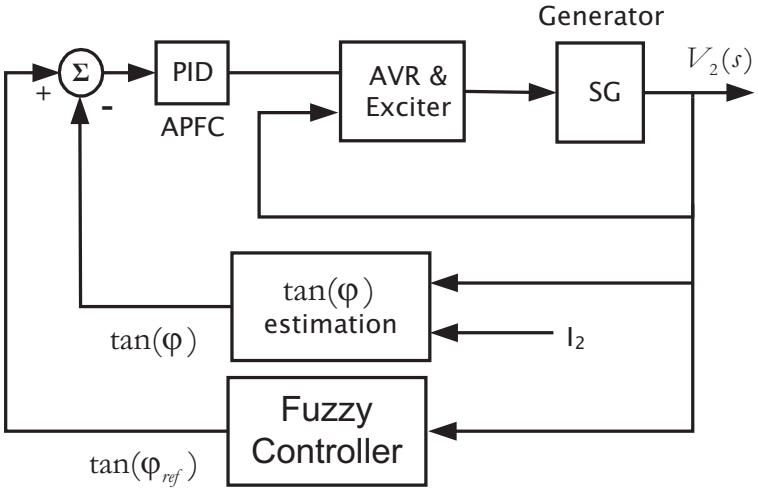

Figure 5.10: *Block diagram of a DG with a Fuzzy Logic Power Factor Controller*

Compared to the block diagram of the AVPFC controlled system, the block diagram shown in Figure 5.10 includes three nested loops. The inner is the same as previously; it is the voltage regulation loop. The middle one performs power factor control with the assistance of the PID controller, and the external loop provides the power factor reference (emerging from $tan(\phi)$) through the fuzzy controller. The latter behaves as a numerical input - numerical output, nonlinear element of a closed-loop control system [93]. It should be stressed that this nonlinear mapping is not unique and is heavily affected by the conversion procedure of the fuzzy control sets [93]. As it will be shown later, exploitation of this characteristic can lead to "tight" or "loose" voltage regulation, specifically designed to match the network characteristics and /or the DNO's requirements. Furthermore, extrapolation capabilities should be given to the fuzzy controller to enable it to produce an output even when the input is outside the design limits. In this case, the protection devices of the generator will ensure that it always operates within its design limits.

5.5.2 Design of the Fuzzy Logic Power Factor Controller

From the two available types of Fuzzy Logic (FL) controllers (Mandamani-type and Sugeno-type), the one proposed by Takagi and Sugeno [94] has superior control performance [95]. Once the desired controller response has been identified, there is a number of steps that have to be followed, namely the design of the input stage (fuzzification), determination of the fuzzy rules, and design of the output stage (defuzzification).

5.5.2.1 Design of the input stage

Since this is a Single Input - Single Output (SISO) controller, the input fuzzy set consists only of the measured terminal voltage V_T, varying over the range $[V_{T_{min}}, V_{T_{max}}]$. Three linguistic labels define voltage; LOW (L), NORMAL (N) and HIGH (H). The (Gaussian) input membership functions are shown in Figure 8(a) and are described by Equations 5.3 - 5.5:

LOW:

$$A_{L(V_T)} = exp\left[-\left(\frac{V_T - V_{T_{min}}}{V_{T_l} - V_{T_{min}}}\right)^2\right] \tag{5.3}$$

$\forall V_T \in [V_{T_{min}}, V_{T_{max}}]$

NORMAL:

$$A_{N(V_T)} = \begin{cases} exp\left[-\left(\frac{V_T - V_{T_1}}{V_{T_l} - V_{T_1}}\right)^2\right], V_{T_{min}} \leq V_T < V_{T_1} \\ 1 \qquad\qquad\qquad\qquad , V_{T_1} \leq V_T \leq V_{T_2} \\ exp\left[-\left(\frac{V_T - V_{T_2}}{V_{T_h} - V_{T_2}}\right)^2\right], V_{T_2} < V_T \leq V_{T_{max}} \end{cases} \tag{5.4}$$

HIGH:

$$A_{H(V_T)} = exp\left[-\left(\frac{V_T - V_{T_{max}}}{V_{T_h} - V_{T_{max}}}\right)^2\right] \tag{5.5}$$

$\forall V_T \in [V_{T_{min}}, V_{T_{max}}]$

5.5.2.2 Determination of the fuzzy rules

A typical rule in a Takagi-Sugeno - type fuzzy model has the form [94]:

IF Input $= x_i$*, THEN Output is* $y_i = a_i x_i + b_i$, where i is the index of the fuzzy rule.

For a zero - order Takagi-Sugeno model, the output level y is a constant ($a = 0$). Therefore the fuzzy rule set becomes:

i. IF ($V_T = LOW$) THEN ($u_1 = PF_{min}$)

ii. IF ($V_T = NORMAL$) THEN ($u_2 = PF_{nom}$)

iii. IF ($V_T = HIGH$) THEN ($u_3 = PF_{max}$)

where u_1, u_2, u_3 are the outputs of the respective fuzzy rules.

5.5.2.3 Design of the output stage

The output level u_i of each fuzzy rule is weighted by the level of activation μ_i of the rule as shown in Figure 5.11. The final output of the system is the weighted average of all rule outputs, computed as:

$$PF_{ref} = \frac{\sum_{i=1}^{3} \mu_i u_i}{\sum_{i=1}^{3} \mu_i} \tag{5.6}$$

5.5.3 Performance of the DG under FLPFC control

To quantify the benefit of using the FLPFC, a simulation on a system identical to the one in Section 4.3.2 was performed, this time with the DG under FLPFC control. The details of the FLPFC are shown in Table 5.3. Application of these data on the FLPFC produced a Look Up Table (LUT) with the response shown in Figure 5.12.

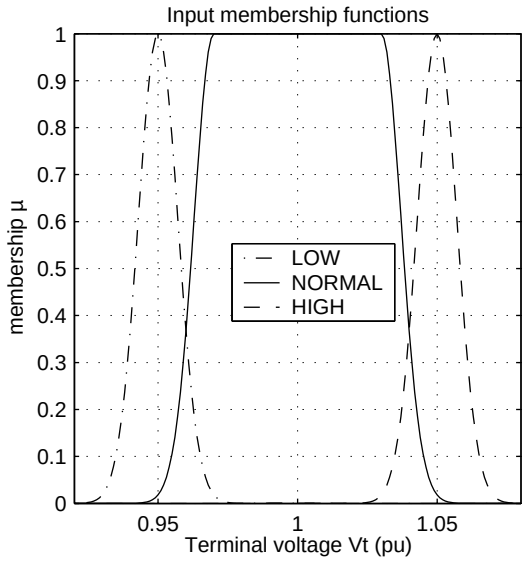

Figure 5.11: *Input membership functions of the Fuzzy Power Factor Controller*

FLPFC Data	
$V_{T_{max}}$:	1.05 pu
$V_{T_{min}}$:	0.95 pu
V_{T_h}:	1.04 pu
V_{T_l}:	0.96 pu
V_{T_2}:	1.03 pu
V_{T_1}:	0.97 pu
$tan(\phi_{max})$:	0.750 ($PF_{min} = 0.8$ lagging)
$tan(\phi_{nom})$:	0.484 ($PF_{nom} = 0.9$ lagging)
$tan(\phi_{min})$:	-0.329 ($PF_{max} = 0.95$ leading)

Table 5.3: *Fuzzy Logic Power Factor Controller data*

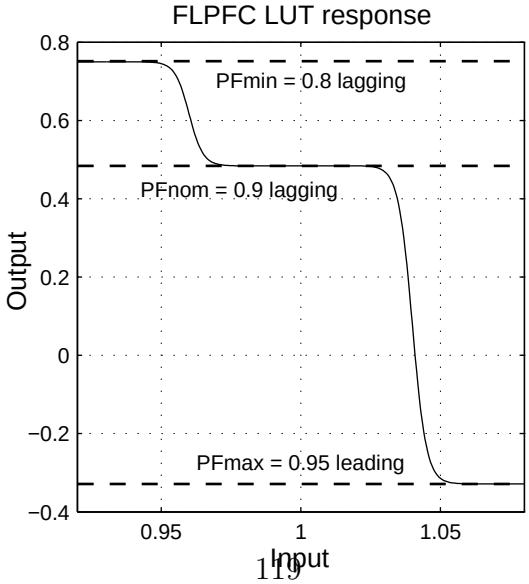

Figure 5.12: *Overall response of the Fuzzy Power Factor Controller*

Triangular membership functions could be used instead of the Gaussian ones shown in Figure 5.11. In that case, the input-output relationship of the fuzzy controller would consist of sections of straight lines. However, Gaussian functions were preferred as they result in a gradual increase of the slope, which has positive effects on voltage regulation, as it will be shown later. The results of the simulation are shown in Figure 5.13. The response of the AVC and APFC controlled DGs are shown in the same graph for comparison.

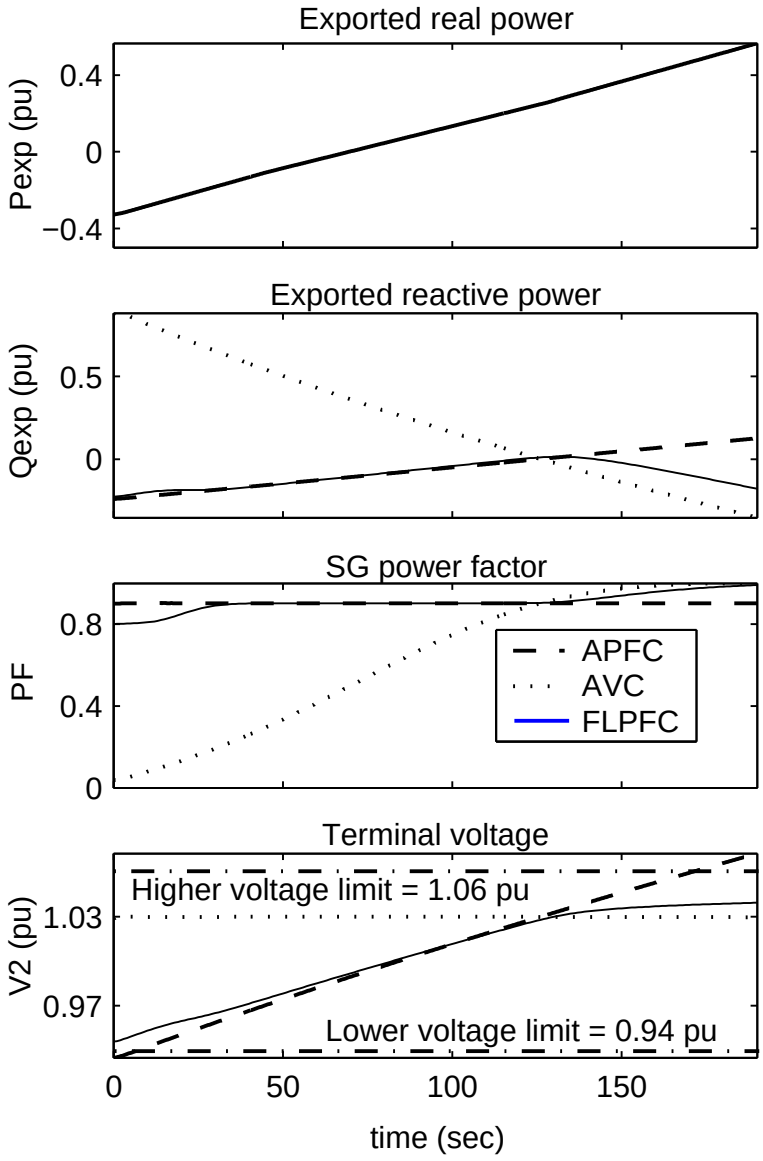

Figure 5.13: *DG loading-up under AVC, APFC and FLPFC control*

Early in the loading process the FLPFC controlled machine operates at a slightly higher voltage compared to the APFC controlled one. This is because the FLPFC allows the SG to operate at 0.8 power factor exporting extra reactive power. In the middle section of the loading process and while voltage lies between 0.97 pu and 1.03 pu the system operates at constant 0.9 PF, almost identical to the APFC and AVPFC cases. When voltage rises above 1.03 pu, the FLPFC starts decreasing the power factor setpoint - increasing $tan(\phi_{nom})$ - and by constraining Q_{exp}, the terminal voltage is held within acceptable levels. It should be noted that the the FLPFC (as well as the AVPFC) will maintain the voltage within the permissible range only as long as the reactive power limits have not been met. These three tests showed that for the same network conditions, utilisation of either AVPFC or FLPFC would be beneficial as their operational margins are wider compared to the traditional fixed power factor operation of a synchronous generator.

5.6 AVPFC and FLPFC controlled DG under real-time varying load conditions

To test the response of the DG under the control of APFC, AVPFC and FLPFC to voltage variations brought about by changes in local load, the load of the 2-bus system in Figure 5.1 was given the time-varying profile shown in Figure 5.14, to simulate the time variation of actual aggregated load at a DN substation. The network characteristics are given in Table 5.4.

The varying demand profile was applied at constant 0.9 power factor over a 24-hour period. It resembles an aggregated 80% domestic - 20% industrial load. The simulation was performed three times; with the APFC, then with the AVPFC and lastly with the FLPFC. The settings of APFC and FLPFC were the same as the ones used for the generator loading tests (see Tables 5.2 and 5.3). Setpoints V_h and V_l of the AVPFC have been changed to 1.05 p.u and 0.95 p.u. respectively in order to match those of the FLPFC. Additionally, the power factor of the generator has been constrained between 0.8 lagging and 0.95 leading to resemble real-life operation in a DN, as a DNO would

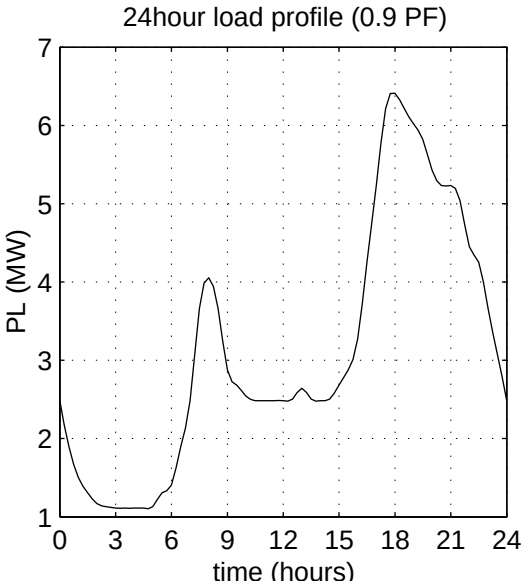

Figure 5.14: *24-hour, 80% domestic 20% industrial load profile*

Network Data	
Machine size:	4.0 MW
Min. Load P_L, Q_L:	1.11 MW, 0.538 MVAr
Max. Load P_L, Q_L:	6.411 MW, 3.105 MVAr
Load power factor PF:	0.9
Line resistance R:	0.1901 pu
Line reactance X:	0.1521 pu
Network Voltage:	1.0 pu
Base Voltage V_{base}:	11 kV
Base Power S_{base}:	10 MVA

Table 5.4: *Test system data*

generally not allow a generator to operate with an unconstrained PF. The response of a typical APFC generator setup is shown in Figure 5.15.

The power factor of the generator remains constant throughout the whole period. However, for the period between 0:45-06:15 hours the generator would be disconnected as the large (constant) amount of generated power in combination with the low local demand would cause excessive power export and thus voltage violation. Additionally, during the 17:15-18:45 hours high local demand period, the bus voltage would be below the 0.94 p.u. statutory limit. Figure 5.16 shows the response of an AVPFC controlled SG under the same circumstances.

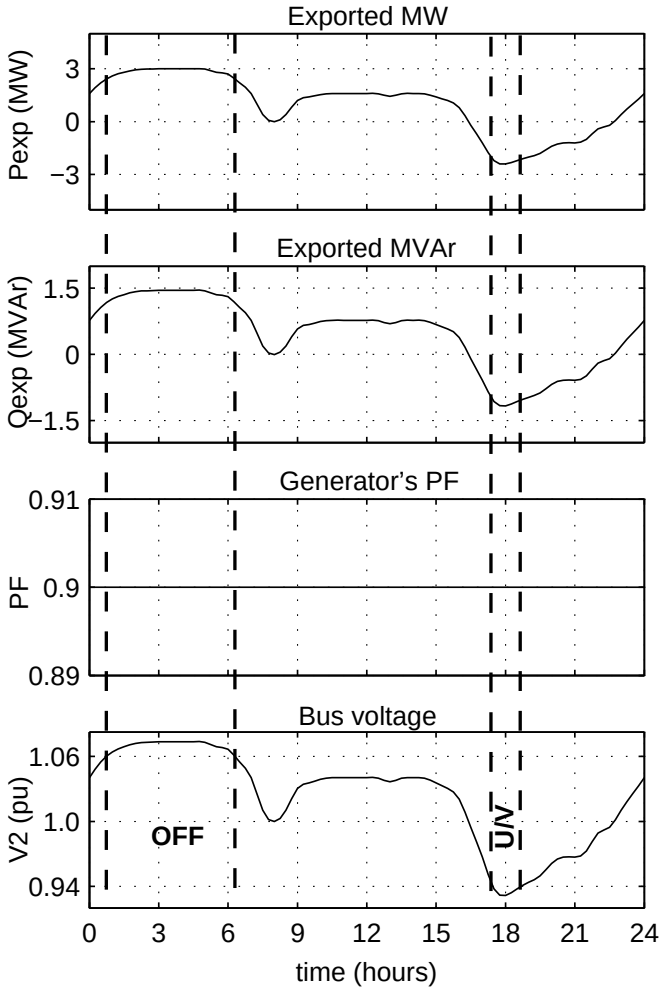

Figure 5.15: *Response of APFC to a varying load*

Compared to the APFC controlled SG response, it is apparent that for the periods while the bus voltage would be in the 0.97 pu - 1.03 pu region, the operation of the two systems is identical. However, during the periods of low (00:30-07:00 hours) and high (17:15-19:30 hours) demand, the AVPFC switches to constant voltage mode and holds voltage at 1.04 pu and 0.96 pu, respectively. This results in a longer period of operation, more energy shipped to the network and therefore increased revenue for the developer. It should be noted that for a short period just before 18:00 hours the voltage falls below the 0.95 p.u. setpoint, because the power factor limit has been met and the generator cannot support voltage any further. Figure 5.17 presents the results of simulations under FLPFC control.

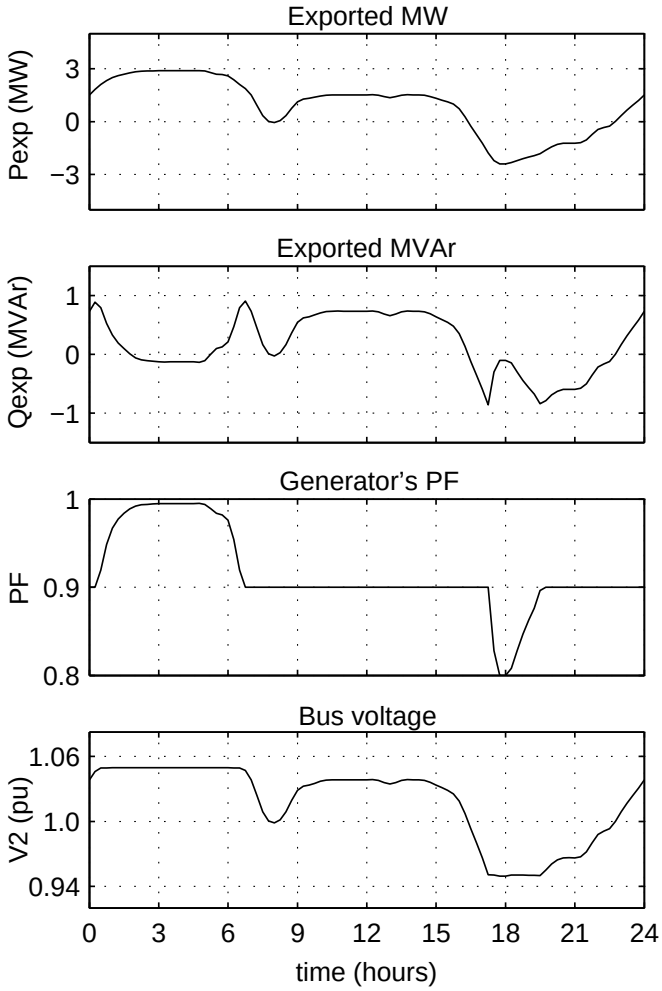

Figure 5.16: *AVPFC response to 24-hour varying load*

Compared to the AVPFC response shown in Figure 5.16, the FLPFC gives quite similar results. It is clear that neither voltage nor power factor exceed their operational range and therefore the generator will remain connected for the whole period of simulation, resulting in an extra 22 MW-hours exported energy compared to APFC operation. For a 4MW machine, this represents considerable increase in output with consequent financial benefits.

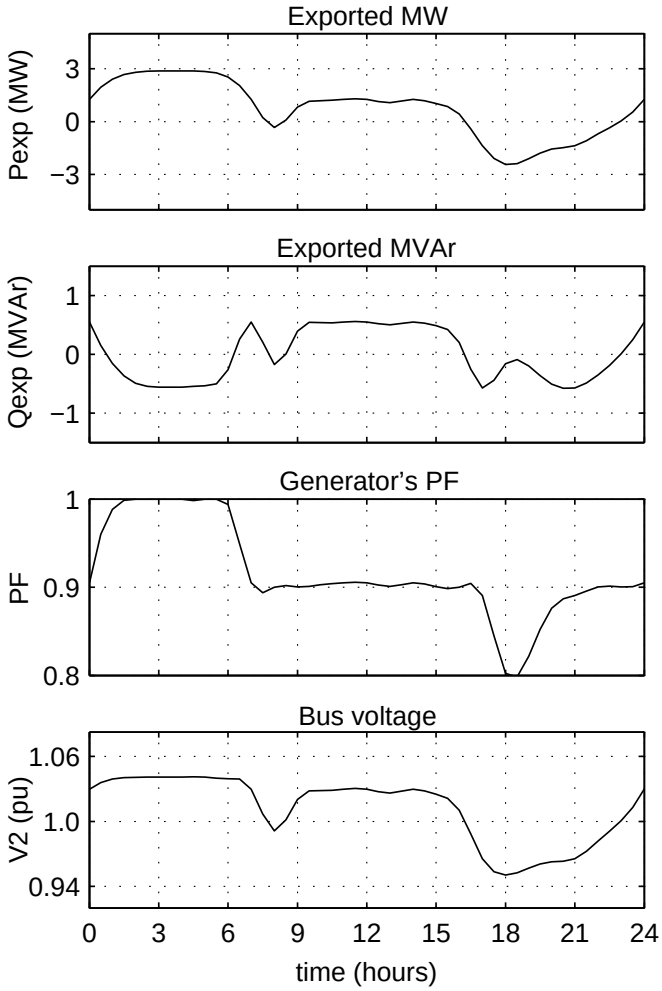

Figure 5.17: *FLPFC response to 24-hour varying load*

5.7 Application of the FLPFC to Wind Turbines with Doubly Fed Induction Generators

The increasing rating of modern wind turbines and in a greater extent the size of the new and proposed wind farms introduce a major concern regarding voltage control in the distribution network. In the case of wind energy, an additional factor of voltage variation to the one of load change is the wind intermittency. Therefore operating the DFIGs in pure power factor control mode is expected to cause wider voltage excursions than in the case of SG-based hydroelectric or CHP plants, and the need for intelligent control is more prominent. Decoupled real and reactive power regulation of the DFIG through

$d-q$ control makes possible the utilisation of the AVPFC and FLPFC controllers in the same manner with the synchronous generators as discussed in the previous sections.

One of the advantages of the fuzzy logic power factor controller is that although it does not fix the voltage at a constant value (an action that has the disadvantage of wide reactive power fluctuations when real power is varying), it can constrain its range, and at the same time it has a reduced variation of the reactive power exchange with the network compared to pure voltage control. This can be a very interesting feature in the case of wind generation, as its inherently intermittent energy source causes wide voltage fluctuations, one of the most important issues that restricts penetration of wind energy. To quantify the possible advantages and disadvantages of the utilisation of FLPFCs in wind energy, a set of simulations was done. FLPFC control was applied to a DFIG wind turbine that was connected to a two bus system like the one shown in Figure 5.1. The real and imaginary parts of the line impedance were $R_l + jX_l = 0.05 + j0.05$ per unit on a 2 MVA base. The load is assumed to be zero and the network voltage 1.0 pu. A method to alter the operation of the FLPFC controller in order to study its characteristics is by changing the non-linear $v - Q$ slope by altering the membership functions. For this example a set of three different $V - Q$ characteristics were used. These relationships are shown in Figure 5.18. The efficiency in regulating voltage is defined by the slope of these curves. The steeper the slope, the easier becomes the reactive power exchange between the DFIG and the network, and the more the controller looks like a usual automatic voltage controller. Of course there lies a trade-off, as increased steepness also leads to increased reactive power fluctuations in case of disturbances. On the other hand, a less steep characteristic resembles more to an ordinary power factor controller (when slope is zero) which has less MVAr fluctuations but a worse voltage regulation. Figure 5.19 shows the power factor and voltage response of the DFIG utilising an FLPFC with each of the three $V - Q$ curves of Figure 5.18, for 120 seconds of operation under varying wind power input. The response of a PF-controlled DFIG is also shown for comparison. The setpoint of the power factor controller was set at 0.95 lagging.

It can be seen that in terms of voltage regulation, the best performance is by curve B, which achieved the lowest voltage and the least variation, then curve A and last curve B.

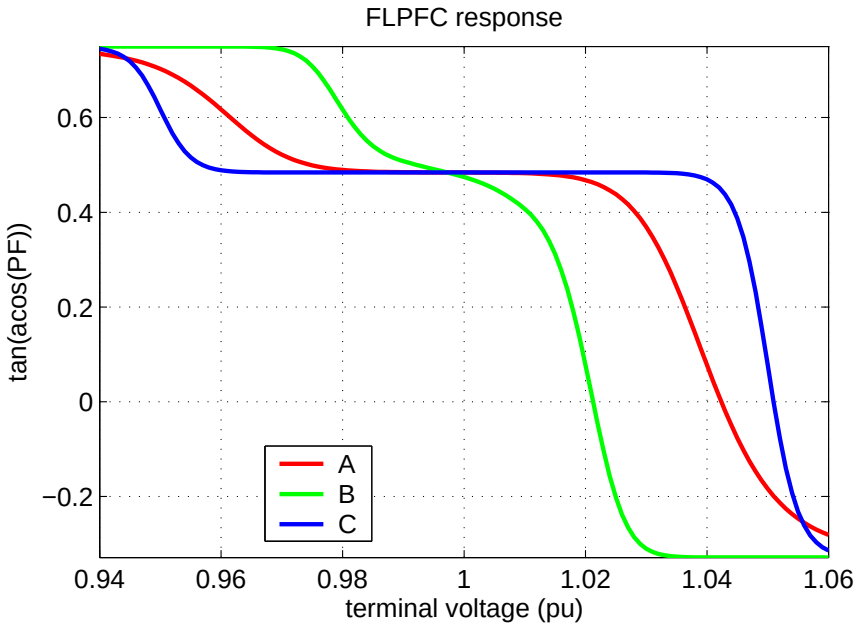

Figure 5.18: *A set of three $V-Q$ curves for the FLPFC*

All three of them though have better voltage characteristics than the APFC controller as expected. It can also be seen that curve A has the widest variation in reactive power. In all cases though, the reactive power exchanged with the network would be less than in the case of pure voltage control. This would have the obvious advantage of lesser network and generator loading. The fuzzy controller gives the opportunity to select a set of rules that match with the network characteristics and the machine and converter reactive capability. Selection of the fuzzy rules could therefore be done in agreement with the DNO on an individual basis.

5.8 Combining Intelligent Voltage Control at Generators and OLTCs

One of the reasons for the DNOs for not allowing constant voltage operation of the distributed generators, is the possibility of conflict with their control equipment such as On-Line Tap Changing transformers. Although AVPFC is partially a voltage controller,

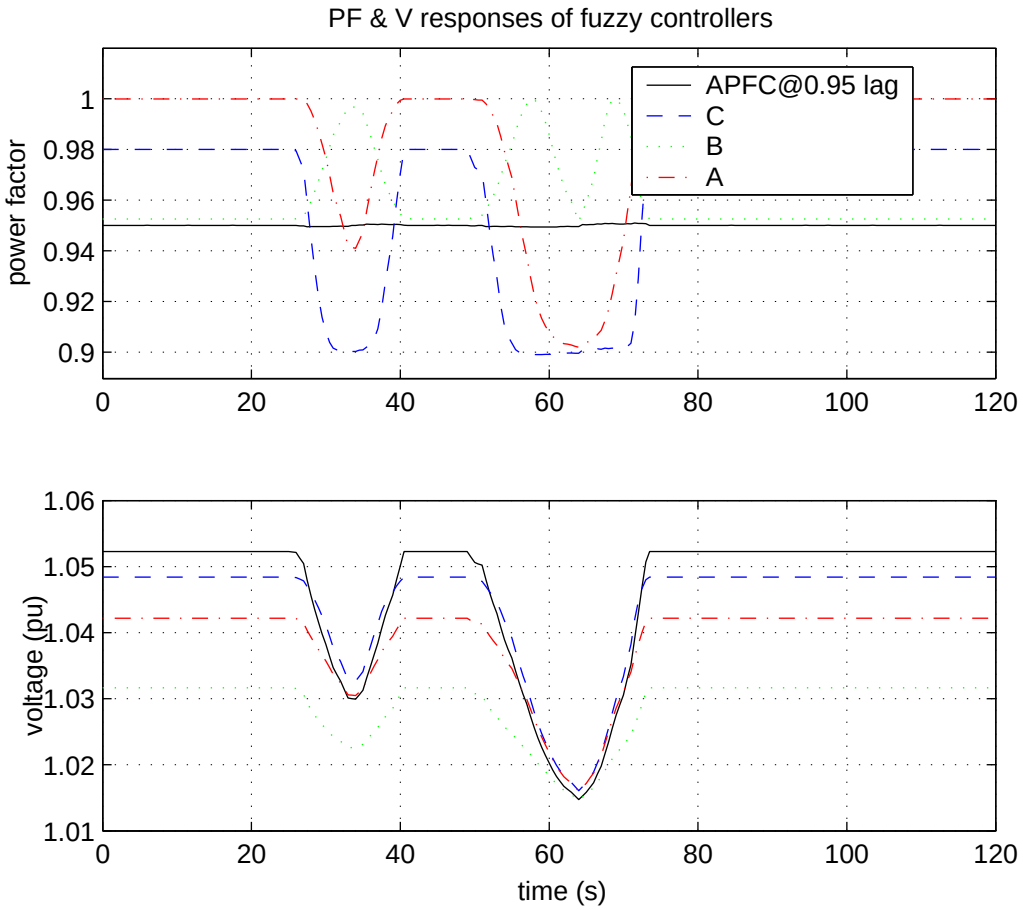

Figure 5.19: *Responses of three different fuzzy controllers and the classic power factor control*

it is possible to coordinate its operation with the network's OLTCs. This will be demonstrated through a simulation of a 4-node radial feeder such as the one depicted in Figure 5.20. The details of the system are shown in Table 5.5 below.

When combining OLTC operation and AVPFC, one of the two controllers has to be given priority for its action over the other in order to avoid hunting between them. Since the AVR of the synchronous generator (or the power electronics converter, in case of a DFIG) is much faster than the OLTC, it can provide more robust voltage regulation. In addition, its operation is smooth and does not cause step voltages as in the case of the OLTC transformer. On the other hand, its range of control is limited by the reactive power capability of the machine (and/or the converter). For these reasons, generator

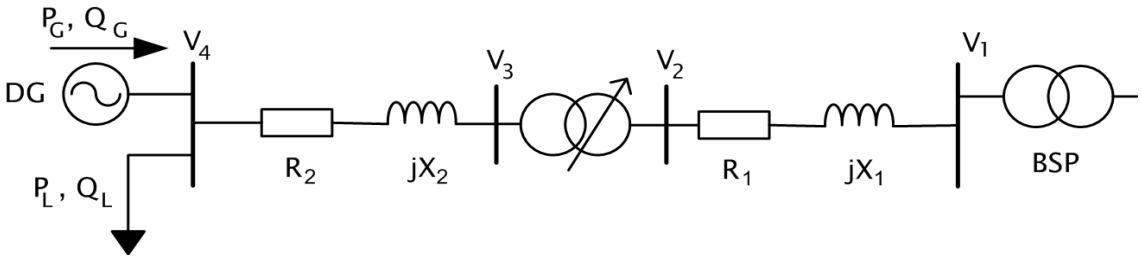

Figure 5.20: *A radial feeder with an OLTC transformer and distributed generation*

control could be used for fast, fine voltage regulation and OLTC control could be used for coarse, secondary control. This can be achieved by assigning the same target voltage to both controllers, and setting the OLTC deadband wider than the AVPFC one. Thus, should voltage rise from the nominal (target) value, it would first reach the AVPFC deadband, switching it to voltage control. The AVPFC would hold voltage steady up to its reactive power capability. Then voltage would start rising further up until it reached the OLTC limit. The OLTC would then act to reduce it, by switching one tap up on the transformer. Lowering voltage under the AVPFC limit would turn it back to automatic power factor control ('normal' mode) etc. The inverse sequence would be followed for undervoltages. Figures 5.21 - 5.28 illustrate the effects of individual and combined AVPFC/OLTC control for the system in Figure 5.20. In this simulation the distributed generation plant is a wind farm that comprises six $1MW$ DFIG wind turbines, and one day of operation with varying wind and demand conditions is shown. Figure 5.21 illustrates the 24-hour voltage profile at the wind farm and neighbouring buses when the turbines operate at constant power factor (0.98). It is shown that at the DG bus (V_4), voltage fluctuates from 0.95 pu to 1.045 pu.

Utilisation of AVPFC reduced the voltage range on the DG bus to [0.955 1.03] pu. It should be noted here that due to the limited reactive power capabilities of the induction generator, its voltage regulation is by default worse than the synchronous machine. The voltage profile at the wind farm and neighbouring buses with the turbines operate under AVPFC control is shown in Figure 5.22.

Figure 5.23 shows the node voltages when the generators operate on constant power

Parameter	**Value**
Network	
S_{base}	$10MVA$
V_{base}	$11kV$
V_1 (slack)	$1.03pu$
R_1	$0.03pu$
X_1	$0.02pu$
R_2	$0.060pu$
X_2	$0.040pu$
Transformer	
V_{nom}	$1.00pu$
V_{step}	$0.0125pu$
$V_{deadband}$	$0.0125pu$
No. of taps on each side	5
R_T	$0.003pu$
X_T	$0.050pu$
Load	
P_{Lmax}	$8MW$
PF	0.9 lagging
Generator	
P_G	$6\times$ $1MW$ DFIG WECS
PF_{nom}	0.98 lagging
PF_{range}	0.95 lagging - 0.99 leading
V_{nom}	1.00 pu
V_{range}	0.99 - 1.01 pu

Table 5.5: *Parameters of the system in Figure 5.20*

factor mode and the OLTC performs Line Drop/Rise Compensation (LDRC). As can be seen in the graph, the voltage on the DG bus is clearly constrained within the OLTC deadband another interesting observation is that the DG voltage is lowered at the expense of node V_3 voltage, which was increased from about 1.01 pu to over 1.02 pu during the peak demand period (after 09:00). Thus the voltage drop across $R_2 + jX_2$ was compensated.

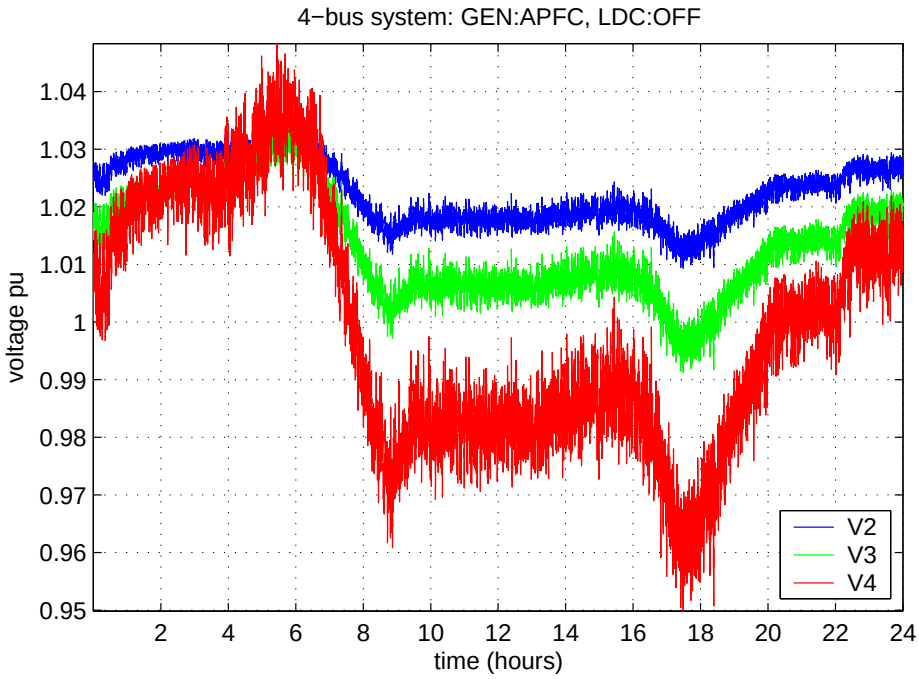

Figure 5.21: *Voltage profile for the APFC controlled wind farm*

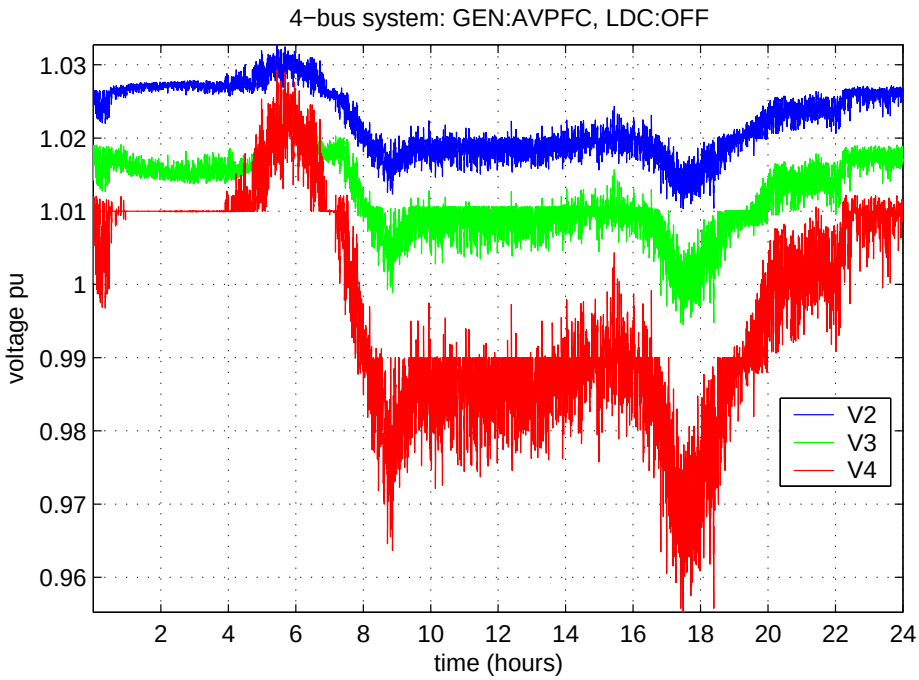

Figure 5.22: *Voltage profile for the AVPFC controlled WECS*

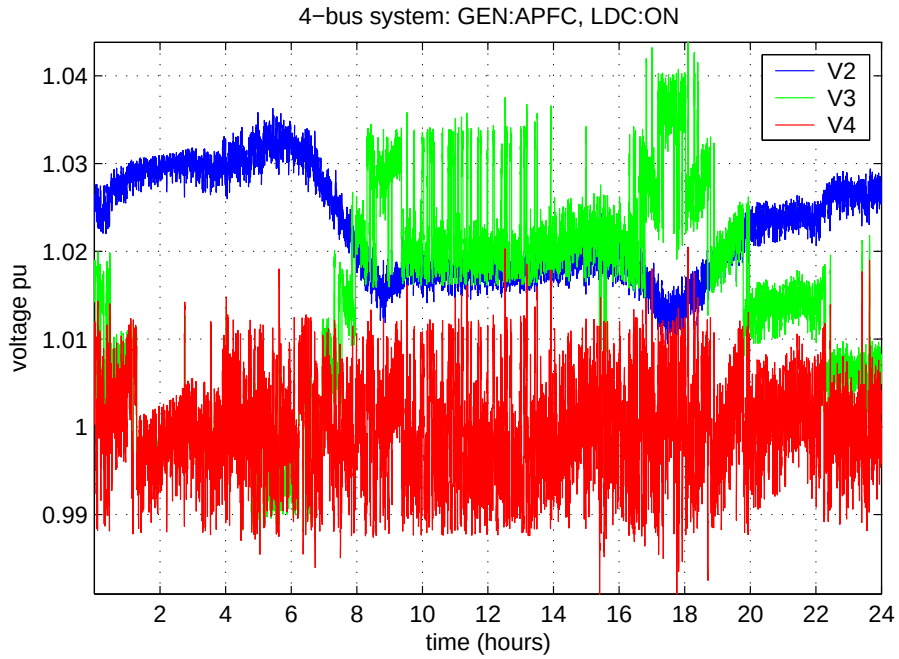

Figure 5.23: *Voltage profile for the APFC controlled WECS with line drop / rise compensation*

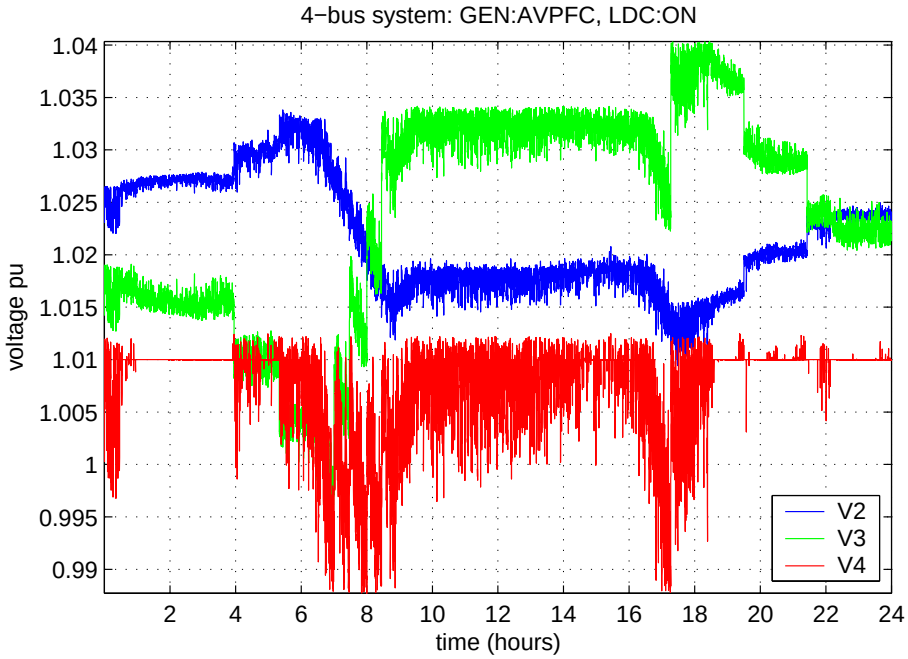

Figure 5.24: *Voltage profile for the AVPFC controlled WECS with line drop / rise compensation*

Combination of OLTC and AVPFC control is depicted in Figure 5.24. Compared to all previous three voltage profiles, the voltage profile for the combined control is further improved. With regard to the AVPFC-only case, combined operation produced better results as it 'centered' the average voltage value within the operating range of the AVPFC, thus allowing it to operate for more time without hitting its reactive power limits. This is illustrated in Figures 5.25 and 5.26, where the respective reactive power outputs (from a single generator out of six) are shown. With regard to the LDRC-only case, combined operation improved the voltage profile as for significant periods (00:30-04:00 and 16:20-24:00 approx.) the generator was able to operate at constant voltage as the reactive power requirement for that was within its capacity. A final but equally important observation that can be made with these simulations, is the drastic reduction of the tap changes at the combined operation, compared to LDRC-only. Figures 5.27 and 5.28 show the tap transitions throughout the simulated period. It is demonstrated that for the simulated wind, load and network conditions, the LDRC-only operation would bring about 197 actions of the tap changer. This is a large number of transitions and would cause quick wear-out of the tap contacts and therefore would increase maintenance costs. Combined AVPFC-LDRC operation reduced the tap changes to only 9 for the same simulated conditions. The reason for this reduction is that AVPFC is able to reduce voltage fluctuation due to wind variability below the OLTC action threshold, and therefore the OLTC needs only to follow the slow load variation. It should be mentioned that in the above simulations operation of the emulating circuit for the LDRC was assumed to be ideal. In reality, the (possible) inaccuracy in estimation of the receiving end voltage would require some extra margin between the LDRC and AVPFC deadbands to ensure that the AVPFC deadband is fully enclosed in the LDRC one.

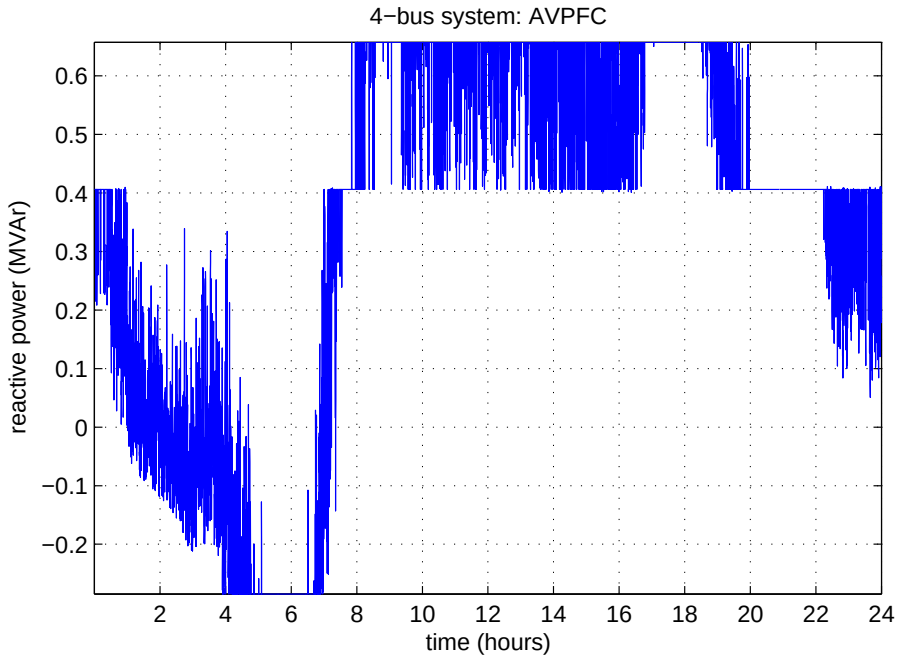

Figure 5.25: *Reactive power exchange from one AVPFC controlled WECS*

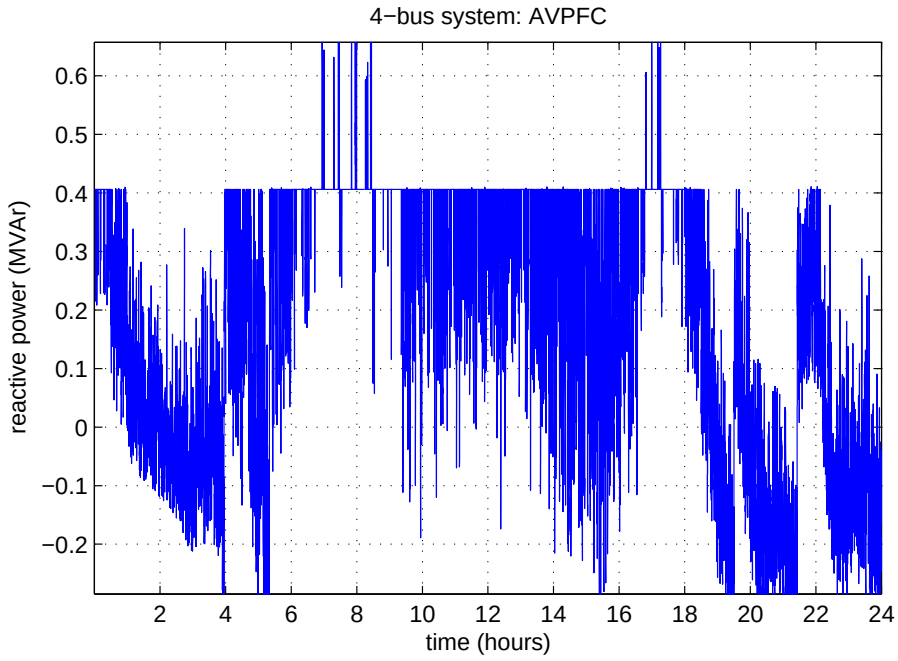

Figure 5.26: *Reactive power exchange from one AVPFC controlled WECS with line drop / rise compensation*

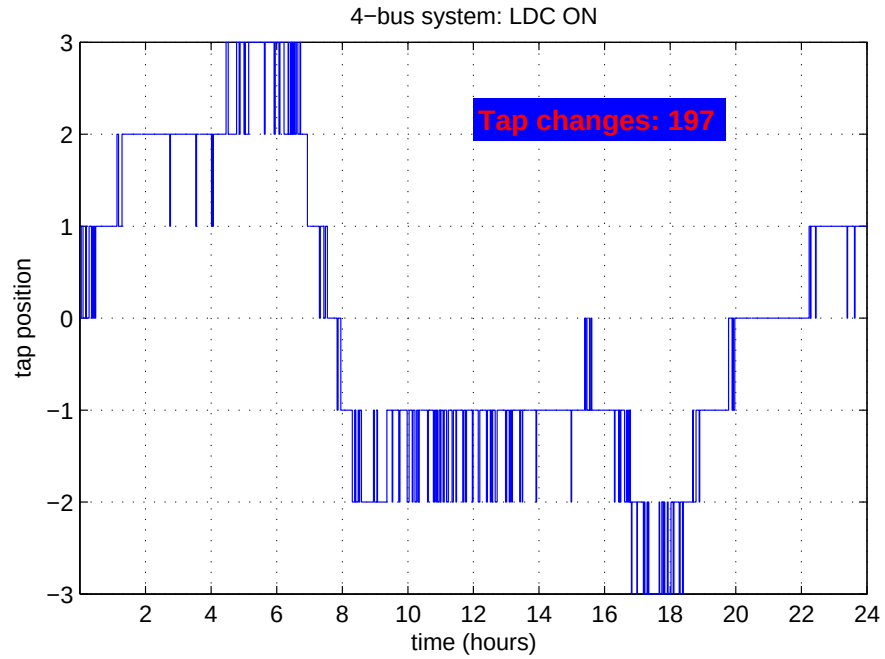

Figure 5.27: *OLTC tap position during the 24-hour simulation with the APFC controlled WECS*

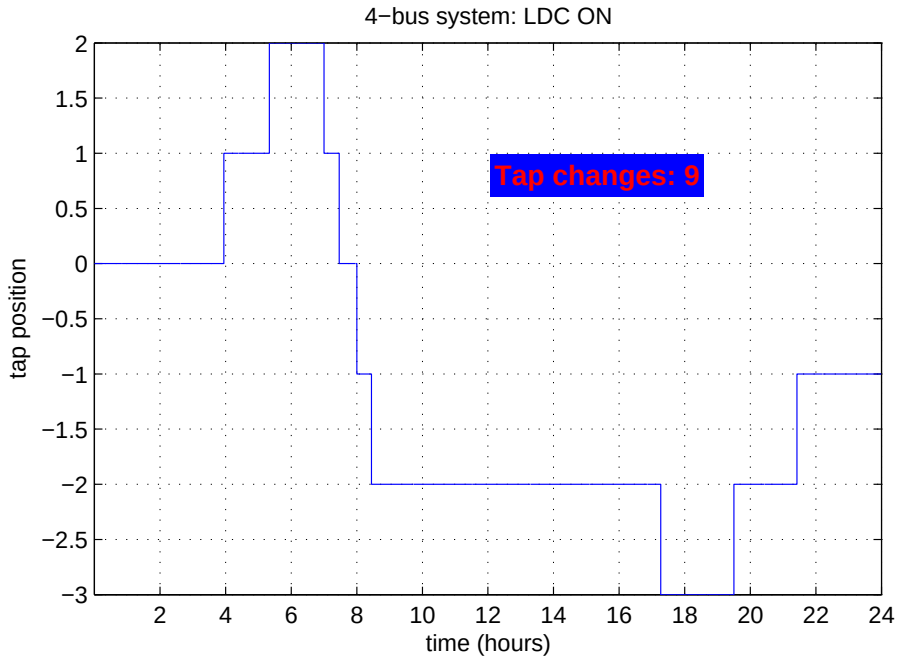

Figure 5.28: *OLTC tap position during the 24-hour simulation with the AVPFC controlled WECS*

5.9 Summary

In this chapter the need for an intelligent control strategy for distributed generators was discussed and two candidate solutions were proposed: a hybrid voltage / power factor controller and a fuzzy logic power factor controller. Both algorithms allowed extension of generator operating period in a weak network and therefore an increase of the revenue from energy export. This was illustrated by simulations of a DG in a radial network using a realistic local load pattern. It is possible to combine operation of OLTC transformers with the proposed intelligent generation controllers. The results of the combination appear to be improved when compared to individual generator or OLTC control. However, the developer should discuss with the DNO beforehand about the adoption of the AVPFC scheme because the generator's settings may conflict with those of the network equipment when in constant voltage mode. On the other hand, adoption of the Fuzzy Controller scheme can be straightforward, provided that the controller is set to operate within the voltage and power factor limits set by the machine specifications and the DNO. In the next chapter the two proposed algorithms will be tested in a real section of the Scottish distribution network in order to quantify the possible merit of their utilisation.

Chapter 6
Case Study: Integrating New Generation in the Scottish DN

6.1 Introduction

This chapter presents a series of simulations of a real section of the Scottish distribution system, which prove that the proposed control strategies can (a) improve voltage profiles in a weak network and (b) increase the capacity of Embedded Generation in the Distribution Network. A number of simulations has been performed using both synchronous generators with a constant or slow-varying source and doubly fed induction generators with a very intermittent source (wind). Firstly, the operation of the test system including synchronous generators with and without intelligent control is presented. The second set of simulations includes transformers with OLTCs performing Line Rise Compensation. The effects of combining OLTCs with intelligent generators are discussed. Finally, wind generation is introduced to the system and the effects of primary source intermittency on network voltage are presented.

6.2 Description of the Test System

This section presents the system under consideration (shown in Figure 6.1), describes the operating conditions and stating the assumptions and simplifications used in the following simulations. This system is a part of the Scottish distribution network. It made of overhead lines and the loads follow a typical rural demand profile. The line data as well as the maximum load values were obtained by the DNO. It is assumed that the demand (shown in Figure 6.2 consists of 80% domestic and 20% industrial loads with a minimum of 30% of the maximum value on each bus and that all loads have constant and equal power factor (0.9).

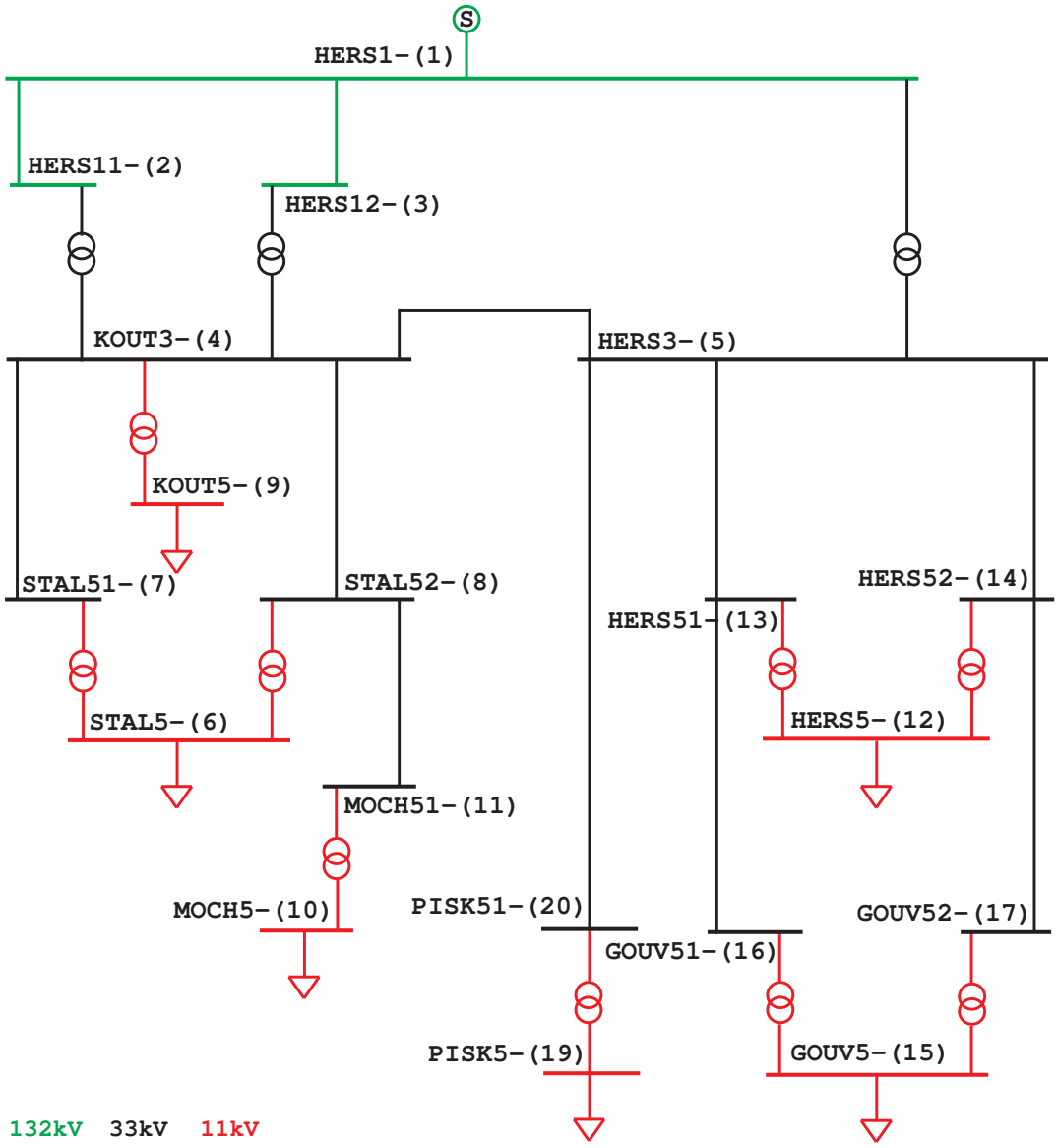

Figure 6.1: *The section of the Scottish distribution network used as a test system. The names of the buses are concealed.*

There are several transformers installed in the system under investigation, some of them serve as step-down transformers to reduce the voltage level from the $132kV$ of the bulk supply point down to $33kV$ and then further to $11kV$, others re-adjust the bus voltages closer to the nominal values using fixed taps, and a few others are equipped with auto tap changers to provide a means of voltage regulation. By dynamically altering the voltage levels, the latter have the ability to assist power transfer from and to the far ends

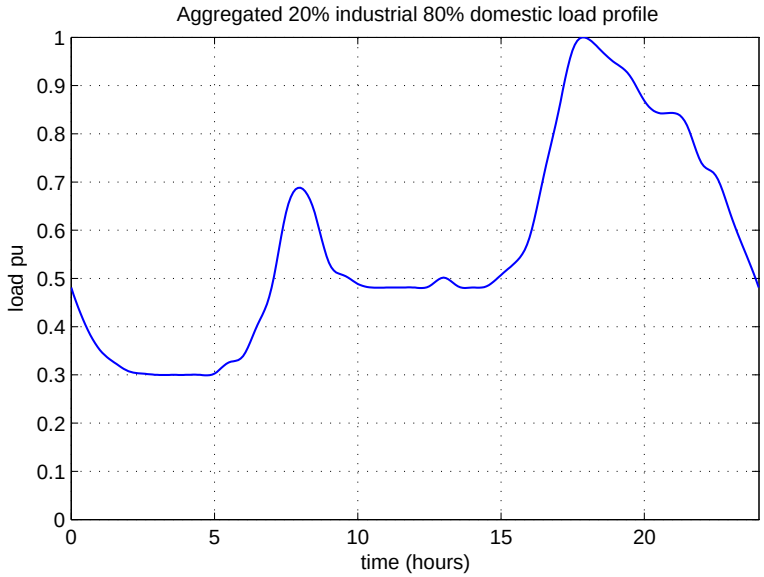

Figure 6.2: *Demand profile in the simulated network*

of the system, thus interfering with the action of the designed controllers. Therefore, in order to have a clear image of the controllers effects, automatic tap-changing on these transformers was disabled in some of the simulations. Unless otherwise stated, the results presented in this chapter are the outcomes of steady-state analysis, as the major concern here is energy capture and not the action of the controllers themselves, as this has been discussed in detail in the previous chapter.

6.3 Operation of the Test System Without Use of OLTCs

In order to have a clear image of the effects and the possible benefits of utilisation of intelligent control of distributed generators, the OLTCs of the test system have been disabled so that their operation will not affect the results of the simulations. In this section two sets of simulations are presented, one with the generators connected to $11kV$ buses and one to the $33kV$ ones. Thus the difference in the performance of the generators when connected both to weak and stiff feeders is shown.

6.3.1 Generators on the 11kV System

The $11kV$ network is more prone to voltage fluctuations and therefore has a lower capacity headroom. Simulations with the generators connected at $11kV$ show that voltage regulation can be assisted by utilisation of intelligent generator control, while the capacity that can be installed is increased. Figure 6.3 shows the voltage profile for 24 hours of operation of the simulated network with an embedded generation of $2MW$ connected to bus GOUV5.

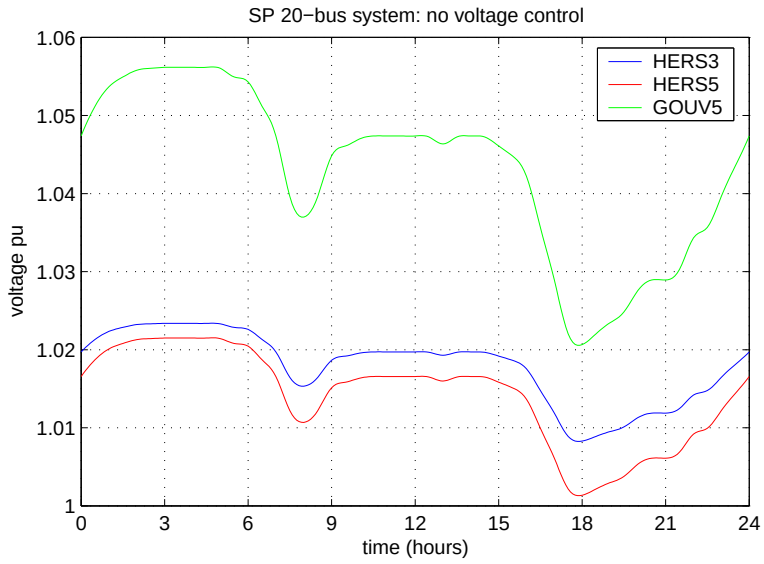

Figure 6.3: *Voltage profiles of buses HERS3, HERS5 and GOUV5 after the connection of a $2MW$ generator at GOUV5 operating in power factor control mode*

The generator is assumed to have constant power output and a power factor of 0.95 (required by the DNO). It is obvious that under the traditional power factor control, the generator would cause an overvoltage on its bus that partially propagates to its neighbouring buses too. Although it does not reach the 1.06 pu statutory limit, operating the generator at such high voltage is a risk, as any sudden change of the network parameters (loss of loads, feeder availability) would drive the voltage outside the 1.06 pu limit and would cause disconnection of the plant. Figure 6.4 shows the voltage profile for the same buses with the generator under AVPFC control. The controller settings are shown in Table 6.1.

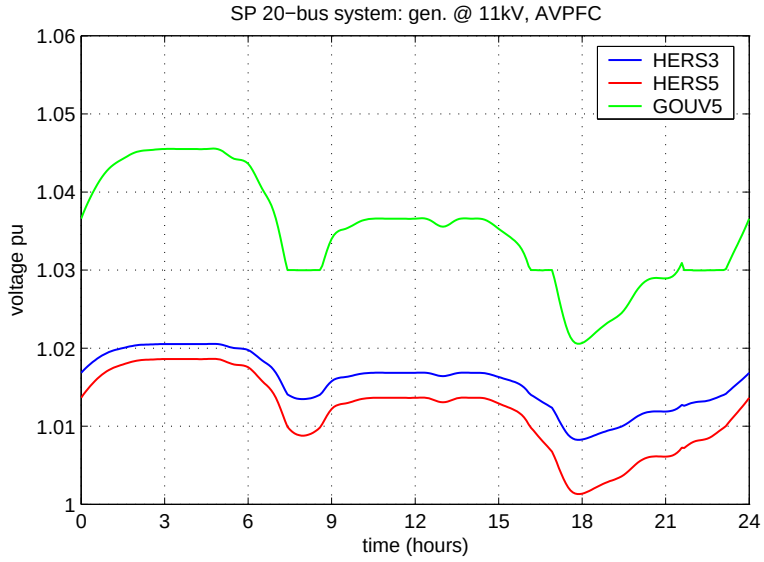

Figure 6.4: *Effect of operating the generator at GOUV5 in AVPFC mode on the voltage profiles of buses HERS3, HERS5 and GOUV5*

V_{high}:	1.03 pu
V_{low}:	0.97 pu
$V_{deadband}$:	0.001 pu
PF_{ref} :	0.95 lagging
PF_{max}:	0.99 leading
PF_{min}:	0.9 lagging
$PF_{deadband}$:	0.0005

Table 6.1: *AVPFC settings*

The controller allowed operation of the generator at lower voltages although only for 8 hours below the 1.03 pu setpoint. This was because for the rest of the time the generator had reached its reactive power capability, as shown in Figure 6.5 and therefore could not import more MVArs to reduce voltage.

It should be noticed however that the voltage was reduced at the neighbouring buses too, which shows that intelligent generator control not only can have a positive effect at the generator bus, but may improve voltage quality throughout a larger area of the distribution network.

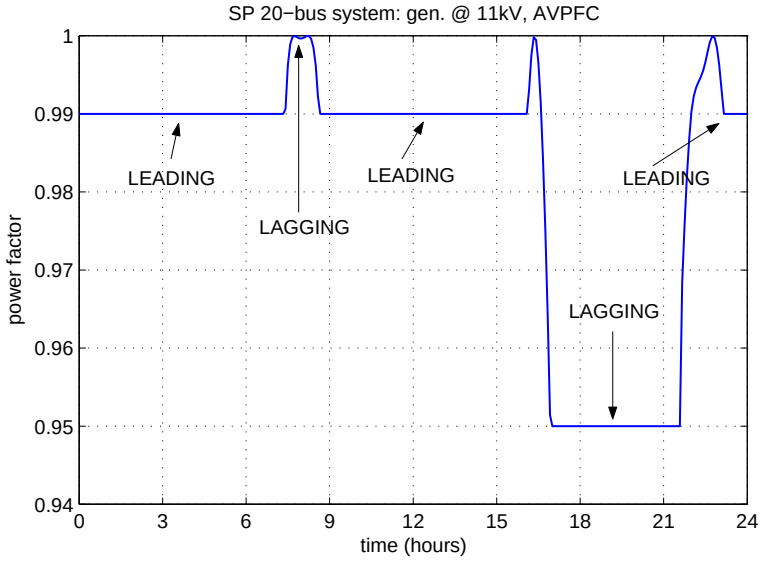

Figure 6.5: *Power factor of generator at GOUV5 operating in AVPFC mode*

Figure 6.6 shows the operating voltage ranges for all the buses in the simulated system. For this simulation a $2.4MW$ synchronous generator operating at a constant 0.95 power factor was connected to bus 15 (GOUV5). The dark blue part of the bars represents undervoltage, light blue and red are the headrooms for undervoltage and overvoltage respectively, and finally yellow is the operating area for each bus. It is shown that voltage at GOUV5 is marginally at the limit for overvoltage, meaning that any further increase of the generating capacity on that bus (or its neighbouring ones, in electrical terms) will lead to overvoltage. Application of the fuzzy logic power factor controller (FLPFC) to the generator led to a reduction of the level and constraint of the range of voltages for all the buses that are electrically close to GOUV5. Figure 6.7 shows the voltage response of the network to the same generator, this time under control of an FLPFC with the volt - $tan(\phi)$ characteristic of Figure 6.8. Therefore for the same load and network conditions, intelligent generation control improves voltage quality in the distribution system.

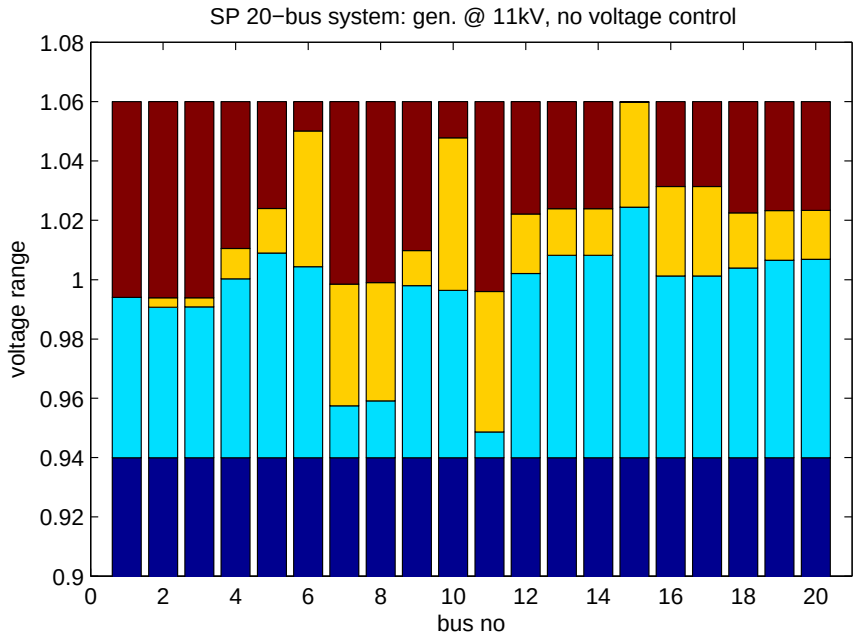

Figure 6.6: *Voltage range on all 20 buses with a 2.4MW generator connected to bus GOUV5*

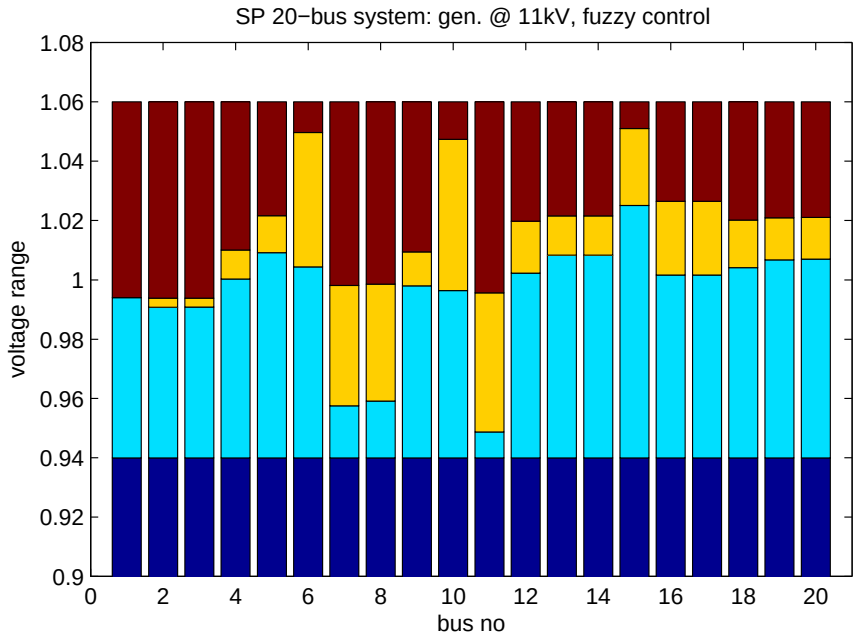

Figure 6.7: *Voltage ranges with the generator controlled by the fuzzy controller*

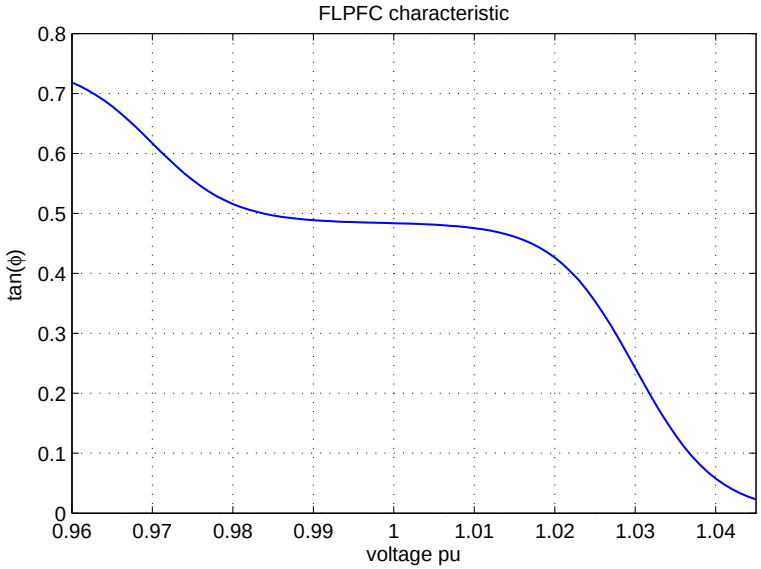

Figure 6.8: *Volt-tan(ϕ) characteristic of the FLPFC*

An alternative way to quantify the merit of utilising intelligent generation control in a distribution system, is to derive the increase of generator capacity before the voltage levels occurred when traditional power factor control was used. The size of the generator at bus GOUV5 was gradually increased until voltage reached 1.06 pu, as in the case of power factor controlled $2.4MW$, 0.95 PF machine. Under FLPFC control, the voltage at bus GOUV5 reached 1.06 pu for a capacity of $4.2MW$, which represents an $1.8MW$ (or 75%) increase. This increase would not otherwise be possible to achieve, unless a network upgrade or installation of an OLTC transformer was performed. The resulting voltage ranges after the $1.8MW$ increase are shown in Figure 6.9.

6.3.2 Generators on the 33kV System

The $33kV$ network can accommodate larger capacity of distributed generation and the voltage fluctuation is less than in the $11kV$ grid. The simulations of the system with the generators connected at $33kV$ show that both in percentage and in absolute terms, the increase of capacity due to the use of intelligent generator control is greater than the $11kV$ case, while voltage regulation is also improved. Figure 6.10 shows the voltage at

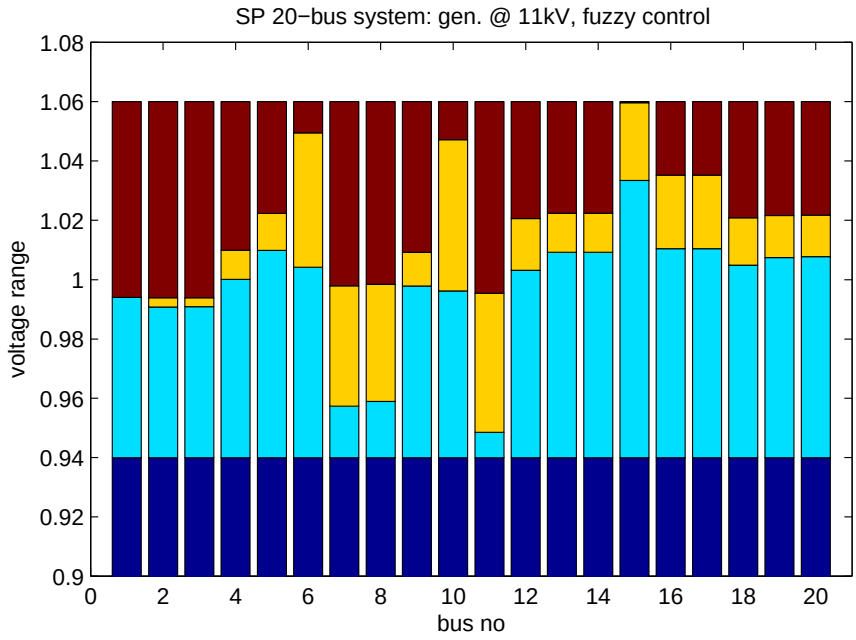

Figure 6.9: *Voltage ranges with a 4.2MW generator under fuzzy control on bus GOUV5*

buses HERS3, HERS5 and STAL5 after the connection of an $8MW$ generator running at a constant 0.95 power factor, this time at bus HERS3.

The first noteworthy point is that compared to Figure 6.3, equivalent voltage levels are observed with a generator with four times larger capacity. Secondly, although the voltage of the generator bus is not high (max. 1.024 pu), the voltage at the bus at the far end of the feeder (GOUV5) exceeds 1.05 pu. This could be resolved by upgrading the feeder or stepping down the transformers that feed GOUV5. However the former is an expensive solution and the latter implies that the generator will be always need to be connected and generating its rated power, which may not be the case for an embedded generator. Enabling AVPFC control of the generator reduces voltage at the generator bus as well as all the way down the feeder. The controller's characteristics are the same as in the 11kV case and are shown in Table 6.1. Figure 6.11 shows the effect of using the AVPFC on the voltage along the feeder.

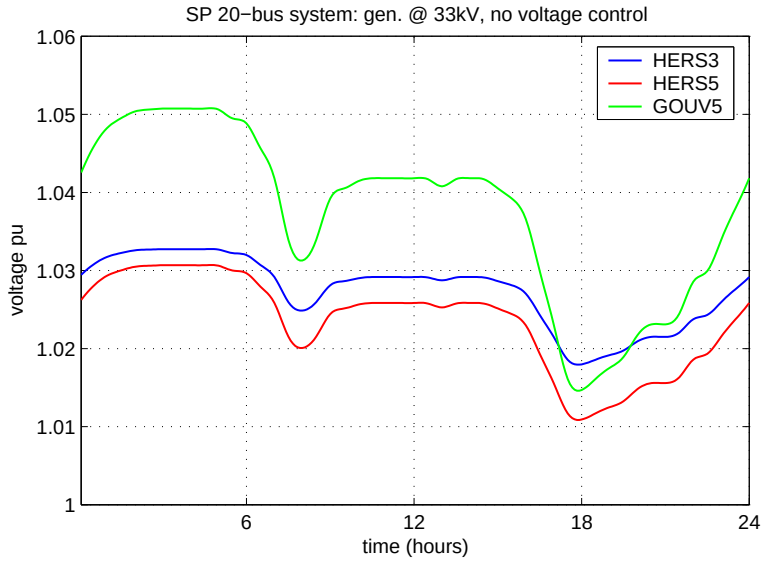

Figure 6.10: *Voltage profiles of buses HERS3, HERS5 and GOUV5 after the connection of a 8MW generator at HERS3 operating in APFC mode*

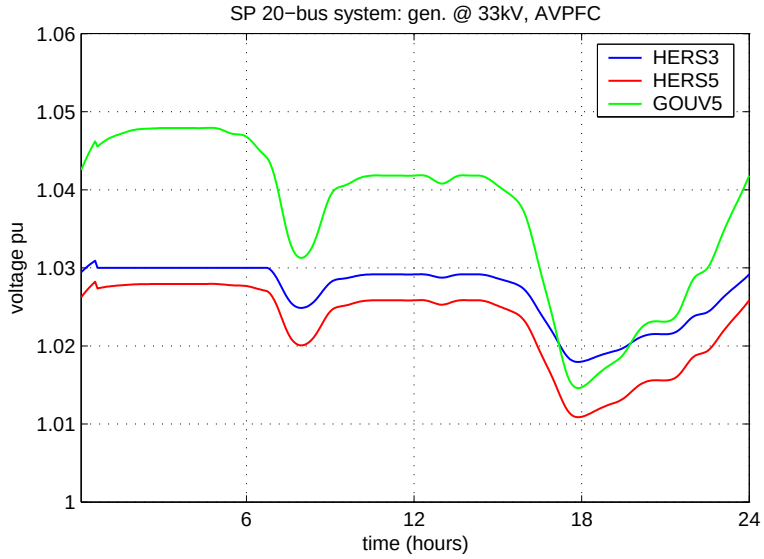

Figure 6.11: *Effect of operating the generator at HERS3 in AVPFC mode on the voltage profiles of buses HERS3, HERS5 and GOUV5*

This time the generator does not reach its excitation limit and is able to hold bus voltage at or below the 1.03 pu setpoint for the whole period of the simulation. Figure 6.12

shows the power factor of the machine and can be observed that it does not need to go into leading (importing MVArs) to hold voltage. Installing a $14MW$ generator at bus HERS3 will cause voltage at bus HERS5 to rise up to the statutory voltage limit of 1.06 pu thus restricting access for further generation in the network.

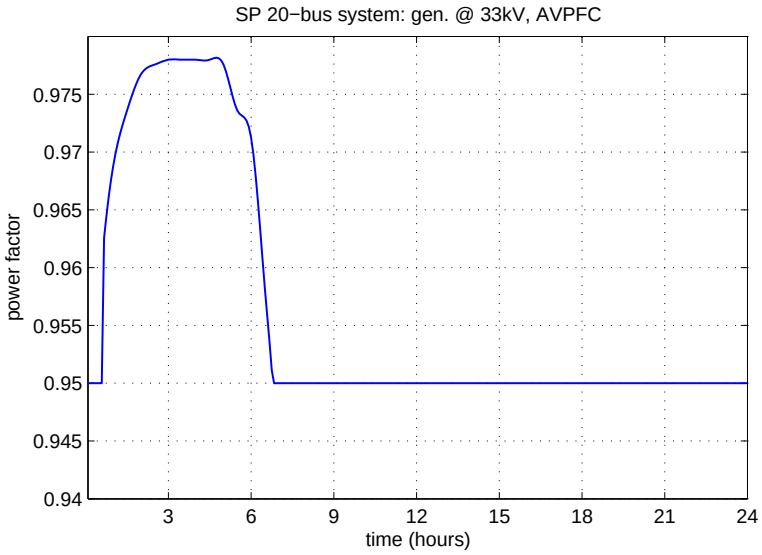

Figure 6.12: *Power factor of generator at HERS3 operating in AVPFC mode*

The operating voltage ranges of the whole system are depicted in Figure 6.13. Use of a fuzzy power factor controller on the generator led to a reduction of the voltage level and range, more noticeably at bus GOUV5 but also in a lesser degree at all buses below HERS3. Figure 6.14 shows the new voltage ranges and it can be observed that bus GOUV5 voltage does not exceed 1.05 pu when the generator is assisted by the FLPFC. Being under FLPFC control, the capacity of the generator at bus HERS3 can be further increased up to $36MW$ before a bus voltage in the simulated system (once again, GOUV5) hits the 1.06 pu limit. Compared to the $11kV$ case, the $22MW$ (or 157%) increase from the initial $14MW$ is more dramatic due to the fact that the generator bus is electrically closer to the bulk supply point and therefore the generated power can be easily exported to the slack bus.

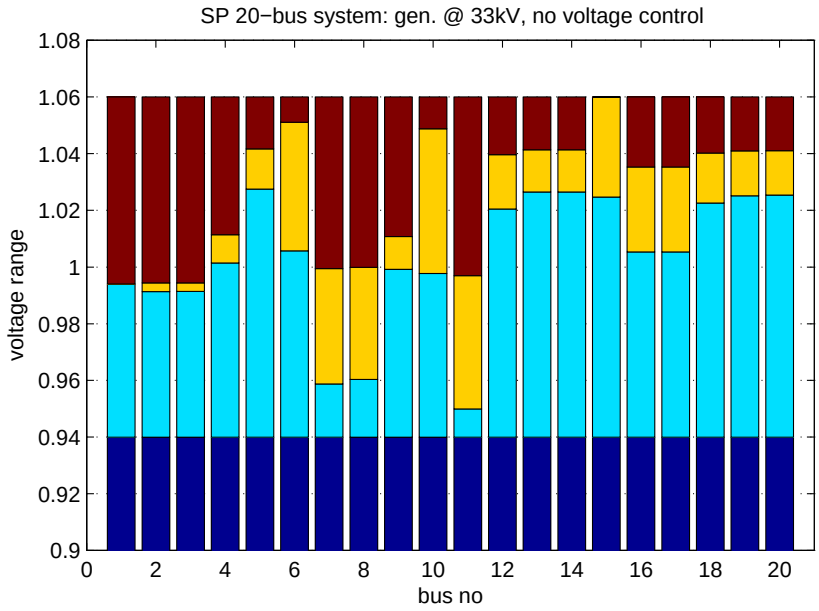

Figure 6.13: *Voltage range on all 20 buses with a* $14MW$ *generator connected to bus HERS3*

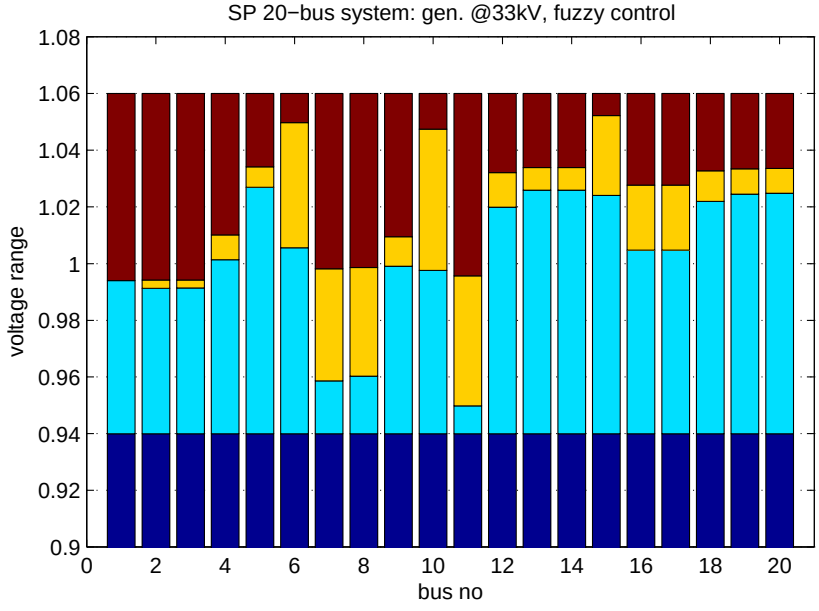

Figure 6.14: *Voltage ranges with the generator controlled by the fuzzy controller*

The resulting voltage ranges for the 20-bus system after the increase of the capacity of the generator at HERS3 are shown in Figure 6.15. One strange phenomenon is that the

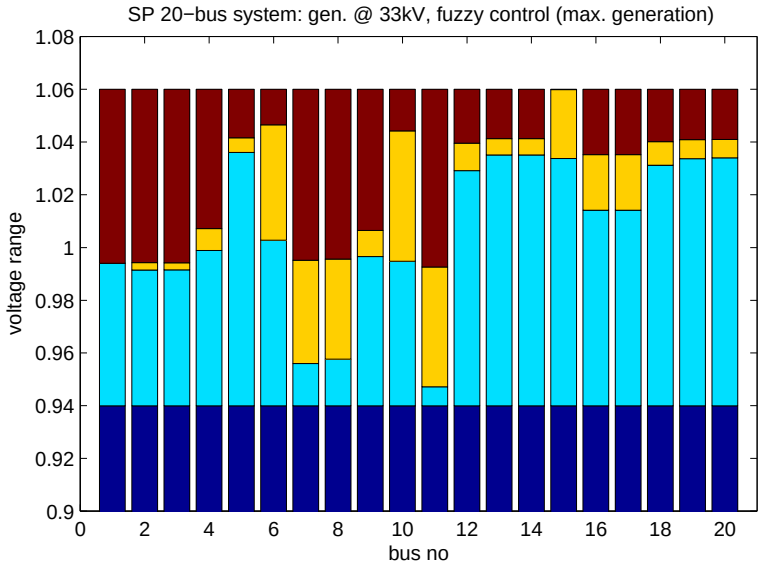

Figure 6.15: *Voltage ranges with a 36MW generator under fuzzy control on bus HERS3*

voltage ranges in some buses (no. 12-14, 16-20) are reduced, although with the increase of local generation capacity the opposite effect was expected. This can be explained as follows: both the minimum and the maximum value of these bus voltages tend to rise due to the increasing generating capacity, but due to its nonlinear nature, the fuzzy controller tries more aggressively to reduce higher voltages, therefore contracting the voltage range at the generator bus and consequently to all its neighbouring buses as well.

6.4 Intelligent Generator Control and OLTCs in the Test System

This section presents a series of simulations that compare and then combine intelligent generation control with OLTC operation in line rise/drop compensation mode. In all cases a 24 hour period was simulated, with a resolution of 5 seconds. It is shown that there is an improvement in voltage regulation as well as a reduction in tap changes, which in turn reduces the maintenance costs and increases lifetime of the tap changers.

6.4.1 Connection of a Small-Hydro Scheme with Synchronous Generator

In this section the effects of connecting a Small-Hydro Generator (SHG) in the test system will be presented through simulation. The characteristic of SHG in power generation terms is that its output is relatively constant (assumed constant for the entire simulated period here) compared to wind generation. In that sense, this simulation could represent any SG-based power plant of that size. In the test system, the transformer that feeds bus HERS3 from the bulk supply point is equipped with an On-Line Tap Changer and it is set to perform line voltage drop/rise compensation across the feeder down to bus GOUV5. At that bus, a 2MW, 0.95 power factor SHG is connected. The OLTC settings are shown in Table 6.2 below.

V_{target}:	1.03 pu
$V_{deadband}$:	0.0125 pu
number of taps:	± 5
time delay:	60 seconds

Table 6.2: *OLTC settings*

Operation of the generator in APFC mode without OLTC operation is shown in Figure 6.3. As it was seen in Section 6.3.1, the voltage on GOUV5 was very close to the overvoltage limit during the period of low demand. After enabling the OLTC, voltage was reduced to $V_{target} \pm V_{deadband}$ as shown in Figure 6.16. It should be noticed however, that the voltage at the upstream buses is not kept between limits, especially during the peak demand period. The voltage on GOUV5 is increased in order to remain within the operational band, but in order to compensate the voltage drop across the feeder, the voltage at the buses between the transformer and the controlled bus is increased even further. Figure 6.17 shows the tap changes, which add up to six.

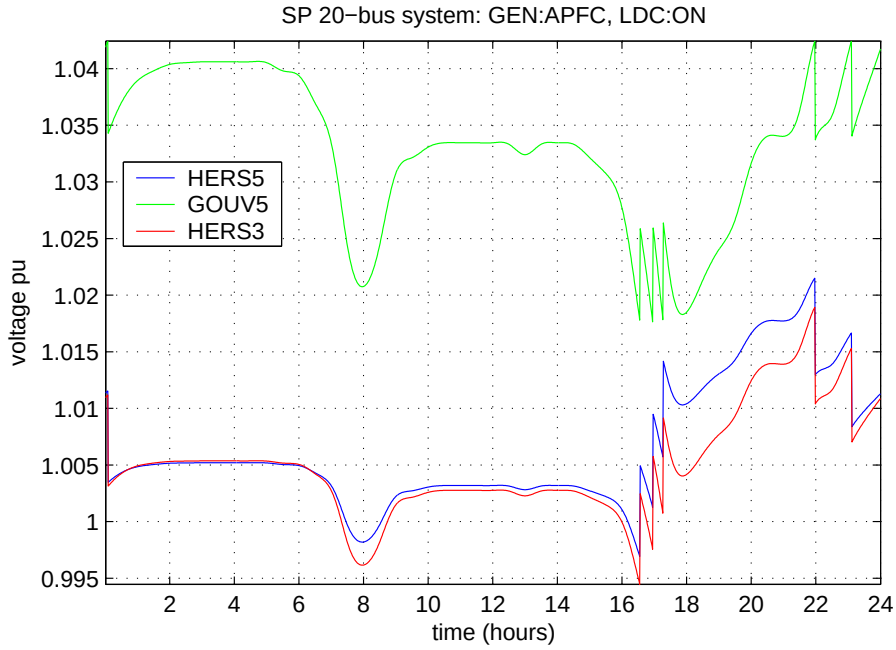

Figure 6.16: *Voltage profile of buses GOUV5, HERS5 and HERS3 with a 2MW synchronous generator at GOUV5 and LDRC operation*

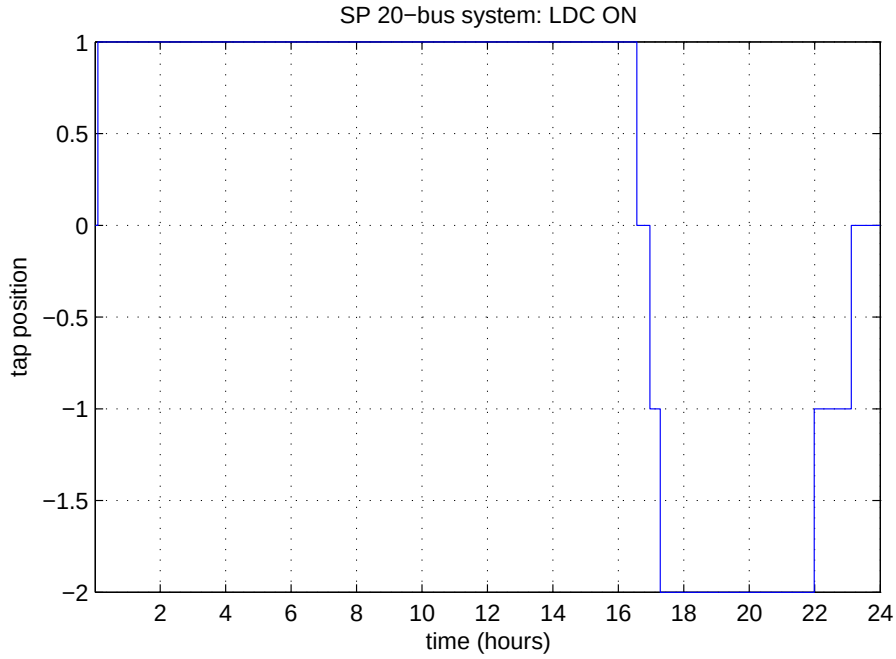

Figure 6.17: *Tap transitions of the OLTC transformer*

Figure 6.18 displays the resulting voltages on buses GOUV5, HERS5 and HERS3 from the combined use of AVPFC on the generator and LDRC on the transformer. The AVPFC settings for this simulation are shown in Table 6.3. The reactive power exchange of the generator (shown in Figure 6.19) was sufficient to keep voltage constant for most of the time that was needed. Only during the extreme states of demand (low at 00:30 and high at 17:00) the MVAr limits of the generator were met. At these instances voltage could not be further controlled by the generator, and appropriate action of the OLTC brought it back within the specified area. The assistance of the AVPFC in voltage regulation is reflected to the number of tap changes, which is reduced to four. The total tap excursion was also reduced, from +1/-2 tap positions to +1/-1. The result of this reduction is that the voltage of the upstream buses experienced a smaller increase.

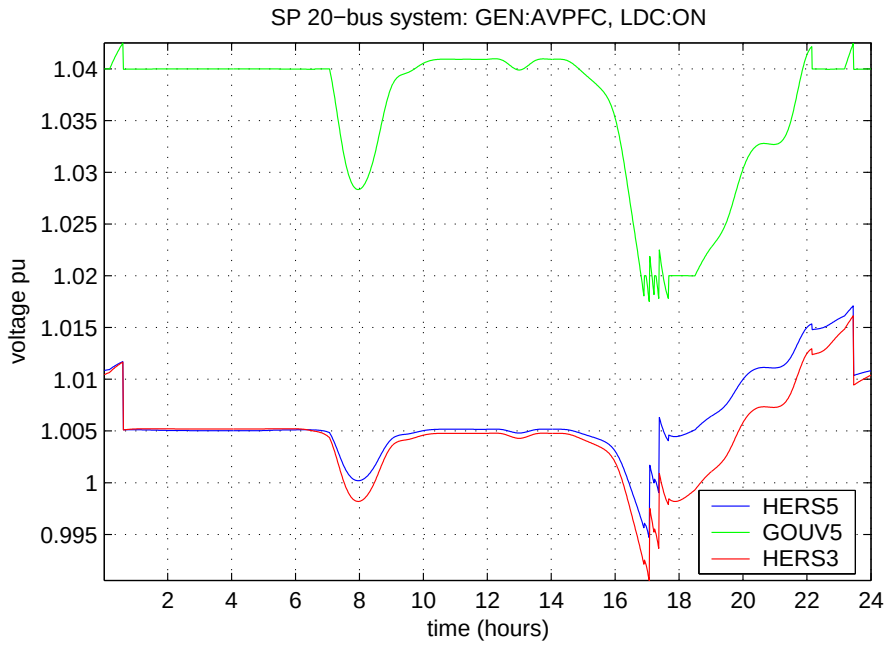

Figure 6.18: *Voltage profiles for combined AVPFC and LDRC operation*

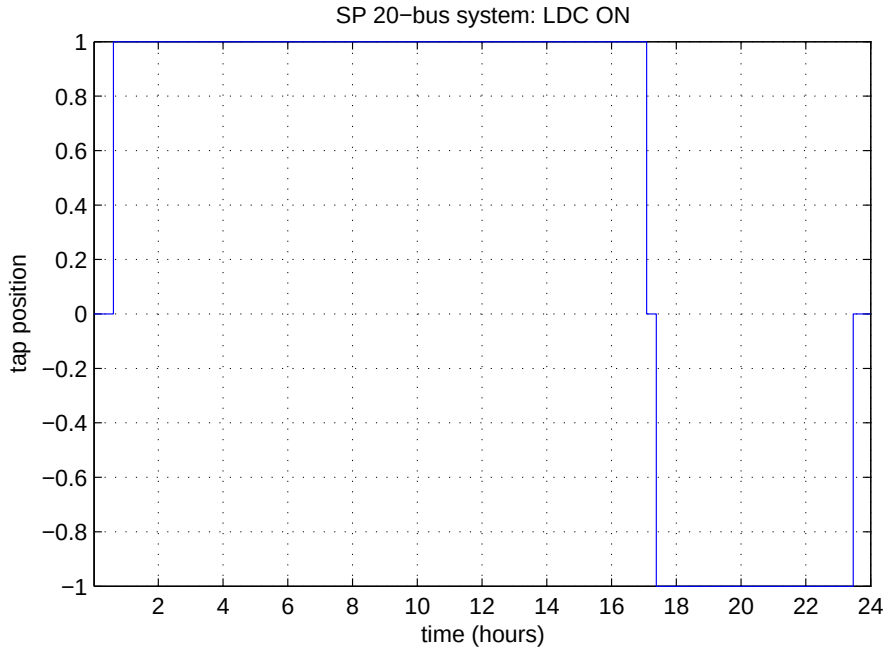

Figure 6.19: *Tap transitions of the OLTC transformer with the generator under AVPFC control*

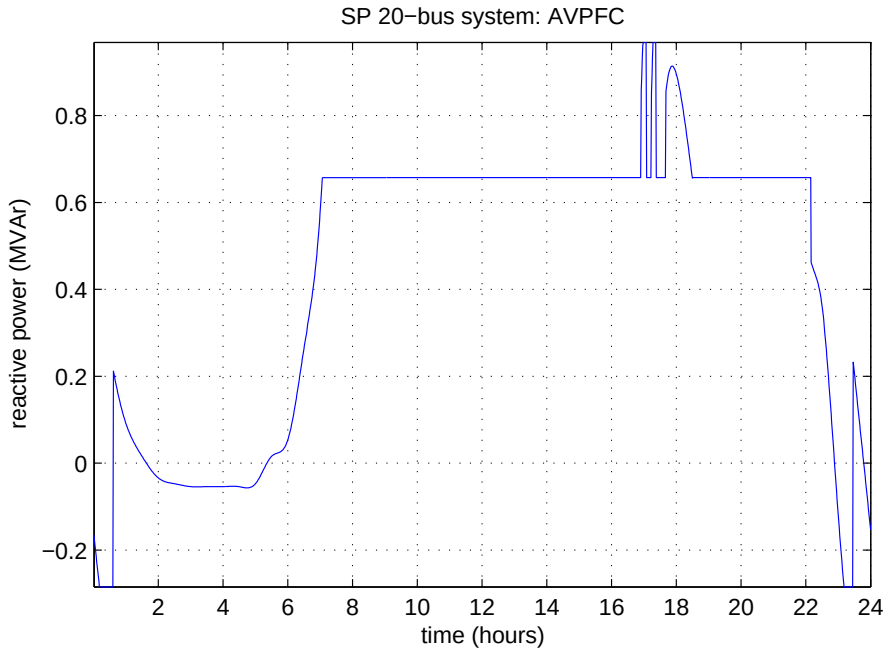

Figure 6.20: *Reactive power exchange or the generator under AVPFC control*

V_{high}:	1.04 pu
V_{low}:	1.02 pu
$V_{deadband}$:	0.001 pu
PF_{ref} :	0.95 lagging
PF_{max}:	0.99 leading
PF_{min}:	0.9 lagging
$PF_{deadband}$:	0.0005

Table 6.3: *AVPFC settings*

6.4.2 Wind Generation in the Test System

Intelligent generation control has also been applied to wind turbines equipped with Doubly Fed Induction Generators (DFIGs). In this section a simulation of the test system including a wind turbine with a DFIG connected on a weak bus is presented. The operation of the generator under constant power factor and automatic voltage/reactive power control is compared. Then, an OLTC transformer is set to perform line drop/rise compensation in order to further assist voltage regulation. Figures 6.21 to 6.28 show the simulation results of the operation of a 2MW DFIG wind turbine at the same bus and under the same load conditions.

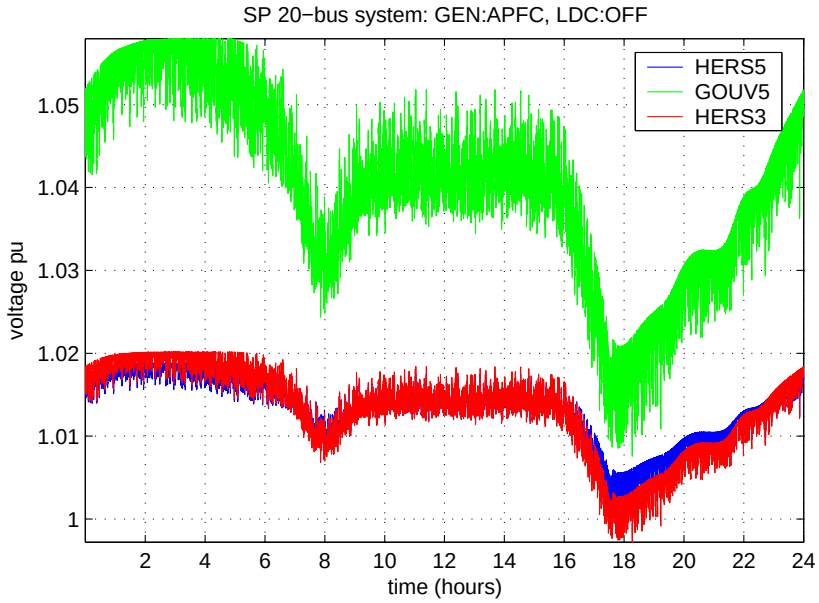

Figure 6.21: *24-hour voltage profile with the wind turbine operating in APFC*

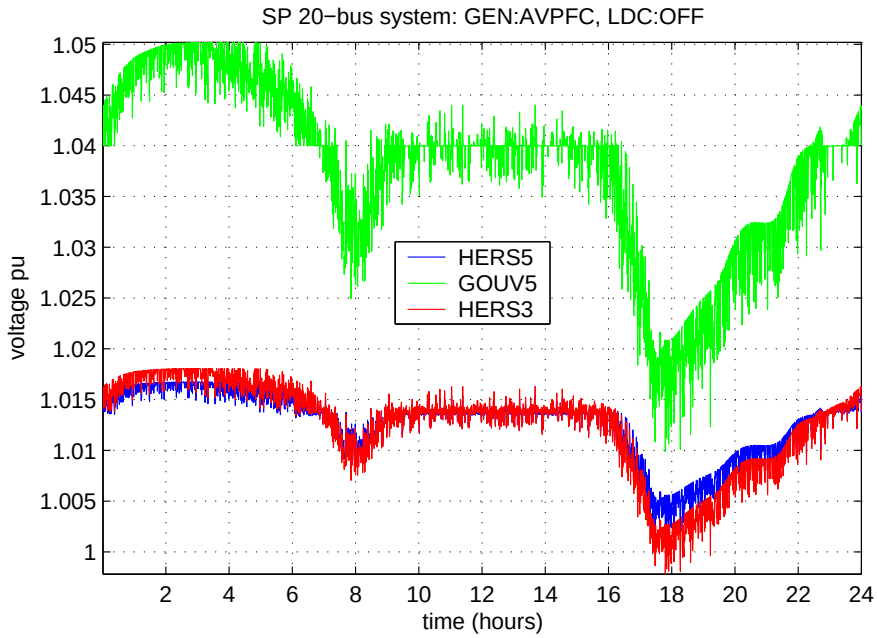

Figure 6.22: *24-hour voltage profile with the wind turbine operating under AVPFC control*

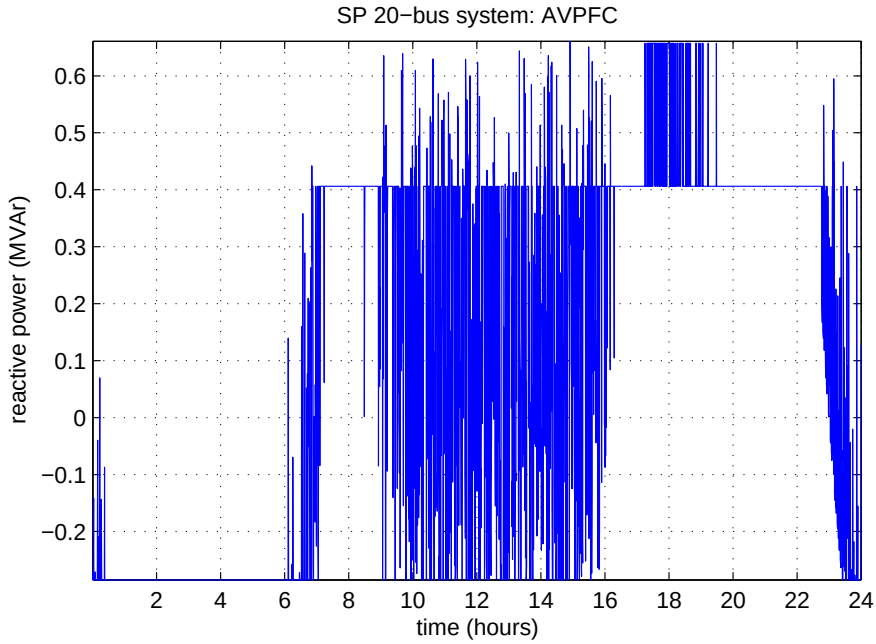

Figure 6.23: *Reactive power exchange of the wind turbine operating under AVPFC control*

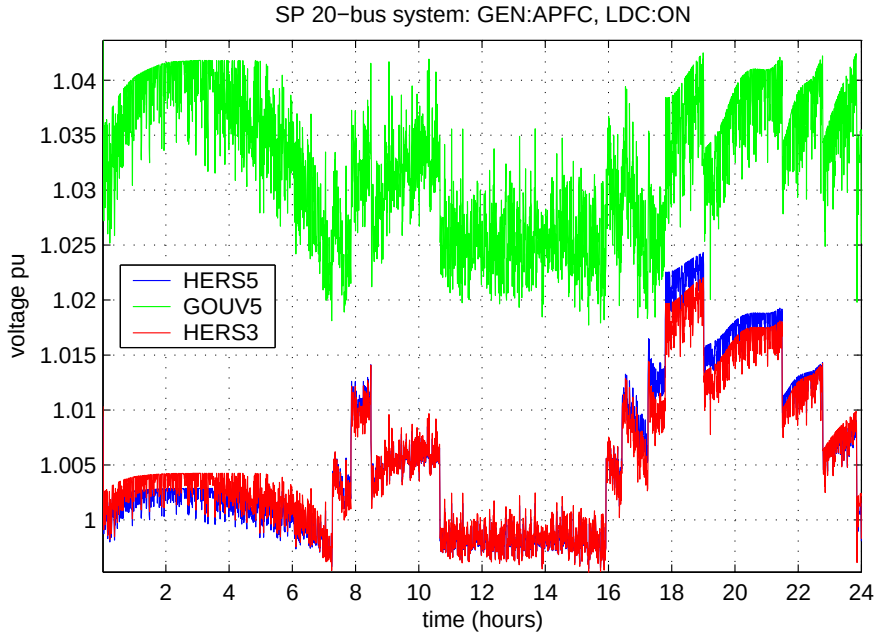

Figure 6.24: *24-hour voltage profile with the wind turbine in APFC mode assisted by line drop/rise compensation*

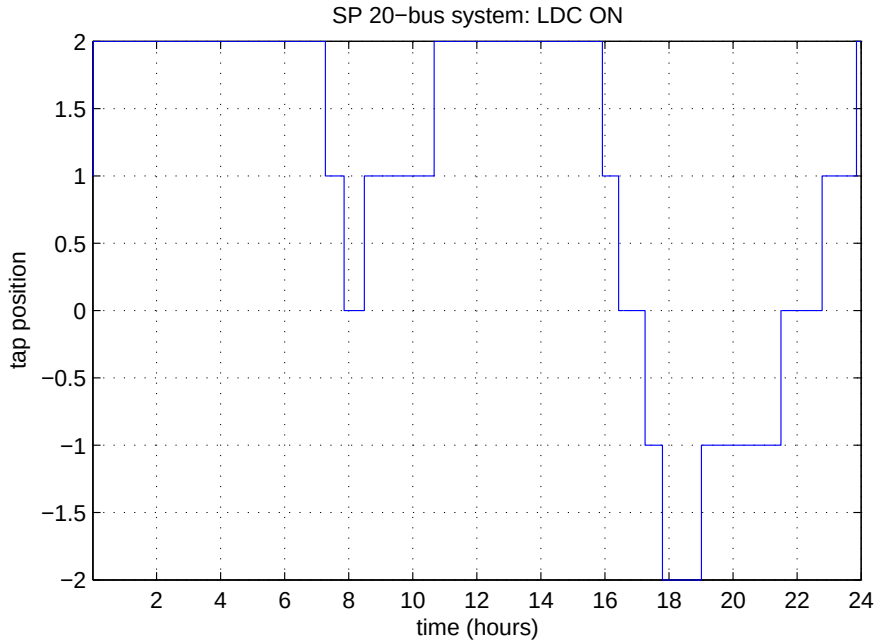

Figure 6.25: *Tap changes throughout the 24-hour period with the generator in APFC mode*

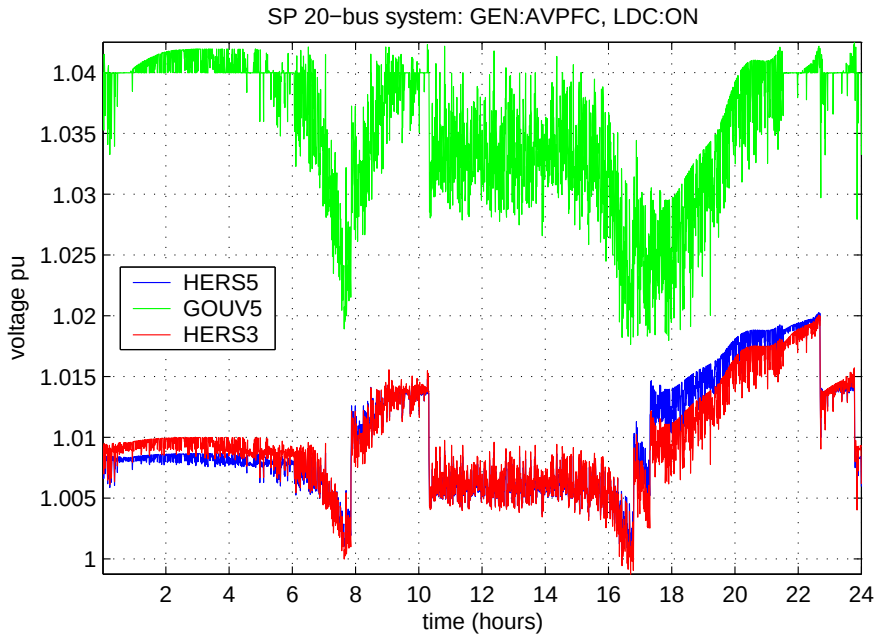

Figure 6.26: *24-hour voltage profile with the wind turbine operating under AVPFC control combined with LDRC*

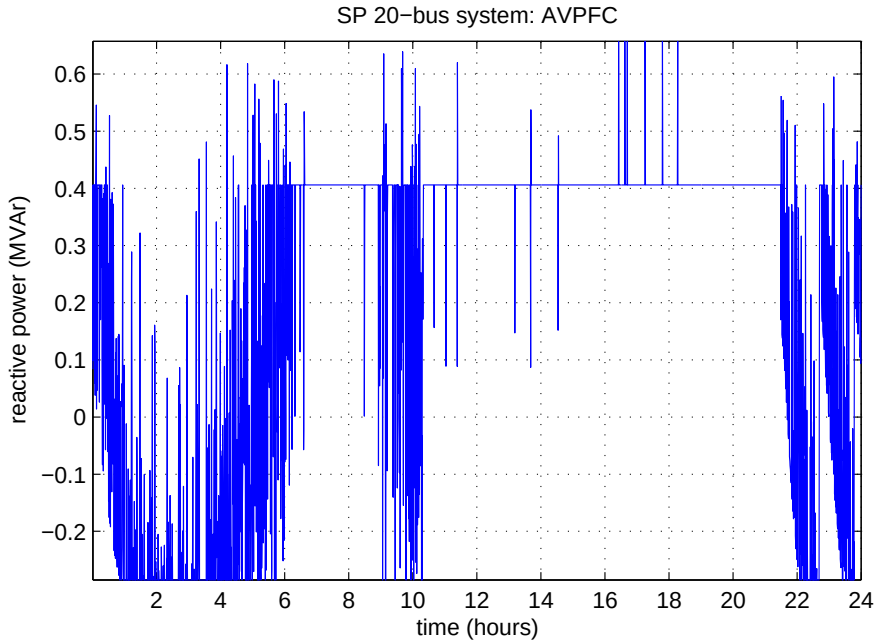

Figure 6.27: *Reactive power exchange of the wind turbine operating under AVPFC control combined with LDRC*

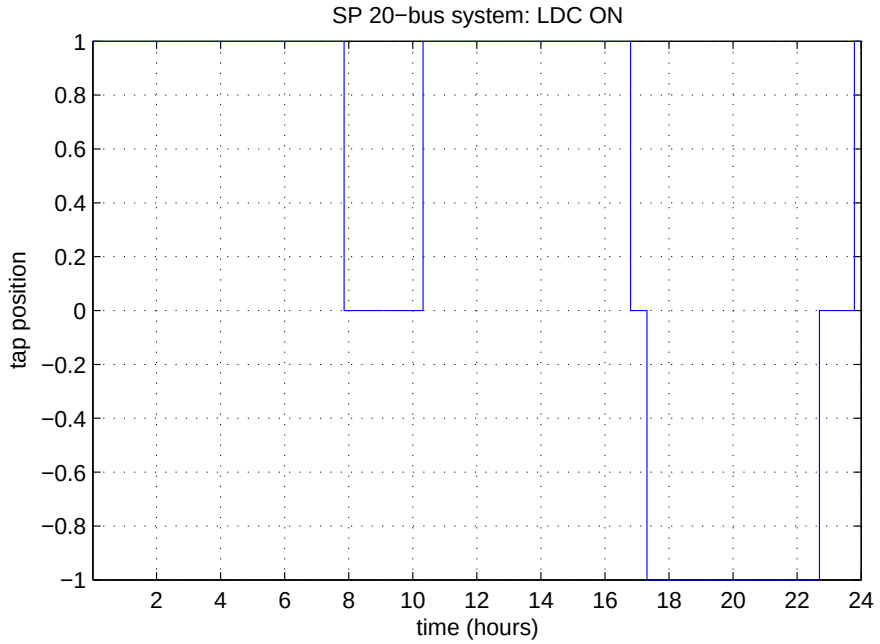

Figure 6.28: *Tap changes throughout the 24-hour period with the generator in AVPFC mode*

The wind speed time series developed in Section 4.2.1 (Figure 4.4) was used as power source input. Figure 6.21 shows the voltage profile with the generator operating at a constant 0.98 power factor (lagging) and Figure 6.22 depicts the voltage profile for AVPFC operation. A first observation reveals that during mid-day, when average voltage is at about 1.04 pu (which is the overvoltage setting in the AVPFC), voltage fluctuation is reduced as there are short periods that it switches to constant voltage mode, but is not eliminated completely as there are other periods that it either operates in constant power factor mode, or it reaches the reactive power limits (see Figure 6.23). This improvement of the voltage profile due to AVPFC operation is also apparent in the neighbouring buses.

Line voltage drop/rise compensation through the OLTC transformer reduced the overall range of voltage at bus GOUV5, but did no good to the short-term variability. In addition, there is a notable alteration of the voltage profile of the middle buses due to tap excursion, which was +2/-2 tap positions and is shown in Figure 6.25.

Combination of AVPFC and LDRC once again brought about an improved overall performance of the system than the individual control cases. Compared to AVPFC-only, the voltage at the controlled bus was always kept within the OLTC bandwidth of $\pm 0.0125pu$, and compared to LDRC-only, the combination resulted in a reduced number of tap changes (6 instead of 12, shown in Figure 6.28).

6.5 Comparison of Intelligent Generator Control with Central "Active" Network Management

Credits: This section describes work done in cooperation with Mr Panagis Vovos and Mr Robert Barrie. As a part of his MEng project [96], Mr Barrie embedded the intelligent generation control algorithms into a capacity allocation program based on Optimal Power Flow (OPF), which was developed by Mr Vovos. Under the supervision of Dr Gareth Harrison and the guidance of Mr Vovos and the author, Mr Barrie set up the simulations and obtained the results presented here.

Voltage control in the distribution system might be achieved by central control, in a similar way that is performed in the transmission system. Distributed generators could have their real and reactive power centrally dispatched, so that the voltage profile throughout the distribution network is flattened. Although traditionally the DN was passively managed, there is now a great interest in active DN management, primarily due to the expansion of distributed generation [97–100]. For obvious reasons, this only concerns generation types that have a predictable and controllable output such as small hydro, biomass etc. Active distribution network management is a promising technology, however its uptake is expected to be slow due to the telecommunications and automation infrastructure that is required, and the associated technical and economic difficulties involved.

In theory, under the assumption of perfect telecoms and infinite availability of information on the conditions throughout the network, the optimal operating regimes for all the connected generators could be estimated at a central point (the control

centre) and then transmitted to them. A capacity allocation program based on Optimal Power Flow, originally presented in [101] was used to simulate central control and dispatch of the DGs. A novelty of the particular program is that it has the additional functionality to consider constraints imposed by protection equipment. Inclusion of the intelligent DG control algorithms to the program, allowed comparison between central voltage control (CVC) of conventionally operating DGs, and DGs under AVPFC or FLPFC control (collectively termed "IntelliGens"). The methodology that allowed inclusion of the DG control algorithms into the capacity allocation program is described in [96, 102, 103].

An OPF algorithm estimates the values for system variables such that an operational criterion is minimised. Several constraints can be imposed mathematically to bound the solution within feasible technical and economic limits. A cost function is assigned to each generator, which represents a "preference factor" according to which a generator is favoured against the others. A series of simulations was carried out in order to compare the benefits of CVC and IntelliGens in terms of capacity increase compared to normal APFC operation of the distributed generators. The network depicted in Figure 6.29 was used as a test base for the simulations.

The bulk supply point (BSP) is considered as a slack bus and is located at bus 12. The network is fed by the BSP through a 90MVA OLTC transformer with 8 steps that holds voltage within ±2% of the nominal value. The controlled generators are connected at buses 1, 10 and 11 through three 30MVA transformers with fixed taps. There is also a 15MW, 10MVAr (max.) generator connected at bus 5. The loads in the network are considered static and their values are shown in Figure 6.29. The network operates at 33kV, except for the BSP which is 132kV and the generator buses (11kV). The transformers and lines characteristics are given in Table 6.4.

It is assumed that the network can exchange 100MW/60MVAr with the transmission grid through the BSP without any effect on its operation and that line 2-5 and 4-9 are constrained by a thermal limit of 14MVA and 40 MVA respectively. The power factor setpoint of the generators is set at 0.9 lagging, and the range is 0.9 lagging to 0.9 leading. The IntelliGens operate in power factor control until voltage reaches the

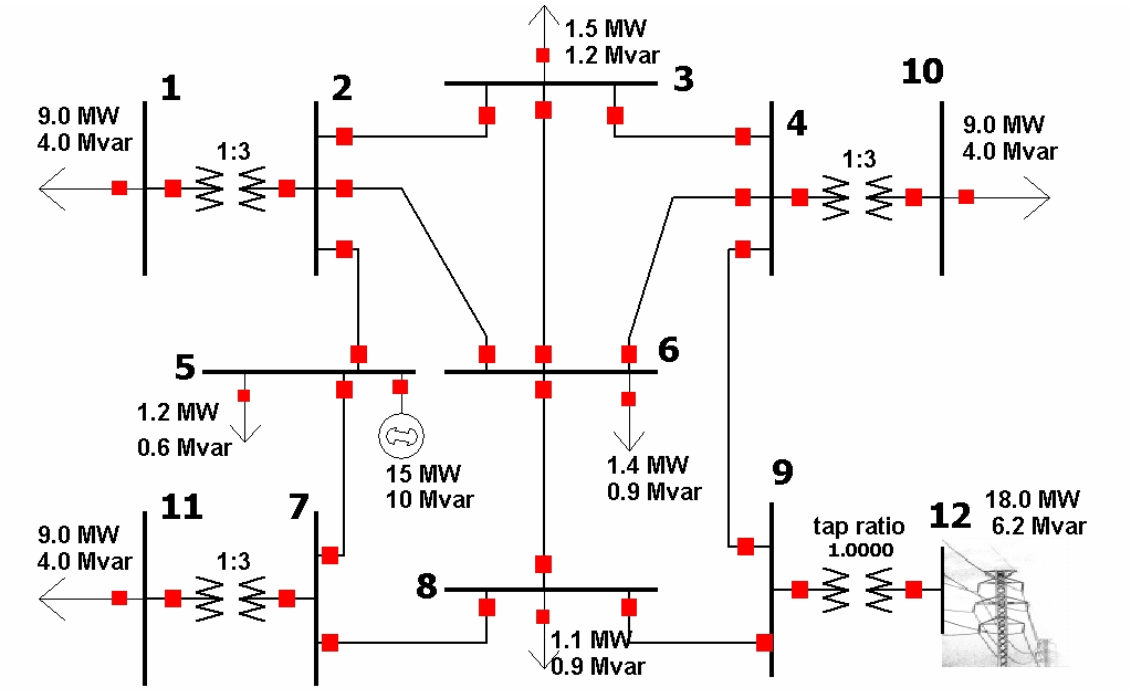

Figure 6.29: *The distribution network used in the OPF simulations*

threshold of 1.05 pu, where they switch to voltage control. Finally, it is assumed that there is no preference to any of the three controlled generators (their cost functions are identical).

The results of the simulations with the generators under APFC, intelligent and CVC control are shown in Table 6.5. The first observation is that intelligent and CVC control roughly doubled the installed capacity compared to the traditional APFC generators. However, the most important outcome of this comparison is that the acceptable total capacities for the IntelliGens and CVC cases are very close (with the CVC higher by 11.1MVA, or 12.3%). This small difference, compared to the cost and technical difficulties related to central voltage control, may justify the utilisation of decentralised "intelligent" control against central "active" control. It should also be noted, though, that this great increase in the installed capacity has the sideffect of an almost tenfold increase of losses. Currently, the DNOs do not take losses into account when determining generator capacities, but with the increase of DG which is expected in the near future, this may become a serious problem.

Type	Buses	R (pu)	X (pu)	B (pu)	Therm. Limit (MVA)
trans.	1-2	0.00	0.3	0.00	30
line	2-3	0.48	0.3	0.0008	∞
line	2-5	0.24	0.15	0.0004	∞
line	2-6	0.72	0.45	0.001	∞
line	3-4	0.64	0.4	0.001	∞
line	3-6	0.64	0.4	0.001	∞
line	4-6	0.48	0.3	0.0008	∞
line	4-9	0.66	0.35	0.0009	40
trans.	4-10	0.00	0.25	0.00	30
line	5-7	0.688	0.43	0.0006	∞
line	6-8	0.768	0.48	0.00	∞
line	7-8	0.56	0.35	0.0008	∞
trans.	7-11	0.00	0.3	0.00	30
line	8-9	0.768	0.48	0.00	∞
trans.	9-12	0.00	0.1	0.00	90

Table 6.4: *Line and transformer characteristics for the network in Figure 6.29*

	APFC	IntelliGens	CVC
Gen @ bus 1	20.0MVA, 0.9 lag	36.6MVA, 0.98 lead	33.7MVA, 0.9 lead
Gen @ bus 10	3.7MVA, 0.9 lag	7MVA, 0.9 lag	20.8MVA, 0.95 lag
Gen @ bus 11	16.9MVA, 0.9 lag	35.2MVA, 0.97 lead	35.5MVA, 0.98 lead
BSP	-16.5MW	-29.7MW	-34.0MW
Total	40.6MVA	78.9MVA	90.0MVA
Losses	3.9MW	30.7MW	34.7MW

Table 6.5: *Capacity allocation from the optimal power flow for APFC, IntelliGens and CVC with the fault level constraints considered*

6.6 Summary

Distribution networks impose serious constraints in the development and operation of distributed and renewable generation. This chapter used a model of an actual section

of the Scottish distribution network to validate the proposed control strategies. The test network has the typical characteristics of a weak rural system. It has a radial topology and can accommodate a small capacity of generation, mainly due to voltage constraints. These characteristics make it an ideal test bed for the assessment of DG operation and the performance of DG control strategies. Through simulations it was demonstrated that adoption of the proposed intelligent generator control techniques may lead to an increase of the generating capacity that may be accommodated in a weak distribution network, and / or an improvement of voltage profiles. Further, it was shown that although OLTC control is an attractive method for voltage regulation, in distribution systems, combination with intelligent generator control may further improve its performance. This becomes more apparent in the case of wind generation, as the OLTC action is not fast enough to mitigate the voltage fluctuations due to wind variability. Finally, simulations using a capacity allocation program based on optimal power flow incorporating fault level constraints, showed that the increase in DG capacity by using intelligent generator control is comparable to the increase that can be achieved if active DN management is utilised. Given the technical and economical burden of the latter, it may well be a more attractive solution for the distribution network voltage control task.

Chapter 7
Discussion and Conclusions

7.1 Thesis Summary

This thesis was structured as following. After the introduction, the problem of voltage variation in the distribution network was discussed. Then, detailed modelling of the DN, small hydro and wind generators was presented. Two possible methods of mitigation were proposed, and finally these algorithms were evaluated in a simulation of a test network. Particularly:

In **Chapter 1** an introduction to this work was given. First, the background of the research was presented. Sustainable energy systems were discussed from a global perspective, and then the current state of renewable and distributed energy resources in the UK was described. An overview of the RNET project was given, and the chapter closed with the thesis statement, the contribution to knowledge and the project deliverables.

Chapter 2 introduced the issues regarding embedded and renewable generation in the DN. This was achieved through a presentation of the current regulations that govern the connection of ERG in the UK, a description of the distribution network structure and the effect of various network parameters on voltage. Finally, the chapter ended with a discussion of the voltage control hierarchy in the distribution network.

In **Chapter 3** a model of a small hydro scheme within a distribution network was constructed. This started with an overview of the design considerations of a SHG and continued with the description of the mathematical model of each component of the SHG. The described model was based on a synchronous generator and two typical methods of SG control were discussed: automatic voltage control and automatic power factor control. The operational limits of the synchronous generator were shown by

means of the 3D "composite" capability diagram. Then, the model of the distribution system including on-line tap changing transformers was presented. The functionality of the full model was presented through a series of simulations.

The complete wind-to-wire dynamic model of a wind energy conversion system based on a doubly fed induction generator was presented in **Chapter 4**. The aspects of WECS modelling were discussed and then wind characteristics and modelling were presented. Then, an analysis of the mathematical model of the turbine, the generator and the controls was performed. The chapter closed with a series of simulation results with the WECS operating with varying wind speed and under automatic power factor, and automatic voltage control.

Chapter 5 presented the developed intelligent generator control control algorithms. The need for intelligent control was illustrated using the universal power circle diagram for the distribution network and the dynamic "composite" capability diagram of the synchronous generator. A brief introduction to artificially intelligent controllers was done, and then the automatic voltage/power factor controller, an expert system, was described. Operation of the AVPFC was illustrated through a simulation of a small hydro generator operating under AVPFC control. A second controller based on fuzzy logic, the fuzzy logic power factor controller, was then discussed. Its operation was also demonstrated using the same simulation as in the case of AVPFC. Both controllers' performance in voltage regulation was compared to the one of the traditional techniques. Their performance was then tested using a varying local load, and the final test was carried out with a WECS operating with varying wind conditions. It was then shown that coordination of intelligent generator control and OLTC operation is possible and reduces tap operations. The final part of Chapter 5 presented a further upgrade of the fuzzy controller, where real power generation of the WECS was also adjusted by means of a fuzzy controller, with the objective of voltage regulation.

In **Chapter 6** a section of the Scottish distribution network was used as a test bed for a real-life assessment of the performance and the advantages of intelligent controllers utilisation. Operation of the system with, and without OLTCs in use was investigated, and the developed algorithms were compared to normal DG operation. In each case,

the benefits of utilising intelligent generator control on voltage regulation and installed capacity increase were shown. The tests involved connection of generators to both 11kV and 33kV buses.

Chapter 7 summarises the thesis, includes a discussion on the findings and draws the overall conclusions.

7.2 Areas of Activity

This work included three main areas of activity:

i. development of two source-to-wire dynamic models of forms of generation that classify as 'distributed'; namely small-hydro schemes and wind energy conversion systems;

ii. development of strategies and algorithms for controlling synchronous and induction DG to maximise capacity and energy production, with minimum network impact;

iii. validation of the proposed control systems on DG in a representative distribution network.

Experience and extensive simulations identify that DG capacity in rural networks is most frequently limited by voltage violation, where and when the generator usually operates in constant power factor mode. DGs must operate within voltage envelopes to gain access and, once connected, to avoid protection shutdown, loss of production and revenue. The operational envelope is constant and pre-defined by the power factor limits of the generator and the voltage limits set by the DNO and system conditions. The DG operating point is dynamic and varies with changing local power flows, network configuration (action of transformer on-load tap changers, network re-configuration etc.) and prime mover input. The relatively high impedance of radial feeders in the distribution network exaggerates the effects of these changes on voltage level. This work developed a control mode for continuous DG operation within the operational envelope.

7.3 Discussion of the Research Outcomes

The outcomes of this research can be broken into two sections: distributed generation and network modelling, and intelligent generation control algorithm development. The following sections discuss the findings.

7.3.1 Distributed Generation and Network Modelling

Steady-state and dynamic models of a small-hydro generating plant and an active pitch-controlled wind energy conversion system utilising a doubly fed induction generator were constructed in Matlab and Simulink. The developed models were built according to widely accepted bibliography and their results matched those of the originals. The original and novel modes of operation proposed (AVPFC and fuzzy logic PF control) were incorporated and their operation was tested in several weak networks, including a simple two-bus system, a radial network and a section of the test system. The variations of voltage under real load profiles and the response of the system to increasing capacities of DG were studied. The studies confirm that the new control modes developed in this work can effectively mitigate the impact of DG on the network.

7.3.2 Intelligent Generation Control Algorithm Development

Extension of the synchronous machine capability diagram on the network to the three-dimensional space P-Q-V enabled projection of the network voltage response to varying P and Q and generated a 3D surface locus of acceptable operation of the machine for every possible network condition. Adding the DNO voltage constraints as horizontal surfaces identified the allowable operational regime for the DG. The initial approach to the problem was to use an extension of the traditional excitation control system to constrain the operation of the machine within voltage and power factor limits. The novel controller developed smooth transfers from power factor to voltage control (PFC to AVC) or back dependent on network conditions. It is implemented as an algorithm

operating on voltage and mechanical power set-points and is termed Auto-voltage Power Factor Control (AVPFC). The controller enables greater export during low demand periods and can also provide voltage support at times of high demand. Extensive simulations compared operation of a water-turbine driven synchronous generator using only a PFC system and with the new AVPFC scheme. Under PFC, the voltage rose above the upper statutory limit during periods of low demand and in consequence the generator was disconnected with significant loss of production. Secondly, excessive local demand drew voltage below the lower voltage limit, and under-voltage protection disconnected the DG when it might have provided voltage support. In AVPFC, however, the voltage was continuously maintained within statutory limits, allowing the DG to remain connected. While PFC used to be obligatory, some DNOs may now permit voltage controlled operation for DGs at weak parts of the network for voltage support. This has to be evaluated carefully as the behaviour larger DGs can cause network voltage control systems to operate in response. However, the combination of power factor control together with voltage control of DGs may offer significant benefit to developers if it enables acceptable access to weak areas of the network and allows continuous operation of the plant when co-ordinated with varying local demand.

Further development led to a fuzzy control system where the generator operates constantly in PFC mode, but the fuzzy controller alters the power factor set point in response to the terminal voltage of the generator. The whole control system has the effect of applying a non-linear voltage droop to the machine. Simulations of a synchronous generator and a variable speed, pitch-controlled Wind Energy Conversion System (WECS) with a Doubly Fed Induction Generator (DFIG), operating under the control of the fuzzy system has demonstrated that, in both cases, the voltage not only remained within the statutory limits for longer periods than with the conventional power factor control, but its distribution was more concentrated around the nominal value, thus improving the overall voltage quality.

7.4 Contribution to Knowledge, Novelty and Potential Impact of Study

This work made a contribution to knowledge through:

i. introduction of a holistic approach for the determination of the generator's acceptable operating area, taking into account both network and plant induced constraints;

ii. development of intelligent generator control techniques for synchronous and induction DG to enhance network integration and maximise capacity of new plant that can connect;

iii. demonstration of a method to combine network and generator voltage control that overcomes the widely known problems due to their co-existence; and

iv. validation of the proposed control systems on representative distribution networks.

While automatic voltage and automatic power factor control are well-established modes of operation, this combination of the two using an expert system to change from one to the other according to network conditions is a novel technique. Furthermore, the proposed use of fuzzy logic to adjust the power factor setpoint of an APFC (collectively termed "FLPFC") for the purpose of minimising voltage fluctuation and increasing capacity has not been discussed elsewhere.

The application and uptake of these outcomes has increased the available understanding, methodologies, software tools and techniques that quantify and mitigate the effects of DG on the distribution network. The major impact will be the wider development and network integration of distributed generation. An additional benefit is the opportunity for further research to extend and expand to three dimensions the applications of the proposed control algorithms:

- **Depth:** Perform further study of the intelligent generation control by building a prototype and evaluate its operation in an emulated distribution system. Several

generator manufacturers have shown interest in this prospect. A project proposal is planned and an application for a *'Proof of Concept'* grant will be submitted for that purpose.

- **Width:** Use the same philosophy to mitigate other DG-related issues such as the effect of distributed generation to system stability. Work towards this direction is already under way within the 'SUPERGEN' research project, supported by the Engineering & Physical Sciences Research Council, which the Institute of Energy Systems is participating through work done by Prof. Janusz Bialek.

- **Extent:** Investigate the application of intelligent generation control to further kinds of distributed and/or renewable generation. This workpath is also being explored by IES mainly through the author's work within the 'SUPERGEN Marine' research project (led by Dr Robin Wallace), also supported by EPSRC. This study is the fourth out of thirteen work packages of the project and investigates how intelligent generation control can be applied to wave and tidal energy converters, as well as its potential effect as a means of assisting the development and uptake of marine energy.

Finally, this work generated 6 journal publications, 5 conference papers and a lecture in an IEE seminar. All these documents can be found in Appendix A.

7.5 Beneficiaries of this Work

There are many potential beneficiaries of this research, from society at large to specific sections of the industrial and academic community. The dissemination and transfer of the results of this work, and knowledge gained, may be applied within the UK and other countries committed to reducing carbon flows in the energy supply chain. Developing countries may use the developed strategies to supply electricity in areas where the distribution network is under-developed. Increased uptake of renewable energy generation will enable CO_2 reductions and environmental improvements that will increase the quality of life and preserve natural resources. The expanded markets

for new DG plant and their subsequent operation will lead to increased levels of business and employment, ideally indigenous to the areas under development. DNOs will be able to provide wider and greater network access for DG at lower associated cost. This will benefit economically the developers and DNOs and increase the sustainability of distributed renewable generation. Finally the industrial collaborators have had access and input to evolving methodologies and tools that they can apply to their benefit.

7.6 Suggestions and Further Improvements

It is possible that the proposed control strategies may introduce some problems. As already mentioned, the amount of voltage regulation that a particular generator can achieve depends on the network characteristics above the point of connection, the rating and the type of the generator. It is therefore possible that the required reactive power to compensate over- or undervoltage is close to, or above the capability of the machine. In such cases excitation limiters should be carefully set as the generator may overheat if adequate counter measures are not taken. This will consequently increase the wear on the machine and hence the maintenance costs. Overheating is expected to be more prominent in DFIGs, as their reactive power capability is more constrained than with the synchronous machines. Typical design power factor limits of the latter are 0.8 lagging to 0.9 leading, which are well outside the DNOs requirements therefore are more difficult to be met. Additionally, overheating due to high reactive power exchange may appear at the power electronic converter that feeds the rotor circuit of the DFIG.

By (partially) solving the voltage rise issue the next problems that may arise from the network point of view are the increased losses (especially in weak networks) as an effect of the increased power transfer, as well as overloading of the system especially during high demand periods, when the generator will try to export high reactive power. The (imported) real and (exported) reactive power add up vectorially and may reach the feeders' and transformers' ratings.

Another potential problem is the poor coordination between intelligently controlled generators or between generators and network voltage control devices. This can be

more serious in the case of AVPFC when it operates in voltage control mode. Therefore care must be taken so that both network voltage controllers and generator adhere to the setpoints agreed between the DNO and the developer. This is less important with the FLPFC as an FLPFC controlled generator is essentially still under power factor control (therefore terminal voltage is allowed to vary in order to allow reactive power sharing).

There are also some potential improvements that can be made to the proposed control strategies. In extreme situations when voltage cannot be kept within the statutory limits by using solely power factor control, the output of the generator could be reduced. This may not be possible in schemes such as some heat-led CHP units, but it is possible in others, such as small hydro or wind turbines. In effect this implies decomposition of the generator to a decoupled pair of real and reactive power sources. The effect of reducing real power output on voltage regulation can be very significant in networks with high resistance. However, this comes at the expense of reduced revenue when compared to a generator of the same size with fixed output.

Additionally, in the case of wind generation (as well as other intermittent sources), further voltage regulation could be achieved by means of intermediate energy storage. Mechanical power could be stored temporarily before it is fed to the electric network, thus removing the transient effects of the primary source. A possible means of intermediate storage could be hydraulic accumulators connected via pump/motor pairs.

7.7 Overall Conclusions

There is a global movement towards the reduction of fossil fueled generation of electricity and the increase of renewable energy resources uptake. The drivers of this trend are economical, political and environmental. Current oil prices are reaching $60 per barrel and rising. Countries that are not major fossil fuel producers seek to reduce their dependency on oil. National and international regulations are also being set in order to promote reduction of greenhouse gases. Increased utilisation of RES (and replacement of fossil fuel fired power plants) is a step towards that direction. However this means

that central, conventional generation will give its place to distributed generation, often powered by intermittent, unpredictable (and therefore non-dispatchable) energy sources, such as wind, small hydro, marine etc.

Increased generation capacity in the distribution network is expected (and already experienced) to introduce several technical and operational problems to both the network operators and the potential developers. The most prominent of these problems is voltage fluctuation due to variation of the energy source and the local power demand. The fact that the distribution network is weak (high resistance and low X/R ratio), particularly close to its remote ends, augments the fluctuation of voltage, and this brings about the need for an alternative operation of both the network and the generator. Distributed generation plants with inherently varying output such as wind farms, small hydro schemes and others, should not be considered as firm (guaranteed) capacity since they cannot be centrally dispatched according to the demand, but rather as energy sources, which should be controlled with the objective to best accommodate their varying output and reduce their impact on the system.

The traditional control methods for the generators, such as automatic power factor and automatic voltage control may not suffice for optimal operation of distributed generation. This can be verified by the results of simulations of DG operation in weak networks. A set of distributed generation models (small hydro and wind) illustrated the effect of such plants on voltage profile. These models were used as a base for development of novel control techniques that would reduce voltage fluctuation. The developed algorithms allowed connection of larger generating capacity in the network before the statutory overvoltage limits were hit, and at the same time the overall quality of supply was improved, as voltage fluctuation was reduced, when compared to automatic power factor control. Additionally, the developed controllers were able to assist voltage regulation when the demand/generation ratio was high and the undervoltage limits would otherwise be hit. However, their ability is constrained by the reactive power generation capability of the plant. Therefore directly coupled synchronous generators (with no power electronic converter in the middle) will have better performance than doubly fed induction machines, as the latter have a smaller

reactive power capability. In terms of reactive power flow (and consequently loading of the generator and the network), the developed algorithms were shown to have superior performance than the automatic voltage control, as they featured lower MVAr import to / export from the generator, while they also allowed cooperation with network voltage control devices such as on line tap changing transformers. However, combination and coordination of the two should be discussed in advance between the developer and the network operator.

The proposed control strategies can be an alternative to centrally operated, active network management as they are able to exploit network resources without the need of dedicated communication links.

7.8 Thesis Statement

The original thesis statement as expressed in Section 1.7 was that: *"Intelligent voltage and reactive power control algorithms of small-scale generators, which are connected to weak distribution networks, can allow increase of their capacity before the statutory voltage limits for quality of supply are violated."*

This work showed that the above thesis statement is true by proposing two candidate control strategies and proving that they can assist network integration of distributed generation through a series of simulations of their operation in a test network. Application of these control algorithms to synchronous generator based small-hydro schemes as well as wind turbines and farms featuring doubly fed induction machines, was shown to have a positive impact on capacity and overall voltage quality within the distribution network.

References

[1] E. Lakervi and E. Holmes, *Electricity Distribution Network Design*. Power Series 21, London UK: IEE, 2nd (revised) ed., 2003.

[2] A. R. Wallace, "Protection of embedded generation schemes," in *Colloq. Protection and Connection of Renewable Energy Systems*, pp. 1/1–5, IEE, 1999.

[3] G. P. Harrison, A. E. Kiprakis, and A. R. Wallace, "A new era for mini-hydro," *International Water Power and Dam Construction*, vol. 54, pp. 20–24, November 2002.

[4] A. R. Wallace and A. E. Kiprakis, "Reduction of voltage violations from embedded generators connected to the distribution network by intelligent reactive power control," in *Proc. 5th Int. Conf. on Power System Management and Control*, (London, UK), pp. 210–215, IEE, April 2001.

[5] DTI, *Energy, its impact on the environment and society*. London, UK: The UK Department of Trade and Industry, 2002.

[6] EIA, *International Energy Outlook 2003*. USA: Energy Information Administration (EIA), 2003.

[7] S. Bull, "Renewable energy today and tomorrow," *Proceedings of the IEEE*, vol. 89, pp. 1216–1226, August 2001.

[8] DTI, *Energy, its impact on the environment and society, 2003 Update*. London, UK: The UK Department of Trade and Industry, July 2003.

[9] United Nations Framework Convention on Climate Change, "The Kyoto protocol," December 1997.

[10] RCEP, *Energy - The Changing Climate*. London, UK: Royal Commission on Environmental Pollution, June 2000.

[11] G. Boyle, B. Everett, and J. Ramage, *Energy Systems and Sustainability*. Oxford, UK: Oxford University Press, 2003.

[12] H. Geller, "Energy revolution. policies for a sustainable future," *Renewable Energy World*, vol. 6, pp. 36–49, July-August 2003.

[13] D. Helm, "The energy policy britain needs," *IEE Maxwell Lecture*, April 2003.

[14] DTI, *Digest of United Kingdom Energy Statistics*. London, UK: The UK Department of Trade and Industry, July 2003.

[15] G. P. Harrison, A. E. Kiprakis, and A. R. Wallace, "Distribution networks: Constraining renewable energy development," in *Re-Gen*, vol. 1, pp. 50–59, Wilmington Publishing, April/May 2003.

[16] C. Masters, "Voltage rise: The big issue when connecting embedded generation to long 11 kv overhead lines," *IEE Power Engineering Journal*, vol. 16, pp. 5–12, February 2002.

[17] C. Dai and Y. Baghzouz, "On the voltage profile of distribution feeders with distributed generation," in *Proc. IEEE Power Engineering Society General Meeting*, pp. 1136–1140, IEEE, 2003.

[18] G. Harrison and A. Wallace, "Maximising renewable energy integration within electrical networks," in *Proc. World Renewable Energy Congress (WREC2005)*, World Renewable Energy Network, WREN, May 2005.

[19] H. Saadat, *Power System Analysis*. Electrical Engineering Series, McGraw Hill, 1st ed., 1999.

[20] N. Jenkins, "Embedded generation (part 1)," *Power Engineering Journal*, vol. 9, pp. 145–150, June 1995.

[21] N. Jenkins, "Embedded generation (part 2)," *Power Engineering Journal*, vol. 10, pp. 233–239, October 1996.

[22] Econnect Ltd. and ILEX Associates, *A Technical Guide for Connection of Embedded Generators to the Distribution Network*, November 1998.

[23] N. Jenkins, R. Allan, P. Crossley, D. Kirschen, and G. Strbac, *Embedded Generation*. Power and Energy Series, London, UK: IEE, 2000.

[24] M. J. Checksfield and M. A. Redfern, "Assessment of embedded generator stability when connected to a utility distribution system," in *Proc. 30th Universities Power Engineering Conference*, 1995.

[25] N. Jenkins and G. Strbac, "Impact of embedded generation on distribution system voltage stability," in *Proc. IEE Colloquium on Voltage Collapse*, IEE, 1997.

[26] Engineering Recommendation G 59/1, "Recommendations for the connection of embedded generating plant to the public electricity suppliers distribution systems," tech. rep., The Electricity Association, London, UK, 1991.

[27] R. Barnes, "Harmonics in power systems," *IEE Power Engineering Journal*, January 1989.

[28] B. Ozpineci and L.M.Tolbert, "Simulink implementation of induction machine model - a modular approach," in *IEEE Int. Conf. Electric Machines and Drives*, vol. 2, pp. 728– 734, IEEE, June 2003.

[29] Z. Lubosny, *Wind Turbine Operation in Electric Power Systems*. Power Systems, Springer, 2003.

[30] J. Slootweg, "Representing distributed resources in power system dynamics simulations," in *Proc. IEEE Power Engineering Society Summer Meeting*, pp. 176–178, IEEE, 2002.

[31] G. Berube and L. Hajagos, "Modelling based on field tests of turbine/governor systems," in *IEEE Power Engineering Society Winter Meeting*, vol. 1, (New York, USA), pp. 567–573, IEEE, February 1999.

[32] A. Feijoo and J. Cidras, "Modelling of wind farms in the load flow analysis," *IEEE Trans. Pwr. Syst.*, vol. 15, pp. 110–115, February 2000.

[33] H. Ramos and A. de Almeida, "Small hydropower schemes as an important renewable energy source," in *Proc. Hydroenergia 99*, (Vienna, Austria), October 1999.

[34] A. R. Wallace, "A review of small scale hydro power in europe," in *Proc. 1st Portugese Mini-Hydro Seminar*, (Lisbon, Portugal), November 1988.

[35] C. C. Warnick, *Hydropower Engineering*. New Jersey, USA: Prentice Hall Inc., 1984.

[36] Working Group on Prime Mover and Energy Supply Models for System Dynamic Performance Studies, "Hydraulic turbine and turbine control models for system dynamic studies," *IEEE Trans. Power Systems*, vol. 7, pp. 167–179, February 1992.

[37] I. Kamwa, D. Lefebvre, and L. Loud, "Small signal analysis of hydro-turbine governors in large interconnected power plants," in *Proc. IEEE Power Engineering Society Winter Meeting*, vol. 2, pp. 1178 – 1183, IEEE, January 2002.

[38] P. Kundur, *Power system stability and control*. The EPRI Power System Engineering Series, New York, USA: McGraw-Hill, 1994.

[39] J. Machowski, J. Bialek, and J. Bumby, *Power sustem dynamics and stability*. London, UK: John Wiley & Sons, 1998.

[40] D. Clemen, *Hydro plant electrical systems*. Kansas, USA: HCI Publications, 1999.

[41] The Brown Book Working Group, *IEEE Recommended Practice for Industrial and Commercial Power Systems Analysis*. New York, USA: IEEE, August 1998.

[42] B. Weedy and B. Cory, *Electric Power Systems*. London, UK: John Wiley & Sons, 4th ed., 1998.

[43] C. M. Ong, *Dynamic Simulation of Electric Machinery*. Prentice Hall, 1998.

[44] IEEE Standards Committee, "IEEE recommended practice for excitation system models for power system stability studies," IEEE Standard IEEE Std 421.5-1992, IEEE, New York, USA, March 1992.

[45] I. Elsedawi, A. Elassal, and E. Azzuz, "Effects of avr systems on the performance of synchronous generators," in *IEEE Canadian Conf. on Electrical and Computer Engineering*, vol. 1, pp. 25–28, IEEE, May 1997.

[46] I. D. E. Force, "Computer models for representation of digital based excitation systems," *IEEE Trans. Energy Conversion*, vol. 11, pp. 607–615, September 1996.

[47] J. Fan and S. Salman, "The effect of integration of wind farms into utility network on voltage control due to the co-ordination of AVC relays," in *Proc. IEEE 4th Int. Conf. Advances in Power System Control, Operation and Management APSCOM-97*, pp. 260–265, IEEE, November 1997.

[48] M. Larsson, *Coordinated Voltage Control in Electric Power Systems*. PhD Thesis, Department of Industrial Electrical Engineering and Automation, Lund University, Lund, Sweden, 2000.

[49] S. Salman and I. Rida, "ANN-based AVC relay for voltage control of distributed network with and without embedded generation," in *IEEE Int. Conf. Electric Utility Deregulation, Restructuring and Power Technologies*, (London, UK), pp. 263–267, IEEE, April 2000.

[50] S. Salman, F. Jiang, and W. Rogers, "The effect of private generators on the voltage control of 11 kV network and on the operation of certain protective relays," *IEEE Joint Int. Pwr. Conf. Athens PowerTech*, vol. 2, pp. 591–595, September 1993.

[51] S. Salman, F. Jiang, and W. Rogers, "Investigation of the operating strategies of remotely connected embedded generators to help regulating local network voltage," in *Int. Conf. on Opportunities and Advances in International Electric Power Generation*, pp. 180–185, IEE, March 1996.

[52] C. Taylor, "Line drop compensation, high side voltage control, secondary voltage control - why not control a generator like a static var compensator?," in *Proc. IEEE/PES Summer Meeting*, (Seattle, USA), IEEE, July 2000.

[53] Beckwith Electric Co. Inc., "M-0067E tap changer control," instruction book, Florida, USA, 1999.

[54] M. Thomson, "Automatic voltage control relays and embedded generation (part 1)," *IEE Power Engineering Journal*, pp. 71–76, April 2000.

[55] J. Choi and J. Kim, "Advanced voltage regulation method at the power distribution systems interconnected with dispersed storage and generation systems," *IEEE Trans. Power Delivery*, vol. 15, pp. 691–696, April 2000.

[56] M. Kashem and G. Ledwich, "DG impact on rural lines: Voltage control and line protection issues," in *Proc. 1st Int. Symposium on Distributed Generation: Power System and Market Aspects*, June 2001.

[57] J. Chow, M. Glinkowski, R. Murphy, T. Cease, and N. Kosaka, "Generator and exciter parameter estimation of fort patrick henry hydro unit 1," *IEEE Trans. En. Conv.*, vol. 14, pp. 923–929, December 1999.

[58] Scottish Power UK plc, Scotland, *Transmission Seven Year Statement*, April 2003.

[59] L. S. T. Ackermann, "Wind energy technology and current status: A review," *Renewable and Sustainable Energy Reviews*, vol. 4, pp. 315–374, 2000.

[60] M. Davidson, "Interaction of a wind farm with the distribution network and its effect on voltage quality," in *IEE Colloquium on the Impact of Embedded Generation on Distribution Networks*, pp. 9/1–9/5, IEE, October 1996.

[61] K. G. T. Ackermann, "Embedded wind generation in weak grids - economic optimisation and power quality simulation," *Renewable Energy*, vol. 18, pp. 205–221, 1999.

[62] Z. Chen and E. Spooner, "Grid power quality with variable speed wind turbines," *IEEE Trans. En. Conv.*, vol. 16, pp. 148–154, June 2001.

[63] K. Burges, A. M. D. Broe, and A. Feijoo, "Advanced power control in a wind farm network," in *Proc. IEEE Bologna PowerTech Conf.*, (Bologna, Italy), IEEE, June 2003.

[64] H. Petersen, "Evaluation of wind turbine performance," Tech. Rep. ENS-51171/00-0016, Danish Energy Agency, Denmark, 2000.

[65] J. F. Manwell, J. G. McGowan, and A. L. Rogers, *Wind Energy Explained, Theory Design and Application.* UK: John Wiley & Sons, 2002.

[66] J. G. Slootweg and W. L. Kling, "Is the answer blowing in the wind?," *IEEE Power & Energy Magazine*, vol. 1, pp. 26–33, November/December 2003.

[67] A. Betz, *Wind-Energie und ihre Ausnutzung durch Windmuehlen.* Gottingen: Vandenhoeck et Ruprecht, 1926.

[68] A. Leon-Garcia, *Probability and random processes for electrical engineering.* Reading: Addison-Wesley Publishing Company, 2nd ed., 1992.

[69] C. Masters, J. Mutale, G. Strbac, S. Curcic, and N. Jenkins, "Statistical evaluation of voltages in distribution systems with embedded wind generation," *IEE Proc. Gen. Transm. Distrib.*, vol. 147, pp. 207–212, July 2000.

[70] V. Akhmatov, H. Knudsen, and A. H. Nielsen, "Advanced simulation of windmills in the electric power supply," *Journal of Electrical Power and Energy Systems*, no. 22, pp. 421–434, 2000.

[71] V. Akhmatov and H. Knudsen, "Modelling of windmill induction generators in dynamic simulation programs," in *Proc. IEEE PowerTech Budapest*, (Budapest), IEEE, August 1999.

[72] W. E. Leithead, S. A. de la Salle, D. Reardon, and M. J. Grimble, "Wind turbine modelling and control," in *International Conference on Control*, vol. 1, pp. 1–6, 1991.

[73] S. Heier, *Grid Integration of Wind Energy Conversion Systems*. Chicester, UK: John Wiley & Sons Ltd., 1998.

[74] J. G. Slootweg, H. Polinder, and W. L. Kling, "Dynamic modelling of a wind turbine with doubly fed induction generator," in *Power Engineering Society Summer Meeting*, vol. 1, pp. 644–649, IEEE, July 2001.

[75] D. Henderson, "Synchronous or induction generators? The choice for small scale generation," in *Proc. Opportunities and Advances in Int. Power Generation Conf.*, IEE, March 1996.

[76] E. N. Hinrichsen, "Controls for variable pitch wind turbine generators," *IEEE Trans. Pwr. Appar. & Syst.*, vol. PAS-103, pp. 886–892, April 1984.

[77] J. Ekanayake, L. Holdsworth, X. Wu, and N. Jenkins, "Dynamic modeling of doubly fed induction generator wind turbines," *IEEE Trans. Power Systems*, vol. 18, pp. 803–807, May 2003.

[78] W. Hofmann and F. Okafor, "Optimal power utilisation with doubly-fed full-controlled induction generator," in *Proc. IEEE 6th AFRICON*, vol. 2, pp. 693– 698, October 2002.

[79] G. Arnold and S. Heier, "Grid control with wind energy converters," in *Proc. 2nd Int. Workshop on Transmission Networks for Offshore Wind Farms*, March 2001.

[80] H. B. (ed.), "Power control for wind turbines in weak grids," Project summary Risoe-R-1117(EN), Risoe National Laboratory, Roskilde, Denmark, March 1999.

[81] A. R. Wallace and A. E. Kiprakis, "Intelligent voltage and reactive power control of mini-hydro power stations for maximisation of real power export," in *Proc. Waterpower XIII*, (Buffalo, USA), HCI Publications, July 2003.

[82] A. E. Kiprakis and A. R. Wallace, "Hybrid control of distributed generators connected to weak rural networks to mitigate voltage variation," in *Proc. 17th Int. Conf. Electricity Distribution CIRED*, (Barcelona, Spain), CIRED, May 2003.

[83] A. E. Kiprakis and A. R. Wallace, "Maximising energy capture from distributed generators in weak networks'," *IEE Proc. Gener. Transm. & Distrib.*, vol. 151, pp. 611–618, September 2004.

[84] R.Chedid, "Intelligent control for wind energy conversion systems," *Wind Engineering*, vol. 22, no. 1, pp. 1–16, 1998.

[85] A. Ekwue, D. Cheng, and J. Macqueen, "Artificial intelligence techniques for voltage control," in *Artificial intelligence techniques in power systems* (K. Wardwick, A. Ekwue, and R. Aggarwal, eds.), 22, pp. 109–120, London, UK: IEE, 1997.

[86] W. J. Laycock, "Intelligent networks," *IEE Power Engineering Journal*, pp. 25–29, February 2002.

[87] M. Marei, E. El-Saadany, and M. Salama, "A novel control algorithm for the DG interface to mitigate power quality problems," *IEEE Trans. Power Delivery*, vol. 19, pp. 1384–1392, July 2004.

[88] G. Ramakrishna and N. Rao, "Fuzzy inference system to assist the operator in reactive power control in distribution systems," *IEE Proc. Gener. Transm. Distr.*, vol. 145, pp. 133–138, March 1998.

[89] Y. H. Song and A. T. Johns, "Applications of fuzzy logic in power systems, part 1," *IEE Power Engineering Journal*, vol. 11, pp. 219–222, October 1997.

[90] C. Su and C. Lin, "A new fuzzy control approach to voltage profile enhancement for power systems," *IEEE Trans. Power Syst.*, vol. 11, pp. 1654–1659, August 1996.

[91] H. Al-Duwaish, "Adaptive output feedback controller for wind turbine generators using neural networks," *Electric Machines and Power Systems*, vol. 27, pp. 465–479, 1999.

[92] R. Bansal, "Bibliography on the fuzzy set theory applications in power systems (1994-2001)," *IEEE Trans. Pwr. Syst.*, vol. 18, pp. 1291–1299, November 2003.

[93] W. Pedrycz, *Fuzzy Control And Fuzzy Systems*, pp. 106–116. Taunton, Somerset, England: Research Studies Press, 2nd ed., September 1993.

[94] T. Takagi and M. Sugeno, "Fuzzy identification of systems and its application to modelling and control," *IEEE Trans. Syst., Man., Cybern.*, vol. 15, pp. 116–132, 1985.

[95] H. Ying, "Constructing nonlinear variable gain controllers via the takagi-sugeno fuzzy control," *IEEE Trans. on Fuzzy Systems*, vol. 6, no. 2, pp. 226–234, 1998.

[96] J. Barrie, "Incorporating novel generator control into optimal power flow," meng individual project report, School of Engineering and Electronics, The University of Edinburgh, Ediburgh, UK, November 2004.

[97] Embedded Generation Working Group, "Future network design, management and business environment," rapporteur contribution, DTI/OFGEM, London, UK, December 2000.

[98] J. McDonald, G. Burt, S. McArthur, C. Booth, I. Elders, and S. Bell, "Power network management using intelligent systems," in *Proc. IEE Power System Control and Management Conf.*, pp. 240–245, IEE, April 1996.

[99] G. Dudgeon, W. Leithead, J. O'Reily, and J. McDonald, "Prospects for the decentralised control of small-scale power networks with embedded generation," in *IEEE Power Engineering Society Winter Meeting*, vol. 2, pp. 1399–1404, IEEE, 2000.

[100] Z. Saoud, M. Lisboa, J. Ekanayake, N. Jenkins, and G. Strbac, "Application of STATCOMs to wind farms," *IEE Proc. Gener. Transm. Distrib.*, vol. 145, pp. 511–516, September 1998.

[101] P. Vovos, G. Harrison, A. Wallace, and J. Bialek, "Optimal power flow as a tool for fault level constrained network capacity analysis," *IEEE Trans. Power Systems*, vol. 20, pp. 731 – 741, May 2005.

[102] P. N. Vovos, A. E. Kiprakis, G. P. Harrison, and J. R. Barrie, "Enhancement of network capacity by widespread intelligent generator control," in *Proc. 18th Int. Conf. Electricity Distribution CIRED*, (Torino, Italy), CIRED, June 2005.

[103] P. N. Vovos, A. E. Kiprakis, G. P. Harrison, and A. R. Wallace, "Augmenting network capacity by widespread intelligent generator control," *Submitted to IEEE Trans. Power Systems*, 2005.

Appendix A
Publications

A.1 Journal Papers

i. **P. N. Vovos, G. P. Harrison, A. E. Kiprakis and A.R. Wallace**, '*Augmenting network capacity by widespread intelligent generator control*', submitted to IEEE Trans. Power Systems *(not included)*

ii. **A. E. Kiprakis and A. R. Wallace**, '*Maximising Energy Capture from Distributed Generators in Weak Networks*', IEE Proc. Gener., Transm., Distrib., 151, 05, 611-618, September 2004

iii. **A. E. Kiprakis, G. P. Harrison, D. S. Forrest and A. R. Wallace**, '*Increasing Distributed Generation Capacity: A Holistic Approach*', Renewable Energy 2004, WREN-UNESCO, 98-11, 2004

iv. **G. P. Harrison, A. E. Kiprakis and A. R. Wallace,** '*Distribution Networks: Constraining Renewable Energy Development*', Re-Gen, Wilmington Publishing, 1, 1, 50-59, April/May 2003, ISSN 1479-0351

v. **G. P. Harrison, A. E. Kiprakis and A. R. Wallace,** '*A new era for mini-hydro*', International Water Power and Dam Construction, Wilmington Publishing, 54 (11), November 2002, pp. 20-24

vi. **A. E. Kiprakis and A. R. Wallace**, '*Novel Control Algorithms for Distributed Generators to Mitigate Voltage Fluctuation Phenomena*', PhDEE (Departmental Journal), School of Engineering & Electronics, The University of Edinburgh, November 2002 *(This is a reduced edition of item A.1(i) and is not included.)*

A.2 Conference Publications

i. **A.E. Kiprakis, A.R. Wallace**, '*Voltage Control in the Distribution Network: Traditional Techniques and New Developments*', World Renewable Energy Congress (WREC2005), 22-27 May 2005 *(Invited paper)*

ii. **P. N. Vovos, A. E. Kiprakis, G. P. Harrison, J. R. Barrie,** '*Enhancement of Network Capacity by Widespread Intelligent Generator Control*', Proceedings 18th International Conference on Electricity Distribution CIRED 2005, June 2005, Torino, Italy

iii. **A. R. Wallace and A. E. Kiprakis**, '*Intelligent Voltage and Reactive Power Control of Mini-Hydro Power Stations for Maximisation of Real Power Export*', Proceedings of the Waterpower XIII Conference, July 2003, Buffalo, USA

iv. **A. E. Kiprakis and A. R. Wallace**, '*Hybrid Control of Distributed Generators Connected to Weak Rural Networks to Mitigate Voltage Variation*', Proceedings 17th International Conference on Electricity Distribution CIRED 2003, 12 - 15 May 2003, Barcelona, Spain.

v. **A. R. Wallace and A. E. Kiprakis**, '*Reduction of Voltage Violations from Embedded Generators connected to the Distribution Network by Intelligent Reactive Power Control*', Proceedings IEE 5th International Conference on Power System Management and Control PSMC 2002, April 2002, London, UK

A.3 Seminar Lectures

i. **A.E. Kiprakis**, '*Doubly Fed Induction Generators for Offshore Wind Energy Systems*', IEE Seminar on Electrical Aspects of Offshore Renewable Energy Systems, 24-25 February 2004 *(Presentation only, not included)*